THE UNIVERSITY OF HULL

An optical label-free aptasensor based on dye doped leaky
waveguide (DDLW) for biomarker detection

Being a Thesis submitted for the Degree of

Doctor of Philosophy (PhD)

In the University of Hull

By

Nasser. A. Alamrani

BSc. MSc.

July 2019

Contents

Acknowledgements

List of abbreviations

Ab	Antibody
Ag	Antigen
ARROW	Anti-resonant reflecting optical waveguide
Biotin-BSA	Biotin labelled bovine serum albumin
BSA	Bovine serum albumin
CL	Chemiluminescence
CMOS	Complementary metal oxide silicon
CS	Chitosan
DDLW	Dye-doped leaky waveguide
FITC	Fluorescein isothiocyanate
FRET	Fluorescence resonance energy transfer
FTIR	Frustrated total internal reflection
GOx	Glucose Oxidase
GO	Graphene oxide
HEPES	(4-(2-Hydroxyethyl) piperazine-1-ethanesulfonic acid)
HRP	Horseradish peroxidase
ISE	Ion-selective electrode
IUPAC	International Union of Pure and Applied Chemistry
Ka	Association Constant
Kd	Dissociation Constant
LED	Light emitting diode
LOD	Limit of Detection
MCLW	Metal-clad leaky waveguide
MZI	Mach-Zehnder interferometer
NHS-PEG-NHS	N,hydroxysuccinimide-polyethylene glycol- N, Hydroxysuccinimide
NHS	N-hydroxysuccinimide
Oligo	Oligonucleotides
PBS	Phosphate buffer saline
PEG	Polyethylene glycol
PEO	Polyethylene oxide

POC	Point-Of-Care
PSA	Prostate specific antigen
PZ	Piezoelectric
QCM	Quartz crystal microbalances
RB4	Reactive Blue four
RI	Refractive index
RM	Resonant mirror
SAW	Surface acoustic wave
SELEX	Systematic Evolution of Ligands via the exponential enrichment
SEM	Scanning electron microscope
SPR	Surface Plasmon Resonance
Sulfo-NHS-biotin	biotin-3-sulfo-N-hydroxysuccinimide ester sodium salt
TE	Transverse-electric polarised light
TIR	Total internally reflected
TM	Transverse-magnetic polarised light
WLI	White light interferometer
YI	Young's interferometer
µTAS	Micro total analysis systems
6-FAM	6-carboxyfluorescein

Abstract

Due to the rapid increase in routine measurement of biomarkers, such as a protein, in blood samples for healthcare monitoring, different techniques have been developed to facilitate this measurement in terms of cost-effective and fast measurement. Label-free optical biosensors are an attractive technology because they do not require fluorescent dyes or radioactive isotopes for detection, thereby reducing cost and measurement time.

Dye-doped leaky waveguides (DDLW) were developed by our group in 2016 as a label-free and a real-time optical biosensor measurement. They measure the change in the refractive index in a real-time when an analyte interacts with the waveguide. DDLW is a leaky optical mode which features a lower index waveguide material such as a hydrogel. This is advantageous for the sensitivity of the sensors as the analyte can be inserted into the sensing region and hence interact with a large portion of the confinement light, resulting in great enhancement of the sensor signal. Furthermore, DDLW shows other advantages such as low cost and easy fabrication.

In this work, a DDLW was developed as a label-free and a real-time optical biosensor measurement with using for the first time a chitosan hydrogel polymer as a porous waveguide layer. The inexpensive hydrogel offers advantages such as non-toxicity and biocompatibility and also features functional amino groups that are amenable to tethering of bio-recognition elements. Furthermore, aptamers were chosen as the bio-recognition element to capture the analyte due to their selectivity, stability and low cost compared to more commonly used antibodies. This was the first time the possibility of using an aptamer as a bio-receptor in the 3D network leaky waveguide containing chitosan porous hydrogel on glass substrate.

Thrombin and prostate specific antigen (PSA) were selected as key biomarkers for measurement by the fabricated DDLW device. Thrombin is an allosteric serine protease that works as the central protease in the coagulation cascade. With some critical role in the coagulation process, thrombin is linked to Parkinson's and Alzheimer's diseases. Prostate specific antigen has been considered the most validated biomarker in serum for early detection of prostate and breast cancers.

The preliminary result was that chitosan could be successfully prepared to provide a single waveguide mode by using 2% of chitosan solution coated at speed of 3000 rpm. The waveguide obtained showed a high sensitivity to the value of refractive index.

However, the porosity of the waveguide was found to be small, which prevented diffusion of the large molecules into the sensing region. Different methodologies were utilised to enhance the waveguide's porosity. Using a lower concentration of chitosan with a controlled drying time for the coated wet chitosan film was found to be effective at improving the pore size of the waveguide. The best conditions was found to be a 1% chitosan solution coated at spin speed of 900 rpm with 3 min of drying time of the coated film.

For the detection of thrombin, an aptamer molecule was immobilised into the porous chitosan waveguide via a streptavidin and biotin complex. First, the attachment of streptavidin was optimised using three methods: covalent attachment, non-covalent attachment and physical adsorption. Comparing the protocols uses, covalent attachment using glutaraldehyde as the cross-linker exhibited the highest amount of streptavidin immobilised onto the waveguide. An anti-thrombin biotinylated aptamer was then attached to the immobilised streptavidin. The detection of thrombin was achieved by observing a rapid shift in the resonance angle upon applying 1μM of thrombin solution for 15 min. The sensitivity of the sensor to detect thrombin was found to be enhanced upon increasing the incubation time of thrombin molecules. Based on this, a calibration curve was then obtained for different concentrations of thrombin, and the limit of detection (LOD) of the sensor was found to be ≈3.7 nM after one hour of incubation. This limit of detection (LOD) was comparable to those were previously reported for detection of thrombin such as SPR. The applicability of the DDLW device for the measurement of thrombin in a clinically relevant sample was evaluated. It was found that the shift observed for the first four hours of incubation of spiked thrombin (50 nM) in 10 % human serum sample was close to the shift obtained when 50 nM of thrombin was measured in an aqueous buffer. Therefore, it was concluded that thrombin was successfully detected in a diluted serum sample.

The detection of PSA was more challenging as compared to the detection of thrombin. An enhancement was obtained upon the thermally treated anti-PSA aptamer prior to immobilisation. This was thought to prevent the folding of aptamer molecules and hence improve the binding of PSA. The detection of PSA was comparable to the detection of thrombin with the thermal treatment of aptamer. Based on this, a series of concentrations of the PSA ranging from 25 nM and 75 nM were then successfully detected in an aqueous

buffer. It was concluded that the fabricated DDLW device could be applied to other applications using an aptamer as a recognition element.

1 Introduction

Biomarkers are commonly tested in laboratories in order to monitor human health. However, this requires large equipment with an increase in time and cost of analysis. Therefore there is high demand for a technique that can overcome the drawbacks associated with the conventional methods. Biosensors are a promising method that can offer sensitivity, specificity, portability, cost-effective and fast measurement[1]. The first emergence of biosensors was based on the work by Leland C. Clark, who first showed the detection of glucose using glucose oxidase entrapping onto the oxygen electrode. Later on the biosensor of glucose for analysis became commercially available in 1975[2].

A typical biosensor device contains[3];

- **Analyte**: a molecule of interest which is required to be measured, for example biomarker.
- **Bio-recognition**: a compound that recognises the target analyte can be a bioreceptor, for example an antibody or aptamer.
- **Transducer**: this usually transfers the bio-recognition event into a detectable signal known as signalisation.

The typical characteristics of biosensors are[3];

- **Selectivity**. This is achieved via using a bio-recognition element to detect the specific analyte in a mixture of sample and contaminants.
- **Reproducibility**. This is reproducibility of the output signal after repetition of the measurement.
- **Stability**. This is to be non-susceptible to changes in ambient conditions such as pH and temperature in order to avoid an error in the output signal.
- **Sensitivity**. This is defined by its limit of detection (LOD). The aim should be to detect quantities in the range of concentration as small as ng/mL to confirm the present of the analyte in the sample.
- **Linearity**. This is represented by the response of the biosensor device. A small change in the concentration of a target molecule would lead to a difference in the output signal.

Different biosensor devices have been established and developed such as surface plasmon resonance (SPR) and interferometers. In this thesis, an optical label-free aptasensor based

on a leaky waveguide mode will be investigated as a relatively inexpensive and easy-to-use tool for scientific analysis and detection of biomarkers.

1.1 Biosensors

Biosensors have been developed and exploited for the detection, quantification and monitoring of a specific biochemical species[4]. The definition of biosensor given by International Union of Pure and Applied Chemistry (IUPAC) is *"a self-contained integrated device that is capable of providing specific quantitative or semi-quantitative analytical information using a biological recognition element (biochemical receptor), which is in direct spatial contact with a transducer element"*[5]. The purpose of using a recognition element is to obtain a high degree of selectivity to the analyte to be measured[5]. The output signal observed from the recognition system is then transferred by a transducer, into a mostly electrical domain, with the measurement being proportional to the concentration of the present analyte. The transducer part of the sensor is also called detector, sensor or electrode[5]. Figure 1.1 shows a typical biosensor device containing a bio-recognition element immobilised into a transducer to capture the analyte. A biosensor achieves highly sensitive detection by combining the high analytical specificity with the processing power of a modern electronic transducer. This allows for the detection of a broad spectrum of analytes in complex samples[6]. Furthermore, it is a self-contained integrated device with all parts packed together in a small unit leading to easy operation, rapid measurement and portability which is an important factor for point-of-care systems (POC systems)[4, 5, 7]. By comparison to a conventional instrument, many steps are no longer required, such as sample preparation that consumes reagents; purification; and separation.
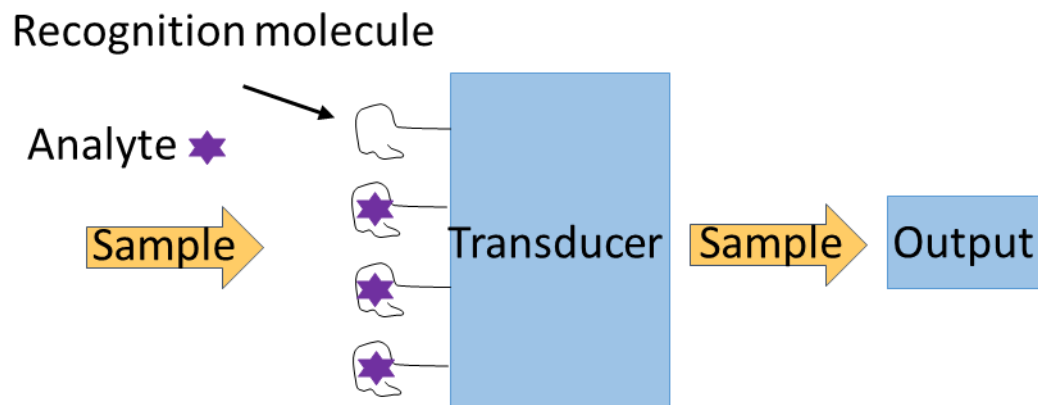
Figure 1.1 *Schematic diagram of biosensor device. Analyte is captured by immobilised recognition molecule on a transducer leading to change in the output signal.*

1.2 Recognition elements

Recognition elements can be classified into two groups; the catalytic type and the affinity type.

1.2.1 Catalytic type

These recognition elements are based on a catalysed reaction which occurs via an immobilised macromolecule that is in its original biological form or has been isolated previously or synthetically prduced[8]. The measurement of the analyte is achieved by the reaction with biocatalyst molecules immobilised into the sensor. The most common biocatalysts used are enzymes (mono- or multi-enzyme), whole cells (bacterial, fungi and yeast) or tissue (plant or animal)[8]. The analytes, usually known as substrate S and substrate S', reacting with the biocatalyst molecules yielding one or more products that are named P and P' based on the equation1.1[8]:

$$S+S' \xrightarrow{\text{Biocatalyst}} P+ P' \qquad \text{Equation 1.1}$$

The transducer can then monitor the consumption of the analyte S or the consumption of the co-substrate S', and hence the signal decreases from its initial value. The consumption of S (analyte) can also be observed through monitoring one of the reaction products (P) and thus the corresponding signal increases[8].

One of the most investigated biosensors based on catalysed reactions is that for glucose. This was first reported by Clark and co-authors in 1962 from the Children's Hospital of Cincinnati[9]. The sensor relied on using the enzyme known as glucose oxidase (GOx) and was based on the following reactions [10]:

$$D\text{-glucose} + O_2 \xrightarrow{\quad GOx \quad} D\text{- gluconolactone} + H_2O_2 \qquad \qquad Equation\ 1.2$$

$$D\text{- gluconolactone} + H_2O \xrightarrow{\quad\quad\quad} D\text{- gluconate} + H^+ \qquad \qquad Equation\ 1.3$$

The concentration of glucose can be found based on the amount of oxygen consumed or on the amount of hydrogen peroxide produced or it can be calculated based on the decrease in pH which is a result of conversion of D-gluconolactone to D-gluconic acid[10].

1.2.2 Affinity type (Antibody-antigen)

The antibody-antigen reaction has been considered one of the most widely used biological recognition techniques. An antibody is a specific protein called an immunoglobulin ($\approx$ 150 kDa) and is generated by the body's immune system to attack an invader pathogen (antigen). The antibodies that have a Y shape (Figure 1.2) can specifically bind to the antigen (analyte) with a very strong affinity with association constant between 10^{12} and 10^{14} (Ka) forming a stable complex with noncovalent binding[6, 10].

The antibody-antigen reaction is performed either a competitive or a sandwich assay[6]. In a competitive format, the antigens (Ag) compete with labelled antigens (Ag*) to bind to immobilised antibodies (Ab). In the other format the labelled free antibodies (Ab*) compete with free antigens (Ag) to bind to immobilised antigens (Ag). In a competitive assay, analytes (antigens) with small molecular weights are usually conjugated with a protein in order to enhance the immobilisation and the interaction with the antibody. This format is usually preferred in order to overcome all issues associated with antibody immobilisation such as correct orientation of the antibody[6]. In a sandwich assay, the antigens (Ag) are first bound to immobilised antibodies (Ab) followed by addition of secondary labelled antibodies (Ab*) that bind to the second binding site of the antigen. Therefore the antigens (Ag) are sandwiched between two antibodies as shown in figure 1.2[6].

Although antibody-antigen reactions have shown high sensitivity and specificity resulting in a good detection limit, the quality of the antibodies can heavily affect the detection process as their preparation via animal immunisation can take several months and may suffer with regards to stability or modification[11]. A large variability from batch to batch can therefore often be observed. Further limitations are also seen with using antibodies such as low temperature stability and high production cost[12].
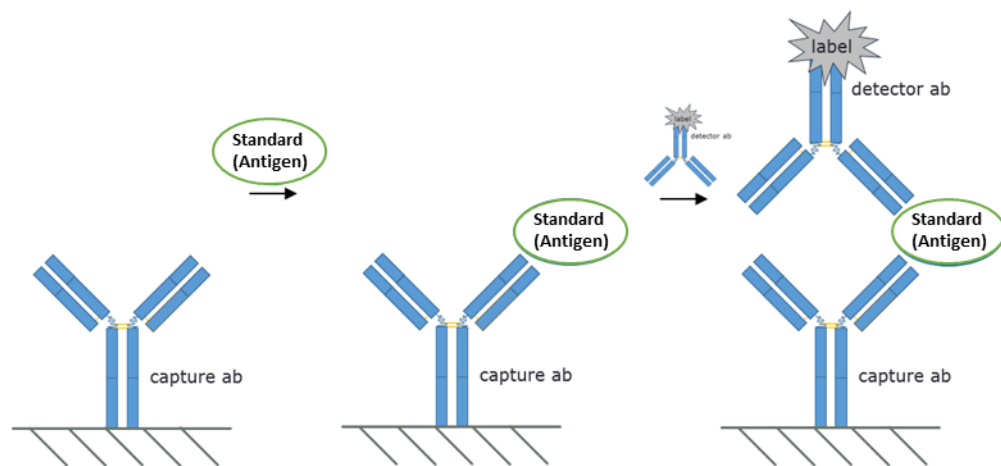
Figure 1.2 *Antigen captured by immobilised antibody followed by capture by the second labelled antibody to form a sandwich assay.*

1.2.3 Affinity type (Aptamer)

An aptamer is a single strand of DNA or RNA that can bind with high affinity and specificity to analytes of different sizes, ranging from small molecules to whole cells due to its flexibility that leads to binding to its ligand via three-dimensional structure[11, 13]. Aptamers were first reported by Ellington and Szostak in 1990 using RNA molecules to recognise a variety of organic dyes[14]. The name aptamer is based on the Latin word *aptus* which means fit and the Greek word *meros* that means part or portion, referring to the folding properties of the aptamer into its target leading to their three-dimensional structure[13]. The mechanism of aptamer binding is to fold into unique overall shapes to form intricate binding furrows for target molecules. This leads to a conformational alteration of the structure of the aptamer such as from a hairpin or duplex structure to a G-quadruplex upon binding to the target analyte as shown in figure 1.3. Therefore, it has attracted research attention in the field of biodetection schemes[11, 13]. The binding of aptamer molecules to the target may be due to hydrogen bonds, van der Waals forces and electrostatic interactions which depends on the type of target analyte[15]. Aptamers are usually produced in variable lengths from 25 to 90 (mer) while their affinities (Kd) are in a range of 1 pm to 1mM with most being between 1 nM and 10 nM[16].
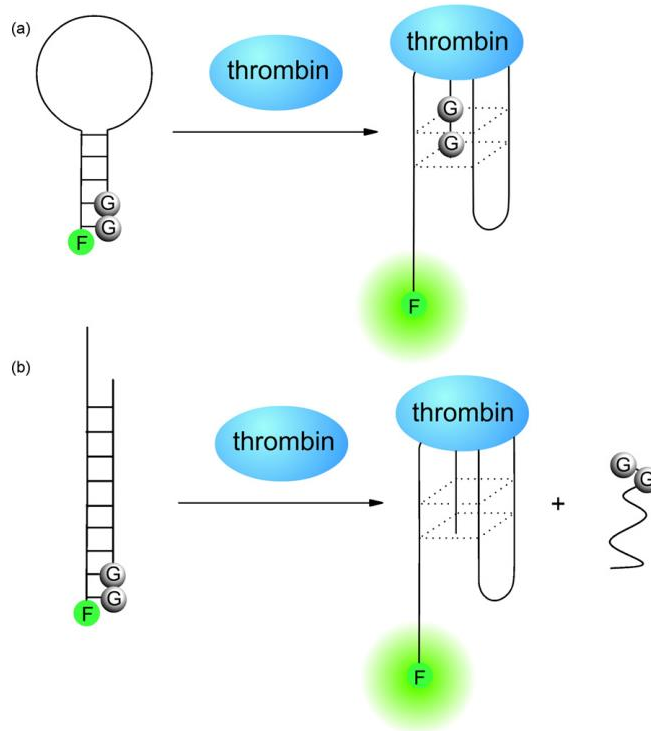
Figure 1.3 *Diagram of a conformation alteration structure of aptamer from (a) hairpin and (b) duplex design to G-quadruplex upon binding to a protein (Thrombin)[17].*

1.2.3.1 Synthesis of Aptamer (SELEX)

The synthesis of an aptamer is carried out by Systematic Evolution of Ligands via the exponential enrichment (SELEX) method (figure 1.4)[16, 18]. A library of synthetic nucleic acids which could contain more than 10^{15} different sequences with a variable region of 30 bases with fixed primers of 20-25 bases is normally utilised to generate an aptamer against a specific target. A random sequence oligonucleotide is introduced to a solution containing the target molecules at a given temperature. After binding the random oligonucleotide to an analyte, unbound DNA is washed out and the recognition sequence of DNA is eluted, usually by affinity chromatography or filter binding. This is then followed by amplification of the recognition sequences by PCR techniques to enrich the library to be used for the second cycling. The whole process is usually repeated for 15-20 rounds until various sequences with high affinities to the target can be obtained. To this end, the selected sequences are then cloned and their binding to the target investigated using techniques such as surface plasmon resonance (SPR). The length of aptamer obtained can then be shortened by removing the bases such as the fixed primer and those not considered to be in the consensus motif (sequences required for binding). The binding efficiency and selectivity of the aptamer against the target are enhanced with each round

leading to the formation of aptamer–target complexes from low micromolar to high picomolar levels[16, 18].
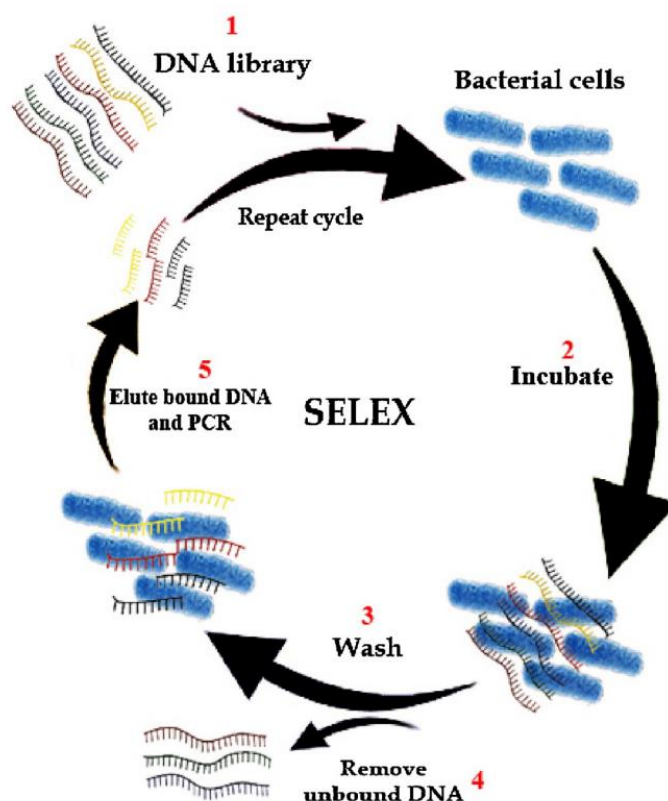
Figure 1.4 *Schematic diagram of the SELEX method utilised for selecting an aptamer to bacterial cells. In stage 1 a random synthesised DNA library is selected; in stage 2 this is incubated with bacterial cells (target analyte); in stages 3 and 4 nucleic acid sequences unbound to bacterial cells are washed and separated from the attached DNA. Finally, in stage 5 the attached sequences are eluted and then amplified by PCR before the next round[16].*

1.2.3.2 Aptamers versus Antibodies

Aptamers are not just an alternative method to antibodies; they have proven advantages over antibodies. As the aptamer is synthetically generated in the laboratory, the use of animals is avoided, making aptamers more animal-friendly and ethical. In addition to this superior benefit, they are cost-effective, offer high reproducibility and selectivity, are produced faster, and demonstrate excellent stability and robustness in complex biochemical matrices[11]. Aptamers can be modified with any functional group without affecting their affinity to the target and thus can be easily deposited on the sensing surface[19]. Furthermore, they can bind ions and small molecules which cannot be

recognised by antibodies indicating the widening applications of biosensors based on aptamer. Aptamers have a higher temperature and pH stability than antibodies[20]. They can recover their native active conformations after thermal denaturation. They are stable to long-term storage and can be transported at room temperature. In contrast, antibodies are more temperature and pH sensitive and suffer from irreversible denaturation and also have a limited shelf life[12]. The binding nature that involves specific conformations such as G-quaduplex, leads to a great construction of aptamer-based biosensors that rely on the conformational variations before and after binding into its target.

1.2.3.3 *Aptasensor*

An aptasensor is a biosensor device that utilises an aptamer as the recognition element to confer selectivity and a transducer to confer sensitivity by producing an analytical signal from the binding event between the aptamer and the target analyte. The first aptasensor device was reported by Potyrailo *et al.* in 1998 when an aptamer labelled with fluorescein isothiocyanate (FITC) was immobilised on a microscope cover slip to detect a human alpha thrombin. The measurement was achieved using a one-step direct detection of the analyte by monitoring the change in fluorescence anisotropy upon the binding event[21]. Lee and Walt also reported in 2000 an aptasensor device for thrombin measurement utilising a competitive mode of assay. An anti-thrombin DNA aptamer was immobilised on silica microspheres beads and the non-labelled thrombin molecules were detected in a competitive mode with fluorescein-labelled thrombin (F-thrombin)[22]. Several aptasensor devices have been published since then using various types of transducers for different applications such as medicine[23, 24], forensics[25, 26], food[27, 28] and environment[29, 30].

1.3 Transducers

Biosensors can be classified based on the type of transducer utilised. The most widely used transducers are electrochemical, piezoelectric and optical transducers.

1.3.1 Electrochemical transducer

Electrochemical biosensors use an electrode as the transduction element and are considered an important type of sensor[31]. According to the IUPAC, the definition of an electrochemical biosensor is *"a self-contained integrated device, which is capable of providing specific quantitative or semi-quantitative analytical information using a biological recognition element (biochemical receptor) which is kept in direct spatial contact with an electrochemical transduction element"*[5, 8]. The principle of the transducer is to measure the current that is produced from oxidation and reduction reactions. The

electrical signal obtained is directly related to the recognition process and hence is proportional to the concentration of the analyte. Electrochemical biosensors have advantages such as high sensitivity, simplicity, speed, and low cost[31, 32]. There are different categories of electrochemical biosensors which depend on the nature of the electrochemical changes during the biorecognition event as shown below.

1.3.1.1 Amperometric sensors

An amperometric sensor is based on measuring, as a function of time, the current that is produced from the oxidation and reduction reaction occurring from the recognition process at a fixed potential. The setup for amperometric sensors usually contains three electrodes: a working electrode (WE) made of carbon (C) or gold (Au) or platinum (Pt); a reference electrode (RE) made from either silver or silver chloride (Ag/AgCl) with a fixed potential that controls the potential of the working electrode; and the third electrode, known as the counter electrode (CE). Upon oxidation and reduction, electrons are transferred from the target molecule to the working electrode or vice versa. The flow of electrons can be directed by the electric potential applied to the working electrode. An oxidation reaction occurs if the working electrode is driven to a positive potential and the current flow measured depends on the concentration of the analyte (electroactive species) that is diffused to the working electrode surface. A reduction reaction occurs if the working electrode is driven to a negative potential. A counter electrode (CE) is used to assist the measurement of current flow by minimising the electrical current flowing through the reference electrode[31, 32]. The reduction reaction of the analyte or other electroactive species such as enzyme horseradish peroxidase (HRP) at the working electrode usually occurs at a very low rate due to small electron transfer. Mediator or redox species such as hydroquinon (HQ) or hydrogen peroxide (H_2O_2) are usually used in order to reduce the enzyme or the analyte rapidly and hence enhance the electron transfer rate due to their higher mobility[33].

A recent amperometric based aptasensor has been reported by Paniagua *et al.* for the detection of a cancer biomarker (carcinoembryonic antigen (CEA))[34]. The device was designed with a nanoparticle that had gold (Au) and silica opposite faces known as Janus-type nanoparticles. The enzyme horseradish peroxidase (HRP) was used as an oxides species. It was functionalized on the silica surface to provide a signalling element while an anti-CEA aptamer was immobilised on the Au face to capture the analyte as shown in figure 1.5 (a). The aptamers were modified by a thiol group at the 3' end for covalent

attachment on the Au surface while they were functionalized with a biotin group at the 5'end. This sensing mechanism was based on capturing the CEA molecules causing unfolding of the aptamer which unmasked the biotin residues as shown in figure 1.5 (b) (route A). The complex was then captured by avidin modified with a magnetic nanoparticle followed by deposition on the working electrode surface of carbon screen-printed electrodes using a permanent magnet. The amperometric analytical signal was then recorded by addition of H_2O_2/HQ (Hydrogen peroxide / Hydroquinone) which caused the reduction of the enzyme horseradish peroxidase (HRP) attached to the complex, hence the amperometric signal is on. In the absence of CEA molecules, the aptamers retain their hairpin structure which covers the biotin residues and hence the complex cannot be captured by the avidin-modified magnetic nanoparticle and thus cannot be deposited on the working electrode. Consequently, the enzyme (oxides species) is absent and thus the amperometric analytical signal is off as shown in figure 1.5 (b) (route B). The detection limit of the CEA molecules was at 0.4 pM in a buffer solution and was at 1.2 pM in 100-fold diluted human serum sample which covered the cut-off level of CEA molecules in a healthy individual person[34].
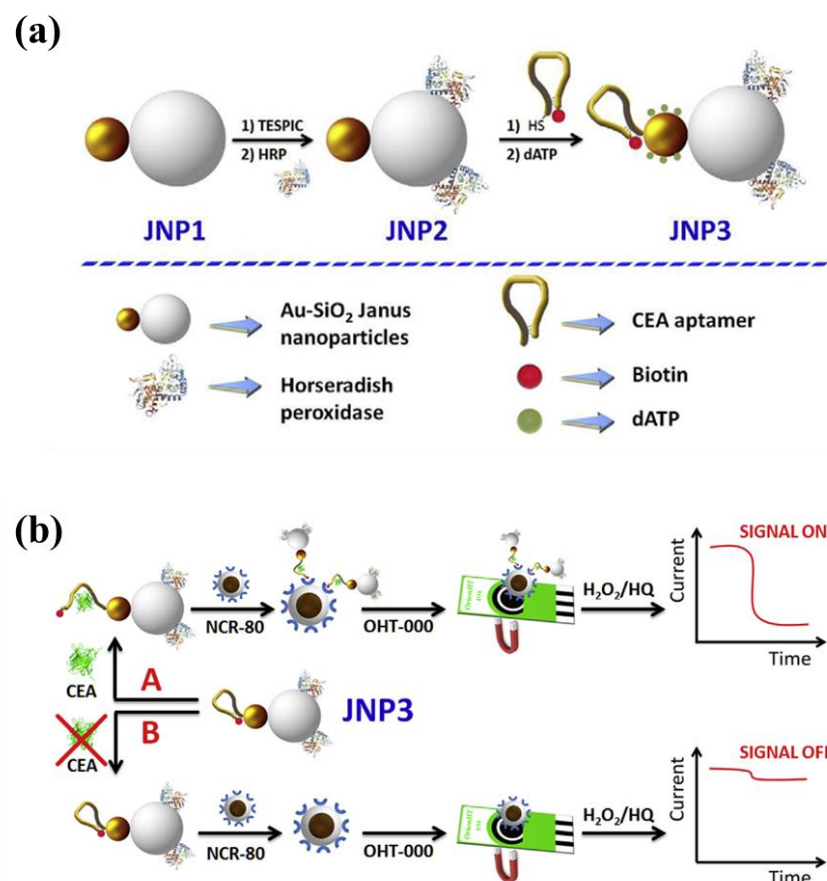
Figure 1.5 **(a)** *Schematic diagram of Janus-type nanoparticles with steps of immobilisation of the enzyme horseradish peroxidase (HRP) (JNP2) and anti-CEA aptamer (JNP3).* **(b)** *Strategy of detection of CEA molecules using Janus-type nanoparticles at the step of JNP3 via two routes;* **A** *with using CEA molecules and* **B** *in the absent of CEA molecules[34].*

1.3.1.2 Potentiometric sensors

Potentiometric biosensors depend on using two electrodes, an indicator electrode and a reference electrode (usually Ag/AgCl) in order to provide an analytical signal that is related to the recognition process. The principle of the potentiometric transduction is to measure the potential difference observed between an indicator electrode and a reference electrode that occurs during the recognition process in an electrochemical cell while the amount of current flowing through the electrode is zero or negligible. An indicator electrode is usually called an ion-selective electrode (ISE) due to being made of a permselective ion-conductive membrane. The membrane can be either plasticized polymer or a solid (e.g. glass, inorganic crystal). In an ISE the potential that is associated with the ion of interest via a selective binding process at the membrane-electrolyte

interface is measured. The concentration of analyte is measured in a logarithmic manner that is proportional to the potential difference obtained. This type of transducer shows several advantages such as rapidity, selectivity, simplicity and low cost. Nevertheless, the devices lack sensitivity and are slower than amperometric transducers[31, 32].

Ding *et al.* fabricated a potentiometric aptasensor device for the detection of *Listeria monocytogenes* (LM); a pathogen that is common in the environment (figure 1.6). The device utilised protamine, a group of arginine-rich polycationic proteins. In the absence of target molecules, the negatively charged anti-LM cells aptamer interacted electrostatically with the positively charged guanidinium groups of protamine, forming a complex. This prevented binding of protamine onto the polycation sensitive membrane rotating electrode and hence inhibiting the potential response of protamine. In the presence of the target bacterium, aptamer molecules bound specifically to the target leading to elimination of the reaction with protamine. The remaining protamine could then bind on a polycation-sensitive membrane electrode via formation of cooperative ion pairs, hence producing a large and reproducible potentiometric response toward protamine. The fabricated device was able to detect LM bacterium in aqueous buffer at levels down to 10 CFU mL^{-1} [35].
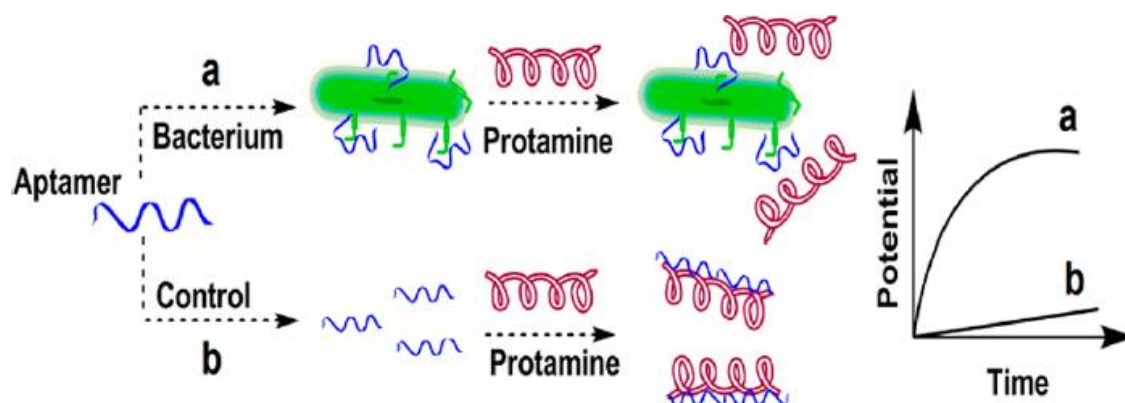
Figure 1.6 *Illustration of potentiometric aptasensing for detection of bacterial cells utilising a polycation-sensitive membrane electrode*[35].

1.3.2 Piezoelectric transducer

The mechanism of piezoelectric transducer is based on the piezoelectric (PZ) effect that was discovered by the Curie brothers in 1880. The piezoelectric (PZ) effect is produced when piezoelectric materials such as quartz crystals or biological matter are mechanically deformed; pressed or pulled. This leads to the generation of an electrical charge (voltage) across the object. It is conversion of mechanical stress into an electrical charge. The effect

can also be used in the opposite way when piezoelectric materials are deformed by application of a voltage[36]. The most common transducers based on the piezoelectric (PZ) effect are quartz crystal microbalances (QCM) and surface acoustic wave (SAW) sensors.

1.3.2.1 Quartz crystals microbalance (QCM)

For analytical applications the frequencies of mechanical oscillations that occur due to an imposed voltage on piezoelectric materials can be used to determine an analyte. The quartz crystal microbalance (QCM) sensor is fabricated by coating thin slices of quartz with a gold or silver layer which serves as an electrode on both sides. The quartz is derived from a signal crystal with optimal mechanical, chemical and electrical properties for analytical applications. An electric field is then generated by applying a potential difference on the electrode which leads to modification of the physical orientation of the crystal lattice. Consequently, a mechanical oscillation with a characteristic vibrational frequency is produced across the bulk of the quartz disk. If an analyte is bound to the quartz disk the mass will change which causes a decline in the resonance frequency which leads to detectable signals and hence can be utilised to monitor analytes at nanogram levels[37]. A QCM transducer offers several advantages such as high sensitivity at nanogram level, reliability, low cost, label-free, widely available and can be used in real-time monitoring for binding events[38, 39].

Chen *et al.* fabricated an aptasensor device based on a QCM transducer for the detection of thrombin. The QCM transducer was used with a dissipation monitoring (QCM-D) technique in order to give information about the viscoelastic properties of the mass bound and hence to simultaneously monitor the change in the frequency and dissipation factor. The anti-thrombin aptamer (TAB 15) was covalently immobilised to the crystal via a thiol self-assembly monolayer. The frequency of the QCM-D signal decreased whereas the dissipation signal rose with an aptamer immobilisation. Upon introducing thrombin, an immobilised aptamer captured the target analyte in the G-quadruplex conformation leading to a further shift in the frequency signal as shown in figure 1.7. The detection limit obtained was 10 nM. A significant enhancement in the limit of detection was obtained via performing a sandwich assay. After capturing thrombin molecules via an immobilised aptamer, a second aptamer (TAB 29) conjugated with gold nanoparticles was introduced to bind to the captured thrombin in the second binding sites. The frequency and dissipation signal was significantly amplified due to a rigid core of gold nanoparticles and therefore the LOD was observed at 0.1 nM[40].
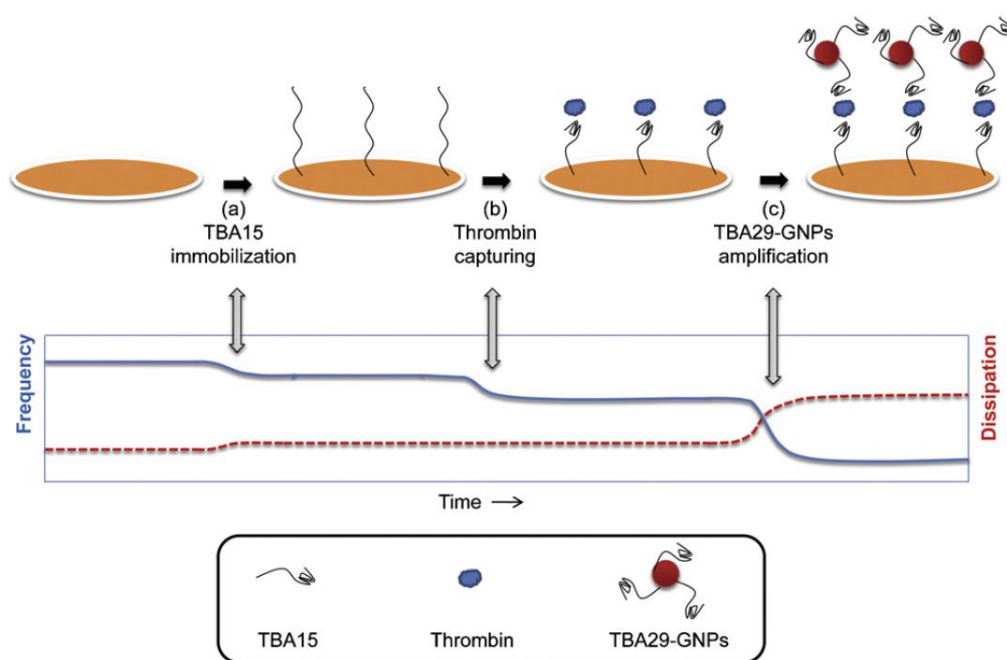
Figure 1.7 *Schematic diagram of an aptasensor based on quartz crystal microbalance (QCM) transudate coupled with dissipation monitoring (QCM-D). The anti-thrombin aptamer (TAB 15) was immobilised to the crystal chip. The frequency of the QCM-D signal decreased whereas the dissipation signal rose with an aptamer immobilisation. Upon introducing thrombin, an immobilised aptamer captured the target analyte (thrombin) leading to a further shift in the frequency signal. A second aptamer (TAB 29-GNPs) conjugated with gold nanoparticles was introduced to bind to the captured thrombin in the second binding site. The frequency and dissipation signal was significantly amplified due to a rigid core of gold nanoparticles[40].*

1.3.2.2 Surface acoustic wave (SAW)

A surface acoustic wave (SAW) is an acoustic and mechanical wave that is generated using piezoelectric materials. In a typical approach, an AC voltage is applied onto electrodes known as input interdigital transducers (IDTs) produced by photolithographic techniques and usually made of alloys or inert metals such as Au and Cr. Consequently, an acoustic wave is generated which travels parallel to the crystal surface usually in an independent guiding layer and not in the bulk of the piezoelectric material. Thus the acoustic energy waves are concentrated within the guiding layer. The velocity and amplitude of the waves are strongly affected by any medium on the surface such as a binding mass. Finally, the waves reach the output interdigital transducers (ODTs) where they are converted to an electrical signal. The input and output signals are then transferred

into a signal of frequency or phase changes that can be correlated with the binding mass[41, 42]. In principle, SAW sensors are operated at frequencies between 25 and 500 MHz which is higher than the operating frequencies of the quartz crystal microbalance (QCM) which are between 5 and 30 MHz. Therefore, the sensitivity of SAW sensor is higher than the QCM[43].

Horiguchi *et al.* designed a label-free aptasensor based on a surface acoustic wave (SAW) transducer for the detection of thrombin[43]. An anti-thrombin aptamer was covalently immobilised onto a gold surface via a thiol group (figure 1.8). Poly (ethylene glycol)-block-poly ((2-N,N-dimethylamino)ethyl methacrylate) (PEG-*b*-PAMA) was also covalently attached to the sensing surface in order to reduce the nonspecific adsorption of proteins and also to eliminate unwanted conformations of the aptamer on the hybrid sensor surface such as fallen chains. The limit of detection obtained for the fabricated sensor was at 7.5 pmol[43].
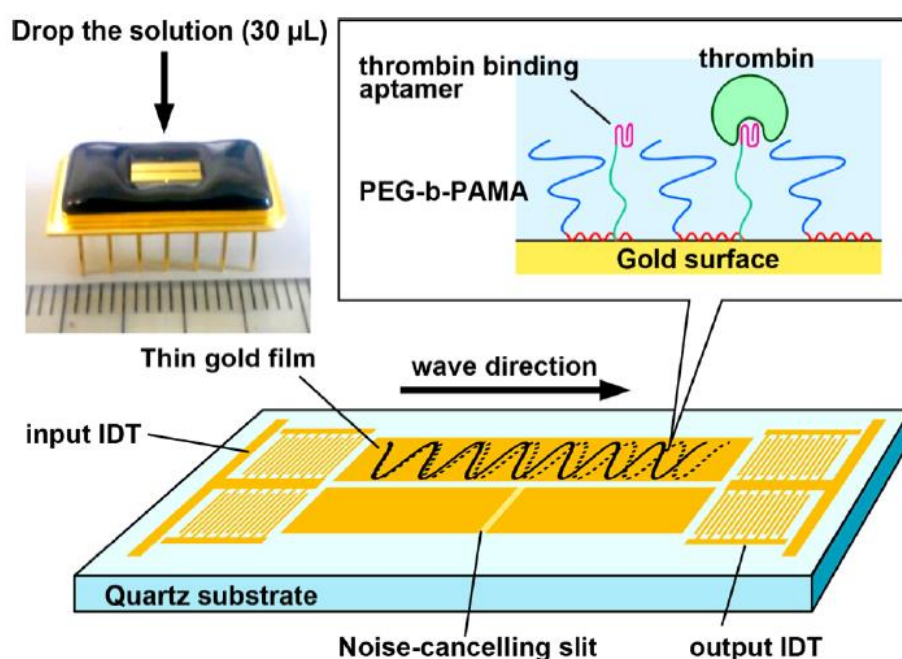
Figure 1.8 *Illustration of an aptasensor device based on surface acoustic wave (SAW) transducer for detection of thrombin. The sensor was fabricated by coating a quartz substrate with a thin gold layer[43]. Thrombin was captured by an immobilised aptamer leading to the change in the velocity and amplitude of the waves.*

1.3.3 Optical transducers

Optical transducers are the most common transducers used in biosensing. They are based on measuring a change in optical properties in the presence of the analyte. The sensing mechanism can be operated in two general modes; label-based and label-free. In the label-based method the optical signal is produced by a fluorescent, luminescent or colourimetric method using a label. In the label-free mode, the optical signal is generated based on the direct interaction between the transducer and a bio-recognition element[44]. In both mechanisms, incident light from a source reaches the sensing surface and the optical signal is then monitored by a photodiode detector before and after attachment of a bio-recognition element and also after the subsequent reaction with the target analyte. The changes in the optical signal due to the reaction of the analyte with the receptor can then be plotted as a dependence of signal *vs* analyte concentration[45]. Optical biosensors have been widely utilised due to their great advantages such as sensitivity, specificity and fast response, enabling direct and real-time measurement along with cost-effectiveness[44].

1.4 Label-based optical transducer

1.4.1 Fluorescence

Fluorescent techniques have led to a revolution in a biochemical research in the last 20 years due to their enormous advantages such as high sensitivity, flexibility, selectivity, simplicity and rapid response[46]. Fluorescence is based on the three steps: excitation, lifetime in the excited state, and fluorescence emission. This process happens in small molecules known as fluorophores. Fluorophore molecules can be either small or large or nanoparticles (e.g., quantum dots) which can be utilised to label bio-recognition elements or target analytes[47]. At an appropriate wavelength, the fluorophore molecules absorb a photon from the incident light which leads to the molecules being excited and hence reaching a higher energy level. An emission of light then occurs usually at a longer wavelength and this is known as fluorescence. It is indicated by the returning of the excited molecules to a ground state. Fluorophore molecules can repeat the cycle of absorption/emission yielding several photons, thus leading to an extremely sensitive measurement[46]. The detection of fluorescence is usually carried out using: (1) light source for excitation; (2) a fluorophore, (3) wavelength filters to separate emission photons from excitation molecules, (4) a detector to monitor the intensity of emitted light and produce a measurable value[47]. Fluorophore molecules can interact directly with the target analyte in which may lead to quenching or enhancement of the emission of light. This type of sensor is called a fluorogenic sensor which is usually used to detect metal ions. In contrast,

fluorophore molecules can be conjugated directly to a bio-recognition element that specifically binds to the target analyte and hence the fluorophore molecules are not participating in the binding process. This type of sensors are the most common and offer good design flexibility[46].

Liu *et al.* reported a novel fluorescent aptasensor for detection of human cardiac troponin I (cTnI); a biomarker of cardiovascular diseases (CVDs)[48]. The sensing mechanism was based on graphene oxide (GO) as a fluorescence quencher (figure 1.9). Graphene oxide (GO), an oxidized form of graphene, contains 2D carbon sheet structure with several functional groups such as oxygen, carboxyl, hydroxyl groups and epoxy. Anti-cTnI aptamer conjugated at the 5 end with a fluorescence dye namely 6-carboxyfluorescein (6-FAM) was immobilised on graphene oxide (GO) via hydrogen bonding and π–π stacking interaction. Upon adsorption, GO rapidly quenched the 6-FAM. The quenching mechanism is based on the fluorescence resonance energy transfer (FRET) technique. This was based on transferring the energy from the fluorescence dye at the excited state through excitation of electron−hole pairs to the graphene[49, 50]. This happens when two different molecules, one with a fluorescence spectrum that overlaps the excitation spectrum of the other, are placed close enough. The energy of the radiation-excited first molecule is then transferred to the second molecule in form of non-radiative energy and hence the fluorescence emission from the first molecule is quenched[51].

In the presence of the target analyte (cTnI), aptamer molecules bind to cTnI with high affinity. Therefore aptamer molecules left the surface of GO and consequently a recovery of fluorescence intensity was obtained. The intensity of the fluorescence was correlated with the concentration of analyte. The detection limit obtained was 0.07ng/mL which was lower than the concentration of cTnI in normal healthy persons (0.4 ng/mL)[48]. The system was investigated in serum samples diluted 50 times and the recovery was between 92.9 and 109.1%.

The main drawback of this technique is that most fluorophores are quickly bleached once exposed to light and they are very sensitive to the change in environmental conditions such as the solution's pH value[52].
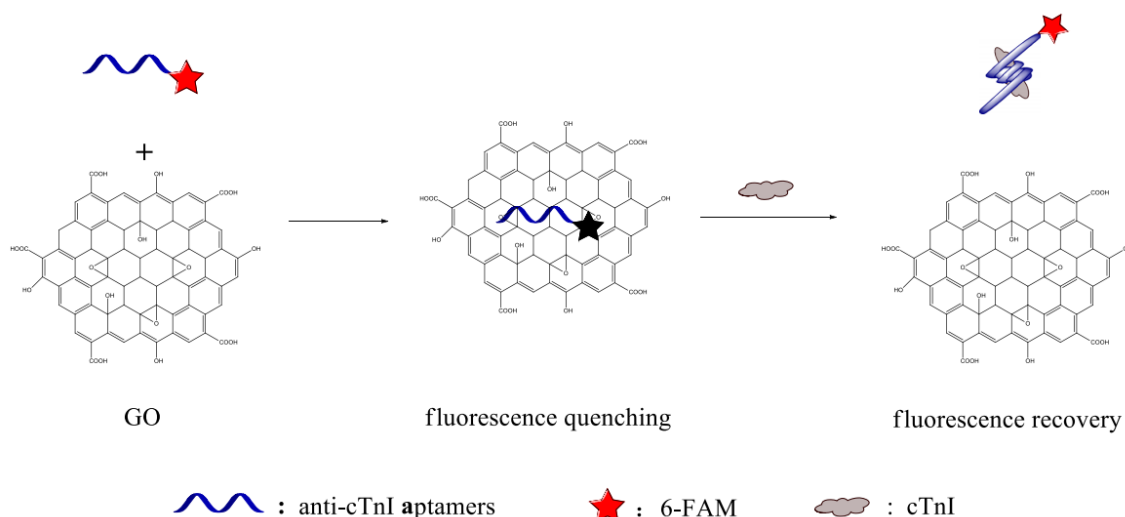
Figure 1.9 *Diagram of a fluorescent aptasensor based on graphene oxide (GO) for detection of human cardiac troponin I (cTnI)[48]. Fluorescent labelled aptamer was first immobilised on graphene oxide (GO) in which the emission light was then quenched. Upon introducing analyte, the aptamer was bound with high affinity to its target leading to a recovery of fluorescent light.*

1.4.2   Chemiluminescence (CL)

Chemiluminescence (CL) is the emission of light as a result of a chemical reaction[53]. It is similar to fluorescence; however, the excitation of the electron to a higher energy level is caused by a chemical reaction and not by the absorption of a photon. In chemiluminescence, an electron is promoted to an excited state by a large amount of energy obtained from an exothermic chemical reaction. These chemical reactions are based on redox reactions in which one molecule is oxidised and the other reduced. Luminol is the molecule that is utilised as reductant agent and it is oxidised by hydrogen peroxide (H_2O_2) usually in the presence of horseradish peroxidase (HRP) as a co-factor agent. The product formed is in the excited state while its extra energy is emitted as a photon leaving the product to return to the ground state. The intensity of the emitted light is correlated with the concentration involved in the chemiluminescence reaction. Due to the excitation being the result of chemical reaction, a light source and emission filters are not required. Therefore this eliminates background interferences[54]. The chemiluminescence (CL) technique also offers further advantages such as high sensitivity, low cost, low detection limits and a simple setup as it only needs a detector to monitor the emission light[53]. Due to its advantages, chemiluminescence (CL)-based sensors have

been used in various fields such as food, toxicology, environment, diagnosis and pharmaceutics[53].

An ultrasensitive chemiluminescence aptasensor has been reported by Sun *et al.* for thrombin detection[55] (figure 1.10). The sensor was prepared by utilising a chitosan polymer (CS) modified with magnetic (Fe_3O_4) and graphene oxide (GO) to produce a composite. The chitosan polymer was used as a biocompatible material, graphene oxide (GO) due to its large surface area, and Fe_3O_4 for easy magnetic separation. A porphyrin compound (hemin (HM), an iron porphyrin) was used as a co-factor in order to improve the production of O_2 and hence catalyze the chemiluminescent reaction of luminol in the presence of hydrogen peroxide (H_2O_2). The anti-thrombin aptamer and hemin (HM) were immobilised on the composite surface. The aptamer molecule was attached to the surface by a π-π stacking effect and the charge-attracting effect while hemin (HM) immobilisation was based on electrostatic attraction between the negative charge of the aptamer molecules and the positive charge of the hemin (HM) molecules. In the presence of thrombin, HM molecules were desorbed from the surface due to a specific interaction between the aptamer and thrombin. Finally, HM molecules were separated magnetically from the surface leading to a significant change in the chemiluminescence (CL) which was proportional to the thrombin concentration. The limit of detection was observed at 1.5×10^{-15} mol/L[55]. Thrombin was detected in practical serum samples and the recovery was between 95% and 103%.
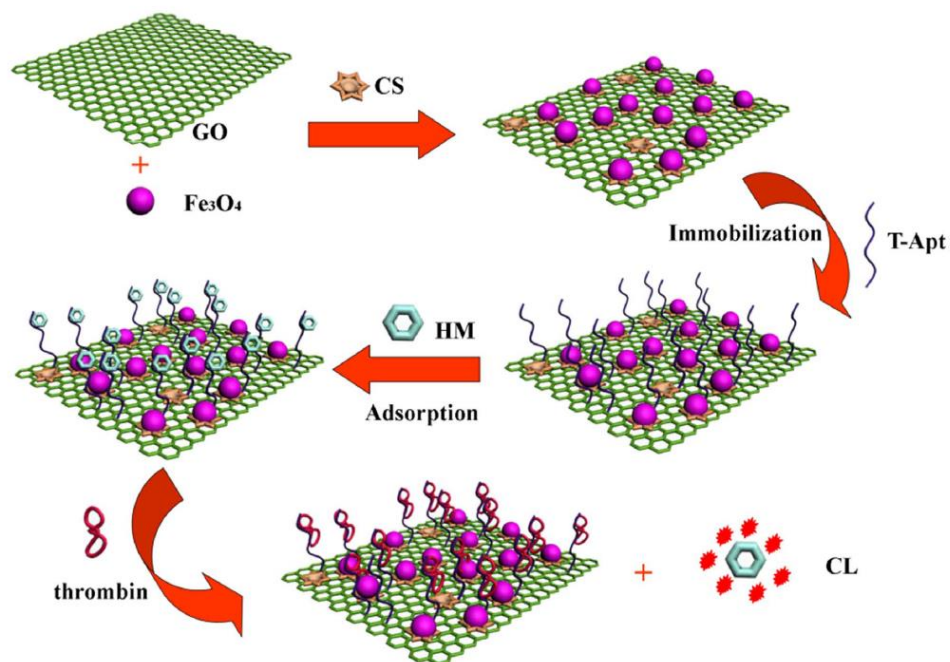
Figure 1.10 *Schematic construction of an aptasensor based on chitosan (CS), iron oxide (Fe₃O₄) and graphene oxide (GO) to form a composite. Anti-thrombin aptamer (apt) and hemin (HM) were immobilised on the composite surface. Upon introducing the analyte (thrombin), HM molecule was desorbed from the surface due to a specific interaction between the aptamer and thrombin. This resulted in catalysis of the chemiluminescent reaction of luminol leading to an emission of light with intensity being proportional to the concentration of analyte*[55].

1.4.3   Labelled versus Label-free

Most optical biosensors are prepared by attaching a label to the target analyte or to the re-cognition elements in which the amount of label detected is assumed to be correlated with bound targets[56]. The label molecules can be fluorophores, active enzymes, magnetic beads or radiolabels which lead to an easy measurement of the target conjugation. However, utilising a label is considered to generate a series of drawbacks such as high cost, consumption of time, generation of highly pollutant or toxic waste, possible deterioration or modification of the target analyte and its interaction with recognition elements and finally, the coupling reaction (target-label) is extremely variable. In contrast, label-free biosensors can measure the reaction between biomolecule and bio-receptor without using an element adhered to the biomolecule. Therefore, target molecules or bio-recognition species are no longer required to be labelled or altered: hence, they can be detected in their natural forms. Moreover, a label-free biosensor can be operated for

detecting the binding event in a real time measurement which is not possible in a label-based operation. Two major advantages can be obtained in a real time measurement. First, the time averaging of binding/unbinding events enhances the detection accuracy. Second, affinity constants can be determined using a curve fitting of the sensor output as a function of time[56, 57]. Furthermore, label-free biosensors offer other advantages such as high sensitivity, selectivity, minimum damage to the analytes, low sample consumption, simplicity and safety[52, 58]. Therefore, several techniques have been developed based on using label-free assay such as surface plasmon resonance (SPR) and optical interferometers where the presence of analytes on the sensing surface leads to a change in the optical properties.

1.5 Label-free optical transducer

One of the optical properties that is changed upon the binding event is the refractive index (RI)

1.5.1 Refractive Index (RI)

Refractive index (RI) is a dimensionless physical number which is specific for a certain medium while its value (n) describes the propagation of light in this medium. In two different media, RI is defined as the ratio of the speeds of light giving $n = c/v$, where c represents the speed of light in a vacuum, while v is the speed of light in a medium. Light is partially reflected and partially refracted when it strikes the interface between two media having different values of RI. This would indicate how much light is transmitted or bent (Figure 1.11). This was historically described by *Snell's law* of refraction yielding $n_1 \sin \theta_1 = n_2 \sin \theta_2$, where θ_1 and θ_2 are the angles of incidence and refraction, respectively, of a ray crossing the interface between two media with refractive indices of n_1 and n_2 respectively[59].
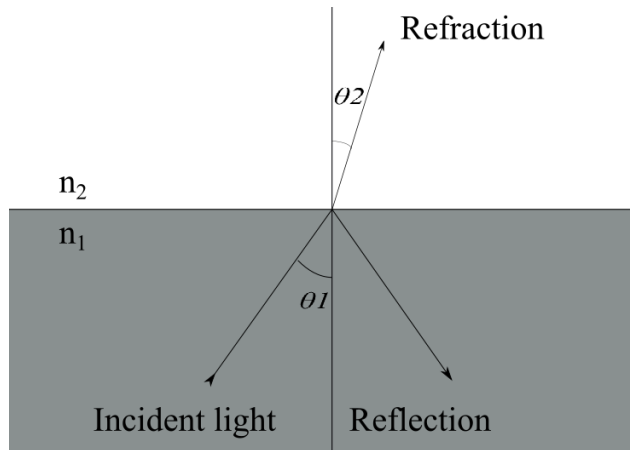
Figure 1.11 *Propagation of light through two media having different values of refractive index (RI) ($n_1 \neq n_2$). This results in partial reflection and partial refraction of the incident light.*

1.5.2 Fresnel Reflection

Fresnel reflection occurs at any interface between two materials with different refractive indexes. In the case of light travelling from a medium of higher refractive index to a medium of lower refractive index, the reflection light is called internal, while in the opposite case, it is called external. In the case of internal reflection, the incident angle is always smaller than the refraction angle, while it is higher in the case of external reflection (Figure 1.12).
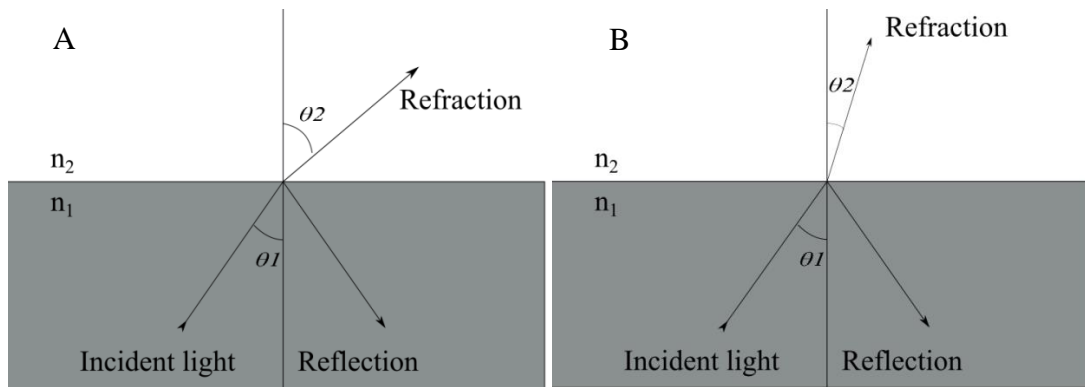
Figure 1.12 *Shows different types of reflected light:* A) *Internal reflection ($n_1 > n_2$ and $\theta_1 < \theta_2$)* B) *External reflection ($n_1 < n_2$ and $\theta_1 > \theta_2$).*

The reflectance of light at an interface between two materials is described by the Fresnel equation (1.4 and 1.5)[59]. Two polarisations of radiation reflect differently.

$$rs = -sin\,(\theta-\phi)\,/\,sin\,(\theta+\phi) \hspace{4cm} \text{Equation 1.4}$$

$$rp = -\tan\,(\theta-\phi)\,/\,\tan\,(\theta+\phi) \hspace{4cm} \text{Equation 1.5}$$

θ represents the angle of incident light, whereas ϕ is the angle of refracted light. *rs* and *rp* are the reflected light of the polarised TE and TM modes, respectively. These Fresnel amplitude coefficients specify the electric field amplitudes and phases of the reflected light as functions of incident angle, polarisation, amplitude of the electric field of the incident light, and the refractive indices of the two materials[59].

1.5.3   Evanescent Wave

The evanescent wave is an electromagnetic field that occurs between two media with different refractive indexes (RI). Light is totally internally reflected (TIR) when it meets the interface with a lower IR at an angle that is greater than the critical angle (Figure 1.13). In this case, the incident beam will establish an electromagnetic field known as an evanescent wave. This wave will penetrate a small distance, the order of a wavelength, into the medium with low IR and propagate parallel to the plane of the interface before it exponentially decays to zero. Therefore, molecules that are closed to the interface will be excited by this wave[60].
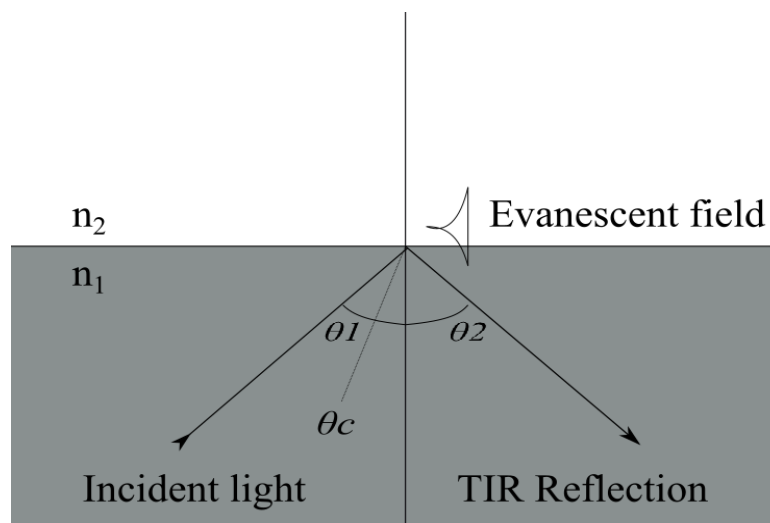
Figure 1.13 *Shows the propagation of light through two media where $n_1 > n_2$. Total internal reflection (TIR) occurs when the incident angle (θ_1) is above the critical angle (θc). Consequently, an evanescent field is generated.*

The evanescent electric field intensity $I(z)$ decays exponentially with perpendicular distance z from the interface[60]:

$$I(z) = I_0 e^{-Z/d,} \hspace{4cm} \textit{Equation 1.6}$$

where I_0 is the intensity of the evanescent wave at the reflecting interface and d is the penetration depth which is a function of the incident angle (incidence $\theta > \theta c$) and the wavelength of light λ_0 in the vacuum is given by:

$$d = (\lambda_0/4\pi)(n_1{}^2 sin^2\theta - n_2{}^2)^{-1/2} \hspace{2cm} Equation\ 1.7$$

The depth of the evanescent wave is independent of the polarisation of the incident light but depends directly on the wavelength. The evanescent field is highly sensitive to two types of ambient change. The liquid/gaseous sample that presents in the media of low RI and the molecules from a liquid/gaseous sample which adsorb to the surface lead to an altered RI in both media. Therefore the change in RI can be exploited as a tool for monitoring the adsorption/binding of any kind of chemical or biological molecule[61]. Different transduction approaches have been operated and developed using an evanescent field as a sensing mechanism by monitoring the shift in the refractive index as shown below.

1.5.4 Surface Plasmon Resonance (SPR)

Surface plasmon resonance (SPR) is an optical label-free measurement based on the generation of an evanescent field. This technique is considered one of the most important methods for investigating biomolecular interactions because it provides highly accurate results which are real-time and label-free. The SPR technique has been widely utilised in the research field because it is highly sensitive, with the possibility of operation within a large dynamic range and without electromagnetic interference[62].

An explanation for the SPR effect was achieved in 1968. The principle is based on irradiation of a surface that is mounted onto a prism by a TM-polarized beam of visible monochromatic light. This is known as a Kretschmann configuration (Figure 1.14). At angles above the critical angle (θc), the surface that is coated with a metal layer either gold or silver reflects the incident light under conditions of total internal reflection (TIR). At a resonance angle (θr) that is above the critical angle (θc), a portion of light energy is absorbed by the free electrons of a thin metallic layer leading to it being propagated parallel to the metal surface due to excitation. The electron movement is now called a plasmon and its oscillation leads to an electric field known as an evanescent wave ranging around 300 nm from the boundary between the metal surface and the sample solution. As a result of absorption, the intensity of the reflected light is decreased giving a sharp dip in reflectivity. The plasmon occurs at a specific angle known as the resonance angle (θr)

which is affected by the refractive index of the material presenting within 300 nm of the metallic surface. In SPR, when target molecules interact with the immobilised bio-recognition species, there is a change in the refractive index at the surface and thus a shift in the resonance angle (θr) with the degree of shift being proportional to the concentration of the analyte [63, 64]. SPR technology has been widely used in the biomedical, environmental and industrial fields. It is considered an acceptable method for drug discovery, disease diagnosis and foodborne pathogen detection[64]. Two types of information can be obtained through SPR technology: 1) the rate of interaction (association, dissociation) which gives information about kinetic rate constants and analyte concentration; and 2) the binding level which leads to affinity constants that can be used for qualitative or semi-quantitative application[62]. SPR instruments are now produced commercially by various companies such as Biacore. The instrument contains a sensor chip that is coated with a gold surface, a functional layer for ligand immobilisation, an optical detector and an integrated fluidics system to flow the sample through the sensor chip[44].
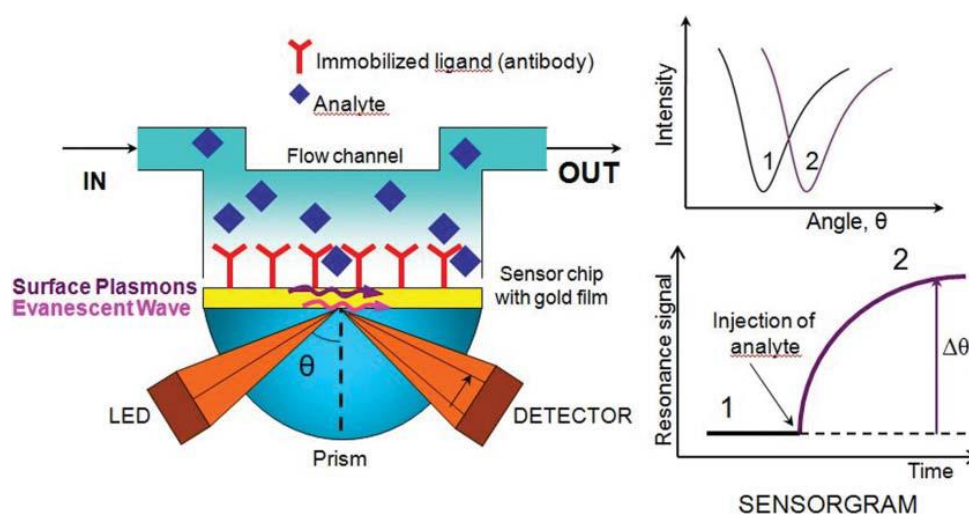
Figure 1.14 An example of SPR biosensor technology monitoring the change of refractive index[62]. The bio-recognition species is immobilised on a gold surface followed by flushing the surface with the analyte through a flow cell (in and out). The change in the refractive index upon binding the analyte is then monitored in real time using the SPR phenomenon. The sensorgram shows changes in SPR resonance angle in real time as a function of time in second.

1.5.5 Waveguide sensor

The waveguide sensor is another class of label-free optical biosensors based on the generation of the evanescent field. The use of the waveguide method has attracted interest over other label-free optical biosensors such as SPR due to its capabilities to be operated at wide range of wavelengths. This can be used for simultaneously refractive index monitoring and absorption spectroscopy upon introduction the analyte to the waveguide. This is not applicable with SPR sensor as the excitation of plasmon on the metal surface in order to visualise the resonance angle, has to be occurred above the 600 nm whereas the absorption maximum of many biological species such as haemoglobin and serum ferritin is below 600 nm[65, 66]. Moreover, waveguide sensor shows a broad dynamic range and long interaction length that can be between several millimetres up to a few centimetres. In contrast, SPR sensor has a trade-off between the dynamic range and resolution[67]. Other advantages of the waveguide sensor can be seen by its versatility, sensitivity, small sample requirement, high throughput applications and real-time measurement capabilities[61, 68]. The explanation of the waveguide phenomena is usually linked to Jean-Daniel Collad who first demonstrated a light fountain in 1842[67]. He explained that light can be guided into a transparent material under total internal reflection (TIR) when the refractive index of the guided material is higher than the surrounding ambience. This phenomenon has been later utilised in various applications such as those used for telecommunications.

1.6 Planar optical waveguides

Lukosz and his colleagues in the 1980s reported that the characteristics of light propagated inside a waveguide can be altered when a change in the neighbourhood environment, such as ambient humidity, is observed. This fundamental discovery has led to an extensive use of planar optical waveguides in chemical and biochemical sensors[61]. The planar optical waveguide consists of three layers; a substrate (s), a transparent waveguide layer thin film (w) and a cover medium (c) as shown in figure 1.15. Light can be coupled into the waveguide film layer (w) and propagated by total internal reflection (TIR) at the waveguide-cover and waveguide-substrate boundaries. This can occur when the refractive index of the film (w) is higher than that of the substrate (s) and that of the cover medium (c) ($n_S < n_w > n_C$); and when the angle (θ) of ray propagation relative to the interface normal is higher than the critical angle (θc) at the two boundaries. Upon propagation of the light, an evanescent field is generated at both waveguide interfaces

due to the occurrence of TIR. The coupling angle is usually called the resonance angle (θr)[67].

The resonance angle (θr) can be excited using a transverse-electric (TE) polarized light where the electric field vector is parallel to the surface of the planar waveguide. Also a transverse-magnetic (TM) light can be used to excite the resonance angle (θr) in which the electric field vector is perpendicular to the surface of the waveguide. Both polarised lights (TM and TE) are shown a distinct different resonance angles (θr)[69]. This is unlike the SPR method where the generation of plasmon only occurs with the TM mode. Light in a waveguide mode can travel without losing power in the ideal case such as no scattering and absorption.
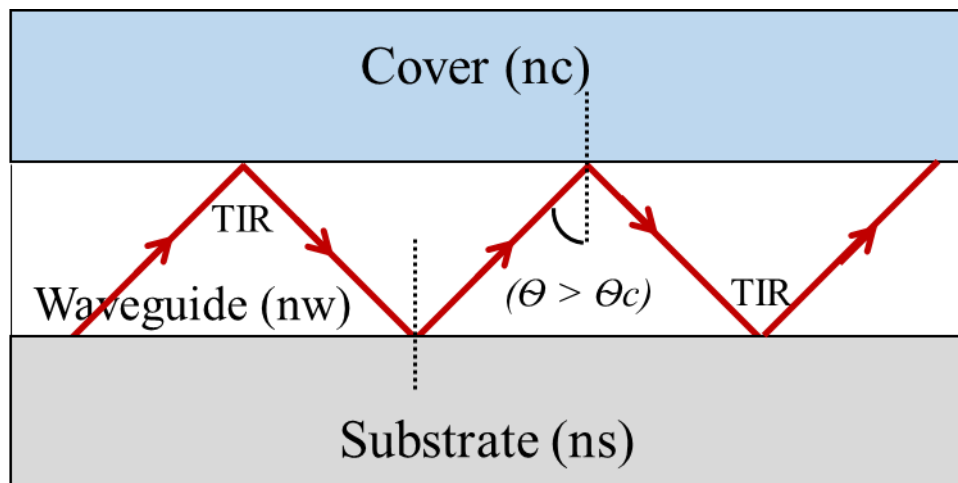
Figure 1.15 *Diagram of light coupling in a planar optical waveguide and propagating under total internal reflection (TIR) when the refractive index of the waveguide (*nw*) is higher than that of the substrate (*ns*) and that of the cover (*nc*), $n_S < n_w > n_C$; and when the angle of ray propagation relative to the interface normal is higher than the critical angle (θc) at the two boundaries.*

1.6.1   Operation mode

A waveguide can be operated under two classifications: multimode and single mode. Multimode is when the light is confined at the waveguide at more than one resonance angle (θr) while when it is propagated at only one specific resonance angle (θr), it is single mode.

Multimode waveguide is usually fabricated with a large thickness film that is thicker than the wavelength of the coupling light. It is typically in the range of several microns. The film is made from inexpensive material such as glass, silica or polymer with lower

refractive index value. The coupling of light into a multimode waveguide is considered to be simple due to the film thickness. However, this has resulted in low levels of signal intensity coupling into the waveguide. A single mode waveguide is usually made with a very thin high refractive index film such as ZrO_2, Nb_2O_5, TiO_2 and Ta_2O_5. The thickness of the film is highly lower than the wavelength of the coupling light, in the range of 100 to 200 nm. The film is deposited on a low index glass substrate through deposition methods such as ion deposition. This class of waveguide offers greater sensitivity due to the large differences in the refractive index between the film and the substrate which results in maximising the strength of the electric field at the waveguide surface. The difference in terms of refractive index between the waveguide film and the substrate should be at least 0.3 to achieve high sensitivity[70]. Furthermore, a single mode waveguide enables thousand reflections per centimetre of light propagation for visible wavelengths, which is two orders of magnitude higher than the equivalent in a multimode waveguide[67, 69]. Therefore a single mode waveguide is considered more sensitive than a multimode waveguide.

For a single mode waveguide, the typical refractive index of the substrate (*ns*) is 1.5 while it is between 1.8 and 2.5 for the waveguide film (*nw*) which depends on the waveguide material. An aqueous buffer with a refractive index of 1.33 is usually used as a cover medium (*nc*). The single mode waveguide is usually referred as a conventional high index waveguide.

1.6.2   Sensing mechanism
Although most of the light is confined within the guiding layer, a small portion extends out into the substrate and into the cover which is known as an evanescent field as shown in figure 1.16. The penetration depth of the evanescent field is typically between 100 and 200 nm.
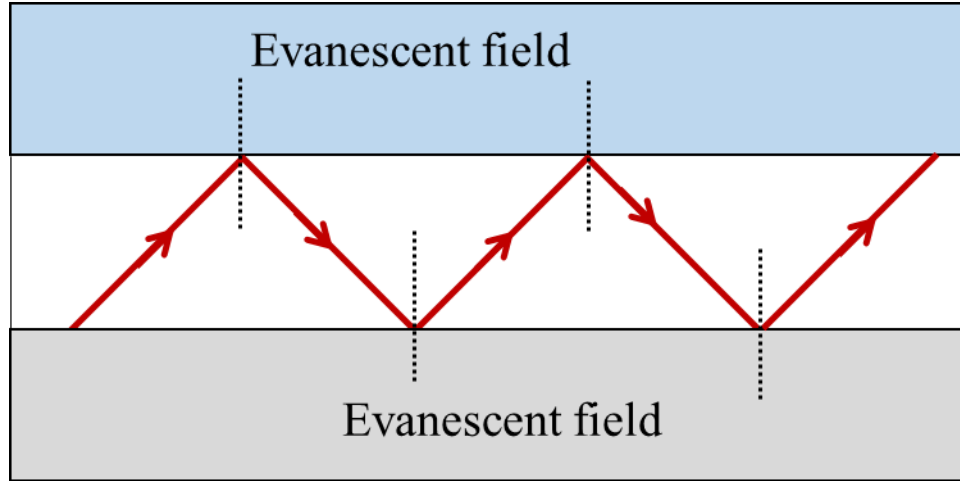
Figure 1.16 *Diagram of propagating of light into a planar waveguide under total internal reflection (TIR) leading to generation of an evanescent field at the both waveguide boundaries. The penetration depth of the evanescent field is between 100 nm and 200 nm.*

The evanescent field exponentially decays from the waveguide surface in a perpendicular direction (z) that is described by the expression decay factor shown in equation 1.8[61].

$$Exp \left(- \frac{2\pi}{\lambda 0} \sqrt{n_c^2 \ sin^2\varphi - nw^2} . \ z \right)$$
Equation 1.8

In which λ_0 is the wavelength in a vacuum while n_c and n_w are the refractive indices of the cover and the waveguide respectively. Φ is the angle of reflection at the waveguide/cover interface. Based on the exponentially decaying field outside the waveguide film, a simple planar waveguide can be utilised as a sensor. Once biomolecules are adsorbed onto the waveguide surface, a thin adlayer of a specific refractive index n_{ad} is then formed at the top of the waveguide. Consequently, the phase velocity v_p of the guided mode inside the waveguide is decreased by $V_p = C/ n_{eff}$ where C is the speed of light in the vacuum while n_{eff} is the effective refractive index of the waveguide that depends on the following parameters (equation 1.9).

$$n_{eff} = f\left(\lambda, \ n_s, \ n_w, \ n_c, \ d, \ n_{ad}, \ t_{ad} \ polarization\right)$$
Equation 1.9

where λ, n_s, n_w, n_c, d, n_{ad}, t_{ad} are the wavelength, refractive index of the substrate, refractive index of the waveguide, refractive index of the cover, waveguide thickness, refractive index of adlayer, and adlayer thickness respectively[61]. Measuring the change in the phase velocity v_p or the alteration in the effective refractive index n_{eff}, the amount of analyte bound on the surface can be obtained. Most waveguide biosensor monitors the

change in the coupling angle (resonance angle (θr)) which is also a function of the effective refractive index n_{eff}.

1.6.3 Coupling light

Coupling light into the waveguide layer can be carried out with different techniques. End-fire coupling through lens is based on focusing the irradiated light on the cleaved edge of the waveguide as shown in figure 1.17 (a)[67, 71]. This method is considered the simplest way for coupling light and also as appropriate for remote sensing applications. However, the sensitivity to vibrations present in the sensing system and the nanometre scale core (waveguide thickness) leads to low coupling efficiency. Similar to end-fire coupling, optical fibre can couple a light in direct contact with the cleaved edge of the waveguide usually through immersion oil. However, this technique also suffers from low coupling efficiency as the alignment between optical fibre and waveguide is crucial. This can be affected by the vibrations present. Coupling the light into a waveguide layer via a prism is usually performed using a thin tunnelling substrate (air gap) or immersion oil that is inserted between the prism and the waveguide. The refractive index of the prism is higher than that of the substrate (air gap) while the refractive index of the substrate (air gap) is lower than that of the waveguide core. This method was first reported by P.K Tien et al in 1969 [72]. At the incident angle, TIR occurs between the prism and the substrate (air gap) generating an evanescent wave that passes into the waveguide core of high refractive index as shown in figure 1.17 (c). This method is preferable for coupling light in optical sensing due to its simple configuration and easy coupling operation. The main disadvantage of this method is using a mechanical pressure to push the waveguide surface on the prism. This could lead to slight deformation of the waveguide surface while in case of using immersion oil, the surface of the waveguide could be contaminated. The grating coupler system performs the optical diffraction induced by periodic patterns engraved on a waveguide layer as demonstrated in figure 1.17 (d). The grating works as a diffractive element to provide higher order diffraction angles within the waveguide that accomplish the condition of TIR. The benefits of this method can be seen by its straightforwardness in which light can be coupled from free space into the expanded grating elements. Moreover, no immersion oil is required. However, the major drawback of this method is that the production of this type of waveguide is technology-intensive. Furthermore, the device is sensitive to mechanical vibrations, leading to lower coupling efficiency[67, 71].
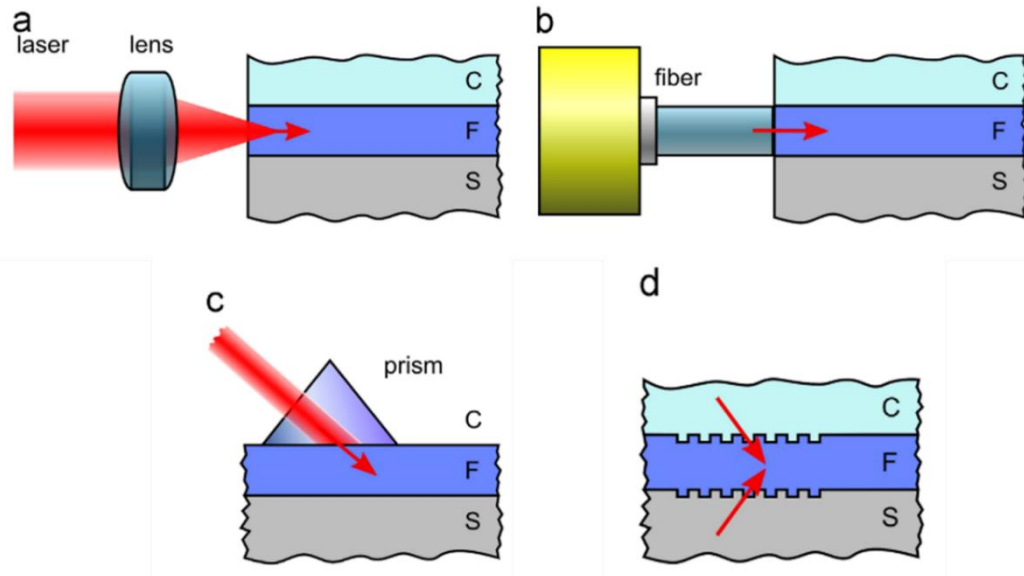
Figure 1.17 *Shows different coupling strategies:* **a**) *End-fire by lens;* **b**) *End-fire by optical fibre;* **c**) *Coupling by prism;* **d**) *Coupling by grating*[67].

1.6.4   Interferometry

Interferometry is based on the generation of the evanescent field using a waveguide. This method can be operated using two different instruments: the Mach-Zehnder interferometer (MZI) and Young's interferometer (YI).

In the integrated Mach-Zehnder interferometer (MZI), a single polarised light is introduced into a waveguide where it propagates under TIR conditions. At a Y junction, light is separated equally into two arms, a sample arm and a reference arm as shown in figure 1.18 (a)[67]. The sample arm has a window over the top of it which allows the sample component to interact with the existed evanescent field while a reference arm is protected from the sample by a thick cladding layer. The two arms are recombined at the output where the light is then detected by a photodetector. When the analyte is bound to the surface in the sample arm, the effective refractive index n_{eff} is changed. Consequently, a phase difference $\Delta\varphi$ between the two arms is observed which results in an intensity modulation of the output light caused by the interference of the two arms at the waveguide output. Measuring the interference intensity at the output waveguide, the concentration of analyte can be detected. The phase difference $\Delta\varphi$ can be calculated based on equation 1.8[73].

$\Delta\varphi = 2\pi / \lambda \text{ times } \Delta\, n_{eff}\, L$ *Equation 1.10*

In which λ, n_{eff}, L represent the operating wavelength, the effective refractive index of the waveguide and the length of the sensing region respectively.

Another interferometric configuration has been developed known as an integrated Young's interferometer (YI). In a YI, a single polarisation light is separated into sample arm and reference arm. Instead of recombining the guiding light at the output as in MZI configurations, the two arms reach the detector to produce interference fringe patterns on the monitor (Figure 1.18 b)[57]. When analyte is bound to the surface, the phase velocity of the guided light and the effective refractive index n_{eff} of the sample arm is then changed. Consequently, a shift in the position of the interference pattern occurs and it can be then analysed to yield information about the analyte bound[74].

In an interferometry system, the reference channel is used with sample solutions or buffers in order to reference the fluctuations in the refractive index (IR) that could be due to the variation in the temperature or because of non-specific adsorption when complex buffer matrices are used. This renders the system particularly for an application involving complex buffers such as cell lysates[61]. A YI configuration is now commercially available from Fairfield Scientific: the product is known as AnaLight®[57].
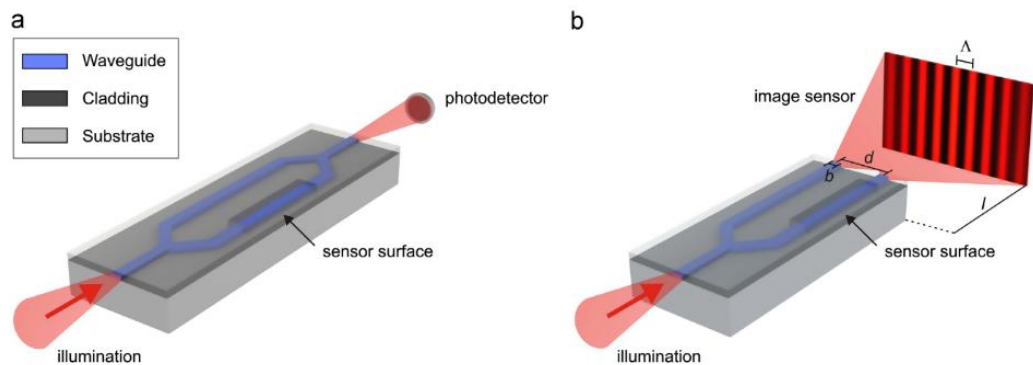
Figure 1.18 *Diagram of (**a**) Mach–Zehnder and (**b**) Young interferometer configurations[67]. Light is coupled into the waveguide in both interferometer structures (**a** and **b**) before splitting into two channels and passing simultaneously through sensor and reference channels. Light beams are recombined in the Mach–Zehnder structure into the same path before reaching the detector. In the Young interferometer, the beams are projected onto a detector producing interference fringes image.*

1.6.5　Resonant mirror sensors

One of the challenges with a conventional waveguide is to couple a light with a high efficiency into a high thin index single mode waveguide[75]. Cush *et al.* demonstrated a waveguide sensing system in 1993 in order to facilitate the coupling light into the waveguide by the effect known as a frustrated total internal reflection (FTIR)[76, 77]. When the evanescent wave is generated at the interface between two media having different refractive indices and the incident light is at an angle above the critical angle (θc), the waves pass into a third medium that is located less than several wavelengths from the interface. This phenomenon is called frustrated total internal reflection (FTIR).

The configuration of a resonant mirror (RM) consists of four layers; a thick substrate, a dielectric layer of lower refractive index, a waveguide and a cover. A dielectric layer of lower refractive index is inserted between a waveguide layer of high refractive index and a thick substrate of high refractive index (Figure 1.19). At resonant angle (θr), light is interfaced between the substrate and the dielectric layer generating evanescent waves due to the TIR effect. The waves generated are passed through the high refractive index waveguide layer due to the FTIR effect. Light is then guided inside the waveguide layer generating evanescent waves at the waveguide/cover boundary due to the TIR effect while at the opposite boundary, the electromagnetic waves are fed back into the substrate due to the FTIR effect. Therefore, a RM sensor is considered to be a leaky mode. This is different to the conventional waveguide where the total internal reflection (TIR) takes place at both boundaries of the waveguides; waveguide-cover and waveguide-substrate.
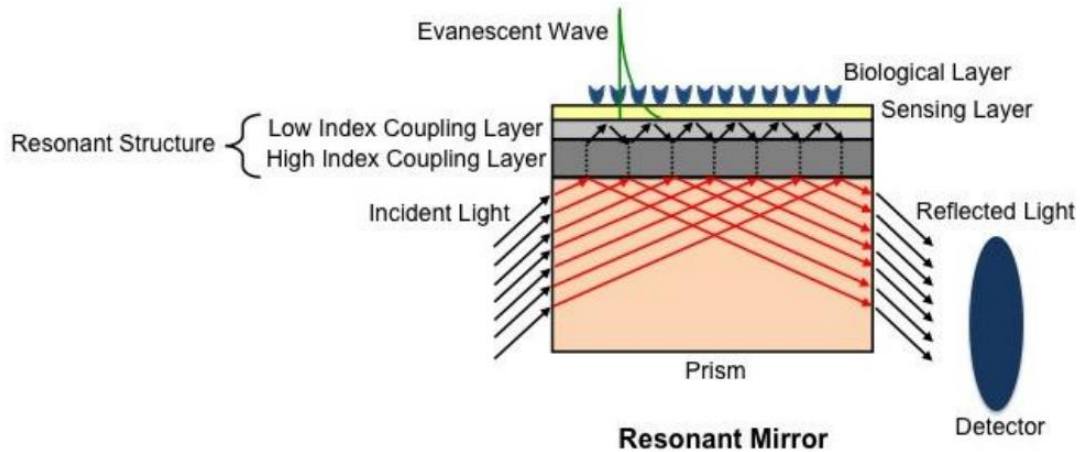
Figure 1.19 *The basic diagram of a resonant mirror waveguide (RM)*[78]. *The device consists of four layers: substrate (a thick high index coupling layer (≈1 mm thick glass slide, ns ≈1.72), dielectric layer (low index coupling layer (≈ 550 nm of silica)), waveguide (a thin high index sensing layer (≈ 80 nm of silicon nitride)) and cover (biological layer). The device is placed on a prism for coupling light. Light travels inside the waveguide (sensing layer) generating evanescent waves at the biological layer due to the TIR effect while at the opposite boundary, the electromagnetic waves are fed back into the substrate due to the FTIR effect (frustrated total internal reflection).*

The fabricated device was named resonant mirror (RM) as it contains a resonant cavity that works as a perfect reflector for incident light above the critical angle[79]. In the SPR method, the resonance angle (θr) is determined by the position of the dip in reflectivity, which is the result of absorption of the free electrons on the metal layer. Even though the resonant mirror (RM) is a leaky mode, the amount of light lost is very low. Thus, there is no dip present in reflectivity when the light is reflected. However, there is a shift in the phase of the reflected light at resonance angle (θr). The phase shift goes a full 2π change when the light passes through the resonance angle (θr) (Figure 1.20 a). 2π is the distance between two front waves that have undergone total internal reflection (TIR) at both waveguide boundaries. This would indicate that the light is successfully confined into the waveguide. This phase shift is then monitored to detect the shift in the resonance angle (θr) which would be due to the change in the effective refractive index n_{eff}[77].

In a resonant mirror (RM), TE and TM modes are used to measure the phase change. This is because both modes have widely separated resonance angles (θr) which can work as a reference. This can be accomplished by cancelling out the variation on the phase-shifting

caused by the ambient environment such as temperature, as both beams follow near identical paths. TE mode (perpendicular to the plane of incidence) and TM mode (parallel to the plane of incidence) are irradiated with equal intensities into the planar waveguide surface. This causes interference at the output. By passing the output beams through an analyser at 45° to the polarisation axes, only light that has undergone a full 2π phase change will pass. Thus output beams that are far away from resonance are given a zero value and sharp peaks for each mode (TE and TM) are then obtained at the resonance angle (θr) as shown in figure 1.20 (b)[75, 77]. The position of the peak changes upon the change in the refractive index near the sensing region (waveguide layer). To monitor the shift in the peak position, a monochromatic light is utilised with suitable optics to generate a converging wedge beam at the sensor. This will cover a sufficiently wide range of input angles which will allow the resonance angle (θr) to be determined in a wide range upon change in the refractive index of the surface. The shift in the peak position can be used to detect the amount of analyte bound. RM waveguide-based biosensors by Thermo Lab-systems, Affinity Sensor (IAsys, Cambridge, UK) and Neo Sensors (Durham, UK) are now commercially available [57, 71].
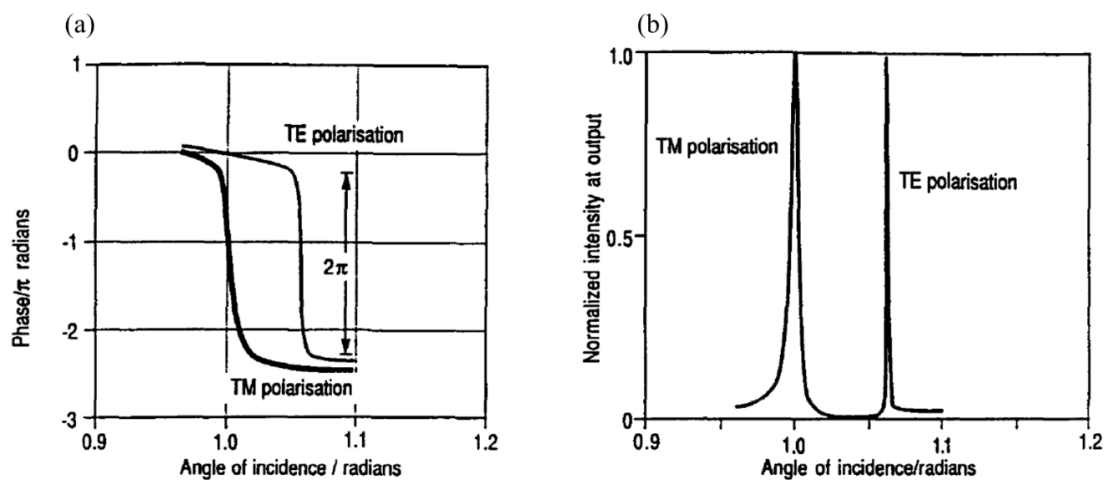
Figure 1.20 **(a)** *Phase shift in reflected light from Resonant Mirror device as a function of incident angle for TE and TM polarised light. Light is shifted by 2π for both modes of incident beam as a result of passing the resonance angle (θr).* **(b)** *Intensity of reflected light as a function of incident angle showing two sharp peaks at two different resonance angles (θr) for both TE and TM polarised beams[77].*

1.6.6 Reverse symmetry waveguide sensors

A reverse symmetry waveguide was first fabricated by Robert Horvath in 2002[80]. The aim of the structure was to increase the penetration depth of the evanescent field into the sensing region and hence increase the interaction with large biomolecules such as cells. The device contains three layers: substrate layer, waveguide and cover. The refractive index of the substrate ($ns = 1.19$) is lower than that of the cover ($nc = 1.33$) ($ns < nc$). This is unlike a conventional high index waveguide where the refractive index of the substrate ($ns \approx 1.5$) is usually higher than that of the cover ($nc = 1.33$) ($ns > nc$) while the waveguide layer ($nw \approx 1.8$) has the highest refractive index ($ns < nw > nc$) in order to allow a TIR effect at both boundaries.

Based on the refractive index of the substrate that is higher than the cover in the conventional waveguide, a large fraction of the mode power propagates at the waveguide-substrate interface compared to the waveguide-cover boundary[81]. Therefore less light passes into the sensing region (cover) and hence it has lower sensitivity towards the analyte present. This can be seen by the penetration depth of the evanescent field that is between 100 nm to 200 nm for the conventional waveguide. Most analyte molecules are covered with this depth. However, large molecules such as bacteria or living cells that are in micrometre size, are only partially covered and thus lower detection sensitivity was obtained. Due to the refractive index of the substrate being lower than that of the cover ($ns < nc$) in a reverse symmetry waveguide, light is more concentrated at the waveguide-cover boundary resulting in higher penetration depth of the evanescent field.

Figure 1.21 (a) shows a reverse symmetry waveguide structure consisting of a thick nonporous silica substrate ($ns = 1.193/thickness\ 1\ \mu m$), a thin polystyrene waveguide layer ($nw = 1.58/thickness\ 160\ nm$) and aqueous cover ($nc = 1.33$). The nonporous silica substrate is sufficiently thick not to allow light to exist in the low glass support. Figure 1.21 (b) displays the comparison in terms of the penetration depth of the evanescent field between the conventional and the reverse symmetry waveguide sensors for various sizes of analyte[80, 82]. From the figure, it can be seen that adsorbed protein can be covered within the range of the evanescent field in a conventional waveguide, while large biological units such as cells and bacteria are fully covered when a reverse symmetry waveguide is used.

The penetration depth of the evanescent field in a reverse symmetry waveguide was reported to be at 500 nm. This was led to a sensitivity and a limit of detection of the sensor respectively to be 4 times higher and 800 times lower than the conventional waveguide

such as resonance mirror (RM) for non-specific detection of bacteria named *Escherichia coli*[83].
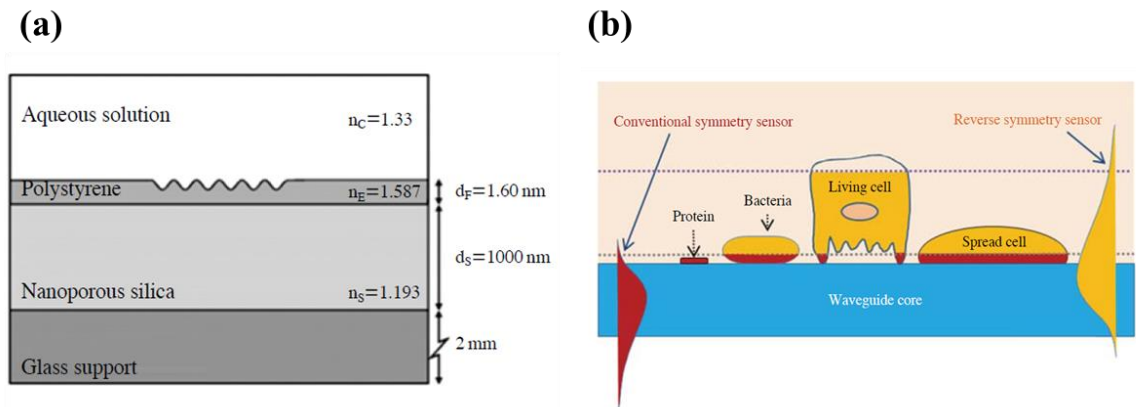
Figure 1.21 (a) A reverse symmetry structure consisting of nonporous silica substrate (ns = 1.193 /thickness 1000 nm), polystyrene waveguide (nw= 1.58 / thickness 160 nm) and aqueous cover (nc= 1.33). A sinusoidal surface-relief grating is printed into the polystyrene waveguide for coupling light. **(b)** A comparison of the penetration depth of the evanescent wave between conventional and reverse symmetry waveguide for different analyte[71].

1.6.7   Anti-resonant reflecting optical waveguide (ARROW)

The anti-resonant reflecting optical waveguide (ARROW) was first demonstrated by Duguay *et al.* in 1986[84]. The ARROW sensor has been developed mainly to be integrated with an optical device such as micro total analysis systems (µTAS) as the configuration allows the light to be guided into material of lower refractive index such as silicon dioxide, This is compatible with standard silicon processing techniques for fabrication of a micorchip[85]. Furthermore, lower index waveguide is advantageous as the light can be guided into lower index material such as hydrogel, liquid and gaseous medium. A second advantage of the waveguide of the lower refractive index is that light can be easily coupled in and coupled out of the waveguide using a prism[86]. A major drawback of using a waveguide of lower refractive index is to find a substrate that has an index lower than that of the waveguide in order to allow the TIR effect. A waveguide of lower refractive index can be deposited onto a higher index substrate such as glass, the most common and cheapest. This would permit the TIR effect at the waveguide-cover boundary, while it is leaky at the waveguide-substrate interface which could suffer from a weak guiding mode. The radiation losses into the substrate can be highly reduced by increasing the thickness

of the waveguide but this can also lead to a multiguide mode. The ARROW sensor features a thick waveguide of low index with a high intensity of light confined into the waveguide operated at a single mode with a significant reduction in the light loss into the substrate[84].

The ARROW sensor consists of five layers which are substrate, second cladding layer, first cladding layer, waveguide and cover as shown in figure 1.22 (a). The first cladding layer and the second cladding layer are used as a sandwich between the waveguide layer and the substrate. The refractive index of the waveguide and the second cladding layer are the same ($n_w = n_2$) while it is higher for the first cladding layer ($n_1 > n_w$ and $n_1 > n_2$) and it is further higher for the substrate ($n_s > n_1$ and $n_s > n_w$ and $n_s > n_2$). The waveguide layer is prepared with a thick low refractive index layer (thickness $\approx$ 4 μm) rather than with a thin layer of high refractive index (thickness $\approx$100 nm) in a conventional waveguide. The first cladding layer that is inserted between the waveguide layer and the second cladding layer, is a thin layer of high refractive index and it works as a reflector by a condition known as a Fabry-Perot interferometer (anti-resonant mode). This is based on the fact that the index step between the high refractive index layer (first cladding layer) and the surrounding lower refractive index layer (waveguide) can be used as a reflector[87]. Light is in anti-resonance when it interferes destructively with itself inside a Fabry-Perot cavity; the reflectivity of the interferometer is then at its maximum[88]. An ARROW sensor utilises this effect to provide a high degree of reflectivity of light into the waveguide core and hence significantly reduce the radiative loss into the substrate.
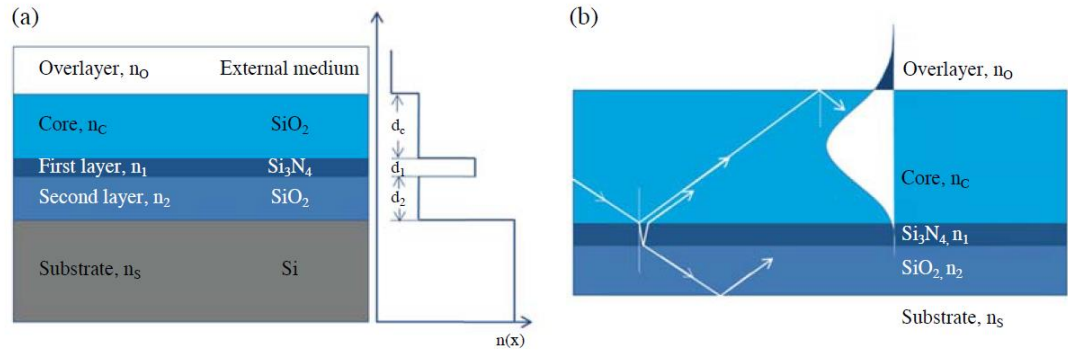
Figure 1.22 (a) *Anti- resonant reflecting optical waveguide (ARROW) structure consisting of five layers: substrate (polycrystalline silicon); second cladding layer (SiO₂ /thickness ≈ 2 μm); first cladding layer (Si₃N₄ /thickness ≈ 100 nm); waveguide (SiO₂ /thickness ≈ 4 μm); and cover. The refractive index of the waveguide and the second cladding layer are the same, while it is higher for the first cladding layer and it is even higher for the substrate.* (b) *light propagation in ARROW waveguide by total internal reflection (TIR) at the waveguide-cover interface, and by anti-resonant reflections at the waveguide-first cladding interface[71].*

In an ARROW sensor, light propagates inside the waveguide by total internal reflection (TIR) at the waveguide-cover interface while by anti-resonant reflections at the waveguide-first cladding interface as shown in figure 1.22 (b). Therefore, the ARROW sensor is considered as a leaky mode waveguide. However, the amount of light that is refracted at the waveguide-first cladding boundary, is very small due to the antiresonant character of the lower layers (first and second cladding layer) resulting in a higher degree of light reflected into the waveguide in the order of 99.96%[84]. Therefore it was considered that the sensitivity of an ARROW sensor is two to five times higher than the RM conventional high index waveguide[85]. The intensity of fluorescence was found to be 11 times higher when the fluorescence molecules were excited from an ARROW sensor than from an RM sensor[85].

Different materials were used to fabricate ARROW waveguides on silicon substrates, such as Si₃N₄, Ta₂O₅, SiO₂ and polyimide. The ARROW structure has been utilised in various applications such as optical polarisers, lasers and optical sensors[89-91]. One of the great advantages of an ARROW structure is that it allows a single mode waveguide operation even though the thickness of the waveguide is high (≈ 4 μm) and the refractive index is low. This is accomplished by filtering out high order modes (high order modes

is to couple light at different resonance angles (θr) into the waveguide) by loss discrimination due to their lower reflectivity at the interference of the first and second cladding layers. In anti-resonant mode, the reflectivity is a very poor function of the thickness and refractive index of the reflectant multilayers (First and second cladding layers). Therefore, the thickness and the refractive index can be fabricated at various parameters. In contrast, in a conventional waveguide and RM sensor, the thickness of the waveguide layer has to be small in order to allow a single mode waveguide operation[89-91]. The main disadvantage of this structure is that it requires two extra layers between the substrate and the waveguide in order to achieve high sensitivity. This complicates the structure of the sensor as three layers including the waveguide have to be uniformly and carefully deposited on the substrate. This requires a more expensive deposition technique and a longer fabrication time.

1.6.8 Metal-clad Leaky Waveguide (MCLW)

Swalen *et al.* reported in 1979 a modified waveguide structure that contained four layers: substrate, metal layer, waveguide and cover as shown in figure 1.23[92]. MCLW is of a similar structure to that of the conventional high index waveguide but with an extra metal layer inserted between the substrate and the waveguide. The metal layer is used in order to push a greater proportion of light at the sensing region (cover) and hence to increase the light-matter interaction with the analyte and the sensitivity of the waveguide sensor[57]. Moreover, MCLW supports a leaky mode which is an advantage of using a waveguide of lower refractive index deposited on a substrate of high refractive index. The structure can also be compared to the SPR technique in which a waveguide film is deposited on top of the metal coating layer.

The layer of metal such as gold, silver and titanium has a higher refractive index than that of the waveguide film while the waveguide has a higher refractive index than that of the cover ($nm > nw > nc$). At resonant angle (θr) light is guided under total internal reflection (TIR) at the waveguide-cover interface due to $nw > nc$, whereas it is partly transmitted into the metal layer and the substrate and partly reflected back into the waveguide film due to $nm > nw$. Therefore the fabricated sensor is called metal-clad leaky mode. The mechanism of the light leaking at the waveguide-metal interface can be Fresnel reflection[93]. Fresnel reflection occurs at any interface between two media having different refractive index values. At the incident angle some of the light is transmitted and the rest is reflected back. The reflected light is called Fresnel reflection as explained earlier in

section 1.5.2. This is unlike a conventional waveguide where the waveguide is surrounded by lower refractive index layers and thus light is guided by TIR at both boundaries.

Similar to SPR technique, in MCLW sensors and at an incident angle, light is absorbed by the free electrons on the metal layer (plasmon resonance) giving a dip in reflectivity. At off resonance, (when the waveguide mode is not excited), all the energy from the incident light is deposited on the metal layer in the form of heat. At resonance angle (θr), a high energy of light then pushes the waveguide mode further into the sensing region. This results in a sharp dip in reflectivity which is sharper than the dip observed by the occurrence of plasmon resonance as shown in figure 1.23 (b). The sharper dip is preferable in order to be able to resolve small changes in the refractive index of the waveguide[94].
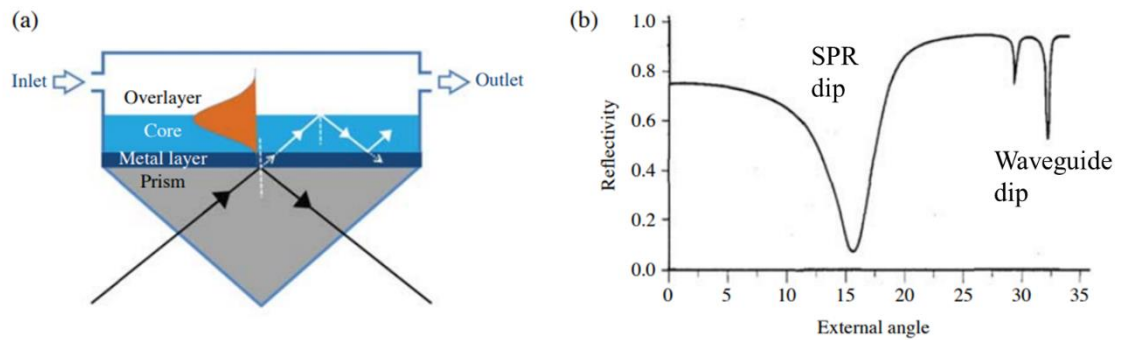
Figure 1.23 (a) *Diagram of metal-clad leaky waveguide (MCLW) consisting of four layers: substrate (prism), metal layer, waveguide core and cover. The refractive index of the metal layer is higher than that of the waveguide layer, while that of the waveguide is higher than that of the cover (nm > nw > nc). (b) typical reflection of MCLW sensor (TM guided mode) showing SPR dip due to the occurrence of plasmon resonance and a sharp dip due to the coupling light into the waveguide region at resonance angles (θr)* [71].

The dip can be used as sensing signals in which changes in the effective refractive index n_{eff} of the waveguide due to analyte adsorption will lead to shift in the dip position[57]. Due to the metal layer, MCLW shows a high penetration depth of the evanescent field into the sensing region at 1µm[95]. This depth is clearly higher than the one observed for conventional higher index waveguides, RM and SPR sensors where the penetration depth is between 100 nm and 200 nm. The MCLW sensor was three times more sensitive to the bulk refractive index change in the solution than the RM sensor[96]. The MCLW sensor has shown a variety of advantages over the conventional waveguide, which can be due to TIR

being no longer applied at the waveguide-substrate interface. This condition leads to flexible choice of waveguide materials of any refractive index, such as silica sol-gels and hydrogels, as they are no longer required to have higher refractive indices than the substrate. However, MCLW suffers disadvantages. The challenging of this method can be seen in its metal layer which is mechanically and chemically unstable for a waveguide layer. Furthermore, the fabrication procedure with MCLW is complicated requiring a vacuum deposition technique, which is expensive[97].

1.6.9 Dye-doped leaky waveguide (DDLW)

The Dye-doped leaky waveguide (DDLW) sensor was first reported by our group in 2016[86, 98]. It is similar to MCLW and ARROW sensors in which it supports a leaky optical mode; therefore, the waveguide was made from a lower index material. This is an advantageous as the light can be guided into lower index material such as hydrogel, liquid and gaseous medium. However, the Dye-doped leaky waveguide (DDLW) device shows greater advantages than other leaky waveguide sensors such as MCLW and ARROW. The device is only fabricated in a single step by spin coating an inexpensive hydrogel material as waveguide layer onto a cheap glass substrate at room temperature followed by manually doping with a few droplets of dye to visualise the resonance angle. This would indicate that using an expensive deposition technique such as puttering to deposit a gold layer on SPR chip, or an e-beam evaporation for deposition of a layer of metal such as titanium in MCLW sensor to visualise the resonance angle or to deposit the first and the second cladding layers in ARROW sensor to enhance the sensitivity, are no longer required in DDLW device. This would further lead to a low fabrication time, easy manufacturing, effectiveness cost and ease of use which are the high requirements nowadays for routine sensor using[99].

In a DDLW, light is confined inside the waveguide layer at resonance angle (θr) and propagates by Fresnel and total internal reflection (TIR) between the substrate-waveguide and sample-waveguide interfaces respectively (Figure 1.24 a). The waveguide was made from a porous hydrogel (agarose) that was spun in a single step on inexpensive microscope glass substrate and subsequently doped manually with reactive blue 4 dye. Dye was used in order to visualise the resonance angle (θr). Due to the advantages of using the hydrogel, dye molecules were diffused inside the waveguide where the light was propagated (Figure 1.24 a). Consequently, the confined light was absorbed by the attached dye molecules resulting in a dip in reflectivity (Figure 1.24 b). This clear dip can

then be monitored upon analyte adsorption, thus allowing quantitative measurements. The device was operated using a low cost white light emitting diode (LED) and a simple and cheap complementary metal oxide silicon (CMOS) camera.

Using a theoretical modelling program, the sensitivity of the DDLW sensor to the refractive index values was identical to that of the MCLW, while its sensitivity to the refractive index was 10 times higher than that of the non-porous waveguide of the same thickness and refractive index (agarose waveguide, thickness 1.53µm and refractive index = 1.356) [86]. The penetration depth of the evanescent field was estimated to be 0.17µm while from a surface profile of agarose waveguide, it was found that 77% of the light travelled inside the waveguide and only 23% was at the top of the waveguide[98]. This indicated the advantage of using porous hydrogel waveguide where the analyte would be diffused and hence interact with a large amount of light.
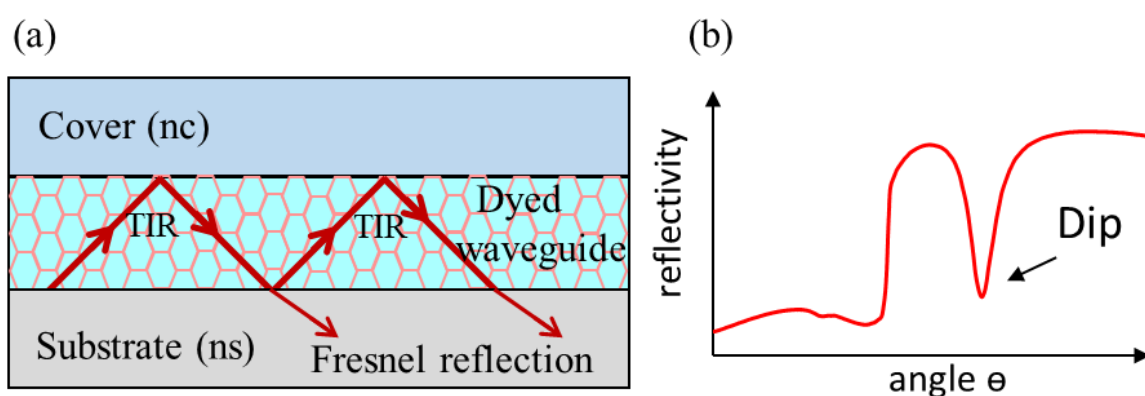
Figure 1.24 (a) *Confinement of light via total internal reflection (TIR) and Fresnel reflection in a dye-doped leaky waveguide (DDLW). The waveguide layer (n_w) is sandwiched between higher refractive index substrate ($n_w < n_s$) and lower refractive index cover ($n_w > n_c$).* (b) *Reflectivity as a function of angle showing a dip at resonance angle (θr) which was as a result of the dye absorption.*

Due to the operation mode of the DDLW device being leaky mode, this permitted the use of a lower index material such as a porous hydrogel. The porous waveguide layer is advantageous as a bio-recognition molecule such as an aptamer or antibody can be immobilized in its entire volume of the waveguide. This would first increase the binding sites for target analytes, and second would allow the analyte to interact with all light present in the waveguide and the evanescent field[86, 100]. Thus the sensitivity of the sensor would be enhanced. Moreover, the resonance angle (θr) was clearly visualised using dye.

Therefore a polariser to filter the output beams and to show only those pass 2π phase change is no longer required. The resonance angle can be simply visualised using LED light source and a CMOS camera as a detector. This further shows the advantages of the DDLW device over other waveguide sensors.

1.6.10 Waveguide material

In the last twenty years there has been a focus on hydrogel materials because of their range of important properties, for instance biocompatibility, responsive behaviour (volumetric changes), storage capacity and the ease with which they can be modified. Agarose hydrogel, a polysaccharide derived from agar, is one of popular material for constructing a waveguide layer. It is a hydrophilic polymer and a chemically inert. The gel is cheap and easy to use for device fabrication[101]. However, a spin-coated agarose waveguide on DDLW devices were found to be largely nonporous to macromolecules such as protein and it was difficult to functionalise for bio-recognition immobilisation[98, 100].

A naturally occurring polysaccharide, chitosan, is an attractive hydrogel to be used as a waveguide layer. Chitosan is the N-deacetylated derivative of chitin, a cationic polysaccharide containing glucosamine and N-acetylglucosamine residues with 1,4-b-linkage (Figure 1.25)[102]. Chitin is a naturally occurring polymer that is considered to be the second most widespread polymer found on earth after cellulose: it exists on the shells of crustaceans and insects[103]. The unique properties of chitosan can be seen through its abundance, biodegradability, non-toxicity and biocompatibility. Furthermore, it is pH-dependent soluble. Its primary amine groups ($-NH_2$) have a pKa value of 6.5 and are positively charged at a lower pH; hence chitosan is soluble. Chitosan becomes insoluble at higher pH as the amines are deprotonated. Therefore, this will help to deposit a stable chitosan film on different surfaces under neutral and basic pH conditions[103]. Moreover, the positively charged amines can be used as an attachment for any biomolecules, such as enzymes, antibodies, and DNA, to a chitosan film through covalent bonding. The attachment can also be carried out through a physical interaction (e.g. surface absorbance, entrapment) when the substance carries a negative charge. The chain of chitosan polymer may also be crosslinked through an amino group, enhancing the strength and chemical resistance of the film. Chitosan film without any modification is transparent and therefore it can be used as a waveguide hydrogel material in an optical sensor[103]. Chitosan

waveguides that rely on TIR for light propagation at both boundaries have been reported previously for sensing relative humidity but not as a biosensor device[104, 105].
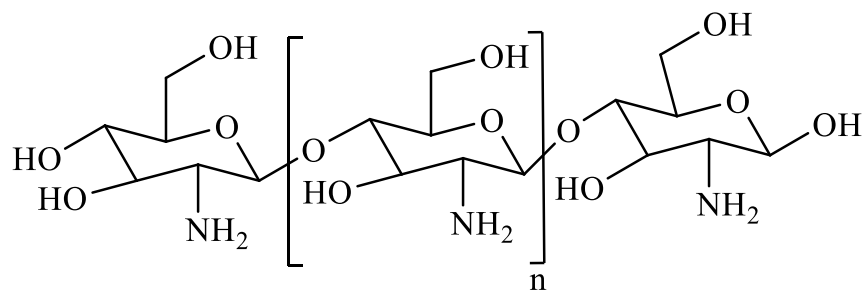
Figure 1.25 Chemical structure of chitosan polymer featuring amine and hydroxyl functional groups.

1.6.10.1 Stained chitosan with reactive dye

Reactive-Blue-4 (RB4) is a water soluble dye that carries two sulphonic groups in its structure and thus it is considered as an anionic molecule (Figure 1.26). Due to the acidity of sulphonic groups, the dye remains negatively charged over the entire pH range[106]. The reaction between chitosan and RB4 dye has been previously reported based on an electrostatic interaction (negative–positive attraction)[106, 107]. Other studies have confirmed that its immobilisation can be performed via a covalent linkage between the dichlorotriazine group on the dye and an amino group on the chitosan membrane under alkaline conditions[108-110]. RB4 dye has a broad absorption spectrum which allows the visualising of the resonance angle (θr) over most of the visible region[65].
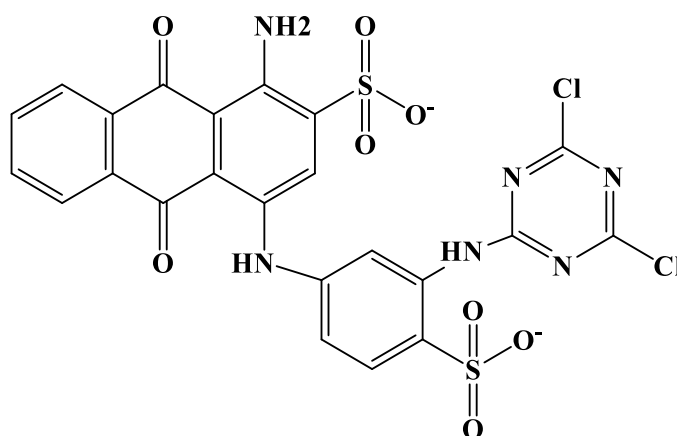
Figure 1.26 Chemical structure of reactive blue four dye (RB4) featuring two sulphonic groups and two dichlorotriazine groups.

1.7 Immobilisation of aptamer

The immobilisation of aptamers has been performed on the surface of polymer, glass, silicon and gold. A modification of either the 5' or 3' end of the aptamer is required for immobilisation on a solid support. The modification of the aptamer end depends on the type of chemistry, orientation of molecules, type of spacer, spacer length and availability of the required ends in the aptamer. The immobilisation of an aptamer on the solid surface should maintain its selectivity and affinity toward the target as exhibited in the solution. The is usually accomplished by covalently or non-covalently tethering the aptamer within close proximity to a transducer in order to induce an analytical signal[68].

1.7.1 Covalent attachment

1.7.1.1 Thiols coupling

Aptamers have been immobilised on gold surfaces such as electrodes and SPR chips via the interaction between the gold atom and thiol. This has a binding energy of 45 kcal/mol. Before immobilisation, the aptamer is functionalised with a thiol group in the following order: a thiol ($-SH$) or disulphide ($-SSR$) terminus, linker chains such as C_6 [$(CH_2)_6$] or C_{11} [$(CH_2)_{11}$], a spacer sequence such as poly A_{20}, and the aptamer sequence[111]. Typically a cleaned gold substrate is incubated in an aqueous buffer solution containing the thiol-terminated aptamer leading to the formation of a monolayer on the gold surface (Figure 1.27). A gold surface offers several advantages such as an easy and a direct immobilisation of the molecules, and the possibility of forming a monolayer with a highly ordered nature. Furthermore, a gold surface shows high stability and affinity towards thiol molecules even in complex liquid media. It is commercially available from different sources as films and particles. Planar gold surfaces are useful for physically characterising the composition, structure, and binding properties of the aptamer. To date, thiol-conjugated aptamers have been widely utilised for monolayers on planar gold surfaces while disulphide- tethered aptamers have been used for gold nanoparticles. This is because aptamer tethered disulphide can easily form a monolayer on the particles while it provides only half of the maximum density on a planar surface. The majority of thiol-conjugated aptamers are designed as stable nonsymmetric disulphides. Free thiol is then obtained by a reduction of the disulphide precursor using dithiothreitol (DTT), forming free thiols. The remaining DTT is then extracted in order not to interface with the aptamer attachment on the gold surface[112].
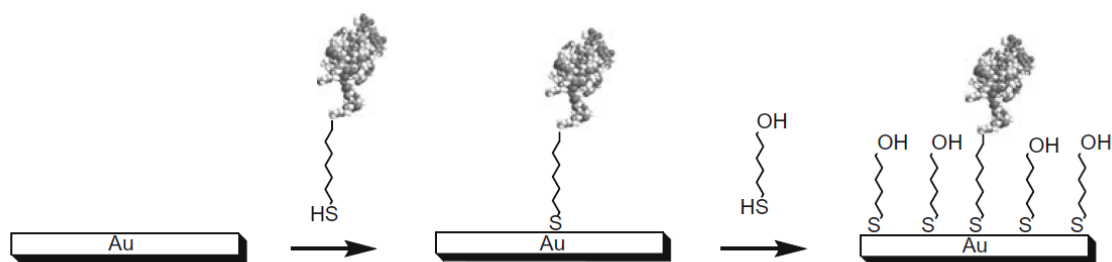
Figure 1.27 *Procedure for direct immobilisation of thiol-terminated aptamer forming a monolayer on gold surface*[112].

1.7.1.2 Amine, hydroxyl and carboxyl coupling system

Aptamers can be immobilised on a solid surface through the three most common functional groups, hydroxyl, amine, and carboxylic acid. Figure 1.28 summarises some of the reaction pathways that can be utilised for aptamer attachment. In hydroxylated surfaces, the functional group is modified with carbonyldiimidazole (CDI) to generate a reactive intermediate which consequently leads to a stable carbamate bond with an amino-conjugated aptamer (Figure 1.28 **a**). An aptamer with amino terminated can be attached to the surface with amine groups via glutaraldehyde, a symmetric bifunctional dialdehyde linker. Glutaraldehyde creates an imine bond known as a Schiff's base with the amino-terminated surface using one aldehyde group while the other aldehyde is free for repeating the same reaction with the amino-conjugated aptamer (Figure 1.28 **b**). Symmetrical diisothiocyanates can also be used as a bifunctional linker to attach either amino-terminated or thiol-terminated aptamers onto a surface of amine groups (Figure 1.28 **c**). Sulphosuccinimidyl 4-(N-maleimidomethyl) cyclohexane-1-carboxylate can be used to activate the amino-terminated surface for a thiol-conjugated aptamer (Figure 1.28 **d**). For a carboxylated surface, amino-terminated aptamer can be immobilised using 1-ethyl-3-(3-dimethylaminopropyl)carbodiimide (EDC) and N-hydroxysuccinimide (NHS) as coupling agents (Figure 1.28 **e**)[112].

The major drawback of the covalent attachment based on hydroxyl, amine, and carboxylic acid functional groups is that aptamer cannot be directly attached into the surface which is required one or two extra regents as an activation buffer. This would further complicate the immobilisation of aptamer. Furthermore, this type of reaction commonly involves toxic reagents such as glutaraldehyde and EDC. Moreover, the coupling of an amino

group to a carboxyl group via EDC and NHS is influenced by temperature as well as pH values affecting the coupling efficiency[113].
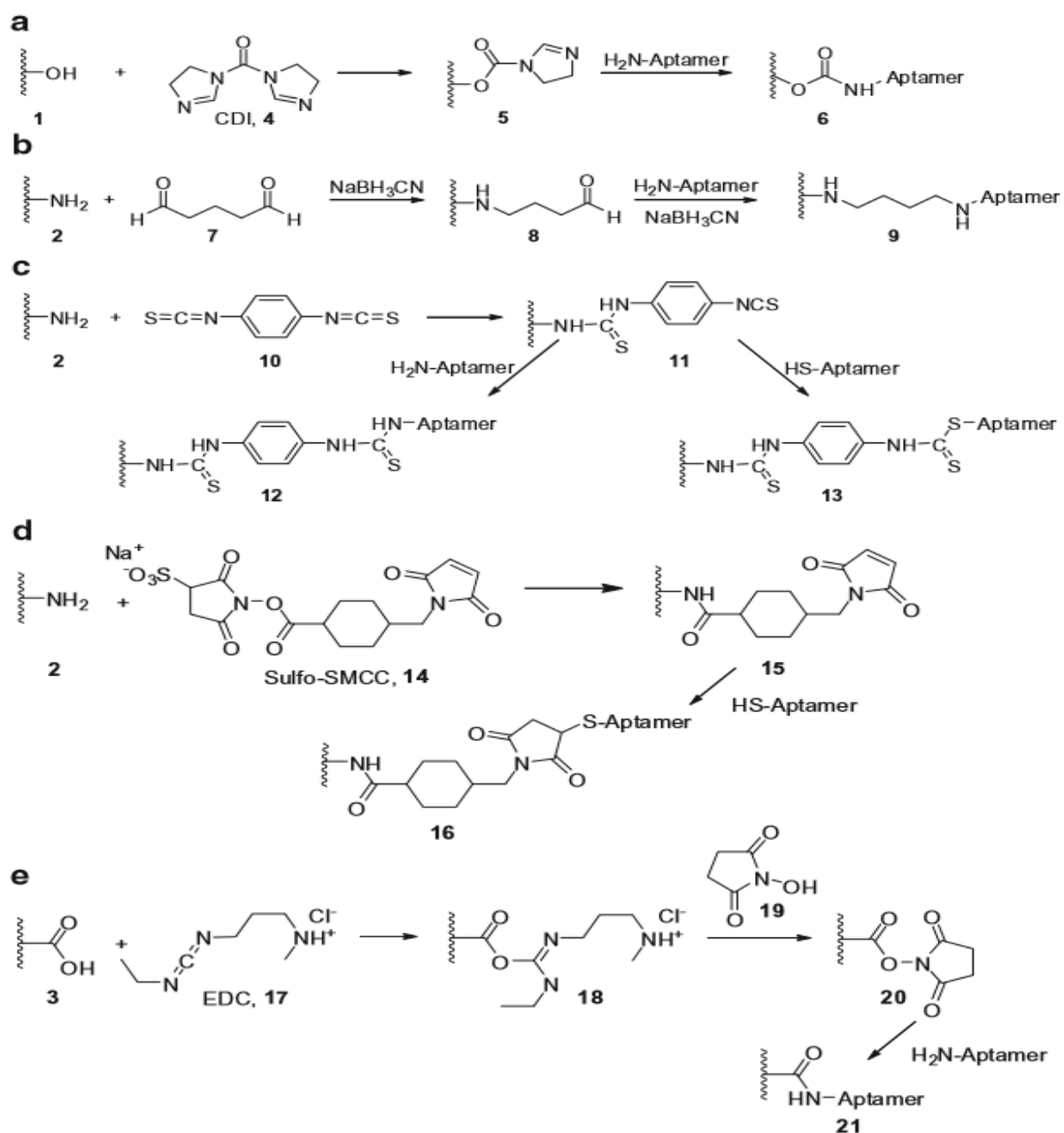
Figure 1.28 *Common reaction pathways for covalent attachment of aptamer into the surfaces usually in presence of carbonyldiimidazole (CDI) or succinimidyl 4-(Nmaleimidomethyl) cyclohexane- 1-carboxylate (SMCC) or 1-ethyl-3-(3-dimethylaminopropyl) carbodiimide (EDC) which depend on the functional group attached to the aptamer and to the surface.[112]*

1.7.2   Non-covalent attachment

1.7.2.1 Biotin-Streptavidin reaction

The most widely utilised technique for aptamer immobilisation is based on the biotin-streptavidin reaction. The noncovalent reaction between streptavidin and biotin was discovered as early as 1941 and is one of the strongest interactions in nature. The reaction is rapid and once it occurs, it is stable under a wide range of pH and temperatures. It has a binding energy of 4.5–6.0 kcal/mol and a dissociation constant, Kd, in the order of 4×10^{-14} M. Avidin is a protein that is usually extracted from chicken egg while biotin is a vitamin that exists in all living cells. Streptavidin, a bacterial protein homologous to avidin, is extracted from the actinobacterium *Streptomyces avidinii*. The streptavidin and avidin proteins have four identical binding sites for biotin with equally high specificity and affinity. However, streptavidin is widely used over avidin owing to the fact that streptavidin can provide a lower non-specific adsorption. This is because the isoelectric point of streptavidin is around 6.8–7.5 which reduces the non-specific interaction onto the biosensor surfaces that are operative at this range of pH.

Furthermore, streptavidin is commercially available in various engineered forms. Due to the strength, reliability and affinity of the biotin-streptavidin interaction, many research and diagnostic applications have utilised this reaction. Streptavidin is a tetrameric protein and hence it can bind biotinylated molecules such as DNA with minimal impact on the biological activity of the attached molecules[114]. The immobilisation of streptavidin onto solid surfaces can be performed either by physisorbtion or non-covalent or covalent attachment. Biotin-terminated aptamer can be then incubated with streptavidin at room temperature to provide an efficient immobilisation of aptamer molecules (Figure 1.29)[111, 115, 116].
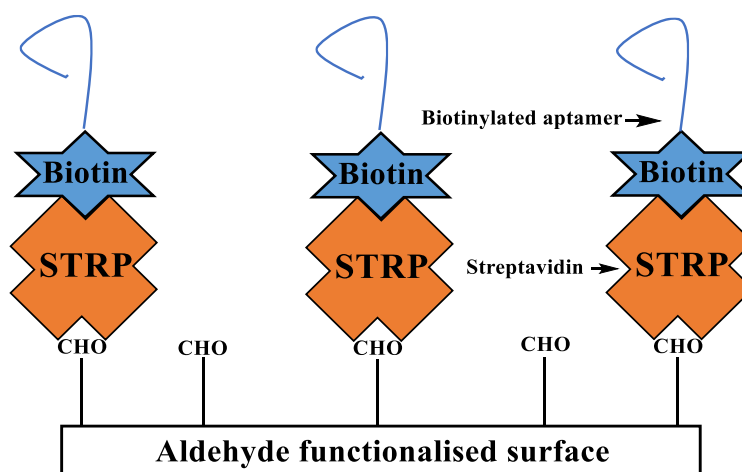
Figure 1.29 *Diagram of covalent immobilisation of streptavidin onto an aldehyde functionalised surface. Biotinylated aptamer is then attached onto immobilised streptavidin through a non-covalent reaction (biotin-streptavidin affinity).*

1.8 Application

1.8.1 Thrombin

Thrombin, Na^+-activated (Figure 1.30 a), is an allosteric serine protease that works as the central protease in the coagulation cascade. After an injury, thrombin is rapidly produced by the inactive zymogen prothrombin through various steps of enzyme cleavages. Activated thrombin cleaves fibrinogen into fibrin and clots are formed at the injury location to eliminate bleeding[117]. With crucial roles in physiological and pathological coagulation, thrombin and inactivated prothrombin are linked to various diseases such as Parkinson's and Alzheimer's[118]. Thrombin generated from bovine sources is also accepted by the U.S. Food and Drug Administration (FDA) as a haemostatic product to prevent bleeding. Under normal condition, thrombin does not exist in blood while its inactive form prothrombin is present at a concentration of 1.2 µM. At injury, thrombin is produced at concentration range from pM to µM levels[117].

Thrombin consists of a light A-chain (49 amino acid residues) and a heavy catalytic B-chain (259 amino acid residues) connected by a disulphide bond. Human thrombin has different forms. The majority of assays deal with the intact α-thrombin (295 amino acids). β-thrombin and γ-thrombin are produced by cleavage of α-thrombin in which cleavage of the B chain of thrombin at the Arg106-Tyr107 bond creates β-thrombin (189 amino acids).β-thrombin is then further cleaved at the Lys190-Gly191 bond to generate γ-thrombin. β-thrombin and γ-thrombin are less active than α-thrombin and their ability to work as a blood clotting agent is significantly decreased[117].

In 1992, Bock *et al.* reported the first aptamer that can bind human α-thrombin[119]. The aptamer consisted of a 15-mer oligonucleotide (5'-GGT TGG TGT GGT TGG-3') and can form a stable intramolecular G quadruplex structure, which is in an antiparallel orientation with a chair-like confirmation as shown in figure 1.30 (**B**)[120]. This aptamer binds to thrombin in one binding site, the fibrinogen-recognition exosite I, with a dissociation constant (Kd) of 100 nM. Tasset *et al*. have shown another aptamer that can recognise human α-thrombin at a second binding site; the heparin-binding exosite II[121]. The aptamer consisted of a 29-mer DNA oligonucleotide (5'-AGT CCGTGG TAG GGC AGG TTG GGG TGA CT-3') and exhibits a higher binding affinity (Kd = 0.5 nM). This aptamer also forms a G quadruplex structure (Figure 1.30 **C**). These two reported aptamers cannot bind β-thrombin and γ-thrombin, due to the binding sites exosite I and exosite II, being fully lost during the cleavage process of α-thrombin.

Thrombin binding to its aptamer is the most commonly used model to demonstrate the proof-of-concept of aptamer-based affinity assays. This is because both thrombin aptamers contain short sequences, 15-mer and 29-mer; which can be easily and inexpensively synthesised. Furthermore, the Kd values of these aptamers are different by two orders of magnitude which can be advantageous and suitable for assays that require different binding affinities. Moreover, a sandwich format can be easily established as a detection method due to both aptamers being bound on two different binding sites of thrombin without any interferences[117].

Figure 1.30 (**A***) Thrombin structure and two frequently utilised aptamers, (***B***) the 15-mer
and (***C***) 29-mer aptamers with G-quadruplex structures on each[117].*

1.8.2 Prostate specific antigen (PSA)

Prostate cancer is one of the most common cancers found in men. There were
approximately 1.1 million cases with 307,000 linked deaths in 2012, based on the statistic
that one in seven men will be diagnosed with prostate cancer during their lifetime. It is
ranked fourth among types of cancer in the world. Among diagnosed patients, 68% of
cases are aged 65 years or more. However, it has been found that prostatic carcinogenesis
is initiated much earlier. To reduce the risk of mortality significantly, an early and
accurate detection of prostate cancer is required[122]. Since the late 1980s, a remarkable
increase in the serum protein known as prostate specific antigen (PSA) has been used for
diagnosis. Prostate specific antigen (PSA), also known as human kallikrein 3 = (hK3), is
a glycoprotein consisting of 261 amino acid residues with a molecular weight of 34 kDA.
PSA is a member of the family of human glandular kallikrein proteins known as serine
proteases. Human glandular kallikrein 2 (hK2) is another member of the same family that
shows similarities to PSA with 78% and 80% identity at amino acid and DNA levels
respectively. Therefore, hK2 is considered as a potential diagnostic biomarker and also
as a negative control in specificity experiments[123]. In the human body, PSA exhibits
different forms such as free PSA (fPSA) and complex PSA (cPSA) which forms a
complex with plasma proteins, particularly serine protease inhibitor α1- antichymotrypsin
(ACT) and inactive PSA. Total PSA (tPSA) is linked to the total amount of free PSA

(fPSA) plus complex PSA (cPSA). PSA is present in blood serum in small quantities; however, prostate cancer causes the level of PSA to increase in the blood and thus it has been used as a biomarker by clinicians. The level of 4.0 ng/mL has been considered as a cut-off level of PSA in serum while higher than this level would be seen as an abnormal[124].

Two aptamers have been developed for PSA detection; RNA and DNA aptamers. The first is an RNA aptamer that consists of 90 mer of nucleotides[125]. However, few studies have selected this aptamer for PSA detection. This was attributed to the long length of the sequence which resulted in difficulties of commercial synthesis of this aptamer[126]. The second aptamer was a DNA aptamer that consists of 32 mer of nucleotides. The aptamer was identified by Savory and co-workers in 2010 with dissociation constant (Kd) in range of several tens of nM[127].

1.9 Aims and objectives

The aim of this project was to develop a label-free optical aptasensor based on a dye-doped leaky waveguide (DDLW) for detection of biomarkers such as thrombin and prostate specific antigen (PSA). Here, for the first time the DDLW device was fabricated with a chitosan hydrogel as porous waveguide material. Chitosan features functional amino groups, and was thus amenable for the tethering of bio-recognition elements. Furthermore, the porous hydrogel layer was advantageous as a waveguide because the bio-recognition molecules would be immobilised in its entire volume. This should result in the enhancement of the detection sensitivity by comparison to a conventional nonporous high index waveguide. To visualise the confinement of the light, in this project the waveguide was dyed with Reactive-Blue-4 (RB4); light is absorbed by the dye resulting in a dip in the reflectivity curve. To succeed a selective sensing, an aptamer was chosen as the bio-recognition molecule. This was to investigate for the first time the possibility of using an aptamer to work as the bio-receptor in the 3D network leaky waveguide containing chitosan porous hydrogel on glass substrate. The aptamer was selected as it offers high stability, selectivity and affinity and also low cost compared to the more commonly used antibodies. The immobilisation of the aptamer was based on the most widely used reaction: streptavidin-biotin affinity. Upon capturing the target analyte (thrombin and PSA), the refractive index of the hydrogel should change and hence the position of the dip in the reflectivity curve shift. This shift in dip position should be proportional to the analyte concentration, thus, allowing quantitative measurements.

The objectives of this project were:

- Fabrication of chitosan film on glass substrate to optimise a single mode optical waveguide. This would be accomplished by investigating various concentrations of chitosan deposited at different spin speeds to gain various film thicknesses.

- At the optimum condition, the dye concentration used to visualise the confinement was then investigated and optimised according to the sensitivity to the refractive index.

- The chitosan film was then characterised in terms of the availability of amino groups on the waveguide. This could be used for attachment of bio-recognition elements.

- The waveguide porosity was then investigated and optimised to be capable for diffusion of large molecules such as proteins into the sensing region and hence providing a high detection sensitivity.

- Streptavidin molecules were then attached onto the waveguide using various techniques such as covalent attachment, non-covalent attachment and physical adsorption. At the optimum condition, biotinylated aptamer was immobilised onto the functionalised waveguide.

- Target molecules such as thrombin and prostate specific antigen (PSA) were then detected in an aqueous buffer. To verify the detection of the analyte, a control experiment was run using a non-specific sequence aptamer that would not recognise the target analyte.

- The sensitivity of detection the analyte was investigated based on different incubation times. Under optimum conditions, the amount of aptamer immobilised was optimised according to the amount of analyte captured. This was performed by using various concentrations of aptamer to detect a constant amount of analyte.

- Upon optimisation of aptamer concentration, a series of concentrations of target analyte (thrombin and PSA) were then measured in order to obtain a calibration curve and hence to calculate the limit of detection of the fabricated sensor.

- The fabricated DDLW was then further investigated for detection of thrombin in a commercial human serum sample. Undiluted and diluted serum samples were applied for detection of spiked thrombin.

CHAPTER 2

Experimental Methodology

2 Experimental Methodology

In this chapter, the chemicals and materials used for the research described in this thesis are outlined, followed by a description of the custom-built optical sensor devices. The designs of the various flow cells utilised during the measurement are laid out. The deposition of the chitosan film on the glass substrate to obtain a dye-doped leaky waveguide is explained, followed by a description of the methods used to characterise the waveguide film, i.e. the number of available surface amino groups, the sensitivity of the waveguide to changes in refractive index and the film's porosity. Finally, the methods used for the immobilisation of aptamers are detailed followed by the protocols employed for the detection of the target analytes, thrombin and prostate specific agent (PSA), in buffer solutions as well as spiked into commercially available serum samples.

2.1 Materials and chemicals

The chemicals and materials used in this project are listed in table 2.1 and table 2.2. All reagents and chemicals were of analytical grade unless otherwise stated. Purified water was obtained from a water purification system (Elga Ltd., UK) at resistivity of 18.2 MΩ cm at 25°C and this was used for the preparation of all solutions unless otherwise stated.

Table 2.1 Chemicals and materials utilised in this project.

Chemicals	Companies
Chitosan lower molecular weight (75-85% DD)	Sigma-Aldrich, UK
Chitosan lower molecular weight (99% DD)	Sigma-Aldrich, UK
Reactive blue 4 dye (RB4)	Sigma-Aldrich, UK
Phosphate buffered saline (PBS) tablets	Sigma-Aldrich, UK
HEPES (99.5% titration)	Sigma-Aldrich, UK
Tris(hydroxymethyl)aminomethane	Sigma-Aldrich, UK
Sodium hydroxide (NaOH)	Sigma-Aldrich, UK
Biotin	Sigma-Aldrich, UK
Biotin 3-sulfo-N-hydroxysuccinimide ester sodium salt (Sulfo-NHS-biotin)	Sigma-Aldrich, UK
Fluorescein isothiocyanate isomer I (FITC)	Sigma-Aldrich, UK
Water (Molecular Biology Reagent)	Sigma-Aldrich, UK
Proteins	Companies
Bovine serum albumin (BSA)	Sigma-Aldrich, UK
Biotin labelled bovine serum albumin (Biotin-BSA)	Sigma-Aldrich, UK

Bovine serum albumin (BSA) labelled fluorescein isothiocyanate isomer I (FITC)	Sigma-Aldrich, UK
Streptavidin	Sigma-Aldrich, UK
Human alpha thrombin	Cambridge Bioscience, UK
Prostate specific antigen (PSA)	Abcam, UK
Salts	Companies
Sodium chloride (NaCl)	Sigma-Aldrich, UK
Magnesium chloride ($MgCl_2$)	Sigma-Aldrich, UK
Potassium chloride (KCl)	Sigma-Aldrich, UK
Calcium chloride dihydrate ($CaCl_2 \cdot 2H_2O$)	Sigma-Aldrich, UK
Polyethylene glycol (PEG)	Companies
PEG (10 kDa)	Sigma-Aldrich, UK
PEG (35 kDa)	Sigma-Aldrich, UK
PEG (40 kDa)	Sigma-Aldrich, UK
Polyethylene oxide (PEO)	Companies
PEO (100 kDa)	Sigma-Aldrich, UK
PEO (200 kDa)	Sigma-Aldrich, UK
PEO (400 kDa)	Sigma-Aldrich, UK
Cross linker	Companies
Glutaraldehyde solution (25% in H_2O, Grade I)	Sigma-Aldrich, UK
Glutaraldehyde solution (25% in H_2O, Grade II)	Sigma-Aldrich, UK
NHS-PEG-NHS (500 Da)	Thermo-fisher, UK
NHS-PEG-NHS (2,000 Da)	Sigma-Aldrich, UK
NHS-PEG-NHS (3,000 Da)	Sigma-Aldrich, UK
NHS-PEG-NHS (10,000 Da)	Sigma-Aldrich, UK
Solvents	Companies
Glycerol (99%)	VWR, UK
Ethanol absolute	VWR, UK
Acetic acid (0.1M)	Honeywell Fluka , UK
Detergent liquid (soap)	Elliott Hygiene, UK

Table 2.2 Oligonucleotides used in this project with their names, sequences, functional groups attached at 5-ends, molecular weights and suppliers.

Oligo number	Oligo name	Sequence	Molecular weight	Supplier
Oligo 1	Random sequence	5'TTCACGGTAGCACGC ATGGCTACCACCGACT CGCCGACCGTGGGACA ACTCACTGAAGTCATCT GACCTCTGTGCTGCT'3	24,500 Da	Sigma Aldrich
Oligo 2	Non-specific biotinylated aptamer	5'- Biotin (C6)-ACTTCAGTGAGTTGTCC CACGGTCGGCGAGTCG GTGGTAG'3	12,793 Da	Integrated DNA Technologies
Oligo 3	Anti-thrombin biotinylated aptamer	5'-BiotinTEG-TTTTTGGTTGGTGTGGT TGG'3	6,728 Da	Integrated DNA Technologies
Oligo 4	Anti-prostate biotinylated aptamer	5'-BiotinTEG-TTTTTAATTAAAGCTCG CCATCAAATAGCTTT'3	10,228 Da	Integrated DNA Technologies

2.2 Optical sensor setup

2.2.1 Measurement concept

The measurement principle of the dye-doped leaky waveguide (DDLW) device is described in depth in section (1.6.9). Briefly, a layer of chitosan polymer solution at a specific concentration was spin coated onto a glass substrate to obtain a film of a certain thickness and porosity so that a waveguide mode can be obtained whilst also allowing space for deposition of biomolecules to carry out bioassay inside the chitosan film. The refractive index of the chitosan waveguide layer (n $\approx$ 1.338) has to be lower than that of the glass substrate (n = 1.51) but higher than the aqueous buffer atop the waveguide (n = 1.333) in order to comply with the confinement condition. At a resonance angle (θ_r) light is confined inside the waveguide and propagates by total internal reflection (TIR) and Fresnel reflection at the interfaces of waveguide-sample and waveguide-substrate, respectively (Figure 2.1). The chitosan waveguide is dyed with Reactive Blue 4 (RB4) resulting in a dip in the reflectivity curve at a resonance angle (θ_r) due to light absorption (Figure 2.2). Bio-recognition molecules such as aptamers can be immobilised in the entire

volume of the waveguide allowing specific binding with the target analyte through the entire volume of the film, provided that the target analytes can diffuse into the film. The molecular binding results in a local change of the refractive index and hence, a shift in the resonance angle (θ_r) (Figure 2.2) as described by equation 2.1[128].

$$\theta_r = sin^{-1}\ \frac{N}{ns} \hspace{4cm} Equation\ 2.1$$

where N is the waveguide mode index and ns is the substrate refractive index. The extent of this shift is proportional to the concentration of the analyte, allowing quantitative measurement.

The quantitative measurement in DDLW is similar to SPR. In SPR, a dip in reflectivity curve at a resonance angle (θ_r) is obtained due to the absorbance of free electron from incident light in the metal layer. The change in the refractive index upon binding an analyte to an immobilised bio-recognition molecule, causes a shift in the resonance angle (θ_r) which is proportional to the concentration of the analyte. In SPR, the result is measured in a real-time by plotting the shift in the resonance angle (θ_r) versus time (a sensorgram) as shown previously in section 1.5.4. In some experiment, a resonance units (RU) is plotted as a function of time. One resonance units (RU) represents the binding of approximately 1 pg of protein/mm^2 [129] while 1000 resonance units (RU) corresponds to a shift in resonance angle by 0.1 degree[130]. The 1inearity of the SPR refers to the ability of the assay to obtain response va1ues that are re1ated to the ana1yte concentration. Ideally, the linear range for detection of protein such as thrombin by SPR is between 0.1 to 75 nM[130, 131]. In DDLW, the change in refractive index due to the binding event is also monitored in a real-time and the result is displayed as a shift in the resonance angle (θ_r) versus time as it will be explained in the following section.
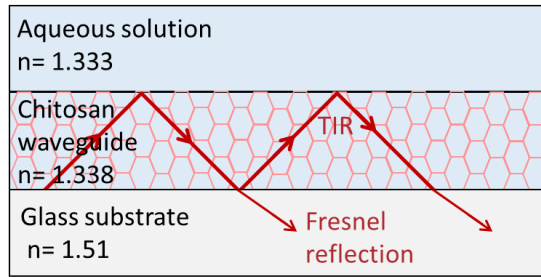
Figure 2.1 *Conceptual drawing of the chitosan waveguide. A porous chitosan gel film (n = ≈ 1.338) is deposited via spin coating onto a glass substrate (n = 1.51). An aqueous solution carrying samples or reagents (n = 1.333) is flown atop the chitosan gel film. Light is confined in the chitosan waveguide at a resonance angle (θr) and travels by Total Internal Reflection (TIR) at the chitosan-water interface and Fresnel reflection/refraction at the chitosan/glass interface.*
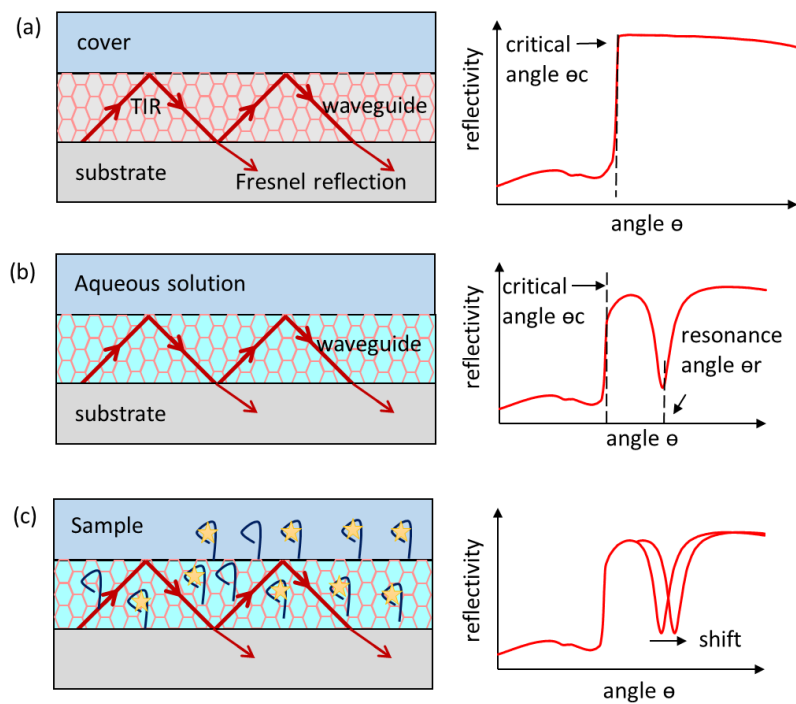
Figure 2.2 *Illustration of light absorption in dye-doped leaky waveguide. (a) Above a critical angle θ_c, light propagates through the waveguide and is picked up with a detector monitoring reflectivity. (b) When the waveguide layer is dyed, in this case with RB4, at a certain resonance angle θr, light is absorbed and there is a dip in the reflectivity curve. (c) When molecular binding events occur in the porous waveguide film, the refractive index changes resulting in a shift of the resonance angle.*

2.2.2 Detection setup

Two custom-built optical systems were used throughout the research presented in the thesis, namely, a photodiode setup for measurement of reflectivity curves; and a setup with CMOS camera allowing two-dimensional data capture. The setups were developed by Dr Gupta as part of her previous work[66, 86, 98].

Photodiode setup with laser light source for reflectivity curves

A red laser (RS components, UK, λ= 650 nm, power output 5 mV) as light source and a photodiode detector (OSD 100-6, Centronic, Surrey, UK) were placed on an optical rail using two goniometers (Figure 2.3 a). The distances between the prism and light source and prism and detector were 1.5 cm and 3.3 cm respectively. The movement of the goniometer was controlled by a computer interface program (Loader software). From the control panel of the software, the start and end angles for movement of the goniometer can be chosen. One goniometer controlled the angular position of the incident light while the other one was utilised to synchronise the detector to a corresponding reflection angle. For waveguide measurements, the chitosan coated glass slide was mounted on a BK7 prism (30 mm by 30 mm, Qioptic Photonics, UK). Angular scans were taken between 75° and 55° with respect to the normal to the base of the prism (Figure 2.3 b, c, d). The acquisition time of the photodiode for an individual data point was set to 25 ms. The number of scans could be specified via the software control panel; a full scan took about 30 s. Schematics of a reflectivity curve typically obtained with the setup are shown in figure 2.2, with the angle plotted on the x-axis and the photodiode output in mV as a measure of reflectivity on the y-axis. The optical system was enclosed in a light tight black box as shown in figure 2.5.
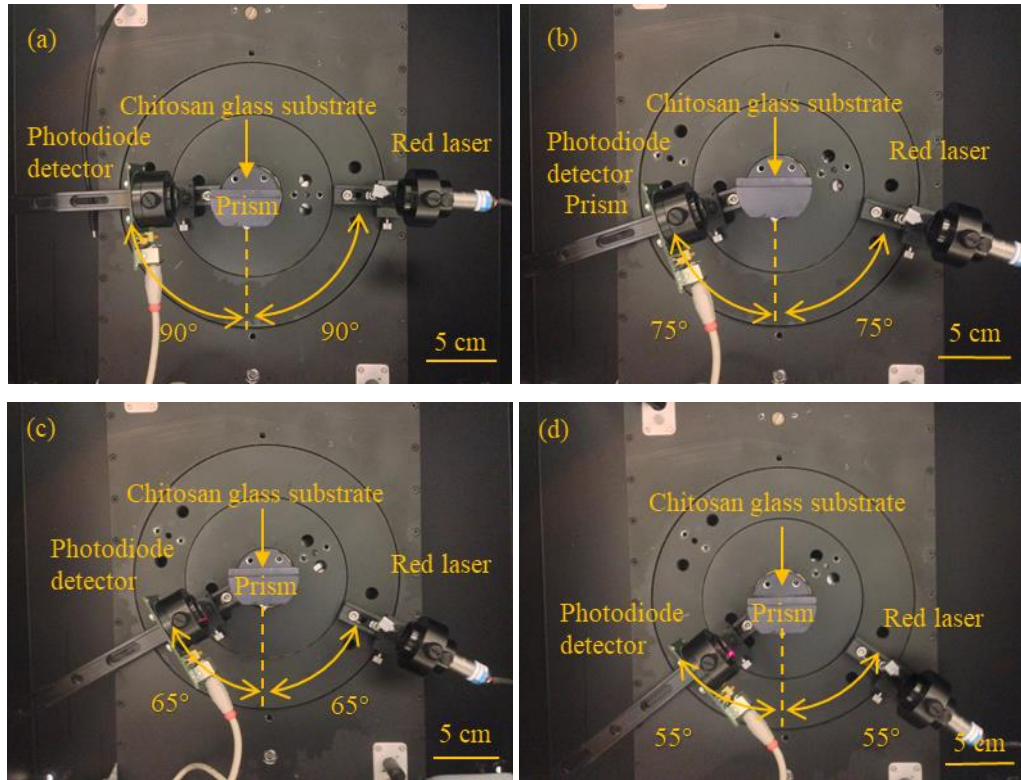
Figure 2.3: *Setup for measurement of reflectivity curves with red laser as light source and photodiode as detector. Both were mounted on a rail to allow synchronised rotational movement around the prism. (a) At 'home' position with an angle of 90° with respect to the base of the prism, (b) at 75°, (c) at 65° and (d) at 55°. Reflectivity curves were usually measured between 75° and 55°.*
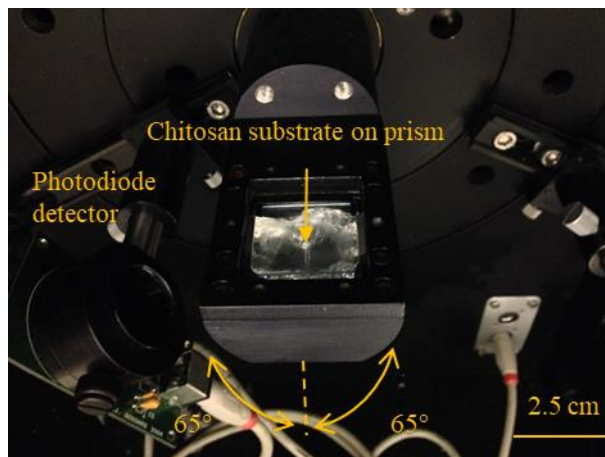
Figure 2.4: *View of the chitosan glass substrate mounted on a BK7 prism before staining with RB4 dye.*
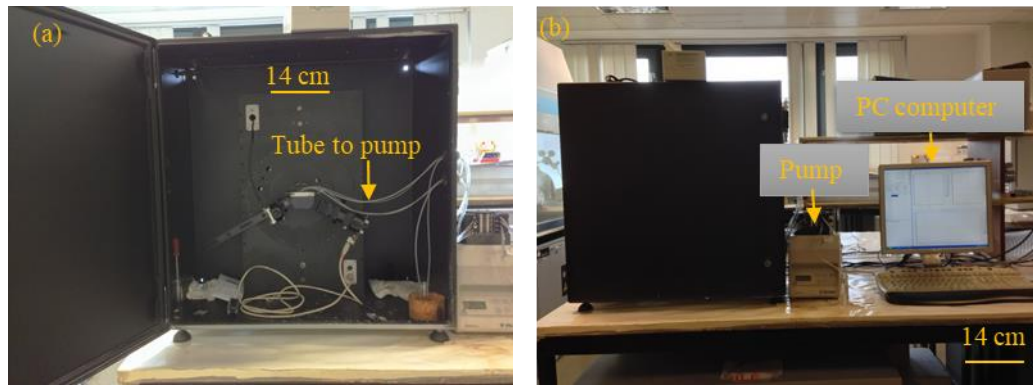
Figure 2.5 *Images of the optical system enclosed in a black box (a) with open door and (b) with closed door.*

CMOS camera setup with LED light source for two-dimensional image capture

For measuring the shift in resonance angle, light from an LED was shaped into a wedge, allowed to propagate through the waveguide layer and detected as a two-dimensional image on the chip of a CMOS camera (Figure 2.6 a). The setup featured a resonant cavity red LED ($\lambda = 650$ nm, RCLED, PR65-F1P0T, Roithner Lasertechnik, Vienna, Austria) as light source. The output of RCLED was collimated and subsequently expanded to 25 mm diameter then passed through a 63 mm focal length cylindrical lens to form a wedge beam to probe the waveguide with a range of angles of incidence simultaneously. The output was recorded using a 10.55 Mpixel CMOS camera (UI-1492LE, IDS Imaging, Obersulm, Germany), which allowed a 4.59 mm wide section of the waveguide to be imaged. The LED and CMOS camera were mounted on the goniometers to allow precise angular positioning with respect to the prism (Figure 2.6 b). Measurements were usually carried out with the LED and CMOS fixed at 65° with respect to the base of the prism, *i.e.* near the resonance angle of the dye-doped leaky waveguide.
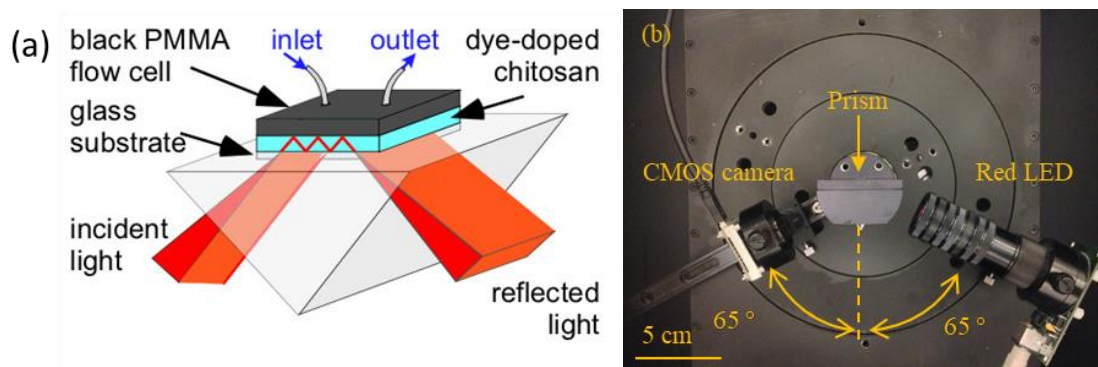
Figure 2.6 *(a) Schematic diagram of a flow cell placed onto a prism with a wedge-shaped beam with incident and reflected light. (b) Photograph of optical setup with red LED as light source and CMOS camera for two-dimensional detection positioned at the resonance angle of 65°.*

The image as captured on the CMOS camera represents width across the waveguide flow cell in the y-direction (*i.e.* a distance measurement) while the x-axis represents an angular reading. The dip in the reflectivity curve appears as a dark line on the CMOS image (Figure 2.7 a). When the refractive index changes in the chitosan waveguide, for example through binding events, the resonance angle shifts and the dark line is found to move along the x-axis (Figure 2.7 b). The movement of this dark line can be tracked by custom written software and recorded in terms of number of pixels and then converted into a shift in angle. For quantitative measurements, the shift in the dip position was monitored as a function of time (Figure 2.8).
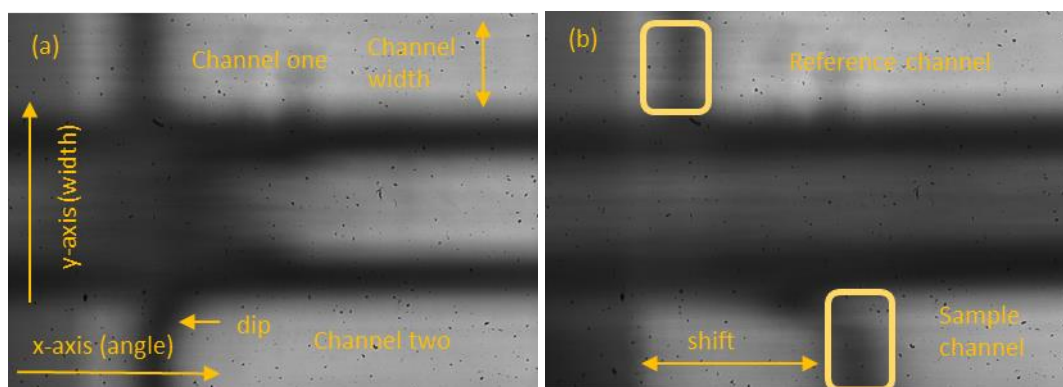
Figure 2.7 *(a) Typical output from the CMOS camera with the y-direction representing the width across the flow cell and the x-direction representing an angle. The dip in reflectivity is observable as a dark line on these CMOS images. (b) Dip shifting in reflectivity curve corresponding to the shift on the dark line on the image taken by CMOS camera.*
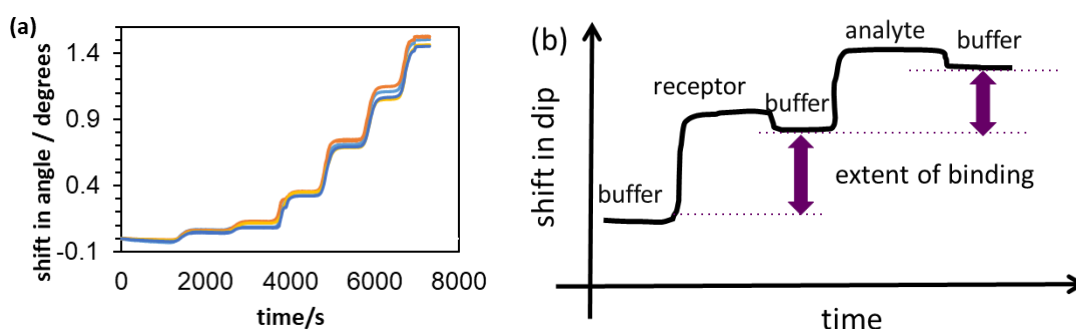
Figure 2.8 *Examples of measurement for shift in resonance angle as a function of time. (a) Flushing of glycerol over waveguide to measure refractive index, (b) flushing of buffer solutions and receptors and analytes over waveguide to measure extent of binding.*

Image processing was achieved through a custom-made system devised by Dr Gupta. The CMOS camera was connected to a computer via USB 2.0 and its settings were controlled by PixeLINK capture OEM software (Pixelink, Ontario, Canada). The image as displayed on screen with 3,000 pixels (x-direction) representing an angle, and 2,208 pixels (y-direction) representing a distance on the y-axis. To monitor movement of the dark line (dip) in the x-direction, GetFrame V8 software was utilised. The software (Figure 2.9) allowed specification of 8 bit or 16 bit image capture and brightness. The user would manually draw 'boxes' around dark line region, i.e. the area of interest (Figure 2.10 a)

and this would then automatically generate various dips in a plot of grey scale intensity as a function of distance in pixels as shown in Figure 2.10 b. Each drawn box was represented by a specific dip that was appeared with a specific colour as shown in figure 2.10 b. The width of the dip was represented by the width of the drawn box where it covered the whole dark region. The depth of the dip was represented by the darkest region which was located in the middle of each drawn box. This would stand for the highest absorbance region of the attached dye molecules into the waveguide. As the dark area shifted due to the binding event, the movement was automatically tracked via a centre of gravity algorithm set to a threshold of 60% of the depth of the dip. This shift over time would be displayed by various lines each with a specific colure while each line represented a specific drawn box as shown in figure 2.11 a.

For tracking a time plot as shown in figure 2.11, the user would start a measurement from zero seconds and data would be saved until the measurement was stopped (Figure 2.11 b). The data was saved as a csv file which was later converted into Microsoft Excel file. For each experiment, typically between 10 and 15 boxes were drawn and processed in parallel. The movement of the drawn boxes in the x-axis for each second of time was recorded in a pixel number. As mentioned earlier; the x-axis in the image captured by the CMOS camera represents an angular reading. Therefore, the number in pixels recorded upon movement was actually corresponded at a specific incident angle.

Before starting the experiment, a relationship between pixel number and incident angle was obtained via a calibration curve. This was accomplished by changing the incident light from angle of 65° to 65.25°, 65.50°, 65.75°, 66° and 66.25°. The dark line in the image was then appeared at different position upon changing the incident angle. Thus, this would lead to different pixel numbers. These pixel numbers are then recorded for each incident angle. A calibration curve is then obtained between various pixel numbers and various incident angles.

At the beginning of the experiment, the incident light was fixed at angle of 65°, while the dark line was moved across the x-axis due to the binding event producing various pixels numbers that are recorded for each second of time. From the straight-line equation of the calibration curve, these recorded pixels numbers for each second of time were then converted into various degree of incident angles. Finally, the movement of the dip in

CMOS camera is plotted as a shift in angle over time for each drawn box (Figure 2.8). The limit of detection of DDLW device to the bulk of refractive index was reported by our group to be at 2.82 x 10^{-6} [86].
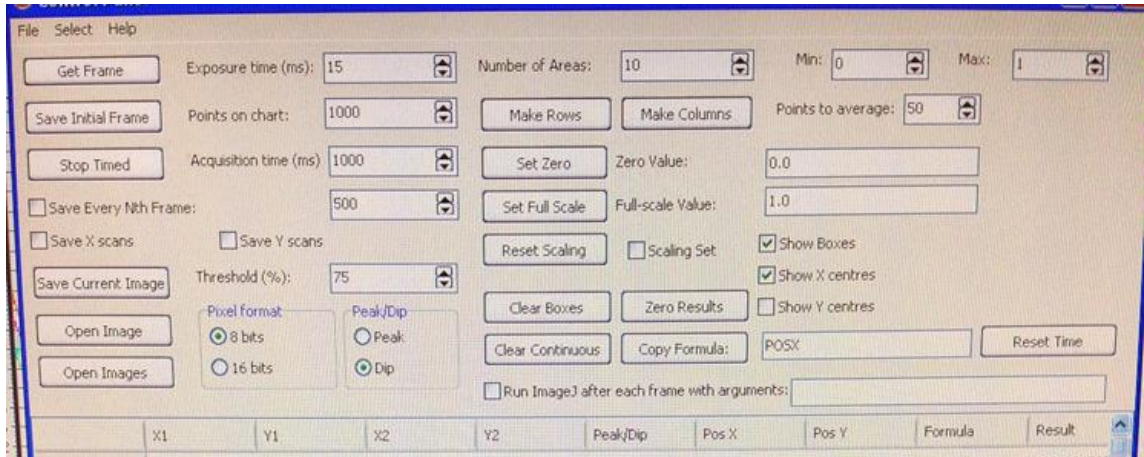
Figure 2.9: *Screenshot of the menu of the GetFrame V8 software showing its functionality.*
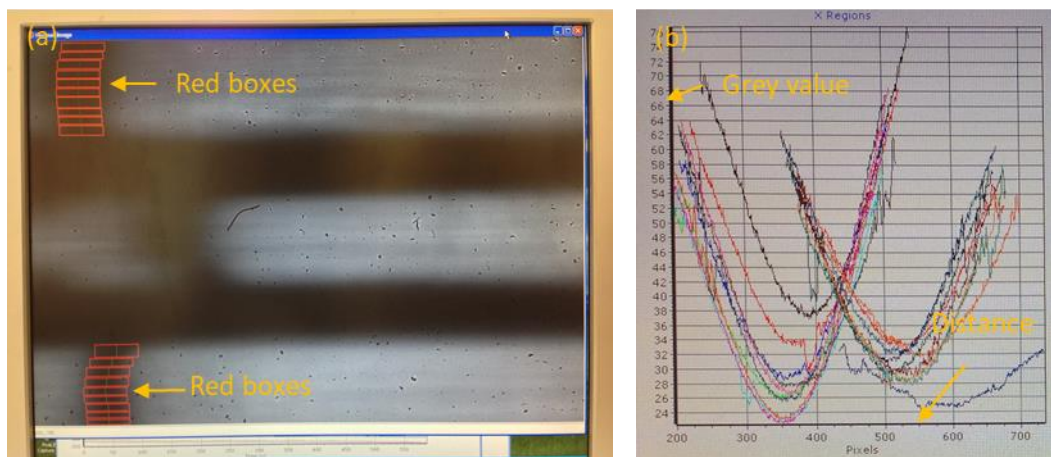
Figure 2.10: *Print screen of GetFrame V8 software showing (a) a dip with red boxes drawn in areas of interest and (b) a plot of grey scale value versus distance in pixels for each drawn box which represented by a dip with a specific colour.*
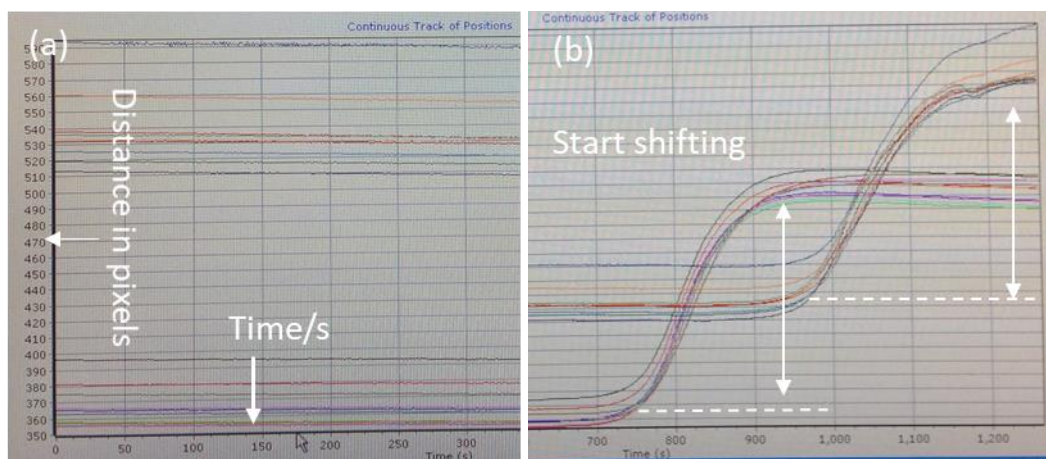
Figure 2.11: Images of tracking position of various boxes in the dip region represented by various lines each with a specific colour (a) when the measurement started, (b) when the movement of the dip begun.

2.3 Flow cell design

The chitosan coated substrate was integrated into a flow cell to allow controlled fluid delivery (Figure 2.12). A range of flow cell devices were utilised in the experiments described in this thesis.
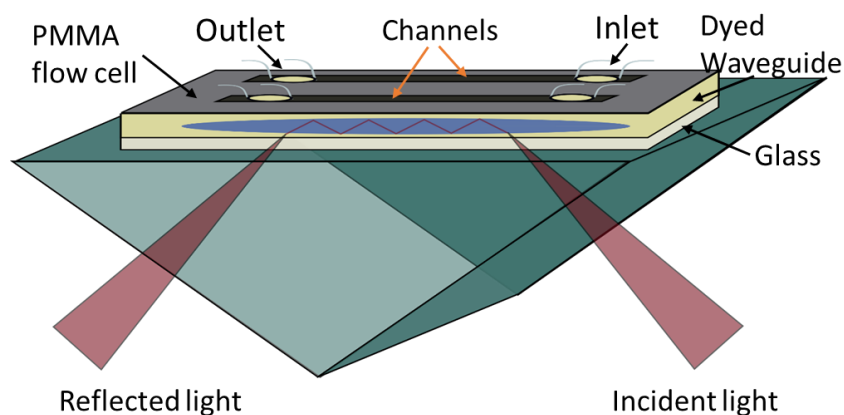
Figure 2.12: Diagram of chitosan coated substrate integrated into a flow cell, here featuring two inlets and two outlets to allow fluid delivery through a sample and reference channel.

2.3.1 Flow Cell Design 1

Flow design 1 featured two parallel channels and was made up of three components, (1) a moulded black piece of PMMA with four access holes of 1.5 mm diameter, (2) a double sided adhesive (3M 467MP), obtained from Viking Industrial Products (UK) of 50 μm

68

thickness with two channel sections of 5 mm width and 8 mm length cut out via laser cutter and (3) a glass substrate coated with chitosan film. The PMMA moulding and laser cutting were carried out at the University of Manchester, courtesy of Dr Gupta. The three layers were assembled and fastened with the adhesive and interfaced as described in section 2.3.4.
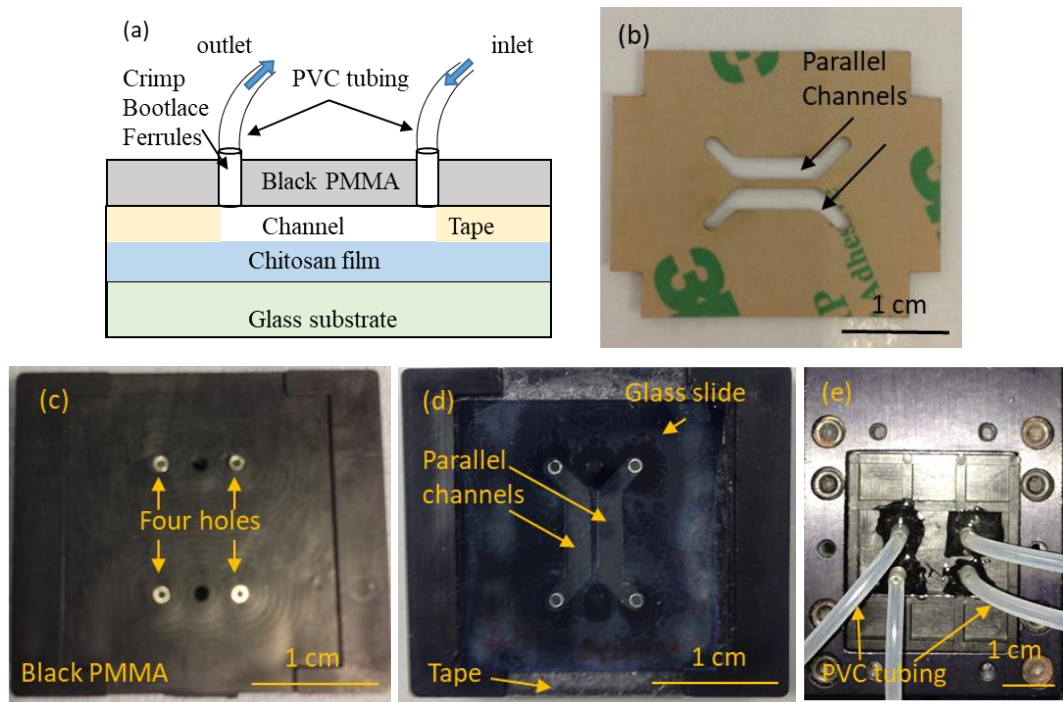
Figure 2.13: *(a) Schematic diagram of flow cell 1, (b) photograph of laser cut 3M tape, (c) bottom view of the black PMMA layer with four access holes, (d) bottom view of flow cell with M3 tape and chitosan glass substrate, (e) top view of fully assembled flow cell with PVC tubing.*

2.3.2   Flow Cell Design 2

Flow cell design 2 featured a single circular flow cavity. It was assembled from a piece of black PMMA (2 mm thick) with a CNC milled circular channel of 20 mm diameter and 0.2 mm depth (Figure 2.14). An O-ring with the same diameter as the circular channel was used for sealing the flow cell with the chitosan coated glass substrate. The flow cell was sealed and stuck on the substrate via pressure provided by a metal holder system as described in section 2.3.4. The flow cell was designed by Prof Nick Goddard and fabricated in his group at the University of Manchester.
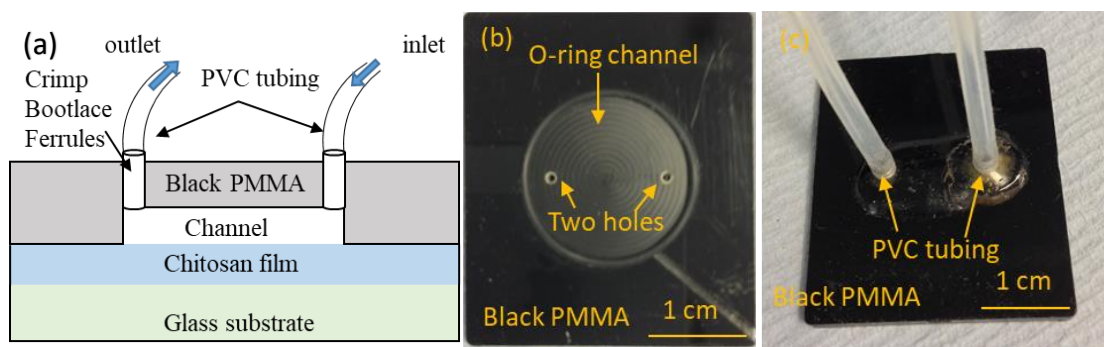
Figure 2.14*: (a) Schematic of flow cell 2, (b) a piece of black PMMA milled with circular channel and fitted with an O-ring rubber, (c) a top view of flow cell 2 with PVC tubing connected.*

2.3.3   Flow Cell Design 3

Flow cell design 3 featured two straight parallel channels, 0.2 mm deep, 3 mm wide and 14 mm long between two access holes of 1.35 mm diameter (Figure 2.15). These were CNC milled into a piece of black PMMA. The channels were surrounded by a recess for an O-ring (Diameter (16mm), Polymax Ltd, UK) to allow sealing onto the chitosan coated glass substrate. This flow cell was designed and manufactured by Dr Alex Iles in the Lab-on-a-Chip Fabrication Facility at the University of Hull (Figure 2.16).
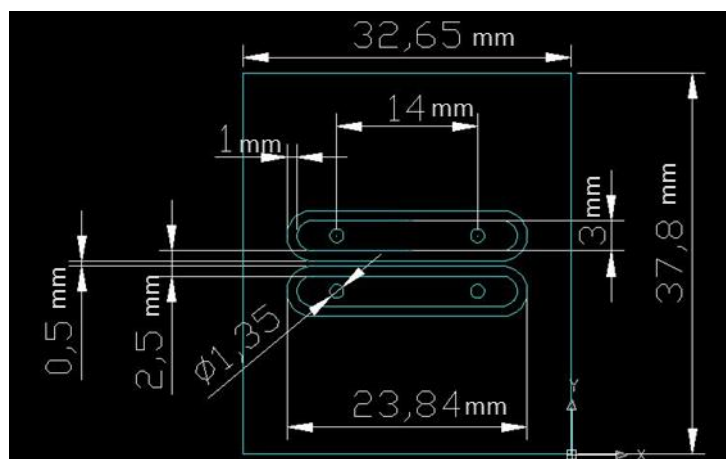
Figure 2.15*: Dimensions of flow cell design 3.*
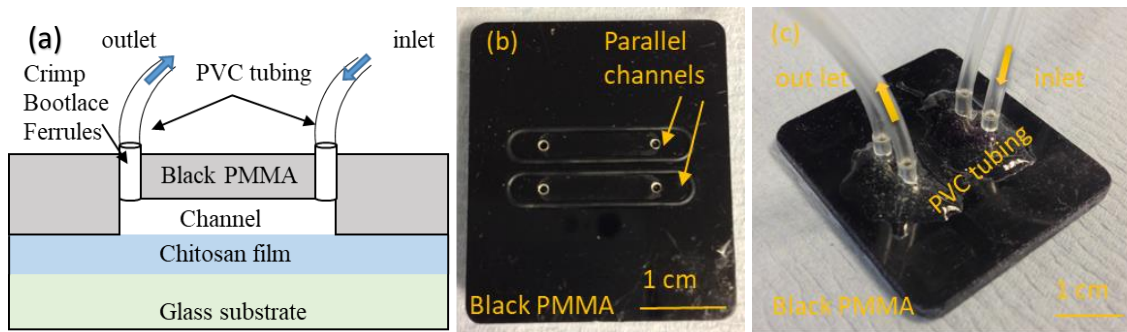
Figure 2.16*: (a) Schematic of flow cell 3, (b) photograph of black PMMA milled with two parallel channels and surrounded by a recess for O-ring, (c) top view with PVC tubing.*

It should be noticed that during the using of the first flow cell (design 1), a leaking from the chitosan chip was observed in some experiments and that was due to the effectiveness of the room temperature on the double sided adhesive resulted in a poor sealing layer. Therefore, a second flow cell (design 2) was designed and utilised instead which was sealed to the chitosan chip via an O-ring as explained in section 2.3.2. However, in some experiments a fluctuation in the refractive index of waveguide was observed and that was linked to the effectiveness of the room temperature. In order to eliminate this impact, a third flow cell (design 3) was fabricated with two channels; reference channel and sample channel in which the sample channel can be subtracted from the reference channel.

2.3.4   Interfacing the flow cells to the optical systems

A custom made metal holder system, devised by Dr Gupta at the University of Manchester was employed to fix tightly the flow cells of design 2 and design 3 to the BK7 prism (Figure 2.17). One drop of refractive index matched oil (Type A; CODE 1248, Cargille Labs, New Jersey, USA) was first applied to a prism. A chitosan-coated substrate was then placed on top of the oil layer. This eliminated any air gap between the chitosan substrate and the prism. Finally, the flow cell (design 2 and design 3) was applied at top of the chitosan substrate and was securely sealed by introducing a metal holder system at the top of the flow cell as shown in figure 2.17.
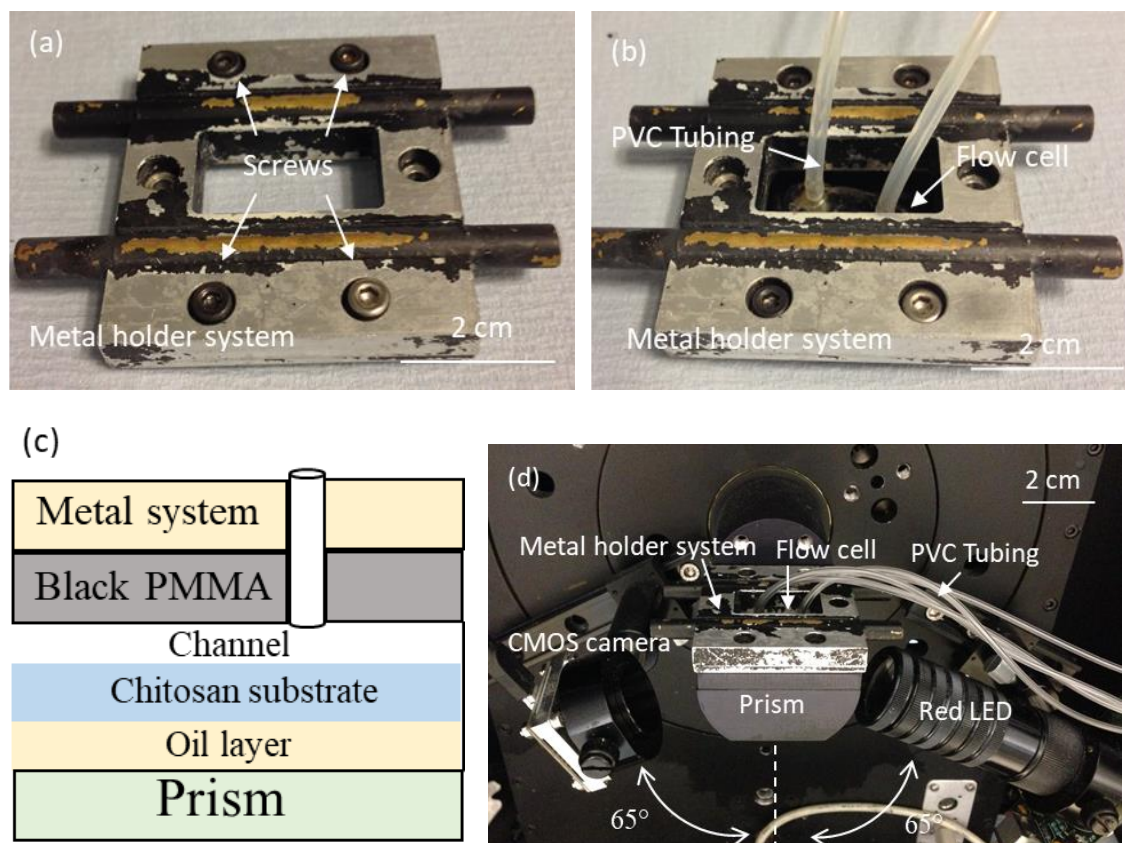
Figure 2.17*: (a) Photograph of the custom-made metal holder system with four screws. (b) Metal holder with a flow cell inserted. (c) Schematic diagram of interfacing metal holder system into black PMMA flow cell. (d) Metal holder mounted on the BK7 prism as part of the full optical setup.*

For fluid pumping, crimp bootlace ferrules (RS Components) with 8 mm pin length and 1.5 mm pin diameter were inserted into the access holes of the black PMMA pieces of all flow cell designs and glued with Loctite Double Bubble 2-Part Epoxy Glue (Figure 2.18). Liquid was pumped through the flow cells via a peristaltic pump (Minipuls®, 3 Gilson, UK) (Figure 2.19). Elkay PVC tubing (i.d. 0.76 mm, o.d. 2.438 mm) was pushed over the ferrules at one end, whilst the other end was dipped into vessels containing the solution to be pumped (Figure 2.19).

A manifold with tubing was devised to allow flushing of the system and displacement of air-bubbles. Polymer syringes (5 mL) (Henke Sass Wolf, Tuttlingen, Germany) were connected to the PVC tubing via T-pieces in order remove the air bubbles (Figure 2.19 a).
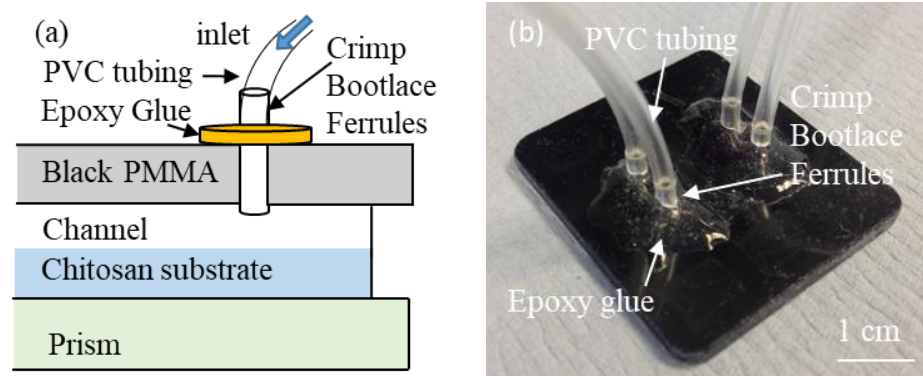
Figure 2.18*: (a) Schematic diagram of interfacing PVC tube into Crimp Bootlace Ferrules, (b) photograph of flow cell glued with Crimp Bootlace Ferrules and connected to PVC tubing.*
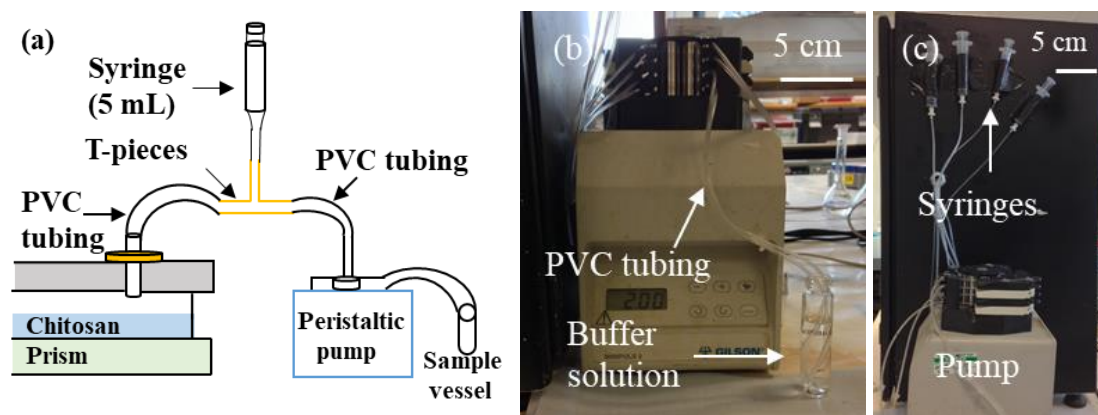
Figure 2.19*: (a) Schematic of fluid manifold, (b) Photograph of peristaltic pump and liquid sample vessel, (c) photograph of manifold allowing manual flushing featuring 5 mL syringes, valves/T-junction.*

2.4 Formation of chitosan film on glass substrate

The dye-doped leaky waveguides were obtained by spin coating chitosan solutions onto a glass substrate and subsequent dying with RB4. To achieve optimum performance, various concentrations of chitosan polymer were investigated at a range of speeds. The films were then characterised by the availability of amino groups on the film obtained.

2.4.1 Cleaning procedure of glass substrate

Before chitosan deposition, the glass substrate had to be cleaned in order to provide a highly hydrophilic surface to which the film would be easily attached. Glass microscope slides (Thermo scientific; ground edges 90°; 1 mm thick) of 25 mm width and 75 mm length were cut into 25 mm x 25 mm squares using a diamond scribe so that the glass

pieces would fit into the flow cells (section 2.3). The slides were washed with 200 mL of detergent liquid (Elliott Hygiene Ltd, UK) for 30 min under ultrasonication (Serial number; 0.38671; Scientific Laboratory Supplies, UK) in a 500 mL beaker. The glass wafers were then taken from the beaker with tweezers and dried on a clean tissue (Product number; 7285 L10 extract+; Bunzl Cleaning and Hygiene Supplies, UK) at room temperature. This procedure was repeated with deionised water (200 mL) and subsequently ethanol (200 mL). After the final drying step, the slides were stored in petri dishes until required.

2.4.2 Chitosan coating procedure

Chitosan solutions of 1%, 1.5% and 2% (w/v) were prepared by dissolving 0.1, 0.15 and 0.2 g of chitosan powder (75-85% DD), respectively, in 10 mL of aqueous acetic acid (0.1 M). The solutions were stirred with a magnetic stirrer bar for 1.5 h to ensure the powder was fully dissolved. For cross-linking, 12.5 μL of glutaraldehyde (25% in H_2O, Grade I) was added to each solution and left again to react for 15 min. Finally, 2 mL of each solution was dispensed on a cleaned glass slide that was held by a vacuum (~10 psi) on the chuck of the spin coater. The solutions were spun at various speeds (2,000, 3,000 and 4,000 rpm) for 30 s. The coated chips were dried at room temperature and stored in petri dishes until required.
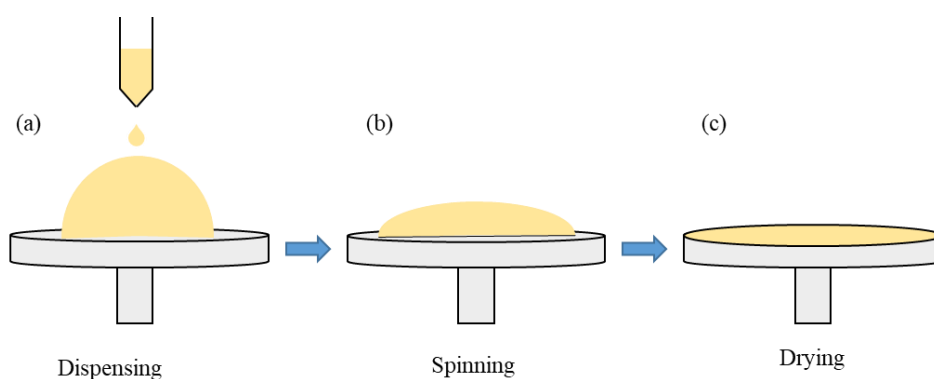
Figure 2.20: *Diagram of coating procedure onto glass slide. (a) Chitosan solution was pipetted onto a cleaned glass slide, (b) the slide was spun at between 2,000 and 4,000 rpm for 30 s, (c) left to dry at room temperature on the bench.*

2.4.3 Evaluation of the chitosan coated glass slides

All coated slides were treated with RB4 dye to obtain the dip in reflectivity described in section 2.2.1 (Figure 2.2). To this end, a stock solution of RB4 (1 mM) was made by dissolving 0.038 g in 20 mL of deionised water. A dilution with deionised water was

made to obtain a concentration of 10 μM. A chitosan coated slide was mounted on the BK7 prism to which one droplet of refractive index matching oil had been applied. A few droplets of water were added and the film was scanned as described in section 2.2.2 (Figure 2.3). This was followed by drying the water droplets from the surface using a soft tissue and then adding a few drops of RB4 dye (10 μM) on top of the slide. The scan was repeated three times upon adding the RB4 dye solution for each chitosan coated slide used.

2.4.4 Dye concentration on chitosan waveguide

Following optimisation of chitosan concentration and spin speed, the effect of the dye concentration on the shape of the dip in the reflectivity curve was studied. A series of RB4 concentrations in the range of 1 μM to 10 μM was made up by dilution with deionised water from a 1 mM stock solution. The chitosan coated slides were inserted into a flow cell of design one (Figure 2.13), the flow cell was mounted on the prism and dye solutions were pumped manually and sequentially starting from 1 μM up to 10 μM using a 5 mL disposable syringe (Figure 2.19). Reflectivity curves were measured for each concentration of RB4 used. Water was flushed through the surface before and after each solution and the measurement was recorded as a reference.

2.4.5 Effect of pH on chitosan waveguide

The effect of pH on the chitosan waveguide was studied by monitoring the change in the dip angle in the reflectivity upon applying phosphate buffer. The buffer was prepared at a range of pH values from 4 to 10 using phosphate salts and phosphoric acid (85%) as shown in Table 2.3. All buffer solutions were made up to 1 L with de-ionised water. The pH was verified with a pH meter (HI 2210, Hanna Instruments, UK). Finally, 250 μL RB4 dye stock solution (1 mM) was diluted in 25 mL of each prepared buffer giving a concentration of 10 μM dye in the different pH buffers.

Slides were spun coated with a 2% (w/v) chitosan solution at 3,000 rpm and interfaced to flow cell design one. The surface was first flushed manually with 5 mL water, followed by the different pH phosphate buffers from pH 10 to pH 4. For each pH, reflectivity curves were taken between incident angles of 55° and 75°. Water was flushed through the channel before and after each buffer and the data were recorded as a reference.

Table 2.3: Volumes taken from salt and acid solutions to prepare phosphate buffers at different pH values before making to 1 L with de-ionised water.

pH	di-basic sodium phosphate (0.2 M) / mL	monosodium phosphate (0.2M) / mL	hydrogen phosphate (0.1M) / mL	Phosphoric acid (85%) / mL
4	19.3			30.7
5	25.7			24.3
6	12.3	87.7		
7	61	39		
8	94.7	5.3		
9			955	45
10			966	

2.5 Calculating moles of amino groups on chitosan waveguide

The number of moles of amino groups (n) on the chitosan waveguide was calculated via equations 2.2 and 2.3.

$$n = c \cdot V \hfill \textit{Equation 2.2}$$

$$V = A_{il} \cdot I \hfill \textit{Equation 2.3}$$

where **C** is the total concentration of amino groups in the chitosan layer of volume **V**, which in turn is the product of the chitosan layer of thickness **I** and the illuminated area **A$_{il}$** of the chitosan film during absorbance measurements.

The concentration **C** of the amino groups was determined by reacting the chitosan waveguide layer with RB4 dye solution. RB4 molecules are expected to bind to the chitosan until all the amino groups within the chitosan film are occupied. Absorbance of the dyed chitosan layer was then measured via a spectrophotometer. From the absorbance measurements, the concentration of RB4 molecules bound to the chitosan film was found using a calibration curve.

2.5.1 Measuring the absorbance of RB4 dye on chitosan film

Three chitosan coated slides were prepared for each concentration of chitosan (1%, 1.5% and 2 % w/v), all coated at a spin speed of 3,000 rpm for 30 s on cleaned glasses. After drying, each slide was incubated in a petri dish with a 100 μM solution of RB4 (Figure 2.21). The slides were incubated for a total of 400 min. Each 10 mins, the slides were taken out of the dish, washed with de-ionised water, left to dry for 5 min on the bench and then transferred to the spectrophotometer for measurement. The slides were then placed back into the incubation dish for another 10 min and this was repeated until 400 min were reached. The absorbance from each slide was taken from two instruments at each incubation time to allow comparison results.
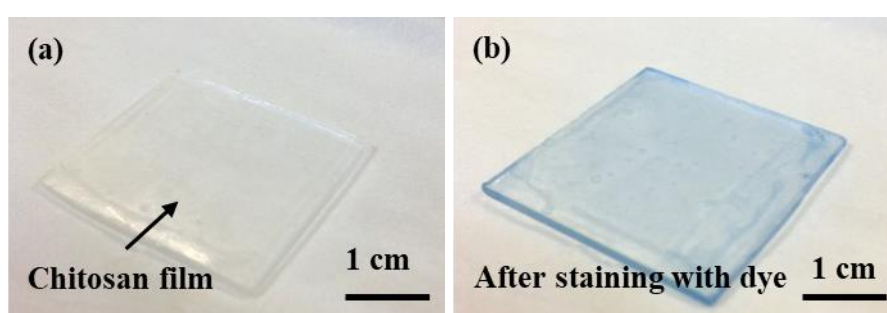
Figure 2.21: Photographs of chitosan glass substrate (a) before and (b) after incubation with RB4 dye (100 μM).

Initial measurements were taken with a modified version of the custom-built optical setup described in section 2.2.2, with a red laser as light source (λ = 650 nm) and photodiode as detector. These were positioned at 90° with respect to the base of the prism to allow absorbance measurements directly through the glass slide positioned in the beam on a custom made holder (Figure 2.22) The absorbance was calculated based on Beer's law (equation 2.4)

$$A = Log \frac{I_0}{I}$$
<div align="right">*Equation 2.4*</div>

with I_0 as the intensity (in mV) recorded for the chitosan-coated slide before staining and I the intensity of the dye-coated slides for the various time periods.

The second instrument was a conventional UV/vis spectrophotometer (Bio Lambda 10). The chitosan-coated slide was placed in front of the light source using a glue to hold it in place. The absorbance measurement was taken from the three different chitosan slides for each concentration (1%, 1.5% and 2 %) on both instruments.
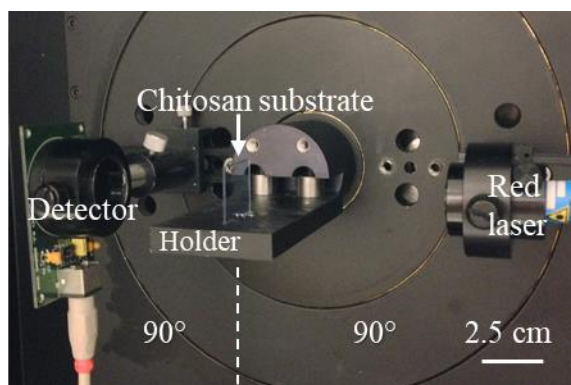
Figure 2.22*: Photograph of the absorbance setup on the custom-built optical device featuring the red laser as light source and photodiode detector positioned at 90° and the chitosan-coated glass substrate mounted on a holder.*

2.5.2   Calibration curve of RB4 dye solutions

A calibration curve for RB4 was obtained by measuring the absorbance of RB4 solutions in a cuvette. First, 0.038 g of RB4 was dissolved in 20 mL of de-ionised water to obtain a 1 mM stock solution. A series of concentrations were then prepared ranging from 0.1 µM to 100 µM in de-ionised water. The absorbance for each concentration was recorded with both the custom-built optical setup and with the commercial spectrophotometer at 650 nm. For the custom-built optical setup, the cuvette was placed on a holder in the path of passing light as shown in figure 2.23. The absorbance was calculated based on Beer's law (equation 2.4) with the intensity (in mV) of an empty cuvette taken as reference (I_0) and the sample solution recorded as I. For the commercial spectrophotometer, absorbance was recorded directly. Three separate measurements were taken from each of three different cuvettes for each concentration of RB4 dye on both instruments.
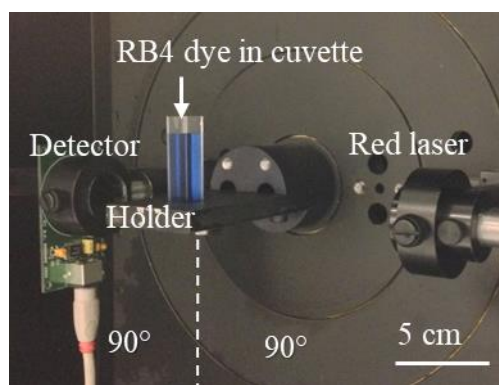
Figure 2.23*: Photograph of the absorbance setup on the custom-built optical device with a cuvette placed in the holder.*

2.5.3 The volume (V) of the chitosan layer

The volume (V) of the chitosan layer can be obtained by measuring thickness I of the chitosan film times the illuminated area A_{il} on the chitosan film during the absorbance measurements.

The thickness of the chitosan film was measured using a white light interferometer (WLI) (Wyko NT1100, Veeco, USA). The WLI can visualise a surface area and the height of any steps on the surface imaged can be quantified. WIL is an optical device that utilises a broadband white light source to illuminate an interferometer. Light interference happens when there is a variation in the distance travelled by the light reflected from the surface to a certain point. WLI utilised this phenomenon to measure the surface roughness of a sample. The incident light is separated by a splitter into two beams known as reference and measurement beams. The reference beam is reflected by the reference mirror while the measurement beam is reflected from the film surface[132]. The returning beams are then recombined to generate bright and dark bands called fringes in the CCD camera. The distance from CCD camera to the reference mirror and from the CCD camera to the sample surface are the same. The roughness of the film causes the optical path length to be unequal resulting in constructive and destructive interference known as interference pattern. The number of lines in the pattern is converted into peaks and troughs where they can be used to estimate the thickness of the film.

Chitosan solutions were made at concentrations of 1%, 1.5% and 2% (w/v) and spun at 3,000 rpm for 30 s onto cleaned glass substrates that were half covered with a piece of masking tape. To obtain the thickness of dry chitosan films, the coated slides were left on the bench to dry totally at room temperature before removing the masking tape. Finally, they were transferred to the WLI instrument and the measurement was taken by a member of staff in the Physics Department. For measurements of wet chitosan films, the slides were kept in a petri dish with deionized water prior to measurement.

The thicknesses of all chitosan films were taken as an average of three readings from three different locations in each chitosan film. For dried film, the measurement was at 87 nm, 116 nm and 137 nm for the films of 1%, 1.5% and 2% respectively. A significant rise in the thickness was seen for the wet chitosan film shown 500 nm, 900 nm and 1300 nm for the films of 1%, 1.5% and 2% respectively. This could be due to the swelling of chitosan film during the incubation with de-ionised water prior to measurement.
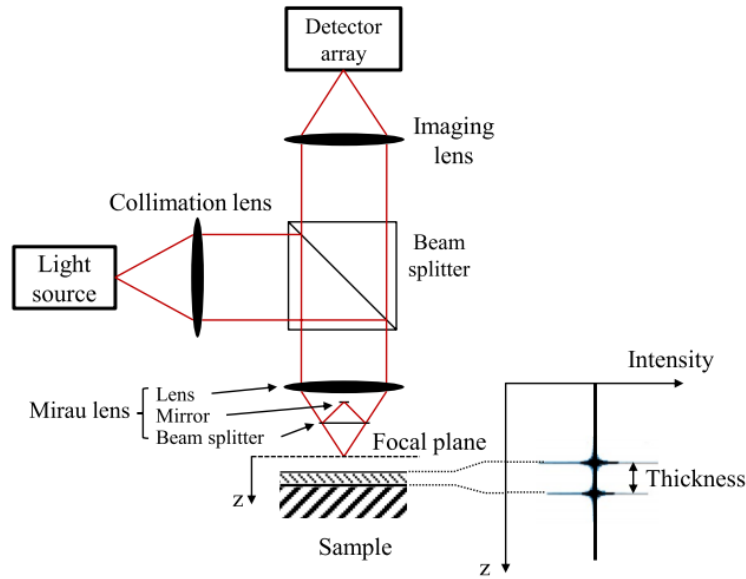
Figure 2.24 *Schematic diagram of a white-light scanning interferometer[133].*

The area (A_{il}) of incident light on the chitosan film during the absorbance measurement was estimated to be 1.2 x10^{-5} m^2 by taken the width and the length of the laser spot light on chitosan coated chip as shown in the figure 2.25.
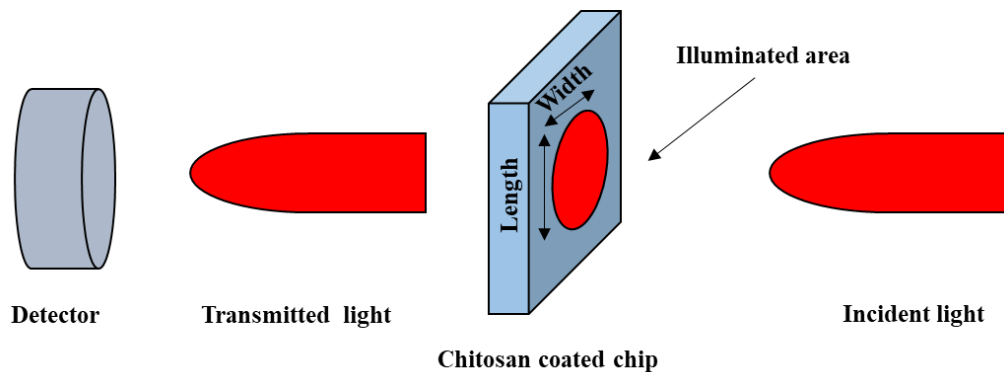
Figure 2.25 *Schematic diagram of illumination a chitosan coated chip with a laser light followed by calculating the area of incident light by taken the width and the length of the laser spot light.*

2.6 Sensitivity of chitosan waveguide to changes in refractive index

Quantitative measurements using the DDLW concept relies on change in refractive index (section 2.2.1). The sensitivity to change in refractive index for a range of dye-doped leaky chitosan waveguides were investigated, including effect of different amounts of RB4 dye present in the waveguide, the type of flushing buffer used and the porosity of the film.

2.6.1 Incubation time with RB4 dye

Glycerol was utilised to provide solutions with known values of refractive index. First, a 2% (w/v) chitosan solution was coated on several cleaned glass slides at 3,000 rpm. After drying, the coated slides were incubated with RB4 solution (100 µM). Each slide was immersed in the incubation bath (petri dish) for 10 min, 30 min, 60 min, 120 min or 200 min before being washed with de-ionised water. Subsequently, the slides were dried on the bench at room temperature and then inserted into the flow cell (design one) and mounted on the prism. A series of solutions of glycerol of known refractive index were made in de-ionised water. First, a stock solution was prepared by making up 5 mL concentrated glycerol (Product number; 24387; VWR PROLABO, UK) to 50 mL with de-ionised water giving a concentration of 10% (v/v). A series of concentrations were then made ranging from 0.5% to 7.5 % (v/v) in de-ionised water. The refractive index of each of these glycerol solutions was measured using a refractometer (M 46.317, Hilger & Watts, UK). Each glycerol solution was then pumped through the flow cell using the peristaltic pump at a flow rate of 250 µL min^{-1} (Figure 2.19) on each slide. The shift in dip was recorded as a function of time (see section 2.2.2). Measurements were repeated three times using three different chitosan slides for each incubation time (10 min, 30 min, 60 min, 120 min and 200 min).

2.6.2 Effect of buffer type

The effect of changing from a PBS to a HEPES buffer was investigated. These buffers were selected because they are commonly employed in biological research. Chitosan coated slides were incubated with RB4 dye (100 µM) for 10 min. Phosphate buffer saline (PBS) was prepared by dissolving one tablet of PBS into 200 mL of de-ionised water. HEPES buffer (4-(2-hydroxyethyl)-1-piperazineethanesulfonic acid) was made at a concentration of 100 mM by dissolving 23.83 g into 1 L of de-ionised water. The pH was adjusted to pH 7.4 by adding NaOH (1 M).

Stock solutions of glycerol (10% v/v) were prepared both in PBS buffer and HEPES buffer. A dilution series was then made up ranging from 0.5% to 7.5 % (v:v) in each buffer. The refractive index of each solution of glycerol in the two buffers was measured with a refractometer (M 46.317, Hilger & Watts, UK). After inserting a chitosan coated slide into a flow cell (design one), the glycerol solutions were pumped through the flow cell at a flow rate of 250 µL min^{-1} and the shift in dip was recorded as a function of time. This was repeated once for each buffer used.

2.6.3 Investigation of chitosan film porosity

The porosity of the film is an important factor for the sensitivity of the DDLW system as it affects how successfully bio-recognition molecules and sample components can penetrate the volume of the waveguide. To examine the film porosity, a selection of compounds with different molecular weights was employed. A model compound for small molecules, i.e. glycerol (M_w = 92 g mol^{-1}) and model compounds for large molecules, i.e. polyethylene glycerol (PEG) (M_w = 10 - 200 kDa), polyethylene oxide (PEO) (M_w = 400 kDa), all featuring the same refractive index value, were pumped through a waveguide flow cell and the shift in dip position was monitored as a function of time.

Glycerol solutions were prepared with different molecular weights of PEG (10 kDa to 40 kDa) and of PEO (100 kDa to 400 kDa) in the PBS buffer. All solutions were made at the same refractive index. This was accomplished by using equation 2.5.

$$X = \frac{C-B}{A-B}$$
Equation 2.5

where **A** represents the initial refractive index of the solution, while **B** is the refractive index of the buffer used (PBS) and **C** is the required value of refractive index. **X** is the volume in mL that needs to be taken from the initial solution (**A**) and be diluted with the buffer used (**B**), in total 1 mL.

Waveguide coated slides were obtained from a 2% chitosan solution through spin coating at 3,000 rpm for 30 s. They were incubated with RB4 (100 µM) for 10 min followed by washing with water and drying on the bench. The slides were then inserted into a flow cell of design two and the flow cell was mounted on the prism.

Glycerol solution was first pumped over the chitosan surface followed by the various PEG and PEO solutions for a period of 20 min each. PBS buffer was introduced before and after each solution for a period of 10 min. The flow rate of the pump was set at 250 µL min^{-1} and the movement of the dip was monitored as a function of time. This experiment was repeated three times using three different chitosan-coated slides.

The porosity of the chitosan hydrogel was further examined using a fluorescence technique. In this experiment bovine serum albumin labelled with fluorescein isothiocyanate isomer I (BSA-FITC) (M_w = ≈ 66 kDa) was used as an example of a large

molecule while fluorescein isothiocyanate isomer I (FITC) (M_w = 389 Da) was used as an example of a small molecule.

A chitosan solution was prepared at 2% (w/v) in 10 mL acetic acid (0.1 M). For cross-linking, 12.5µL (v:v) of glutaraldehyde (25% in H_2O, Grade I) was added to the solution and left to react for 15 min. A volume of 1 mL was then poured into a cuvette and left to dry at room temperature overnight. The dried chitosan hydrogel was then measured by a fluorimeter (Perkin Elmer LS 55 Fluorescence Spectrometer Bio Lambda 10, USA) at an excitation wavelength of λ_{ex} = 490 nm and an emission wavelength of λ_{em} = 525 nm. This was used as the blank reading. FITC and BSA-FITC were then prepared at a concentration of 0.05% (w/v) in the PBS buffer. Two mL of each solution were then pipetted into the chitosan containing cuvettes and left to incubate for 2 h. After incubation, the cuvettes were read again on the fluorimeter. Subsequently, the treated chitosan in the cuvettes was washed three times with 1 ml of PBS buffer. Finally, the washed chitosan was then measured again to investigate whether the fluorescent molecules could be removed. The reading was taken simultaneously from three cuvettes for each solution applied.

2.7 Optimisation of chitosan waveguide porosity

A range of approaches were investigated to optimise the pore size within the chitosan waveguide, which were: varying the amount of cross-linker (glutaraldehyde), trialling the use of a porogen (PEG), and varying the drying time.

2.7.1 Varying the amount of glutaraldehyde cross-linker

Chitosan solutions of 2% (w/v) were prepared in 10 mL of acetic acid (0.1 M) and left being stirred for 90 min to ensure the chitosan was fully dissolved. Glutaraldehyde (25% in H_2O, Grade I) was diluted with acetic acid (0.1 M) to obtain concentrations of 5%, 2% and 1%. A blank of 0.1 M acetic acid was also prepared. Subsequently, 12.5 µL of each glutaraldehyde solution was added to the chitosan solution and left to react for 15min. Finally, the solutions were spun onto glass slides at 3,000 rpm for 30 s.

Tris-buffer was prepared at a concentration of 10 mM by dissolving 0.302 g into 250 mL of de-ionised water. The buffer pH was adjusted to pH 7.4 by adding a few drops of HCl solution (1 M). A stock solution of RB4 dye (1 mM) was made in the same buffer by dissolving 0.038 g into 20 mL and subsequently diluting this to 100 µM. The chitosan coated glass slides were then incubated with the 100 µM RB4 dye for 10 min followed

by drying at room temperature. Finally, the slides were inserted into the flow cell design 2.

Glycerol, polyethylene glycol (PEG) and polyethylene oxide (PEO) of identical refractive index were prepared in Tris-HCl buffer (10 mM) as explained in section 2.6.3 (equation 2.4). These solutions were pumped through the flow cell at 250 µL min^{-1} and the shift in dip was recorded as a function of time.

2.7.2 Introducing a porogen (PEG)

The porosity of a hydrogel film can be increased by mixing a so-called porogen such as polyethylene glycol (PEG), into the chitosan solution. Upon obtaining a dried hydrogel, the porogen can then be extracted for example by using hot water or a high concentration of NaOH, thus leaving a hydrogel with a microporous structure[134, 135]. The pore size can be controlled by varying the concentration as well as the molecular weight of the PEG porogen.

A 2.5% (w/v) solution of chitosan was prepared by dissolving 0.375 g into 15 mL of acetic acid (0.1 M). Solutions of PEG (10 kDa and 35 kDa) were prepared by dissolving 1 g, 0.5 g, 0.334 g and 0.167 g of each polymer into 10 mL of de-ionised water giving concentrations of 10 %, 5 %, 3.34 % and 1.67% (w/v), respectively. The chitosan and PEG solutions were then mixed to yield a volume of 3 mL with ratios of 2/2, 2/1, 1/1 and 1/2. The mixed solutions were stirred for 2h. Next, 3.75 µL of glutaraldehyde (25% in H2O, Grade I) was added. After 15 min, 1 mL of each solution was pipetted into cuvettes and left to dry at room temperature overnight. The cuvettes now contained a hydrogel with embedded PEG porogen. Control cuvettes were prepared with chitosan solution (2 %) but with no polymer added.

The cuvettes were washed with NaOH (0.1 M) for 30 min to neutralise the hydrogel, followed by washing with de-ionised water to remove the NaOH. They were then immersed in a water bath at 80 °C for 8 h to extract the porogen from the hydrogel. Finally, the cuvettes were washed intensively with de-ionised water and incubated with 2 mL of BSA-FITC (0.05%) for 2 h. The fluorescence intensity was measured from each cuvette before, during and after incubation with BSA-FITC solution as described in section 2.6.3. The rationale was that the BSA-FITC would indicate the enhancement of the chitosan's porosity by the diffusion of the BSA-FITC molecules inside the gel. This can be seen by

monitoring the colour of the gel after incubation with BSA-FITC solution and subsequently by measuring the light emitted from the gel.

The above experiment was repeated with the extraction step performed using 5% and 10 % (w/v) NaOH solution for 16 h. This was followed by flushing several times with de-ionised water and subsequent incubation with 2 mL BSA-FITC (0.05%) and measurement of the fluorescence of the gels.

Experiments were also performed with higher molecular weight porogens: 35 kDa PEG and 400 kDa PEO on glass substrates. A 2.5% (w/v) chitosan solution was prepared and mixed with PEG (35 kDa) in a ratio of 2/1 (chitosan / polymer). A second solution of chitosan was prepared by dissolving 0.2 g chitosan powder and 0.1 g PEO (400 kDa) in 10 mL acetic acid (0.1 M). These solutions were spun onto glass slides at 3,000 rpm. The chitosan coated slide with 35 kDa PEG was treated with NaOH (5%) for 16 h followed by washing with de-ionised water. The slides with 400 kDa PEO were immersed in a water bath at 80 °C for 8 h followed by flushing with de-ionised water. Upon drying, the chitosan coated slides were incubated with RB4 (100 µM) for 10 min and subsequently inserted into a flow cell (design 2). Glycerol and PEG (10 kDa and 35 kDa) solutions of identical refractive index were pumped at 250 µL min^{-1} and the shift in dip was recorded as a function of time.

2.7.3 Controlling drying time of chitosan film

The spin-coated chitosan film on the glass slide was initially wet and left to dry at room temperature to obtain a uniform film. It was hypothesised that a high concentration of chitosan (2 %) in the film would lead to a fairly 'dense' film, which would influence the film's porosity. Furthermore, the wet film was porous, the pore size would gradually decrease during drying. Therefore, a series of experiments was carried out to investigate the effect of different drying times on the waveguide film. These were carried out at relatively low concentrations of chitosan. The films were characterised by measuring reflectivity curves and comparing the resonance angle (dip). This was followed by monitoring the shift in dip upon applying glycerol and PEG solutions with different molecular weights but with identical refractive index.

Chitosan solutions were prepared at 0.5%, 1% and 1.5% (w/v) in 10 mL of acetic acid (0.1 M). The 1% solution was spin coated onto several glass slides at 900 rpm for 30 s. The slides were left to dry at room temperature for 1 min, 2 min, 3 min, 4 min, 5 min or

10 min before incubation with HEPES buffer (100 mM) for 10 min. The same 1 % solution was also coated onto glass slides at various speeds, 500, 700, 1000, 1100 and 1500 rpm for 30 s, and the films obtained were left to dry for 3 min before incubation with HEPES buffer. Finally, chitosan solutions of 0.5% and 1.5% were spun at 900 rpm followed by 3 min drying time.

Dye solution (RB4) was made in the same buffer at a concentration of 100 µM (v/v). All coated chitosan slides were then immersed in the RB4 dye solution for 5 min followed by washing with de-ionised water. Upon drying, the coated slides were mounted on the prism (Figure 2.3) followed by adding a few drops of water on top. Subsequently, reflectivity curves were measured between 55° and 75°.

The conditions rendering a film with a sharp single dip in the reflectivity curve were selected and all chitosan films in the following sections were made at these conditions. These conditions were 1% (w/v) chitosan concentration spun at 900 rpm for 30 s and then left to dry at room temperature for 3 min.

2.8 Characterisation of the chitosan waveguide

2.8.1 Sensitivity of chitosan film to changes in refractive index

The sensitivity of the waveguide to changes in refractive index was examined using glycerol solutions with known values of refractive index. A 10 % (v/v) stock solution of glycerol was first prepared in HEPES buffer (100 mM, pH 7.4). A series of dilutions were then made up in the same buffer to obtain concentrations in range of 0.5 % to 7.5 %. The refractive index of each solution was measured using a refractometer (M 46.317, Hilger & Watts, UK). Chitosan coated substrates were then prepared with the above conditions, (1% chitosan solution spun at 900 rpm for 30 s). After drying for 3 min, the slides were incubated with HEPES buffer (100 mM) for 10 min and subsequently with RB4 (100 µM) dye for 5 min. At the end, the coated slide was inserted into a flow cell (design 2) and mounted on the prism. Glycerol solutions were pumped through the channel sequentially starting from 0.5% to 10 % at a flow rate of 250 µL min^{-1}. The position of the dip was measured as a function of time. HEPES buffer (100 mM, pH 7.4) was introduced at the beginning and at the end of the experiment to return the dip to its baseline position. The experiment was carried out three times using three different chitosan-coated substrates (n = 3).

2.8.2 Characterisation of chitosan porosity

Chitosan coated substrates were prepared with the optimised conditions (1% solution spun at 900 rpm for 30 s). After drying for 3 min, the slides were incubated with HEPES buffer (100 mM) for 10 min and subsequently with RB4 dye (100 µM) for 5 min. Glycerol, PEG (10 kDa, 35 kDa and 40 kDa) as well as PEO (100 kDa, 200 kDa and 400 kDa) were made up in HEPES buffer (100 mM) to the same refractive index as explained in section 2.6.3 (equation 2.4). All solutions were pumped through the flow cell (design 2) at a flow rate of 250 µL min^{-1} and the shift in dip was measured as a function of time. This experiment was carried out three times using three chitosan coated slides (n = 3).

2.8.3 Investigating cross-linking of the chitosan film

The porosity of the chitosan film was further investigated using a cross-linker: O,O′ - Bis[2-(N-Succinimidyl-succinylamino)ethyl] polyethylene glycol (NHS-PEG-NHS). This cross-linker was obtained with different molecular weights (500 Da, 2 kDa, 3 kDa and 10 kDa). NHS-PEG-NHS solutions of 1 mM were prepared in the HEPES buffer (100 mM). Chitosan films were prepared in optimum conditions (1 % chitosan spun at 900 rpm for 30 s). After the chitosan film had been dried for 3 min, a few droplets of cross-linker solutions were added on top of each film and left to incubate for 5 min. This was followed by transferring the slides into an incubation bath of HEPES buffer (100 mM) for 10 min and subsequently into RB4 dye (100 µM) for 5 min. Finally, the slides were inserted into a flow cell (design 2) followed by introducing glycerol, PEG (10 kDa, 35 kDa and 40 kDa) and PEO (100 kDa, 200 kDa and 400 kDa) solutions sequentially at a flow rate of 250 µL min^{-1}. The shift in dip was recorded as a function of time.

2.8.4 Effect of pH on cross-linked and non-cross-linked film

The effect of pH on the cross-linked and non cross-linked chitosan films was studied by applying HEPES buffer at different pH values ranging from 4.4 to 8.4. The buffer solutions were prepared by dissolving 23.83 g of HEPES into 1 L of de-ionised water. The pH was then adjusted to 8.4, 7.4, 5.4 and 4.4 using 1 M NaOH or HCl solutions. This was verified with a pH meter (HI 2210, Hanna Instruments, UK). Chitosan films spun onto glass slides were cross-linked with 1 mM of NHS-PEG-NHS (3 kDa) as described in section 2.8.3. A control slide was prepared using a chitosan film without a cross-linker applied. All chitosan slides were then incubated with HEPES buffer (100 mM, pH 7.4) for 10 min and in RB4 dye (100 µM) for 5 min. Finally, they were inserted into a flow cell (design 2), followed by pumping the different HEPES buffers, starting from pH 8.4

down to pH 4.4, at a flow rate of 250 µL min⁻¹. HEPES buffer at pH 7.4 was introduced before and after each pH applied. The shift in dip was recorded as a function of time.

2.8.5 Effect of buffer ionic strength on chitosan film

The binding of aptamers to analytes is usually performed in a high ionic strength buffer as this enhances folding of the aptamer into its target. Therefore an experiment was conducted to examine the effect of buffer ionic strength on the chitosan waveguide layer. For this experiment, oligo 1 (table 2.2) and bovine serum albumin (BSA) were used as they both possess a negative charge at pH 7.4 whereas the chitosan layers feature a positive charge at this pH.

Initially, four buffers were prepared, namely (i) a conventional 100 mM HEPES buffer, (ii) a HEPES buffer with additional salts, (iii) a buffer prepared from Tris salts and (iv) a buffer prepared from TE salts. These are detailed in table 2.4. The HEPES buffer was prepared as explained in section 2.6.2. The HEPES buffer with additional salts and the Tris buffer with additional salts were prepared by dissolving 11.915 g of HEPES and 1.2115 g of Tris, respectively, into 500 mL of de-ionised water. This was followed by adding 2.92 g of NaCl, 0.09g of $MgCl_2$, 0.18 g of KCl and 0.07 g of $CaCl_2$ into each buffer. NaOH (1 M) and HCl (1 M) solutions were then used to adjust the pH to 7.4 for the HEPES and Tris buffers. The TE buffer was purchased already containing Tris (10 mM) and EDTA (1mM) at pH 7.5-8. To 10 mL of this buffer, 0.058 g of NaCl were added.

Table 2.4 List of buffers used in this section with type of salts being added

Buffers	Contents
HEPES buffer	Only HEPES (100 mM, pH 7.4)
HEPES salts buffer	HEPES (100 mM) NaCl (100 mM), KCl (5 mM), $MgCl_2$ (2 mM) and $CaCl_2$ (1 mM) (pH 7.4)
Tris salts buffer	Tris-HCl (20 mM), NaCl (100 mM), KCl (5 mM), $MgCl_2$ (2 mM) and $CaCl_2$ (1 mM) (pH 7.4)
TE salts buffer	Tris-HCl (10 mM), NaCl (100 mM) and EDTA (1 mM) (pH 7.5-8)

A stock solution of oligo 1 was first made by adding 685.9 µL to the commercial TE buffer (with 10 mM Tris and 1 mM EDTA, pH 7.5-8) into a tube to obtain a concentration of 200 µM as instructed by the supplier. Oligo 1 solution was then diluted to a

concentration of 0.5 µM in three buffers; HEPES buffer, Tris salts buffer and TE salts buffer. Bovine serum albumin (BSA) was made up in two buffers; HEPES buffer and HEPES salts buffer; at a concentration of 0.5% w/v by dissolving 0.025 g into 5 mL of each buffer. Chitosan coated slides were made (1% solution spun at 900 rpm for 30 s). After drying for 3 min, the slides were incubated with HEPES buffer (100 mM, pH 7.4) overnight and subsequently with RB4 dye (100 µM) for 5 min. Finally, they were inserted into a flow cell (design 2). The position of the dip was recorded as a function of time.

For oligo experiments, HEPES buffer, Tris salts buffer and TE salts buffer were first flushed through the flow cell for 20 min. Each buffer experiment was performed on different chitosan substrates. Oligo 1 (0.5 µM) solution prepared in the same buffer was then introduced into the flow cell for periods between 1 h and 4 h until the dip position obtained no longer changed, i.e. the solution was at a saturated level. The time depended on the buffer used. Finally, buffer solutions were re-applied to the chitosan surface to return the dip to the baseline. All solutions were pumped at a flow rate of 250 µL min^{-1}.

For the BSA experiment, two running buffers (HEPES and HEPES salts buffer) were used on two separate chitosan substrates. This experiment was repeated three times using three chitosan slides for each buffer applied (n = 3).

2.8.6 Chitosan film characterisation with profilometer, SEM and confocal microscope

The thickness of the chitosan film was characterised under various conditions. Chitosan solutions were prepared at concentrations of 1%, 1.5% and 2% (w/v). The 1% chitosan solution was coated on glass slides at 200 rpm, 500 rpm and 900 rpm, while the 1.5% solution was spun at 300, 500 and 700 rpm. The 2% chitosan solution was deposited at 2,800, 3,000 and 3,500 rpm. All chitosan films were then left to dry at room temperature for 3 min before incubating with HEPES buffer (100 mM, pH 7.4). All coated slides were then transferred to the Physics Department on campus for thickness measurement with the Dektak profilometer (Dektak XT Bruker, UK).

The basic principle of the Dektak instrument is scanning the chitosan film with a diamond-tipped flexible stylus according to a user-programmed scan length, speed, and stylus force. This stylus is linked to a linear variable differential transformer (LVDT) which generates and processes an electrical signal that is related to surface variations of the sample. LVDT consists of a transformer and core. The transformer contains three coils; primary and two secondary coils. All are made from glass reinforced polymer. The

primary coil is located between the two secondary coils and is arranged as a hollow form around the core. The core moves freely inside the bore of the transformer. When voltage is applied on the primary coil, the resulting flux is coupled to the two secondary coils by a core leading to an equal voltage between two secondary coils. When the core moves inside the transformer, this would cause a differential voltage output which can be used to determine the amount of movement[136]. The chitosan film is initially scratched by a scalpel in order to make a measurement channel. In scanning, the stylus is moved across the channel leading to the differential voltage output due to the core position in the LVDT being moved. The LVDT produces an analog signal proportional to the position change. This signal is then converted into a digital format which can be used through a software program to determine the thickness of the chitosan film in nm[137].

Figure 2.26 shows the thickness profile of the chitosan film after scanning. The film was produced at a concentration of 1% with a deposition spin speed of 900 rpm and with 3 min drying time. From the figure, a clear reduction was observed once the stylus crossed the scratched channel showing the thickness of the film to be 100 nm. The thicknesses of all prepared chitosan films at various deposition speeds are displayed in table 2.5. Each film was scanned three times from three different locations on the scratched channel. The scan duration was 10 seconds while the scan length was in the range of 1mm.
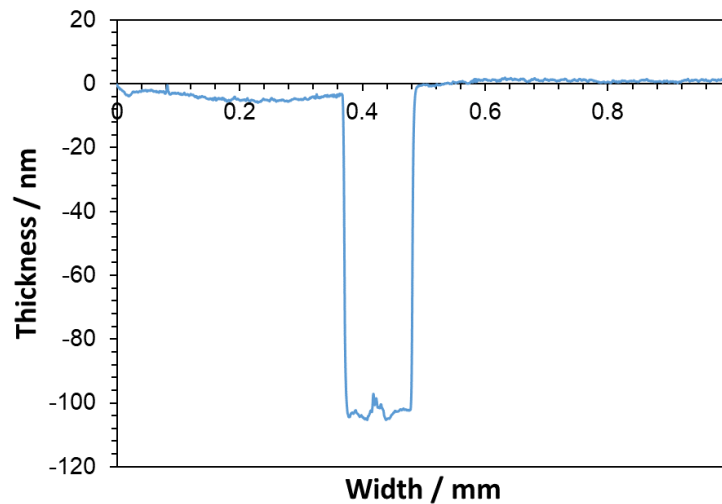
Figure 2.26 *Surface profile of chitosan film upon scanning with a flexible stylus in the Dektak instrument for a distance of 1 mm. The film was made at a concentration of 1% (w/v) with coating spin speed of 900 rpm and with 3 min drying time. The film was then scratched by a scalpel to generate a measurement channel.*

Table 2.5 Thicknesses of all films obtained at various concentrations (1%, 1.5% and 2%) and at different deposition spin speeds (rpm). All films obtained were dried at room temperature for 3 min before measuring the thickness. Each film was scanned three times from three different locations on the scratched channel.

Concentration (%)	Deposition speeds (rpm)	Thickness (nm)			Average	STDEV
1	200	920	876	864	886	29
	500	665	560	531	585	70
	900	97	101	105	101	4
1.5	300	554	597	611	587	29
	700	346	341	396	361	30
	900	263	267	232	254	19
2	2800	210	207	207	208	1.7
	3000	175	168	164	169	5.5
	3400	161	164	183	169	11
	3500	152	149	154	151	2.5

The porous film was further characterized by scanning electron microscope (SEM) (Model EVO 60, Carl Zeiss). A 1% chitosan solution was made up and spun at 900 rpm on cleaned glass slides. The film was left to dry at different times starting from 1 min up to 10 min, followed by incubation with a HEPES buffer (100 mM, pH 7.4). All coated slides were transferred to a different building on campus for SEM measurement. Before measurement, all films were coated with a thin carbon film using a Vacuum Coating machine (Model E12 series, Edwards High Vacuum). Electrons were then emitted from a metallic filament at the top of the microscope (Figure 2.27 a) to obtain a beam (Figure 2.27 b). The beam was then focused onto coated chitosan film by a series of electromagnetic lenses (Figure 2.27 c-d). Upon irradiating the film with an electron beam, the electrons are scattered from the surface leading to generate secondary electrons. These secondary electrons are then collected via the detector provided (Figure 2.27 g) where they were then amplified. The amplified signal was then transferred to the monitor (Figure 2.27 h) where the data is analysed to provide information about the morphology of the film[138]. The entire process occurs in a vacuum to prevent the electrons from interacting with the air. These processes were carried out by a technician (Dr Sinclair).
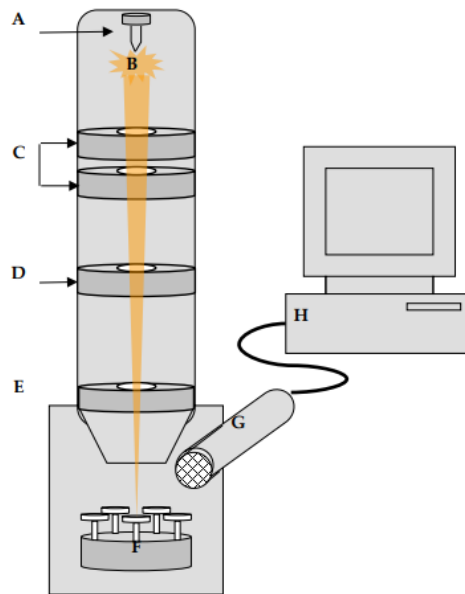
Figure 2.27 *Diagram of scanning electron microscope (SEM). Electrons are produced at metallic filament at (A) and are formed as a beam at the location (B). The beam is then focused onto the sample (F) by a series of electromagnetic lenses (C–E). The scattered electrons from the surface are captured by the detector (G) and finally transferred to a monitor (H)[138].*

Confocal microscopy (Zeiss/ LSM 710) was carried out on films stained with FITC. The basic configuration of the confocal microscopy is shown in figure 2.28. A coherent light produced by the laser system (excitation source) is passed via a pinhole aperture that is located in a conjugate plane (confocal). The laser light is then reflected by a dichromatic mirror where it is then guided towards the sample in a defined focal plane. The fluorescence emitted lights are then transferred back through a dichromatic mirror and are then focused as a confocal point by a second pinhole aperture located in front of the detector (a photomultiplier tube) as shown in figure 2.28. The fluorescence emission lights that are obtained at point above or below the objective focal plane are rejected by the second pinhole aperture and hence permits the light of focussed points to be passed to the detector[139].
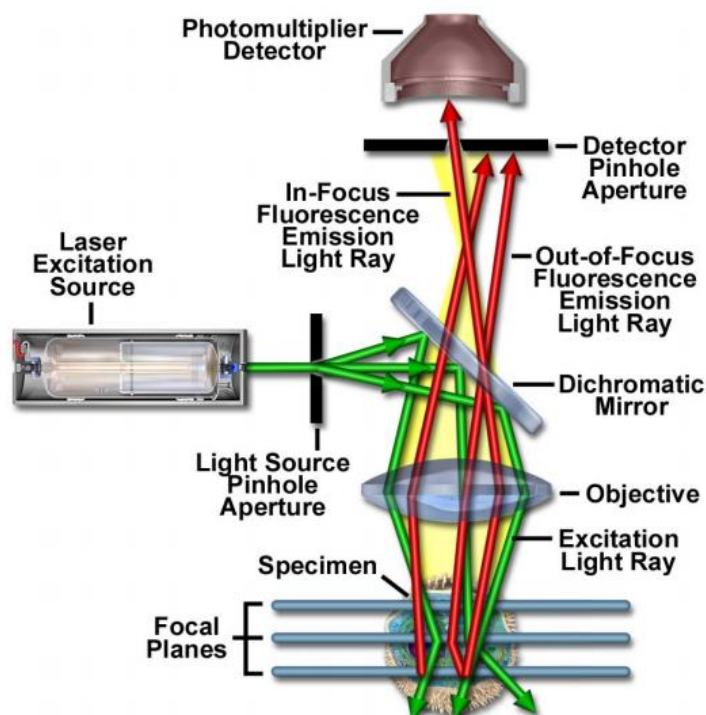
Figure 2.28 *Schematic of a laser scanning confocal microscope[139].*

The FITC solution was prepared at 3 µM in the HEPES buffer (100 mM, pH 7.4). A 1% chitosan solution was spun at 900 rpm onto cover slips, left to dry at room temperature for 3 min and then incubated with HEPES buffer for 10 min. A few drops of FITC solution were added on the top of each film and left for 2 h to incubate. Next, the cover slips were washed with HEPES buffer and subsequently sealed to a glass slide with dimensions of 25 mm x 75 mm using epoxy glue. Finally, the glass slides were placed on the confocal microscope and the images of the surface were taken at excitation of 490 nm and emission of 525 nm and at the objective of 63 times. The measurements were carried out by a technician (Dr Kemp).

The obtained images were then analysed using ZEN lite software (downloaded from Zeiss, UK[129]). The software automatically recognises the images taken by Confocal microscopy (Zeiss/ LSM 710) as both; the instrument and the software; are produced from the same company. The software automatically generates the scale bar for each image taken and based on this, the pore size on each chitosan film was then calculated by drawing a straight line over the pore of the film from the software menu. For each chitosan coated chip, ten measurements were taken from different locations.

2.9 Immobilisation of streptavidin onto chitosan film

Streptavidin-biotin binding is commonly used to immobilise bio-recognition elements onto a biosensor device. Here, the intention was to attach streptavidin to the chitosan film for eventual tethering of the biotinylated aptamers. A range of approaches were compared: covalent bonding through glutaraldehyde, physical adsorption through electrostatic attraction and molecular recognition following embedding of biotin into the waveguide.

In all cases, the chitosan layer was obtained by spin coating a 1% (w/v) solution at 900 rpm, drying for 3 min, followed by overnight incubation with HEPES buffer (100 mM, pH 7.4) and subsequent treatment with 100 µM RB4 dye for 5 min. The coated glass slides were inserted into a flow cell (design 3) and mounted on the BK7 prism. Solutions were pumped through the flow cell at 118 µL min^{-1}. Changes in dip angle were measured as a function of time as described in section 2.2.2.

2.9.1 Covalent attachment (Glutaraldehyde)

Glutaraldehyde is a widely utilised cross-linker for streptavidin attachment. The immobilisation is based on creating a covalent bond between streptavidin and chitosan via aldehyde groups. In the work presented here, bovine serum albumin (BSA) was used as an example of attachment of a protein onto a chitosan waveguide by glutaraldehyde. It was also utilised to block any remaining aldehyde groups after streptavidin attachment. This binding was performed in a high ionic strength buffer (HEPES salts buffer, table 2.4) to minimise electrostatic interactions between BSA and the chitosan waveguide, as was described in section 2.8.5. Biotinylated bovine serum albumin (Biotin-BSA) and biotinylated nonspecific sequence aptamer (oligo 2, table 2.2) were utilised to verify the binding of streptavidin onto chitosan waveguide.

Solutions of BSA 0.5% (w/v), Biotin-BSA (10 µg mL^{-1}), oligo 2 (10 µM) and glutaraldehyde 0.6% (v/v) were all prepared in the HEPES salts buffer. BSA (0.5%), and glutaraldehyde (0.6%) was also prepared in the conventional HEPES buffer (100 mM, pH 7.4). Streptavidin was prepared at concentrations of 1.6 µM and 83 µM in the HEPES buffer (100 mM, pH 7.4) as shown in table 2.6.

Table 2.6 Summary of preparation of different solutions used in this section.

Solutions	Preparation
BSA (0.5%)	Dissolving 0.025 g into 5 mL of HEPES salts buffer (table 2.4)
BSA (83 µM)	Dissolving 0.027 g into 5 mL of HEPES buffer (100 mM, pH 7.4)
Biotin-BSA (10 µg/mL)	Dissolving 10 mg into 1 mL of HEPES buffer (100 mM, pH 7.4) to obtain 10 mg/mL then diluted with HEPES salts buffer (table 2.4) to 10 µg mL^{-1}
Oligo 2 (10 µM)	100 µM solution prepared in water (Molecular Biology Reagent) as per supplier instructions. Dilution in HEPES salts buffer (table 2.5) to 10 µM.
Glutaraldehyde (0.6%) in HEPES salts buffer	Diluted from stock solution (25 % in H$_2$O, Grade II) in HEPES salts buffer to 0.6% (v/v)
Glutaraldehyde (0.6%) in HEPES buffer	Diluted from stock solutions (25 % in H$_2$O, Grade II) in conventional HEPES buffer to 0.6% (v/v)
Streptavidin (1.6 µM)	Dissolving 0.1 g into 1 mL of conventional HEPES buffer (100 mM, pH 7.4)
Streptavidin (83 µM)	Dissolving 1 g into 200 µL of conventional HEPES buffer (100 mM, pH 7.4)

Solutions of chitosan (1%) were spin coated (900 rpm, 30 s) onto glass slides, left to dry for 3 min, incubated in HEPES, dyed with RB4 dye and interfaced to the flow cell (design 3). Flow cells were mounted on the BK7 prism and the shift in dip angle was recorded as a function of time.

Solutions were pumped at 118 µL min^{-1} with the peristaltic pump. Solutions that could not be prepared at large volumes, i.e. the streptavidin and some oligo solutions, were introduced into the flow cells by manual injection using a micropipette as shown in figure 2.27.

For immobilisation of BSA, a 0.5% solution in HEPES salts buffer was pumped over the chitosan waveguide until the dip was established and stable. The surface was then flushed with HEPES salts buffer to return the dip to its original baseline, hence removing the BSA molecules. This step was performed in order to ensure that the BSA molecules were not

permanently adsorbed onto the chitosan waveguide. This was followed by introducing glutaraldehyde (0.6%) for 1 h. Unbound glutaraldehyde was then washed away with HEPES salts buffer. Next, BSA solution (0.5%) was reapplied to attach the BSA molecules to the chitosan waveguide via glutaraldehyde. Finally, unbound BSA was washed away with HEPES salts buffer. This experiment was carried out three times using three separate chitosan waveguides (n = 3).

For immobilisation of streptavidin, the chitosan was first treated with glutaraldehyde in conventional HEPES buffer (100 mM, pH 7.4) for 1 h followed by washing with the same buffer to remove unbound glutaraldehyde. Next, the peristaltic pump was turned off and the PVC tubing was removed from the flow cell (Figure 2.29). A volume of 20 µL streptavidin solution (1.6 µM, 83 µM) was then injected manually and directly into the sample channel via crimp bootlace ferrules using a micropipette. After injection, the PVC tubing was reconnected to the flow cell while the pump was kept off for 2 h. Afterwards, the chitosan waveguide was washed with conventional HEPES buffer to remove unattached streptavidin. HEPES salts buffer was then applied followed by BSA (0.5%) in the same buffer to block any remaining glutaraldehyde molecules. Finally, biotinylated non-specific sequence aptamer (oligo 2, 10 µM) or biotinylated bovine serum albumin (Biotin-BSA, 10 µg mL^{-1}) in HEPES salts buffer was introduced until the dip was stabilised. Unbound material was washed away with HEPES salts buffer. The biotinylated non-specific sequence aptamer (oligo 1, 10 µM) was applied to the chitosan waveguide by manual injection as described above for streptavidin immobilisation.
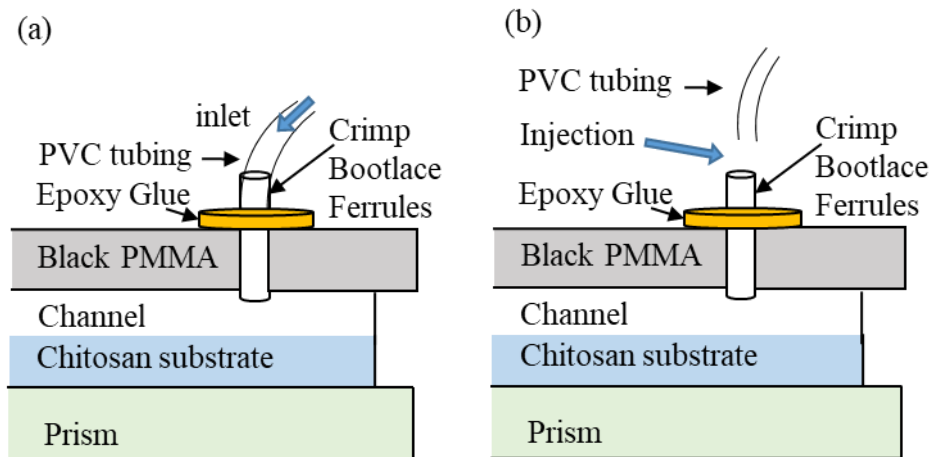
Figure 2.29*: Diagram demonstrating (a) interfacing PVC tubing into Crimp Bootlace Ferrules, (b) Removing PVC tubing from Crimp Bootlace Ferrules for manual injection of solution into a sample channel.*

A control experiment was conducted following the same procedure as above with the exception of using streptavidin molecules. After treating the chitosan waveguide with glutaraldehyde in HEPES buffer, 20 µL BSA (83 µM), the same buffer was injected manually. After 2 h, the surface was flushed with HEPES buffer to remove unattached BSA. HEPES salts buffer was then applied followed by BSA (0.5%) in the same buffer for blocking. Finally, oligo 2 (10 µM) was manually injected until no further movement of the dip was observed.

Glutaraldehyde concentrations were optimised by comparing solutions between 0.2% and 1.4% (v/v). Each concentration was introduced in a separate chitosan waveguide. After 1 h of reaction, unbound glutaraldehyde was washed with the same buffer, followed by manual injection of streptavidin (83 µM) for 2 h. The surface was then flushed with HEPES salts buffer followed by blocking with BSA (0.5%). Finally, biotinylated BSA (10 µg mL^{-1}) was immobilised until observing a stabilised signal. The optimum concentration of glutaraldehyde was considered based on the amount of streptavidin attached to the chitosan waveguide and consequently the amount of biotinylated BSA bound.

2.9.2 Electrostatic interaction

Streptavidin has a negative charge at pH 7.4, whereas chitosan possesses an opposite charge. An experiment therefore was performed to immobilise streptavidin onto the chitosan waveguide via electrostatic interactions. Here, biotinylated nonspecific sequence aptamer (oligo 2, 10 µM) was used to verify the immobilisation of streptavidin. The experimental procedure was as described in the previous section.

HEPES buffer (100 mM, pH 7.4) was first introduced until the baseline was reached. Afterwards, 20 µL streptavidin (83 µM) was manually injected. After 2 h, the pump was turned on and the surface was flushed with HEPES buffer and later on with HEPES salts buffer. Lastly, 20 µL of biotinylated aptamer (oligo 2, 10 µM) was manually injected for 2 h. This experiment was carried out three times using three chitosan waveguides (n = 3).

2.9.3 Physical adsorption (based on biotin-streptavidin affinity)

Streptavidin was attached to the chitosan waveguide through biotin-streptavidin affinity. This was accomplished by treating the waveguide in the beginning with a biotinylated cross-linker, biotin-3-sulfo-N-hydroxysuccinimide ester sodium salt (Sulfo-NHS-biotin). This was bound to the surface through NHS ester generating amide bonds with the amino group in the chitosan. This was followed by immobilisation of streptavidin to the attached biotin. Here, anti-thrombin biotinylated aptamer (oligo 3, table 2.2) was used to confirm the attachment of streptavidin.

First, solutions of Sulfo-NHS-biotin (1 mM), streptavidin (83 µM) and oligo 3 (1 µM) were prepared in HEPES buffer (100 mM, pH 7.4) and also in HEPES salts buffer as shown in table 2.7.

Table 2.7 Summary of solutions preparation used in this section.

Solutions	Preparation
Sulfo-NHS-biotin (1 mM)	Dissolving 1.33 mg into 3 mL of HEPES buffer (100 mM, pH 7.4)
Biotin-NHS (1 mM)	Dissolving 1.33 mg into 3 mL of HEPES salts buffer (table 2.5)
Streptavidin (83 µM) in HEPES buffer	Dissolving 1 g into 200 µL of HEPES buffer
Streptavidin (83 µM) in HEPES salts buffer	Dissolving 1 g into 200 µL of HEPES salts buffer
Oligo 3 (1 µM)	A volume of 1 mL of water (Molecular Biology Reagent) was added into the oligo tube to obtain 100 µM as instructed by the supplier. Dilutions were made in HEPES salts buffer to 1 µM.

Sulfo-NHS-biotin solution (1 mM) in HEPES buffer was first flushed through the chitosan waveguide for 1 h. Unbound Sulfo-NHS-biotin was removed with the same buffer before manual injection of streptavidin (83 µM). After 2 h, the chitosan waveguide was washed with HEPES buffer to remove unattached streptavidin and subsequently with HEPES salts buffer. Finally, oligo 3 solution (1 µM) was introduced through the pump at a flow rate of 118 µL min^{-1} until a stable signal was observed. The experiment was repeated by flushing the surface with Sulfo-NHS-biotin solution (1 mM) in HEPES buffer for 30 min, 10 min, 5 min and 1 min prior to streptavidin injection. Each was performed on a different chitosan waveguide.

Immobilisation of Sulfo-NHS-biotin onto the chitosan waveguide was also performed in a buffer of high ionic strength. Sulfo-NHS-biotin solution (1 mM) in HEPES salts buffer was applied for 1 h, 30 min and 10 min each on separate chitosan waveguides. Next, streptavidin (83 µM) in HEPES salts buffer was injected for 2 h. This was followed by the introduction of oligo 3 solution (1 µM) until a stable signal was observed.

2.10   Detection of Thrombin

The measurement of thrombin was performed by immobilisation of anti-thrombin aptamer onto the waveguide via streptavidin-biotin complex. The attachment of streptavidin was carried out using the glutaraldehyde method. A biotinylated nonspecific sequence aptamer (oligo 2) was utilised in order to perform a control experiment.

2.10.1 Detection of thrombin in HEPES salts buffer

First, a 100 µM stock solution of anti-thrombin biotinylated aptamer (oligo 3) was made by adding 1 mL of water (Molecular Biology Reagent) into the oligo tube as provided by the supplier. A series of dilutions in the HEPES salts buffer then followed to obtain concentrations of 0.1 µM, 0.5 µM, 1 µM, 1.5 µM and 2 µM. Human alpha thrombin was first gained from the supplier at a concentration of 10.1 mg mL^{-1} in 50% (v/v) of glycerol and water. A series of concentrations were made in the HEPES salts buffer, ranging from 1 nM to 1 µM. Glutaraldehyde (0.2% v/v) and streptavidin (83 µM) were prepared in the HEPES buffer, while oligo 3 (1 µM) and BSA (0.5% v/v) were made in HEPES salts buffer.

The chitosan waveguide was first treated with glutaraldehyde (0.2% in HEPES buffer) for 1 h followed by manual injection of streptavidin (83 µM in HEPES buffer) which was left to incubate for 2 h. Any remaining aldehydes were then blocked with BSA (0.5%) in HEPES salts buffer. This condition was used in all flowing experiments and is then called 'surface preparation' unless otherwise stated.

For thrombin measurement, oligo 3 solution (1 µM) was first introduced into the chitosan waveguide until no further movement of dip was recorded. The surface was then flushed with HEPES salts buffer to remove any unbound aptamer. This was followed by applying thrombin solution (1 µM) for 15 min at a flow rate of 118 µL min^{-1}. A control experiment was carried out by repeating the same experiment with oligo 2 (1 µM) instead of oligo 3.

The above experiment was repeated by applying a series of thrombin concentrations in HEPES salts buffer. After immobilisation of oligo 3 (1 µM), thrombin was introduced into the chitosan waveguide sequentially starting from 1 nM up to 1 µM. Each solution was flushed at a flow rate of 118 µL min^{-1}.

In order to enhance the binding of thrombin to the immobilised aptamer, thrombin was flushed through the surface overnight. Thrombin (100 nM) was pumped at a flow rate of

118 µL min^{-1} for about 4 hours. Finally, unbound thrombin was washed with running buffer.

In order to improve the binding of thrombin, different concentrations of oligo 3 were investigated. Oligo 3 solutions of 0.1 µM, 0.5 µM, 1 µM, 1.5 µM and 2 µM in HEPES salts buffer were immobilised on separate chitosan waveguides at a flow rate of 118 µL min^{-1}. Thrombin (100 nM) was flushed through the flow cell for about 4 hours. The optimum concentration of oligo 3 was considered based on the amount of thrombin bound.

Upon optimising the concertation of the oligo, a calibration curve was made at various thrombin concentrations. After surface preparation, the chitosan waveguide was flushed with oligo 3 solution (1 µM) until observing a stable signal. Thrombin (0 nM, 1 nM, 5 nM, 25 nM, 50 nM, 75 nM, and 100 nM) then followed at a flow rate of 118 µL min^{-1} for about 15 hours. Each concentration of thrombin was applied on a separate waveguide. The experiment was carried out three times using three chitosan waveguides for each concentration of thrombin (n = 3). A control experiment was conducted by applying BSA (100 nM) in HEPES salts buffer after immobilisation of oligo 3 (1 µM). The solution was run overnight at the same flow rate.

2.10.2 Detection of thrombin in a commercial human serum sample
A human serum sample was purchased in order to validate the measurement of thrombin in more realistic conditions. Thrombin was spiked at 50 nM into the undiluted serum sample by taking 9.2 µL of thrombin stock solution (27.23 µM) and diluting with serum sample to a total of 5 mL. First, Oligo 3 solution (1 µM) in HEPES salts buffer was immobilised onto the chitosan waveguide. This was followed by pumping the undiluted serum sample until a saturation level was observed. Finally, the spiked thrombin (50 nM) was introduced overnight. This experiment was repeated with diluted serum samples. The dilution was carried out with HEPES salts buffer to 10%. Thrombin was then spiked into this diluted serum sample at 50 nM.

2.11   Detection of PSA
The measurement of prostate specific antigen (PSA) was performed by immobilisation of an anti-prostate aptamer (oligo 4) onto the chitosan waveguide *via* the streptavidin-biotin reaction. A biotinylated nonspecific sequence aptamer (oligo 2) was utilised in order to perform a control experiment.

The PSA buffer (pH 7.4) used for the PSA experiments consisted of HEPES (100 mM), NaCl (150 mM), $MgCl_2$ (5 mM) and KCl (5 mM). This was prepared by dissolving 4.76 g of HEPES into 200 mL of de-ionised water. NaCl (1.75 g), $MgCl_2$ (0.095 g) and KCl (0.074 g) were then added. The pH was adjusted by adding a few drops of NaOH (1 M).

A stock solution of anti-prostate biotinylated aptamer (oligo 4) was obtained at a concentration of 200 µM by adding 0.87 mL of water (Molecular Biology Reagent) into the oligo tube as instructed by the supplier. A concentration of 1 µM was then prepared in the PSA buffer.

A stock solution of prostate specific antigen (PSA) was prepared at 2.2 mg mL^{-1}. A dilution series was then made up in the PSA buffer at 25 nM, 50 nM and 75 nM. Glutaraldehyde (0.2% v/v) and streptavidin (83 µM) were prepared in the HEPES buffer, while oligo 2 (1 µM), oligo 4 (1 µM) and BSA (0.5% v/v) were made in the PSA buffer.

The chitosan waveguide was first treated with glutaraldehyde for 1 h and then with streptavidin (83 µM) for 2 h. Unbound molecules were washed with HEPES buffer; any remaining glutaraldehyde sites were blocked with BSA. The oligo 4 solution (1 µM) was then applied until a stable signal was observed. Finally, PSA solution (75 nM) was pumped at a flow rate of 118 µL min^{-1} for about 4 hours.

In order to enhance the PSA binding, thermal treatment was carried out for the anti-prostate biotinylated aptamer using a thermal cycler PCR instrument (Techne genius). Oligo 4 solution (1 µM) was heated up to 95 °C for 10 min, then the heat was gradually reduced to 25 °C for 30 min. After the thermal treatment, oligo 4 was immobilised in the chitosan waveguide that had initially been treated with glutaraldehyde, streptavidin and BSA. The surface was then flushed with PSA buffer to remove any unbound aptamer. Finally, PSA solutions (25 nM, 50 nM and 75 nM) were introduced overnight at a flow rate of 118 µL min^{-1}. The experiment was carried out three times using three chitosan waveguides for each concentration of PSA (n = 3).

A control experiment was applied by utilising oligo 2 instead of oligo 4. Thermal treatment was also used for oligo 2. The concentration of PSA in this experiment was 50 nM.

2.12 Statistical analysis

A statistical analysis was performed in order to investigate if there is or is not a significant difference between each experiment performed on DDLW device. This is guided by a p-value in which the value above 0.05 is considered there not being significant difference between each run and in this case a null hypothesis is kept. In contrast, when the value was below 0.001, the null hypothesis is rejected and alternative hypothesis is accepted. This would indicate that there is a significant difference between each experiment in terms of the output of the fabricated device. The statistical analysis was performed using a software program named SigmaPlot and the test is called ANOVA one or two way analysis.

CHAPTER 3

Optimisation and Characterisation of Chitosan Waveguide Film

3 Optimisation and Characterisation of Chitosan Waveguide Film

A dye-doped leaky waveguide (DDLW) device was prepared by deposition of chitosan hydrogel polymer onto glass substrate followed by staining with a reactive blue 4 dye to visualise the confinement of the light. The concentration of chitosan polymer and the deposition speed were optimised in order to observe a single dip in reflectivity. The thickness of the film at various parameters was measured in both wet and dry states. Surface characterisation was carried out to calculate the availability of amino groups on the chitosan waveguide which can be utilised as a guide choice for aptamer immobilisation. The sensitivity of the chitosan waveguide to the value of the refractive index was investigated under various parameters, such as the amount of dye attached to the waveguide, the type of buffer utilised and finally the waveguide's porosity. All optimisation, characterisation and investigation experiments are discussed in depth below.

3.1 Chitosan waveguide

3.1.1 Concentration and deposition speed of chitosan waveguide

The aim of this experiment was to obtain a single waveguide mode on the DDLW device. This can be achieved by obtaining a single dip in reflectivity curve. To obtain a dip in reflectivity curve, a setup one was used which allow monitoring the intensity of reflected light as a function of incident angle. Due to dye absorption from the waveguide region, a reduction in the intensity of reflected light is then observed and thus a dip is appeared in the reflectivity curve. The optimisations were carried out by investigating various concentrations of chitosan polymer (1%, 1.5% and 2% (w/v)) deposited onto various glass substrates at various spin speeds as outlined in section 2.4. After drying, the films obtained were mounted onto a prism followed by doping with a few droplets of RB4 dye (10 µM) to visualise the confinement. The films were then scanned with a laser light between incident angles of 55° and 75° while the output was captured by a photodiode detector (OSD 100-6, Centronic, Surrey, UK) as explained in section 2.2.2. The measurement was carried out using three chitosan waveguides for each condition investigated.

As can be seen from figure 3.1, the intensity of the reflected light was very low at lower incident angles (θ) while it was sharply increased after passing the critical angle ($\theta c = 60°$). This was because of the occurrence of the total internal reflection (TIR) above the angle of 60° and thus all incident light being reflected back to the detector. At a resonance

angle (θ_r) that is above the critical angle (θc), light is confined inside the waveguide and absorbed by the dye molecules attached leading to a dip in the reflectivity. For the 1% (w/v) chitosan films in figure 3.1 (a), the dip did not appear at the resonance angle (θ_r) even though the films were deposited at various spin speeds (2000 rpm, 3000 rpm and 4000 rpm), giving different thicknesses. This was also observed for the 1.5 % (w/v) chitosan films in figure 3.1 (b) in which no dip was obtained. This would lead us to say that the conditions still do not support the waveguide mode and that might be due to the low concentrations of chitosan. A single dip was only gained with the 2% (w/v) chitosan film in figure 3.1 (c) when the solution was spun at a speed of 3000 rpm. At 4000 rpm the chitosan film was thinner, therefore cannot provide any dip. At 2000 rpm, the film was thicker, therefore, various dips were seen presenting multimode waveguides. Nevertheless, multimode waveguides are of little advantage, as it can be difficult to monitor the shift of the various dips upon changes in the refractive index. Therefore, 2% (w/v) of chitosan solution coated at a speed of 3000 rpm was considered as the optimum condition and will be used for the following section. The results in figure 3.1 represent one run for each condition applied. However, the results were similar in all three runs.
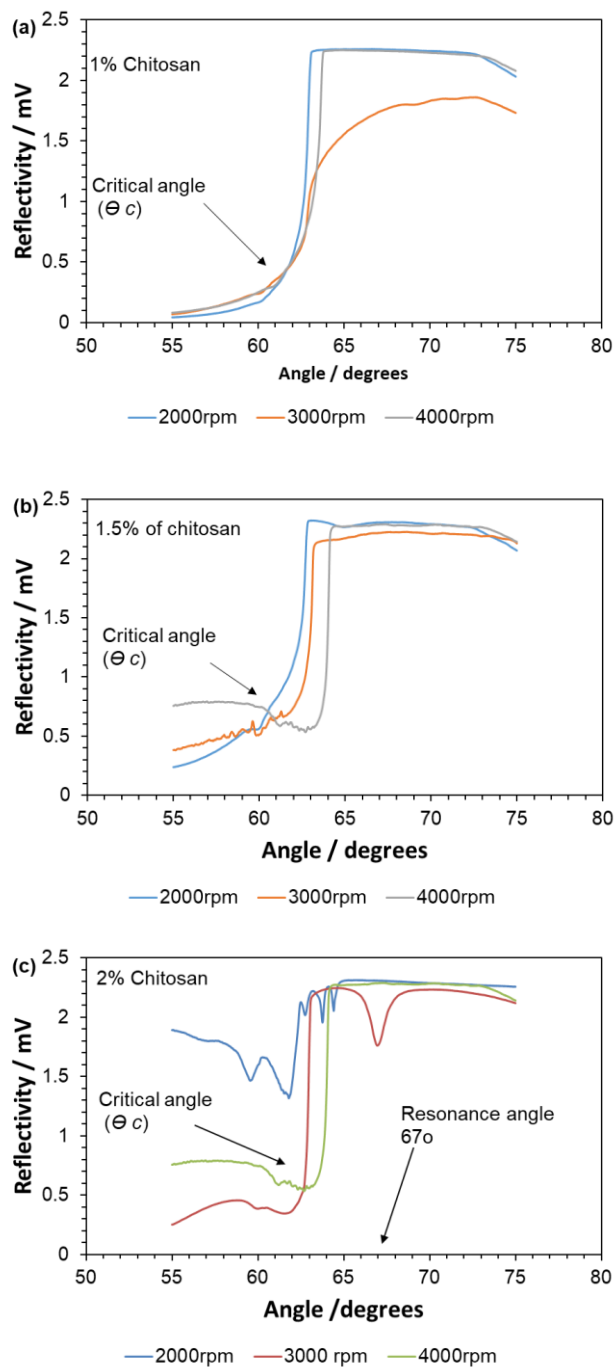
Figure 3.1 *Reflectivity curve as a function of incident angle obtained from chitosan films formed from chitosan solutions of (a) 1 %, (b) 1.5% and (c) 2% (w/v) at different spin speeds (2000 rpm, 3000 rpm and 4000 rpm) as indicated by different colours in each figure. Each film was then stained with a few droplets of 10 µM of RB4 before scanning. All chitosan coated substrates were irradiated with laser light between incident angles of 55° and 75° while the reflections were captured by a photodiode detector. The reading represents one run for each condition applied, however, the results were similar in all three runs.*

3.1.2 Effect of dye concentration on the shape of the dip

The effect of dye concentration on the shape of the dip on reflectivity was studied. Chitosan solution 2% (w/v) was coated on glass substrate at a speed of 3000 rpm. After drying, the film was inserted into a flow cell (design one) and later mounted onto a prism. Next, a series of concentrations of RB4 dye from 1.5μM to 10 μM (v/v) were applied manually and sequentially on one chitosan waveguide as described in section 2.4.4. The reflection was then measured between incident angles of 55° and 75° as explained above. The reflection was captured at each concentration applied.

Figure 3.2 (a) displays the reflection from 2% chitosan waveguide before staining with dye. As expected, no dip was observed due to no dye being attached to the waveguide. Once the surface had been flushed with RB4 dye (1.5 µM) (Figure 3.2 b), a small dip appeared at the resonance angle ($\theta r = 67°$) while the depth of the dip increased when the surface was flushed with higher concentrations of dye. This would indicate the greater absorption of light from the waveguide region. It can be seen that the more dye is attached to the chitosan waveguide, the broader dip is observed. The sharpest dip is considered to shift in angle resulting from a change in the waveguide's refractive index, with higher sensitivity by comparison to the wider and broader dip. Therefore, dye concentration needs to be optimised according to the degree of shift in angle as will be shown in section 3.3.1.
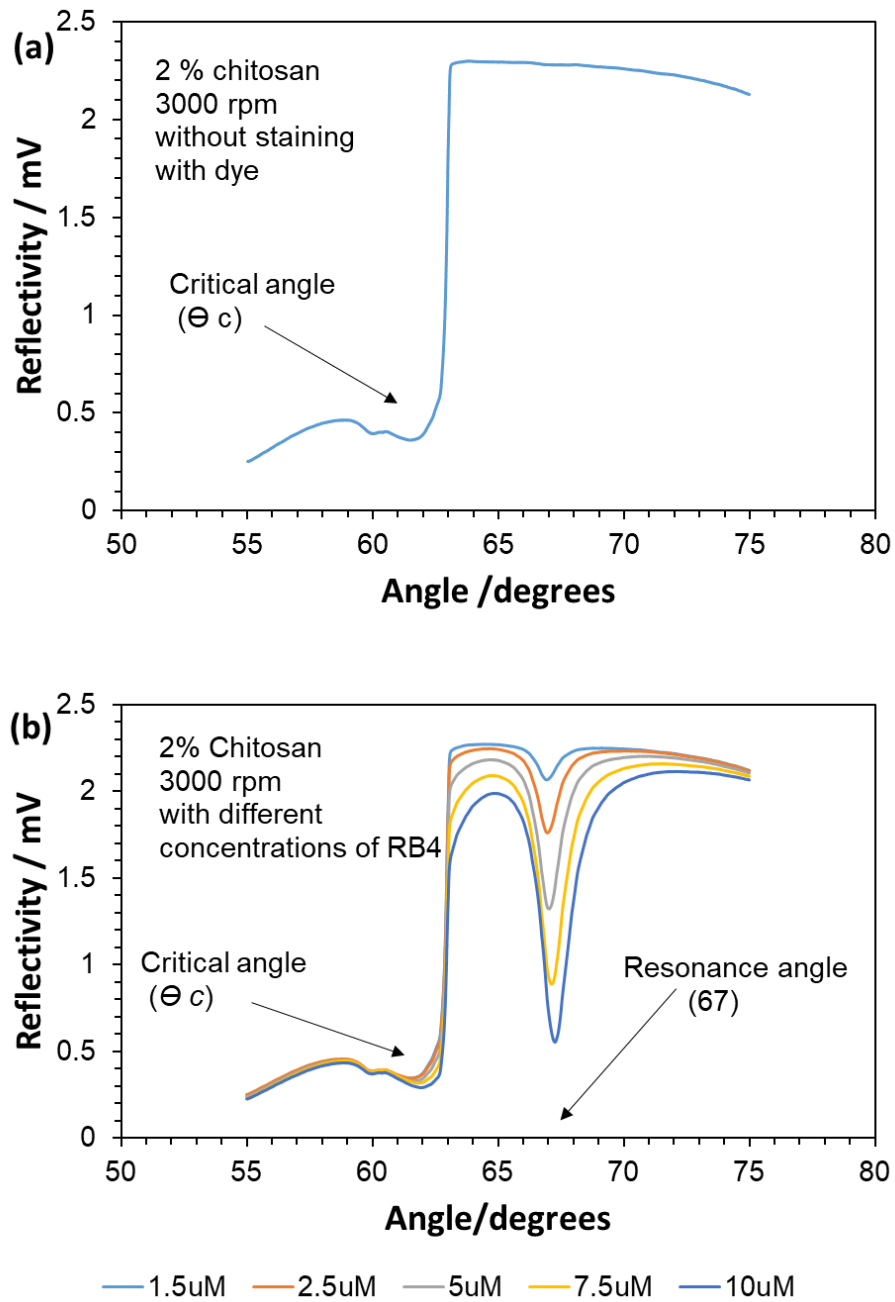
Figure 3.2 *Reflectivity curve as a function of incident angle from chitosan film obtained by deposition of 2% (w/v) chitosan solution on a glass substrate at a speed of 3,000 rpm. (a) Reflectivity curve after flushing the surface with water in the absence of RB4 dye. (b) Reflectivity curves following sequential treatments of the waveguide with RB4 solutions of increasing concentrations from 1.5 μM to 10 μM which each concentration represents a specific colour of the dip. The reflection was captured by a photodiode detector at each concentration applied. The experiment was performed one time using one chitosan waveguide.*

3.1.3   Investigation of chitosan waveguide under different pH

The impact of pH on chitosan waveguide was investigated using phosphate buffer at various pH. Chitosan waveguide was produced from chitosan solution (2% w/v) with deposition speed of 3000 rpm. Phosphate buffer solutions were then introduced into chitosan waveguide through a flow cell (design one) manually and sequentially starting from pH 10 to pH 4. Each buffer was made with 10 µM of RB4 dye as explained in section 2.4.5. The reflection was then measured at each buffer applied and between incident angles of 55° and 75° as explained above.

The reflection from the chitosan waveguide (2%) upon applying different pH is shown in figure 3.3. It can be seen that the depth of the dip gradually increased upon the introduction of buffer solutions, showing a reduction in the intensity value from 1.7 mV to 0.3 mV. This was because each buffer applied was made with10 µM of RB4 dye which led to staining the waveguide with a higher amount of dye, hence a higher absorption of light occurred. The resonance angle (θ_r) was clearly affected by pH as it was shifted from 65.5° to 67° upon the introduction of pH buffer from 10 to 4. This can be attributed to the swelling of the chitosan film in which at lower pH the surface becomes more positively charged due to protonation of amino group (NH_3^+). This results in electrostatic repulsion between the positive charges, hence changing the thickness of chitosan film. The resonance angle (θ_r) is a function of the waveguide thickness and refractive index. At higher pH, the chitosan film was shrunk due to deprotonation of amino group (NH_2) and thus less repulsion force existed. These findings were in good agreement with those of other researchers which showed that the chitosan hydrogel can be swollen and collapsed according to the pH buffer used[140, 141]. Furthermore, the alteration in the thickness of the waveguide hydrogel will result in change in the refractive index and hence in the resonance angle (θ_r) [142]. From the above data, it appears that the chitosan waveguide can be operated at a wide range of pH which could facilitate the immobilisation of bio-recognition molecules in any condition. The chitosan waveguide was further characterised in terms of the availability of the functional amino groups as shown in the following section.
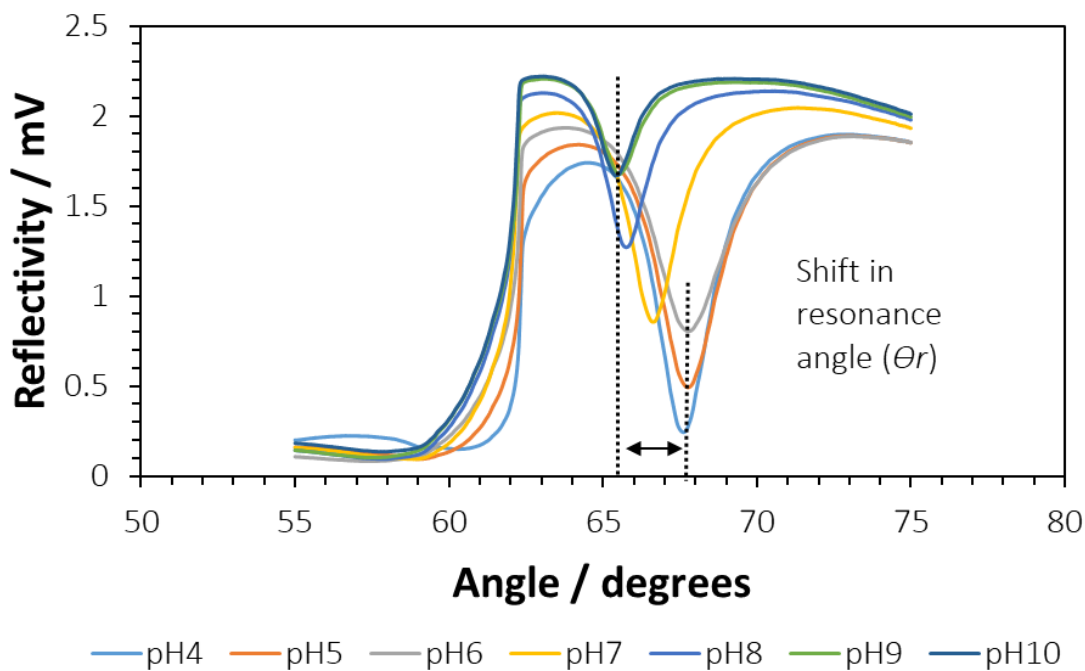
Figure 3.3 *Reflectivity curve from chitosan waveguide (2%) upon applying phosphate buffer at various pH. The waveguide was flushed manually and sequentially with buffer solutions from pH 10 down to pH 4. Each dip appeared with a specific colour represents flushing the waveguide with a specific buffer. Each buffer was made with 10 µM of RB4 dye. The reflection was captured by a photodiode detector at each buffer applied. The experiment was performed one time using one chitosan waveguide.*

3.2 Number of moles of amino groups on chitosan films

The chitosan waveguide was further characterised to estimate the availability of amino groups on the surface. This can be utilised for immobilisation of bio-recognition elements on the waveguide. The calculation is first based on the concentration of amino groups on the chitosan film and second on the volume of the film. These factors are then used in equations 2.2 and 2.3 to estimate the number of moles of amino groups as described in depth in section 2.5. In this section, the setup of the device was consisted of a red laser light (RS components, UK, λ= 650 nm power output 5 mV) and photodiode detector (OSD 100-6, Centronic, Surrey, UK) that were both fixed at incident angle of 90° as shown in figure 2.22. This was required in order to measure the transmitted light from the chitosan film and hence calculating the absorption value as explained in section 2.5.

3.2.1 Absorption spectra of dye from different chitosan films

To calculate the concentration of amino groups, the chitosan film needs first to be stained with RB4 dye until all the amino groups are occupied. This is then followed by measuring the absorbance of the attached dye which can be used later via a calibration curve provided to obtain the total concentration of amino groups on the chitosan film.

Three chitosan films were prepared at concentrations of 1%, 1.5% and 2% (w/v). All films were coated at a speed of 3000 rpm for 30 seconds. After drying, the film was then incubated with 100 µM of RB4 dye for various times. The absorbance from each chitosan film was then taken from a custom-built optical setup. The device consisted of a red laser light and photodiode detector both positioned at 90° as explained above. For gaining comparison results, the absorbance from the same film was taken also by a conventional UV/vis spectrophotometer (λ= 650 nm /model Bio Lambda 10, USA). This experiment was carried out using three chitosan films for each concentration of chitosan applied.

The absorbance of attached dye from three chitosan films (1%, 1.5% and 2%) as a function of staining time is plotted in figure 3.4 (a and b). In figure (a) the absorbance was obtained from the custom-built optical setup at wavelength of 650 nm. The absorbance of RB4 in all chitosan films increased with an increase in the incubation time. Saturation level was reached after 140 min for the films of 1% and 1.5% giving the absorbance value of 0.14 a.u. and 0.23 a.u. respectively. For 2% chitosan film, a stabilised level was reached after 200 min of incubation, showing the highest absorbance value (0.38 a.u.). These absorbance values would be expected with the higher concentration of chitosan used and the larger number of amino groups present. In figure (b), the measurement was recorded from UV/vis spectrometer at wavelength of 650 nm from the same chitosan films. The absorbance values were equivalent to those obtained from the custom-built optical setup (Figure 3.4 a) giving the absorbance values of 0.12 a.u., 0.23 a.u., and 0.37 a.u. for the films of 1%, 1.5% and 2% respectively. To calculate the concentration of amino groups on each chitosan film, a calibration curve of RB4 dye solution was made as shown in the following section.
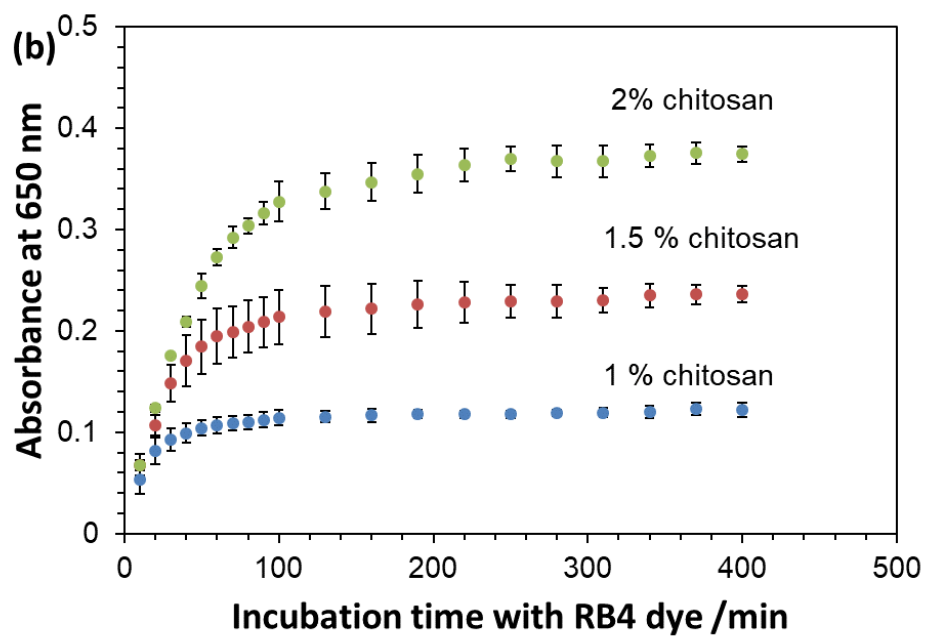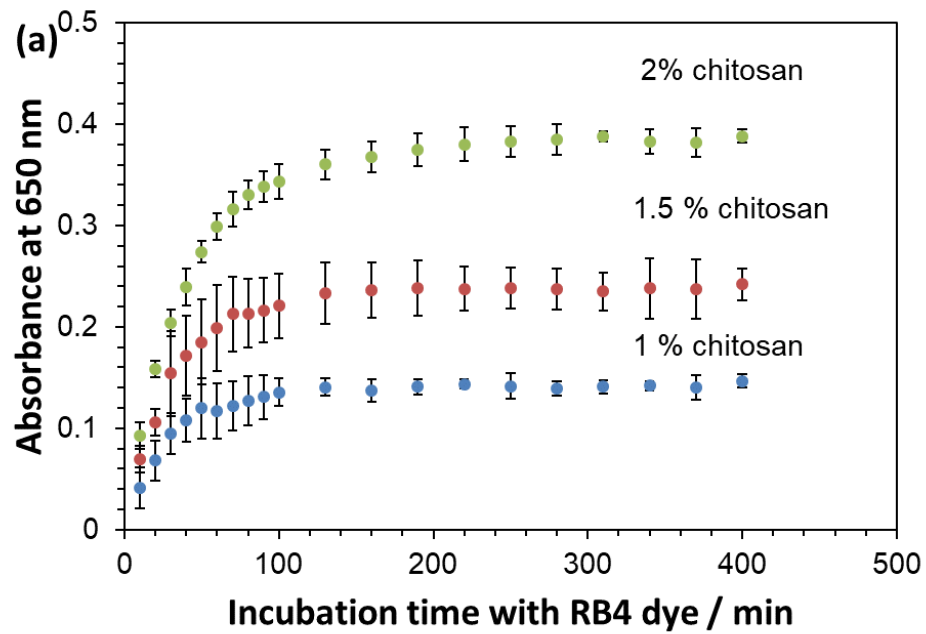
Figure 3.4 *Absorbance from different chitosan films (1 %, 1.5% and 2% (w/v)) stained with RB4 dye as a function of staining times. All devices were coated at spin speed of 3,000 rpm for 30 s. The reading was taken as the average of the three runs using three separate chitosan chips for each condition used. The measurement was performed on (a) the custom-built optical setup and (b) a conventional UV/vis spectrophotometer, both at wavelength of 650 nm.*

3.2.2 Concentration of amino group on chitosan film

A calibration curve of RB4 dye solutions was made in order to read the concentration of RB4 dye attached to chitosan film during the absorbance measurement. This corresponds to the total concentration of amino groups on each film. A series of concentrations of RB4 dye ranging from 0.1 µM to 100 µM were prepared in de-ionised water. The absorbance was then read from each solution in a cuvette using a custom-built optical setup and a UV/vis as explained in section 2.5.2.

As can be seen in figure 3.5, the absorbance of RB4 dye solutions from both spectrophotometer readers was in excellent agreement. The total concentration of RB4 dye molecules on each chitosan film is exhibited in figure 3.6. The concentration was obtained first from the absorbance measurement in figure 3.4 and then read by the calibration curve provided in figure 3.5. From figure 3.6, the concentration was found to be 15 µM, 26 µM and 43 µM for the chitosan films of 1%, 1.5% and 2% respectively, using the custom-built optical setup measurement. The results from the UV/vis were similar, giving the concentration of 13 µM, 25.5 µM and 40 µM for the chitosan films of 1%, 1.5% and 2% respectively. This was also confirmed by two way ANOVA statistical analysis which indicate that there was not significant difference in terms of the measurement of the dye concentration on chitosan films between the custom-built optical setup and the UV/vis. The p-value was 0.082 ($\geqslant$ 0.05). In contrast, it was significantly different between each concentration of chitosan films (1%, 1.5% and 2%) in terms of the amount of dye bound where the p-value was < 0.001. This would be expected as at the higher amount of the chitosan used corresponded to the higher amount of dye bound onto the film due to the higher number of amino groups on the surface. For estimating the number of moles of amino groups, a volume of each chitosan film was calculated as explained in the following section.
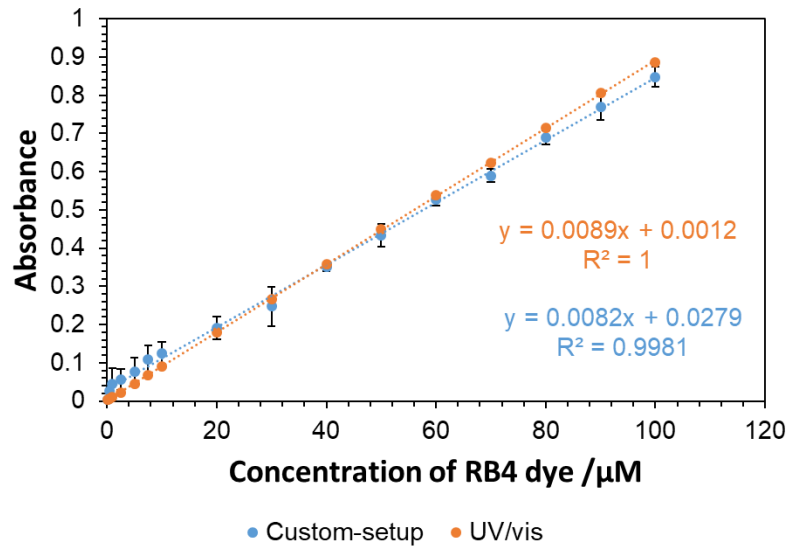
Figure 3.5 *A calibration curve of RB4 dye solutions from the custom-built optical setup and UV/vis spectrophotometry at wavelength of 650 nm. The reading is an average of three runs for each concentration measured.*
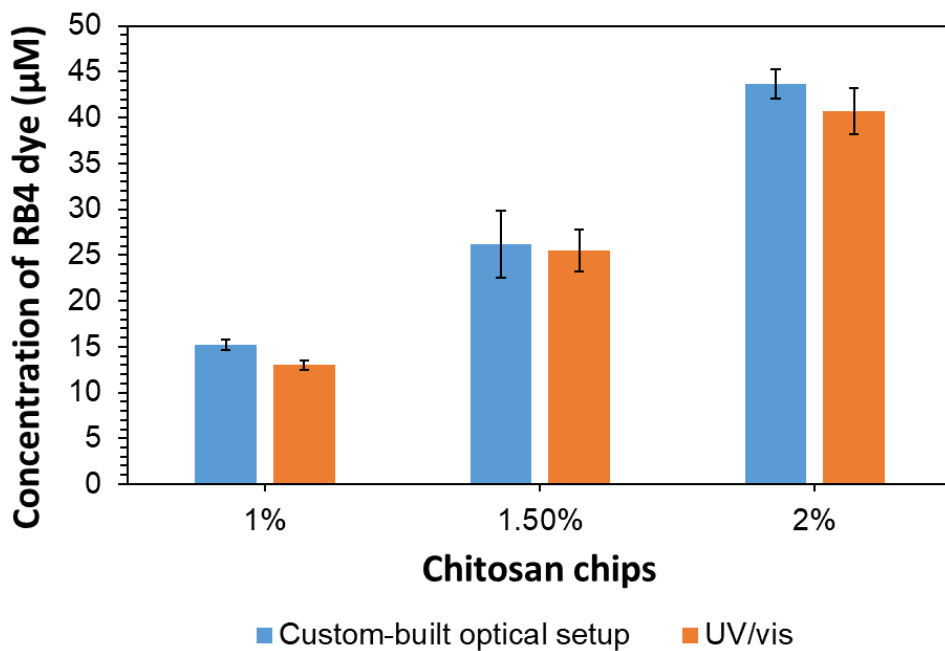
Figure 3.6 *Total concentration of RB4 dye on each chitosan film (1%, 1.5 % and 2%). The reading was taken as the average of three runs from each of three different chitosan films for each condition applied using custom-built optical setup and UV/vis. From the two way ANOVA statistical analysis, there was not significant difference between custom-built optical setup and UV/vis on the measurement of dye concentration (RB4) on the chitosan films as the p-value was 0.082 ($\geqslant$0.05).*

3.2.3   Number of moles of amino groups on chitosan film

The number of moles (N) of amino groups can be calculate based on equation 2.2 and 2.3. (C) stands for the total concentration of RB4 dye on chitosan film (Figure 3.6) which corresponds to the concentration of amino group. (V) is the volume that can be obtained from (I), the thickness of the chitosan film times (A_{il}) the area of incident light on the chitosan film during the absorbance measurement. The thicknesses of all chitosan films for dried and wet films and the estimation value of the (A_{il}) are shown in section 2.5.3.

Table 3.1 summarises the total number of amino groups found on each chitosan film (1%, 1.5% and 2%), measured either by the custom-built optical setup or by a conventional UV/vis spectrophotometer. The number of moles of amino groups was comparable in each method used giving around 9×10^{-14} mole, 2.9×10^{-13} mole and 6.8×10^{-13} mole for chitosan films of 1%, 1.5% and 2% respectively. These numbers represent the amount of available amino groups in each volume of 6.0×10^{-12} m^3, 1.1×10^{-11} m^{3}and 1.5×10^{-11} m^3 for the films of 1%, 1.5% and 2% respectively. These data can be used as a guide choice for immobilisation of bio-recognition elements onto the chitosan film.

Table 3.1 Thickness, volume, concentration of RB4 and number of moles of amino groups on each chitosan film (1%, 1.5% and 2%) measured by custom-built optical setup and by UV/vis.

Chitosan Films (coating speed 3000 rpm)	Thickness (wet film) (nm)	Volume (m^3)	RB4 concentration (Custom) (µM)/ (mole/m^3)	RB4 concentration (UV/vis) (µM)/ (mole/m^3)	Number of moles of amino groups (Custom) (mole)	Number of moles of amino groups (UV/vis) (mole)
1%	505 ± 18	6.06×10^{-12}	15 / 0.015	13 / 0.013	9.09×10^{-14}	7.87×10^{-14}
1.5%	943 ± 21	1.13×10^{-11}	26 / 0.026	25 / 0.025	2.94×10^{-13}	2.82×10^{-13}
2%	1291 ± 19	1.54×10^{-11}	44 / 0.044	40 / 0.04	6.81×10^{-13}	6.19×10^{-13}

3.3 Sensitivity of chitosan waveguide to refractive index

The measurement principle of a DDLW device is based on change in the refractive index. Therefore, the sensitivity of the chitosan waveguide to refractive index was examined under various parameters as shown below. Glycerol was utilised in this section to provide solutions with known refractive index values. It was chosen because it is relatively cheap and is not adsorbed physically into the chitosan waveguide.

3.3.1 Amount of RB4 dye attached onto chitosan waveguide

As was shown previously in figure 3.2, the amount of dye attached into the chitosan waveguide can affect the shape of the dip in reflectivity. The sharpest dip shifts in angle with higher sensitivity to the value of the refractive index than the wider and broader dip. Therefore the amount of RB4 attached to the waveguide was optimised based on the degree of shift in the resonance angle. In order to be able to monitor the shift in the resonance angle in a real-time, a setup two (section 2.2.2) was used. A chitosan waveguide was irradiated with red LED light (RCLED, PR65-F1P0T, Roithner Lasertechnik, Austria) at a fixed incident angle (65°) while the shift in resonance angle was continuously monitored by a CMOS camera (PL-B781, Pixelink, Ottawa, Canada) as a function of time as described in section 2.2.2.

Chitosan waveguides prepared at a concentration of 2% (w/v) and coated at speed of 3000 rpm were stained with RB4 dye (100 µM) for 10 min, 30 min, 60 min, 120 min and 200 min. The waveguides were then inserted into a flow cell (design 1) followed by mounted onto a prim. A series of concentrations of glycerol with known refractive values were then flushed to each waveguide using a peristaltic pump at a flow rate of 250 µL min^{-1}.

Images of the dips after staining with RB4 dye (100 µM) are shown in figure 3.7. It can be seen that the dips become wider and broader in images (b) and (c) by comparison with (a) which is sharper. This was related to the amount of dye attached to the chitosan waveguide leading to absorption of more light from the waveguide region. Incubation with dye for 120 min or 200 min did not show any clear dip as the images were totally dark.
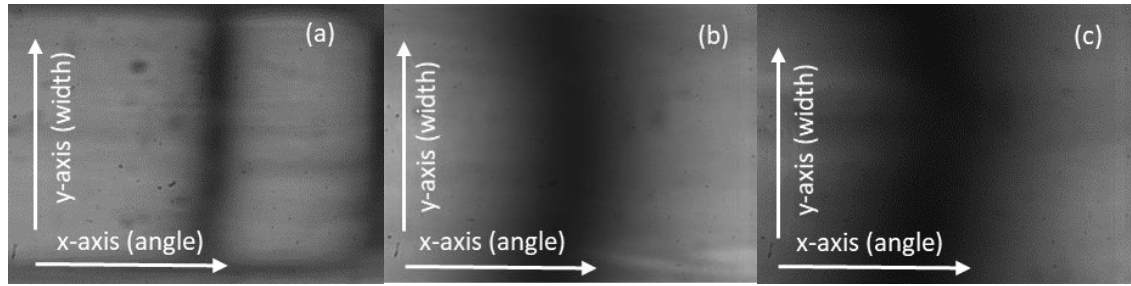
Figure 3.7 Images of dips taken by CMOS camera after staining with RB4 dye (100 μM) for (a) 10 min, (b) 30 min and (c) 60 min. Higher amount of dye present led to more light being absorbed from the waveguide, thus a wider and broader dip being given.

The refractive index of glycerol solutions is plotted in figure 3.8. The measurement was taken using a refractometer (M 46.317, Hilger & Watts, UK) as explained in section 2.6.1. A trend line was obtained between glycerol solutions indicating an increase in the refractive index value with an increase in the glycerol concentrations.
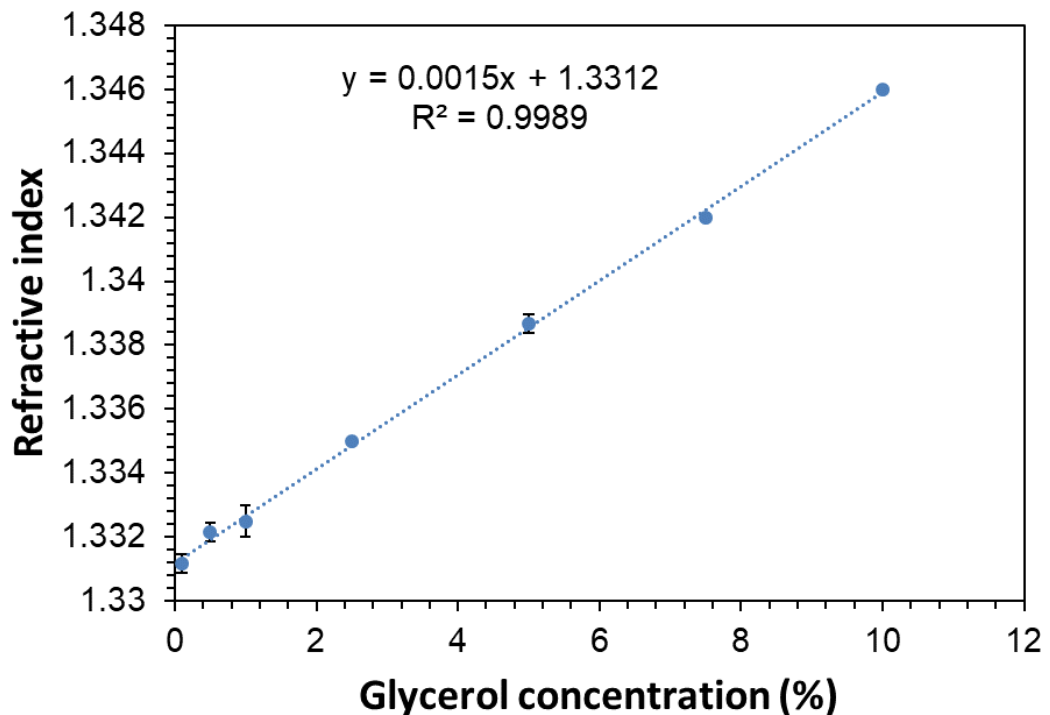
Figure 3.8 Refractive index of glycerol solutions (0.1%, 0.5%, 1%, 2.5%, 5%, 7.5% and 10 % (v/v)) prepared in de-ionised water (n = 3).

Figure 3.9 shows the shift in resonance angle as a function of time upon applying glycerol solutions into chitosan waveguide (2%). The waveguide was initially stained with RB4 dye (100 μM) for 10 min. The dip was at the baseline with water, which has a refractive

index value of 1.331. However, it gradually rose to a higher resonance angle upon gradually introducing glycerol solutions. This was because of the change in the refractive index of the waveguide. The dip reached in average 1.4° with 10% (v/v) of glycerol concentration, which has a refractive index of 1.346. This means that the dip shifted from 0° to 1.4° upon an increment in the refractive index value by 0.015, the refractive index of glycerol (10 %) (1.346) minus the refractive index of water (1.331). In order to see the impact of dye concentration, the experiment was repeated with a longer time of incubation and the findings are summarised in figure 3.10.
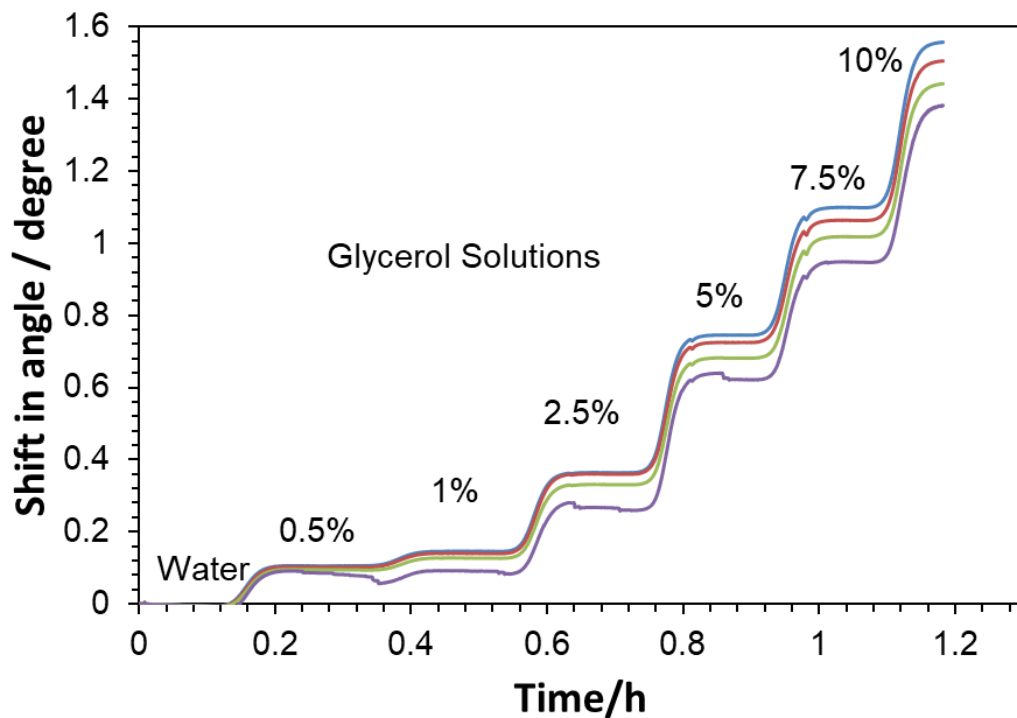
Figure 3.9 *Shift in resonance angle as a function of time upon applying glycerol solutions (0.5%, 1%, 2.5%, 5%, 7.5% and 10 % (v/v)) onto chitosan waveguide (2%). The waveguide was initially incubated with RB4 dye (100 μM) for 10 min. Glycerol solutions were all prepared in de-ionised water. The waveguide was irradiated with red LED light at a fixed incident angle (65°) while the dip movement was monitored by a CMOS camera. The experiment was performed one time using one chitosan waveguide.*

Figure 3.10 summarises the shift in resonance angle as a function of refractive index value from three chitosan waveguides (2%). The waveguides were initially stained with dye for 10, 30 or 60 min. It is clear that the waveguide was more sensitive to the refractive value when it was stained with dye for 10 min, leading the dip to be shifted with the highest

degree in resonance angle. The slope value was given at 100.6° RIU^{-1}. Incubation with dye for a longer time resulted in a lower shifting and hence a lower sensitivity was observed. The steepest slopes for 30 min and 60 min of incubation were of 93° RIU^{-1} and 62° RIU^{-1} respectively. Incubation with dye for 120 min and 200 min did not show any reliable data, due to a large amount of dye attached leading to difficulties in monitoring the dip. Therefore, 10 min was considered as the optimum time for staining with dye. A two way ANOVA statistical analysis was carried out to examine the differences between each waveguide. It was found that there was a significant difference in terms of the shift in resonance angle upon changing the incubation time of the chitosan waveguide (10min, 30 min and 60 min) as the p-value was at < 0.001. This would further confirm that amount of dye attached to the waveguide would influence the shift in resonance angle. The sensitivity of the chitosan waveguide to the refractive index was further investigated using different running buffers such as HEPES and PBS as shown below.
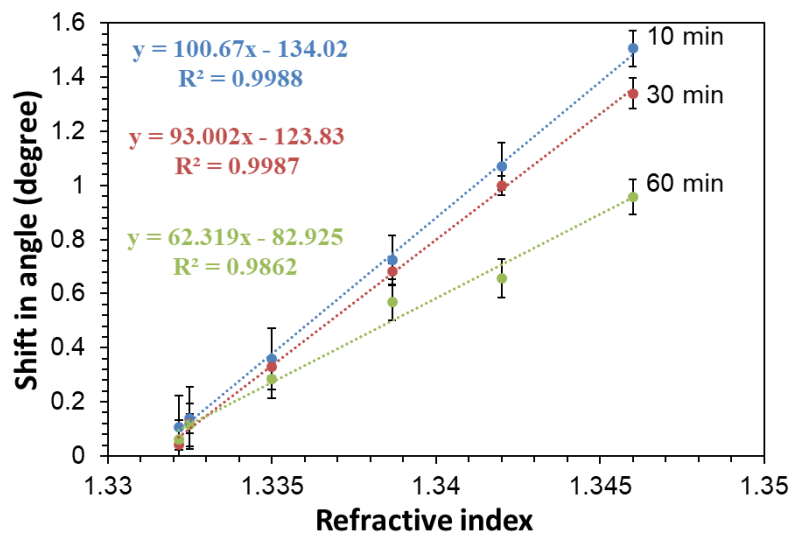
Figure 3.10 *Degree of shift in resonance angle as a function of refractive index for three chitosan waveguides (2%). The waveguides were initially incubated with RB4 dye (100 μM) for 10 min, 30 min or 60 min before applying glycerol solutions with known values of refractive index. A two way ANOVA statistical analysis indicated that there was a significant difference in terms of the shift in resonance angle between chitosan waveguides that were initially incubated with dye for 10 min, 30 min and 60 min as the p-value was at < 0.001.*

3.3.2 Effectiveness of buffers on sensitivity of the chitosan waveguide

Upon optimising the concentration of dye, the sensitivity to the value of refractive index was further investigated using different buffers. Here two types of buffers were compared, namely PBS (Phosphate buffer saline) (pH 7.4) and HEPES (4-(2-Hydroxyethyl) piperazine-1-ethanesulfonic acid) (pH 7.4). These buffers were selected because they are commonly used in biological research. Two chitosan waveguides (2%) were prepared as described in section 2.6.2. All waveguides were stained with dye for 10 min. Glycerol solutions were prepared in both buffers at concentrations ranging from 0.5% to 10% (v/v).

The refractive index of each solution of glycerol in water, in PBS and in HEPES is plotted in figure 3.11. Glycerol solutions have a higher refractive index in HEPES buffer than in PBS and in water. This can be attributed to the original concentration of buffer used: both HEPES and PBS were made in de-ionised water at concentrations of 100 mM and 10 mM respectively.
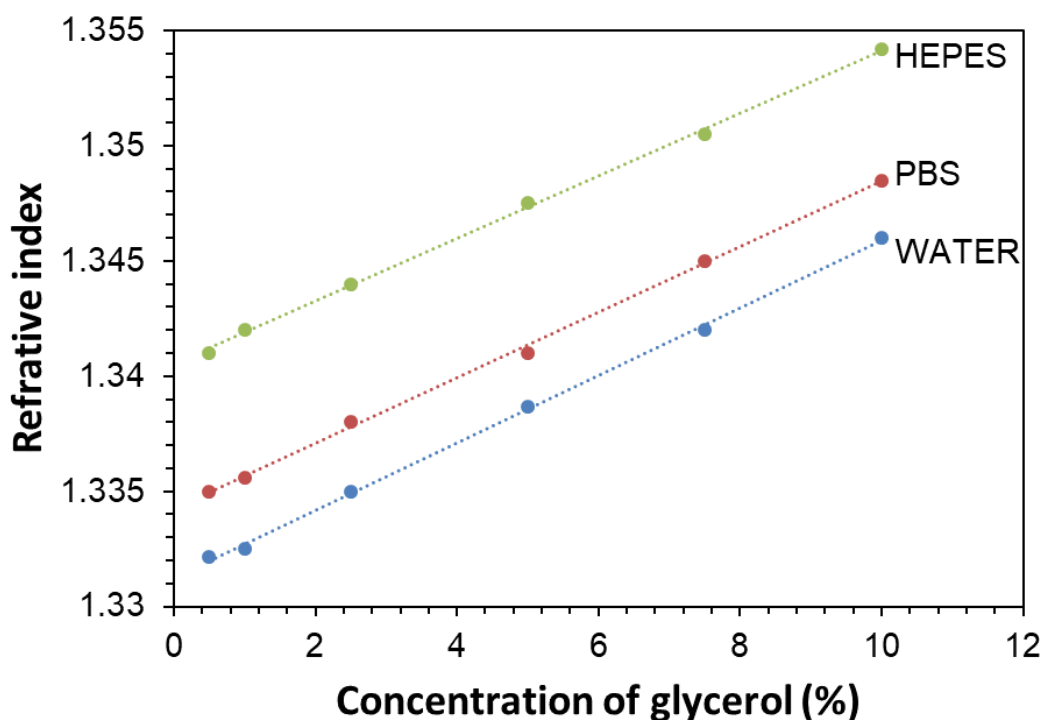
Figure 3.11 *Refractive index of glycerol solutions (0.5%, 1%, 2.5%, 5%, 7.5% and 10 % (v/v)) prepared in de-ionised water, HEPES and PBS (n = 3).*

The shift in resonance angle as a function of time upon applying glycerol solutions prepared in the PBS buffer is shown in figure 3.12. As seen previously, the higher the concentration of glycerol applied, the higher the shift in resonance angle due to the change

in the refractive index. At 10 % (v/v) of glycerol solution, which has a refractive index of 1.348, the dip moved on average to 1.4°. The refractive index of the running buffer (PBS) was 1.334 which means that the dip reached 1.4° with an increment in the refractive index value of 0.014: the refractive index of glycerol (10 %) (1.348) prepared in PBS, minus the refractive index of PBS (1.334). This was almost identical to that previously seen with 10 % (v/v) of glycerol solution prepared in water and applied into the chitosan waveguide (2%) (Figure 3.9). The dip moved by 1.4° with an increment in the refractive index of 0.015. This would indicate that the sensitivity of the waveguide to the refractive index was not changed using the PBS buffer. Further comparisons between water, PBS and HEPES are summarised in figure 3.13.
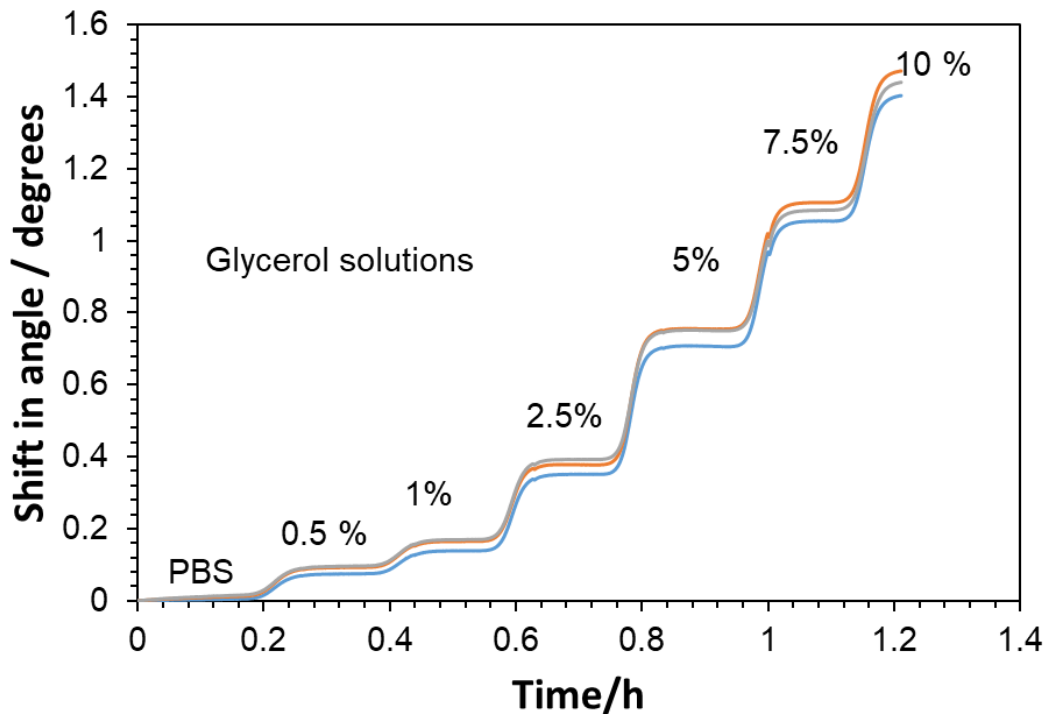
Figure 3.12 *Shift in resonance angle as a function of time upon applying glycerol solutions (0.5%, 1%, 2.5%, 5%, 7.5% and 10 % (v/v)) to the chitosan waveguide (2%). The waveguide was initially incubated with RB4 dye (100 µM) for 10 min. Glycerol solutions were all prepared in PBS buffer. The waveguide was irradiated with red LED light at a fixed incident angle (65°) while the dip movement was monitored by a CMOS camera. The experiment was performed one time using one chitosan waveguide.*

Figure 3.13 compares the water, PBS and HEPES buffers that had been utilised for glycerol preparation (0.5%, 1%, 2.5%, 5%, 7.5% and 10 % (v/v)) before flushing into

chitosan waveguide (2%). The glycerol solution in each buffer was applied in a separate chitosan waveguide (2%). Here the comparison between buffers was based on the degree of shift in resonance angle as a function of glycerol concentrations and not as a function of the refractive index value of the glycerol solutions. This is because glycerol solutions have different values of refractive index in each buffer (Figure 3.14) which would be difficult to utilise for the comparison. In figure 3.13, the dip shifted with the same degree in angle upon applying glycerol solutions made in water and PBS. Therefore, the sensitivity was identical, giving the slope value of $0.146°$ RIU^{-1}. Glycerol solutions in the HEPES buffer show an identical shift in resonance angle to glycerol in water and in PBS buffers particularly at lower concentrations (0.5%, 1%, 2.5% and 5%). At higher concentration (7.5 % and 10 %), a lower shift in resonance angle was observed leading to a lower slope value ($0.13°$ RIU^{-1}). This lower shift could be caused by unexpected air bubbles inside the PVC tubing which would affect the optical signal. Over all, the sensitivity of the chitosan waveguide (2%) to the value of refractive index was not significantly affected by the buffer used. The sensitivity of the waveguide was further examined based on the waveguide's porosity as demonstrated in the following section.
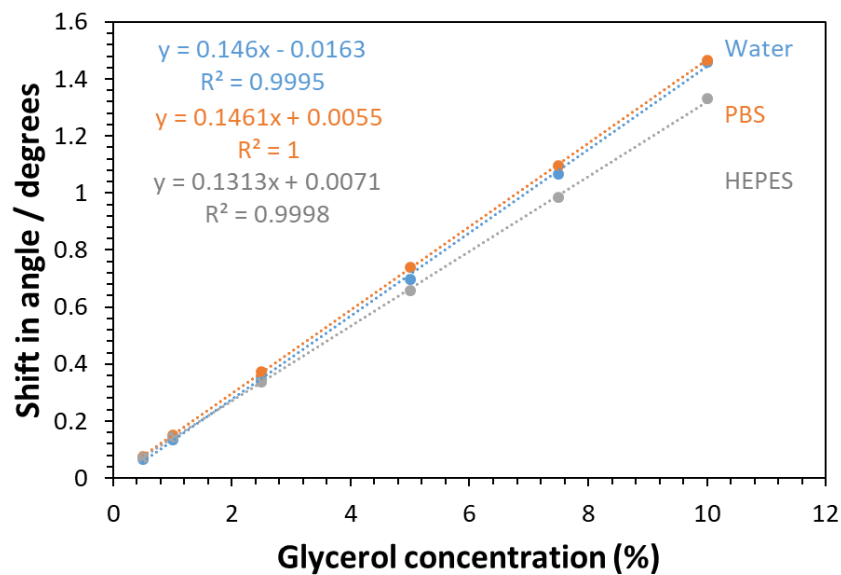
Figure 3.13 Degree of shift in resonance angle as a function of glycerol concentrations made in water, PBS and HEPES buffer. Glycerol solutions (0.5%, 1%, 2.5% and 5%, 7.5 % and 10 %) in each buffer were applied in separate chitosan waveguides (2%). Each waveguide was initially incubated with RB4 dye (100 µM) for 10 min. The experiment was performed one time using one separate chitosan waveguide for each buffer applied.

3.3.3 Influence of waveguide's porosity on sensitivity

The porosity of the waveguide is a fundamental factor for the sensitivity of a DDLW device. It could inhibit the diffusion of bio-recognition molecules in the entire volume of the waveguide. Therefore the porosity of the waveguide was investigated using small and large molecules made at the same refractive index value. If the pore size is large enough, both molecules (small and large) should lead to the same degree of shift in resonance angle as both have the same refractive index value. In order to monitor the shift in resonance angle in real-time upon applying large and small molecules, a setup two was used as explained in section 2.2.2. Chitosan waveguides were obtained at 2% (w/v) with deposition speeds of 3000 rpm as described in section 2.6.3. Solutions of glycerol, polyethylene glycol (PEG) at various molecular weights; (10 kDa, 35 kDa and 40 kDa) and polyethylene oxide (PEO) (100 kDa) were all made in the PBS buffer at a refractive index of 1.335. All solutions were pumped into the chitosan waveguide at a flow rate of 250 μL min^{-1}.

Figure 3.14 displays the dip shifting in resonance angle as a function of time upon applying glycerol and polymer solutions into the chitosan waveguide (2%). PBS buffer was flushed between each solution in order to return the dip to the baseline. Although all solutions have the same refractive index (1.335), a significant shift was observed upon introducing the glycerol solution, where the dip reached on average 1.5°. The dip only moved to less than 0.02° when all PEG (10 kDa, 35 kDa and 40 kDa) and PEO (100 kDa) solutions were applied. This would lead us to say that large molecules such as PEG and PEO cannot be diffused inside the sensing region and provide a remarkable change in the dip position as glycerol. The shift in resonance angle observed upon applying all polymer solutions (0.02°) can be attributed to the change in the refractive index in the evanescent field that is located at the top of the waveguide. To obtain a reproducible result, the experiment was carried out three times using three separate chitosan waveguides (2%). The findings are summarised in figure 3.15.
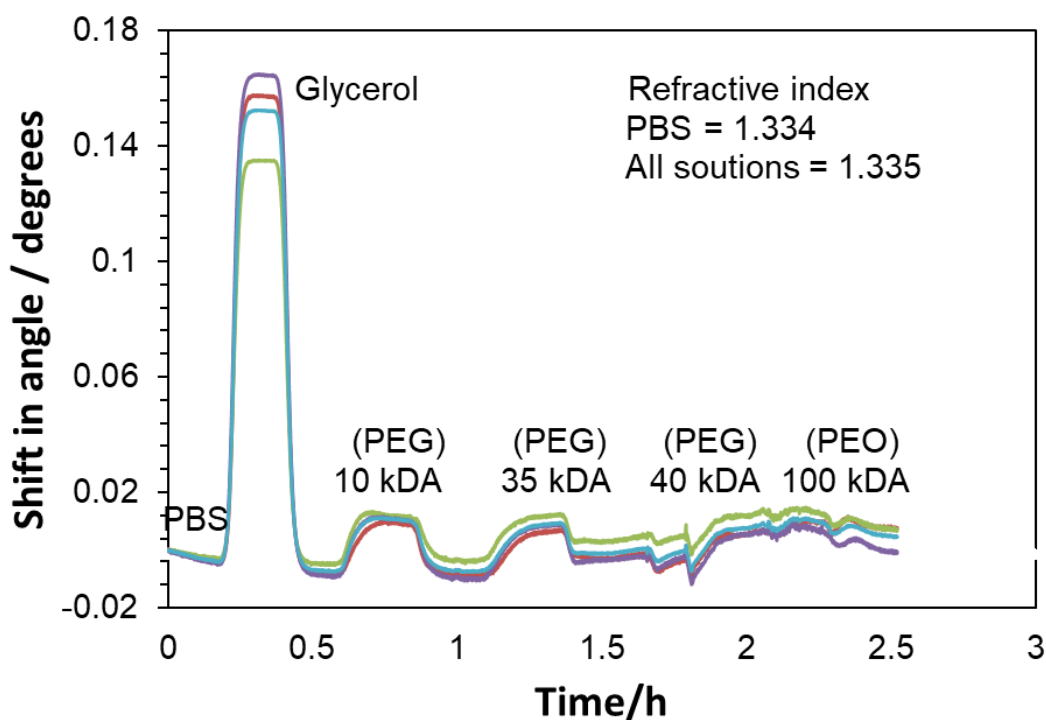
Figure 3.14 *Change in resonance angle upon applying glycerol, PEG (10 kDa, 35 kDa and 40 kDa) and PEO (100 kDa) solutions onto the chitosan waveguide (2%). All solutions were prepared in the PBS buffer at the same refractive index (1.335). The chitosan waveguide (2%) was initially incubated with RB4 dye (100 μM) for 10 min. The waveguide was irradiated with red LED light at a fixed incident angle (65°) while the dip movement was continuously monitored by a CMOS camera. The experiment was performed one time using one chitosan waveguide.*

The average of three runs introducing glycerol and polymer solutions prepared at the same refractive index value into the chitosan waveguide (2%) is shown in figure 3.15. Each run was performed in a separate chitosan waveguide. Although a high error bar was observed upon applying glycerol solution into three chitosan waveguides, the degree of shift in resonance angle was significantly higher than with any other solutions. This was also confirmed by one way ANOVA statistical analysis in which there was a significant difference in terms of the shift in resonance angle between glycerol and other polymer solutions where the p-value was at < 0.001. In contrast, the p-value was at 0.9 when the shift in the resonance angle was only compared between polymer solutions excluding the glycerol. This would lead us to say that chitosan waveguides prepared at concentration of 2% (w/v) and deposited at speed of 3000 rpm feature a very small pore size that cannot diffuse large molecules. Consequently, this would have an effect on the sensitivity of

125

DDLW device as it would influence the immobilisation of bio-recognition element in the entire volume of the waveguide. Further investigation of the waveguide's porosity was carried out using fluorescence spectroscopy as shown below.
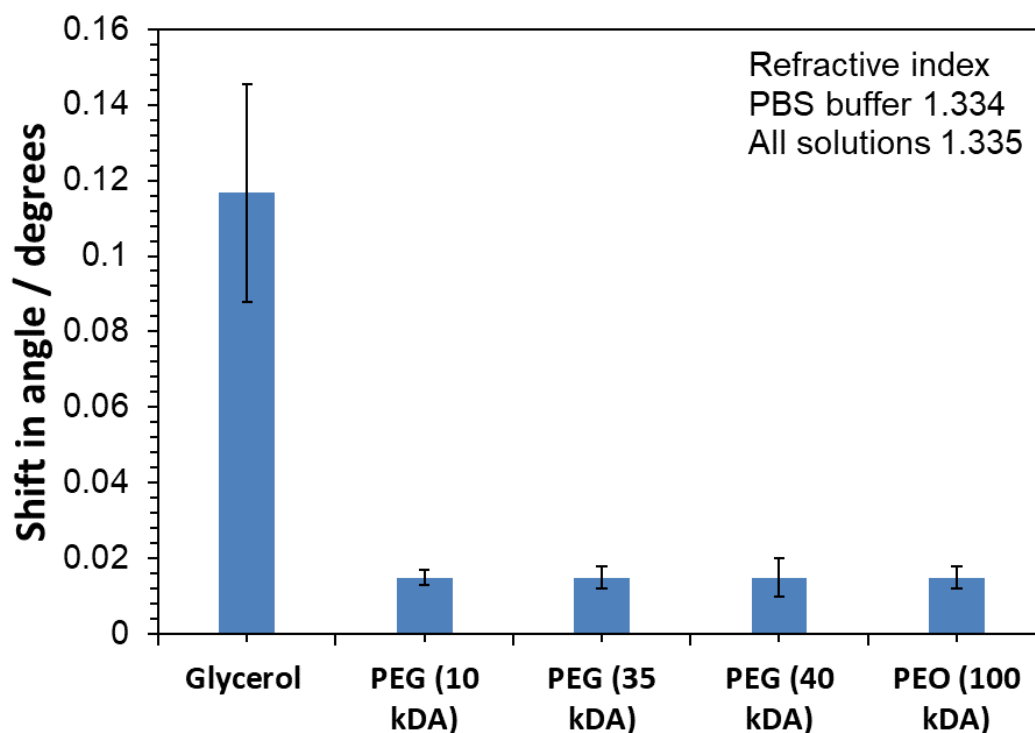
Figure 3.15 *The average shift in resonance angle upon applying glycerol, PEG (10 kDa, 35 kDa and 40 kDa) and PEO (100 kDa) solutions onto three chitosan waveguides (2%). All solutions were prepared in PBS buffer (pH 7.4) at a refractive index of 1.335. The chitosan waveguide was initially incubated with RB4 dye (100 μM) for 10 min. Each run was performed in a separate chitosan waveguide. One way ANOVA statistical analysis indicated that there was a significant difference in terms of the shift in resonance angle between glycerol solution and all other polymer solutions where the p-value was at < 0.001.*

The porosity of the chitosan was further characterised using fluorescence spectroscopy. For this experiment, bovine serum albumin conjugated with fluorescein isothiocyanate isomer I (BSA-FITC) (M_w = ≈ 66 kDa) was used as an example large molecule while fluorescein isothiocyanate isomer I (FITC) (M_w = 389 Da) was used as an example small molecule. Chitosan hydrogel at a concentration of 2 % (w/v) was prepared in a cuvette as described in section 2.6.3. The hydrogel was then incubated with BSA-FITC (0.05%) or with FITC (0.05%) solutions for two hours followed by measuring the fluorescence

intensity with a Perkin Elmer LS 55 Fluorescence Spectrometer (Bio Lambda 10, USA) at excitation of 490 nm and at emission of 525 nm. Images of chitosan hydrogels in cuvettes before, during and after incubation with BSA-FITC and FITC solutions are provided in figure 3.16. After drying overnight, the hydrogel obtained is transparent, as shown in figure 3.16 (a). This was expected because unmodified chitosan is a transparent material and therefore was compatible with optical sensors[143, 144]. The hydrogel remained transparent during (image b) and after (image c) incubation with BSA-FITC solution. In contrast, the gel acquired colour when it was incubated with FITC solution (image d) for two hours. This would first indicate that the FITC molecules were successfully diffused in the chitosan hydrogel. Secondly, this would indicate that two hours of incubation was enough to diffuse the FITC molecules into the entire volume of the chitosan hydrogel as the gel became totally coloured. Furthermore, this would confirm that 2% chitosan hydrogel was impermeable to larger molecules like BSA as the gel remained transparent after incubation with BSA-FITC solutions for the same period of time.

FITC molecules were not eluted from the hydrogel even after washing with PBS buffer (image e) and this was owing to the covalent linkage between the isothiocyanate group on FITC molecule and the amino group on chitosan gel [145]. The fluorescence emission was taken from each cuvette and is shown in figure 3.17.
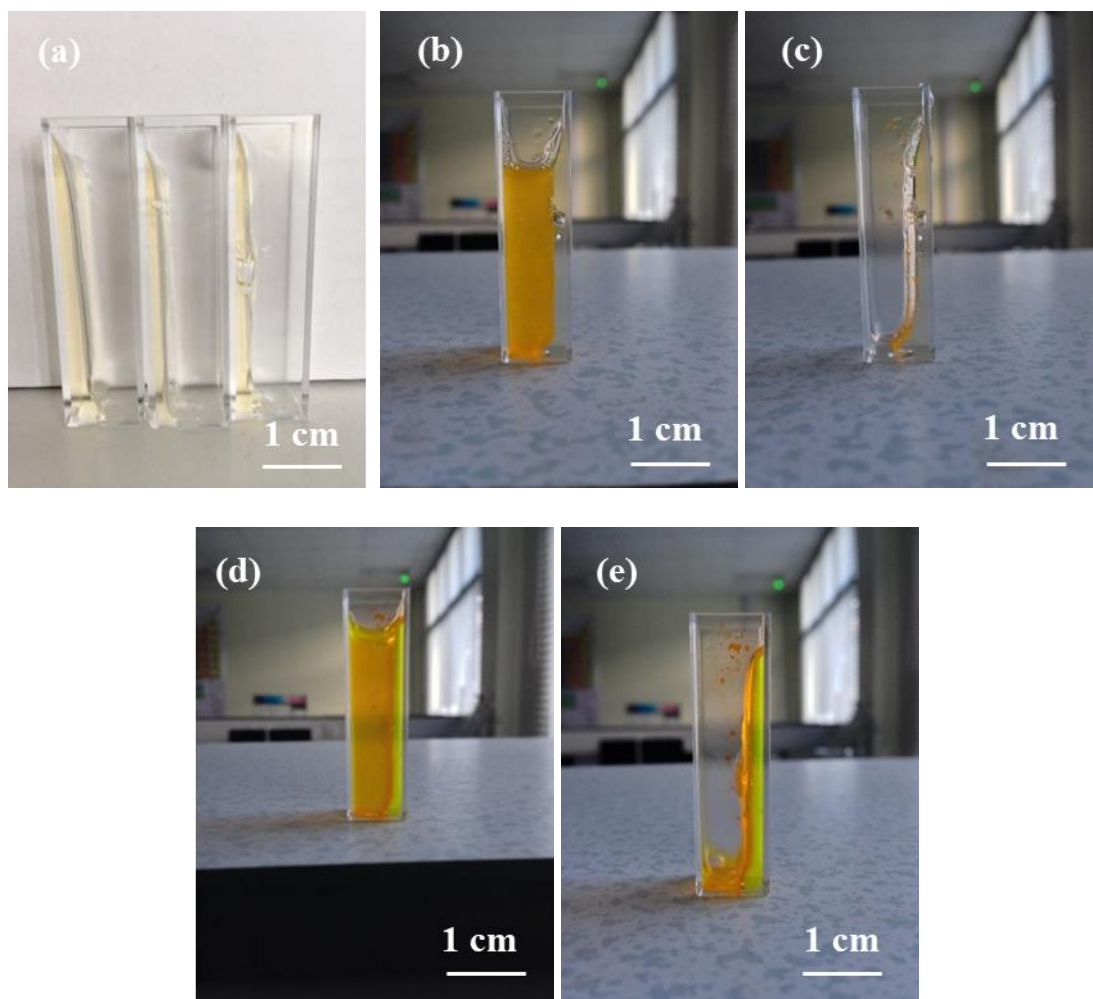
Figure 3.16 *Photographs of cuvettes (a) with 2 mL of 2% chitosan hydrogel after drying for 24 h, (b) during and (c) after incubation with BSA-FITC solution (0.05% w/v) for 2 h, (d) during and (e) after an incubation with FITC solution (0.05% w/v) for 2 h.*

Figure 3.17 represents the average of the fluorescence intensities measured from chitosan hydrogel cuvettes during incubation with BSA-FITC (0.05% w/v) and FITC (0.05% w/v) solutions and after washing with PBS buffer (pH 7.4). Cuvettes incubated with BSA-FITC solution exhibited the highest emission of light while a significant reduction was observed upon washing with PBS buffer (pH 7.4). This could be attributed to impermeable hydrogel to the BSA molecules leading being easily eluted by PBS buffer (pH 7.4). In contrast, cuvettes incubated with FITC solution showed a similar fluorescence intensity during and after washing with PBS buffer. This is thought to be associated first with chitosan's porosity allowing more FITC molecules to penetrate. Secondly, it was linked to the type of reaction between FITC molecules and chitosan's functional group as mentioned above. This leads to the conclusion that 2% chitosan, either

as hydrogel or film, featured a small pore size that is not compatible with the large molecules such as BSA. Therefore, an enhancement to the waveguide's porosity is required.
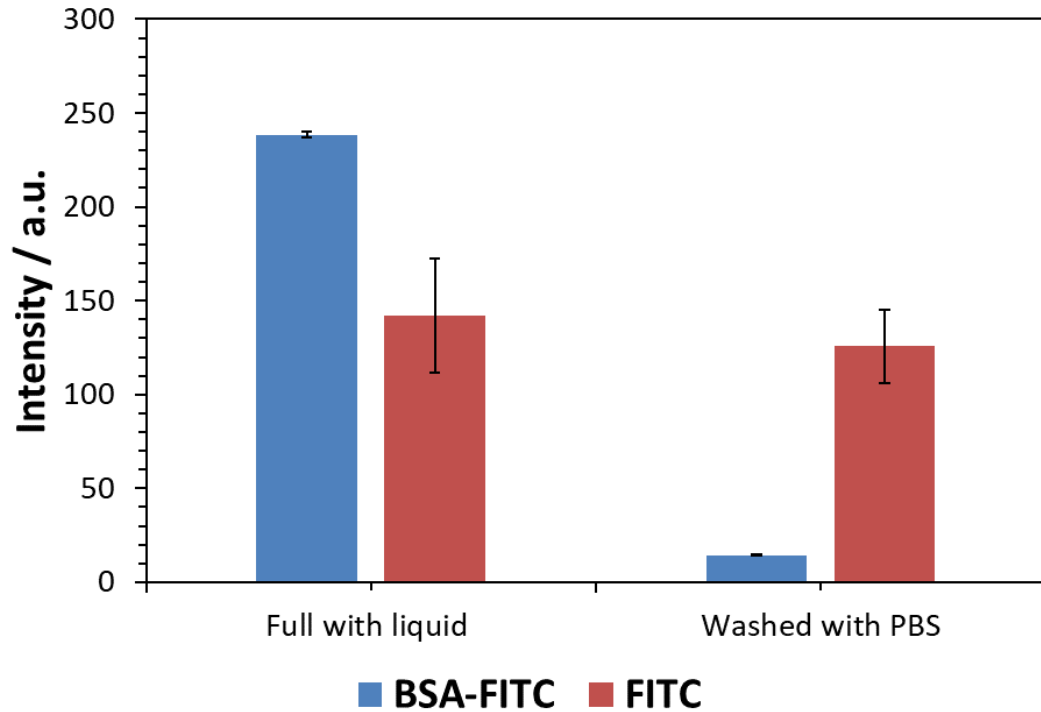
Figure 3.27 *Fluorescence intensity from chitosan hydrogel cuvettes during incubation with BSA-FITC and FITC solutions (0.05% w/v) and after washing with PBS buffer (pH 7.4). The measurements were taken at excitation and emission of 490 nm 525 nm, respectively (n = 3). Two way ANOVA statistical analysis indicated that there was significant difference in terms of the fluorescence intensity emitted during and after incubation with BSA-FITC solution as the p-value was at < 0.001 while the p-value was at 0.796 indicating no significant difference in the fluorescence intensity emitted during and after incubation with FITC solution.*

3.4 Summary

Chitosan polymer has been successfully utilised as a waveguide material on dye-doped leaky waveguide (DDLW) devices. The condition used in this research was obtained by 2% (w/v) of chitosan solution cross-linked with glutaraldehyde at a concentration of 0.03% (v/v). This was followed by deposition onto a glass substrate at speed of 3000 rpm. Although, the resonance angle (θr) was shifted from 65.5° to 67° with pH buffer due to the alteration in the waveguide thicknesses, the waveguide mode remained stable and

showed excellent response in a wide range of pH. This permits a variety of conditions to be applied for bioassay measurement.

As expected, lower concentrations of chitosan resulted in a lower amount of available amino groups giving 9 x 10^{-14} mole and 2.9 x 10^{-13} mole for the surfaces of 1% and 1.5% respectively. This was confirmed by two spectrophotometry readers utilised during the absorbance measurement showing identical findings. The number of moles of amino groups on 2% (w/v) of chitosan surface was found to be 6.8 x 10^{-13} mole for each volume of 1.5 x 10^{-11} m^3. This can be used as a guide choice for future immobilisation.

The sensitivity of the DDLW device to refractive index was highly dependent on the amount of dye attached. Incubation with RB4 dye for 10 min led to the highest slope value (100.6° RIU^{-1}) by comparison with 30 min (93° RIU^{-1}) and 60 min (62° RIU^{-1}). Thus, 10 min was considered the optimum time. The sensitivity was not significantly changed on using different running buffers as the slope value was equivalent (0.146° RIU^{-1}) when using both water and the PBS buffer. It was slightly lower with the HEPES buffer (0.13° RIU^{-1}): that was owing to unavoidable air bubbles in PVC tubing which influenced the optical signal.

The sensitivity was further investigated on the basis of the waveguide's porosity by diffusion of small and large molecules. This was accomplished using an optical waveguide setup and fluorescence spectrophotometry. Although all solutions were made at the same refractive index, a significant shift in resonance angle was observed only when glycerol solution was used. The dip reached 1.4°. In comparison with PEG and PEO solutions, the dip only moved less than 0.02°. This confirmed that the waveguide was of small pore size. Confirmation was seen from the chitosan hydrogel that remained transparent before, during and after incubation with BSA-FITC solution, which indicated that BSA molecule was not diffused. In contrast, the hydrogel became coloured during and after incubation with FITC solution, indicating penetration of FICT molecules. This was expected because of the small size of FITC molecules. It was concluded that 2% (w/v) of chitosan as a hydrogel or as a waveguide was impermeable to large molecules such as BSA, PEG and PEO. Consequently, this would influence the immobilisation of bio-recognition elements such as an aptamer. The following chapter will discuss various approaches for the enhancement of the waveguide's porosity.

CHAPTER 4

Optimisation of the porosity of the chitosan waveguide

4 Optimisation of the porosity of the chitosan waveguide

The porosity of the waveguide is a fundamental factor in the sensitivity of the DDLW device because it influences the ability of analytes to diffuse into the volume of the waveguide. In the previous chapter, it was shown that a waveguide generated from a 2% chitosan solution with added glutaraldehyde deposited at 3,000 rpm was impermeable to large molecules such as BSA, PEG and PEO. Consequently, the effective immobilisation of bio-recognition elements for bioassays would be hampered. Thus, in this chapter, the aim was to improve the porosity of the waveguide. One approach was to reduce the amount of glutaraldehyde cross-linker to test whether this would increase the space between the chitosan chains and thus increase the pore size. Additionally, blending the chitosan with a porogen followed by porogen dissolution was investigated. Finally, the effect of drying time was studied, since the pore size of the initially wet and porous film was found to decrease gradually upon drying. Therefore, controlling the drying time of the chitosan film could control the porosity of the waveguide. These approaches are discussed below.

4.1 Reducing the amount of glutaraldehyde cross-linker

In the previous chapter, chitosan solution was cross-linked with glutaraldehyde before coating onto a glass substrate. This was performed in order to obtain a film which is more chemically resistant and physically harder[146]. The reaction is based on the covalent linkage between chitosan's functional amino groups[147, 148] as shown in figure 4.1. However, Krajewska *et al.* observed that a higher concentration of glutaraldehyde utilised as a cross-linker would result in pore size reduction of a chitosan membrane and consequently a reduction in porosity.[149]

An experiment was conducted to examine the impact of glutaraldehyde concentration on the waveguide's porosity by studying the diffusion of large molecules into the waveguide. Glutaraldehyde concentrations ranging from 0% to 25% (v/v) were added to the chitosan solutions before being coated onto cleaned glasses as described in section 2.7.1. Glycerol, polyethylene glycol (PEG) and polyethylene oxide (PEO) were all prepared in a Tris buffer at a refractive index of 1.3335. The solutions were introduced into flow cell design 2 at a flow rate of 250 µL min^{-1}. Figure 4.2 shows the shift in resonance angle as a function of time on applying glycerol and polymer solutions at various molecular weights (10 kDa, 35 kDa, 40 kDa, 100 kDa and 200 kDa) onto a 2% (w/v) chitosan waveguide. The waveguide had been initially modified with glutaraldehyde solution at a concentration of

5% (v/v). Although all solutions were made at the same refractive index, a significant shift in the dip level was only obtained when the glycerol solution was applied, for which the dip shifted by 0.15°. In contrast, the dip was found to shift by only 0.02° when any of the various polymers were introduced. This significant difference in terms of shifting between glycerol and polymers would indicate that the waveguide was still impermeable to large molecules such as PEG and PEO. The experiment was repeated using different concentrations of glutaraldehyde and the results are summarised in figure 4.3.

Figure 4.3 represents the average shift in resonance angle from five (2% w/v) chitosan waveguides upon introducing glycerol, polyethylene glycol (PEG) and polyethylene oxide (PEO) solutions. Each chitosan waveguide had been initially cross-linked either with 0 %, 1 %, 2 %, 5 % and 25 % (v/v) of glutaraldehyde solution. When the glycerol solution was applied, the dip shifted to 0.14° on average for five runs. This was significantly higher than any of the other polymers applied. The error bars on the polymers solutions were clearly lower than glycerol which indicated small variations between each run. Each run represents a waveguide prepared from a different amount of glutaraldehyde, which means that the shifts were almost comparable in all chitosan waveguides upon applying polymer solutions. Thus, reducing the amount of cross-linker did not show any enhancement in the waveguide's porosity. This was also confirmed by a two way ANOVA statistical analysis in which there was not significant difference in terms of the shifting in resonance angle upon changing the concentration of glutaraldehyde in the waveguide from 0% to 25% for both glycerol and polymer solutions. The p-value was at 0.065 (> 0.05). Thus, it became evident that enhancement of the waveguide's porosity needed to be carried out by other methodologies.
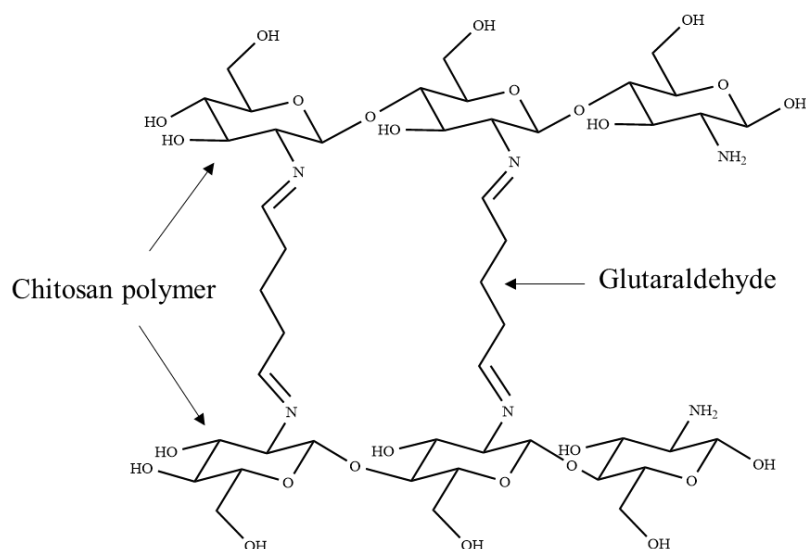
Figure 4.1 *Reaction of glutaraldehyde with chitosan polymer. The reaction is based on creating an imine bond, known as Schiff's base, between amino groups on the chitosan polymer and aldehyde groups on the glutaraldehyde. Since the glutaraldehyde features two aldehyde groups, it can act as a bridge between chitosan chains.*
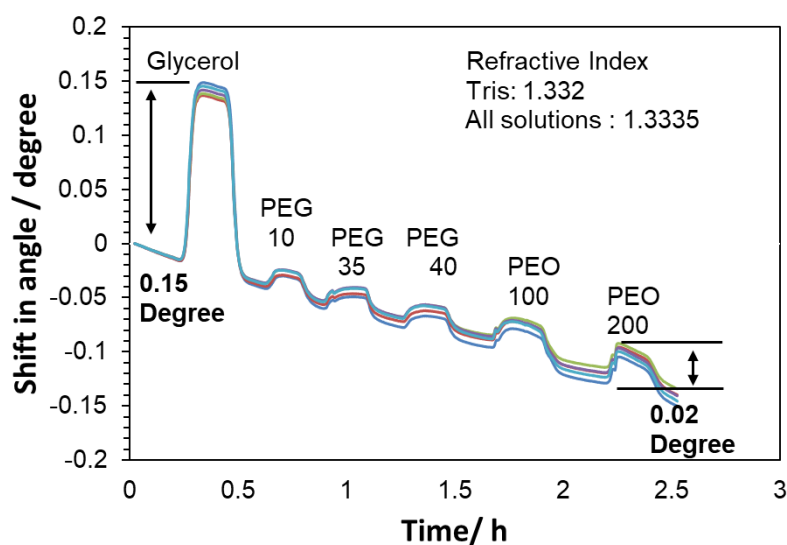
Figure 4.2 *Shift in resonance angle upon pumping glycerol and polymers (PEG and PEO) at different molecular weights (10 kDa, 35 kDa, 40 kDa, 100 kDa and 200 kDa) over a 2% (w/v) chitosan waveguide at a flow rate of 250 μL min⁻¹.The waveguide was obtained from chitosan solution that had been initially cross-linked with 5% (v/v) of glutaraldehyde solution. All solutions were made in Tris buffer at a refractive index of 1.3335. The experiment was performed one time using one chitosan waveguide.*
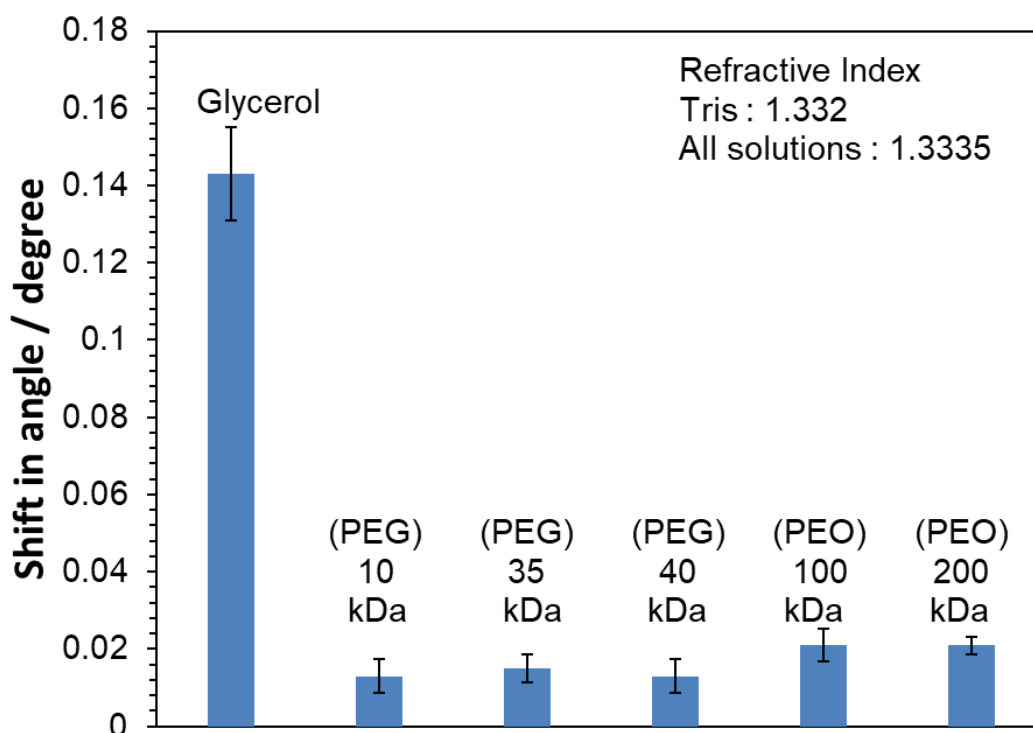
Figure 4.3 *Average shift in resonance angle from five chitosan waveguides (2% w/v) upon applying glycerol, polyethylene glycol (PEG) (10 kDa, 35 kDa, and 40 kDa) and polyethylene oxide (PEO) (100 kDa and 200 kDa) at a flow rate of 250 µL min^{-1}. Each chitosan waveguide was modified with 0 %, 1 %, 2 %, 5 % or 25 % (v/v) of glutaraldehyde solution before applying glycerol and polymers solutions. All solutions were made in Tris buffer at a refractive index of 1.3335. A two way ANOVA statistical analysis indicated that there was not a significant difference in terms of the shift in resonance angle upon changing the concentration of glutaraldehyde from 0% to 25% for both glycerol and all other polymer solutions. The p-value was at 0.065 (>0.05).*

4.2 Introduction of porogens into the waveguide

There are reports in the literature about creating microporous chitosan hydrogels using a selective dissolving method. This involves blending the chitosan solution with a porogen such as polyethylene glycol (PEG). Upon formation of the hydrogel, the porogen can be dissolved in a water bath at 80 °C[150-153] or under alkaline condition at room temperature[154 155] to leave a porous structure with voids left by the dissolved porogen. The pore size can be controlled by using different molecular weights of porogen and mixing them at various ratios with the chitosan. Here, a selective dissolving method was initially investigated with bulk chitosan hydrogel in a cuvette, followed by applying the condition on a spin-coated chitosan waveguide.

4.2.1 Introducing a porogen (PEG) into chitosan hydrogel

Bovine serum albumin labelled fluorescein isothiocyanate isomer I (BSA-FITC) was utilised as a readily visible and detectable indicator of diffusion of a large molecule into the chitosan hydrogel. This was accomplished by observing the colour of the gel after incubation with BSA-FITC solution and also by measuring the intensity of the light emitted from the gel using fluorescence spectrometry. The blended hydrogels were produced as explained in section 2.7.2. Briefly, they were mixed at ratios of 2/1 or 1/1 % (chitosan/polymer). The hydrogels were then neutralised with NaOH followed by dissolution of the polymer in a water bath at 80 °C for 8 h. Finally, BSA-FITC (0.05%) solution was left to incubate with each hydrogel for 2 h before photographing and taking the fluorescence measurement as explained in section 2.7.2.

Table 4.1 shows photographs of hydrogels in cuvettes at various conditions. The hydrogels obtained after drying at room temperature for 24 h are shown in image (a). The cuvettes in image (a) represent different conditions. The gels were found to be transparent in all blended hydrogels. However, as seen in image (b), they turned into a white gel when neutralised with NaOH solution for 30 min. This may have been caused by the insolubility of chitosan in neutral conditions. When heat was applied to dissolve the polymer, the cuvettes were deformed, as seen in figure (c). During an incubation with the BSA-FITC (0.05%), the gel was clearly not immersed in the solution and remained white (image d). Upon washing with the PBS buffer, a yellowish orange thin layer was observed on the surface and at the edge of the hydrogel (e). The hydrogels in images (e), (f), (g), (h) and (i) were modified with PEG or PEO at the 2/1 or 1/1 ratios. Nonetheless, the entire volume of the hydrogel with each condition remained white meaning that the BSA molecules were not diffused even though the incubation time was last for 2 hours which should be enough to diffuse the molecule in the entire volume of the hydrogel as was previously shown in figure 3.16. The incubation time was then extended by repeating the same experiment and leaving the hydrogels with BSA-FITC (0.05%) solution for three days. As shown from images (j), (k) and (l), the colour of the entire volume of the hydrogels was almost the same as those in the previous cuvettes. This leads to the conclusion that the hydrogel was still impermeable to large molecules. Possibly the length of time of the thermal treatment was insufficient to dissolve the polymer. Successful extraction of the PEG component (6 kDa and 20 kDa) from a cross-linked chitosan membrane has been performed in a water bath at 80 °C for 8 h.[151-153] However, the thickness of the chitosan

membranes in these reports were between 40 µm and 250 µm while here it was in the range of 2.5 mm. Furthermore, it has been found that blending chitosan with PEG leads to enhance adsorption of such proteins as bovine serum albumin (BSA).[156] This was attributed to the addition of hydroxyl groups and the hydrophilic chains of PEG to the chitosan membrane. The yellowish orange thin layer was not observed when unblended chitosan hydrogel was incubated with BSA-FITC solution for 2 h (Figure 3.16). This would further confirm that the polymer component was not fully dissolved from the hydrogel during the thermal treatment. Therefore other approaches for extraction the polymer component were investigated instead as discussed below.

Table 4.1 Images of chitosan/polymer hydrogels (2/1 and 1/1 ratio) in cuvettes. The hydrogels were obtained after 24 h of drying at room temperature. The hydrogel was then neutralised with NaOH (0.1M) for 30 min followed by thermal treatment at 80 °C for 8 h to extract polymer component. Finally, the hydrogel was incubated with BSA-FITC solution (0.05%) for 2 h.

Obtained blended hydrogels at ratio 2/1 and 1/1 (chitosan/polymer)	After neutralisation with NaOH (0.1M) for 30 min	After thermal treatment (80 °C) for 8 h

(d) The gel was surrounded by the solution — BSA-FITC (0.05 %) solution — White gel — 1 cm	**(e)** Yellowish orange thin layer at the edge — White gel — 1 cm	**(f)** Yellowish orange thin layer at the edge — White gel — 1 cm
During incubation with BSA-FITC (0.05 %) solution for 2 h.	After BSA-FITC incubation for 2 h and washing with PBS buffer. The mixing ratio was 2/1 (Chitosan/PEO 400 kDa)	After BSA-FITC incubation for 2 h and washing with PBS buffer. The mixing ratio was 2/1 (Chitosan/PEG 35 kDa)

(g) Yellowish orange thin layer at the edge — White gel — 1 cm	**(h)** Yellowish orange thin layer at the edge — White gel — 1 cm	**(i)** Yellowish orange thin layer at the edge — White gel — 1 cm
After BSA-FITC incubation for 2 h and washing with PBS buffer. The mixing ratio was 1/1(Chitosan/PEG 35 kDa)	After BSA-FITC incubation for 2 h and washing with PBS buffer. The mixing ratio was 2/1(Chitosan/PEG 10 kDa)	After BSA-FITC incubation for 2 h and washing with PBS buffer. The mixing ratio was 1/1(Chitosan/PEG 10 kDa)

138

(j) Yellowish orange thin layer at the edge	White gel 1 cm	(k) Yellowish orange thin layer at the edge	White gel 1 cm	(l) Yellowish orange thin layer at the edge	White gel 1 cm
After three days of incubation with BSA-FITC and washing with PBS buffer. The mixing ratio was 2/1(Chitosan/PEO 400 kDa)		After three days of incubation with BSA-FITC and washing with PBS buffer. The mixing ratio was 2/1(Chitosan/PEG 35 kDa)		After three days of incubation with BSA-FITC and washing with PBS buffer. The mixing ratio was 2/1(Chitosan/PEG 10 kDa)	

The fluorescence measurements taken from the blended chitosan gels in the cuvettes after thermal treatment and after 2h incubation with BSA-FITC are presented in figure 4.4. Only the hydrogels prepared at a ratio of 2/1 (chitosan /polymers; PEO 400 kDa, PEG 35 kDa and PEG 10 kDa) are plotted; the other conditions (1/1 chitosan /polymer with PEG 35 kDa and PEG 10 kDa) were excluded due to the effect of the temperature on the shape of the cuvettes: it did not allow fitting the cuvette into the spectrometer. From the figure it is evident that the intensity from the hydrogel prepared with the 400 kDa PEO was higher than 35 kDa and 10 kDa PEG blended hydrogels. However, the error bars were clearly high from 400 kDa PEO and 10 kDa PEG cuvettes indicated that there were variations between each run. This would lead to say that the amount of BSA-FITC molecules adsorbed on the surface of the hydrogels was almost comparable between each condition. This was also confirmed by one way ANOVA statistical analysis indicating that there was not significant difference in terms of the fluorescence intensity emitted from different cuvettes with different conditions as the p-value was at 0.14 (> 0.05).
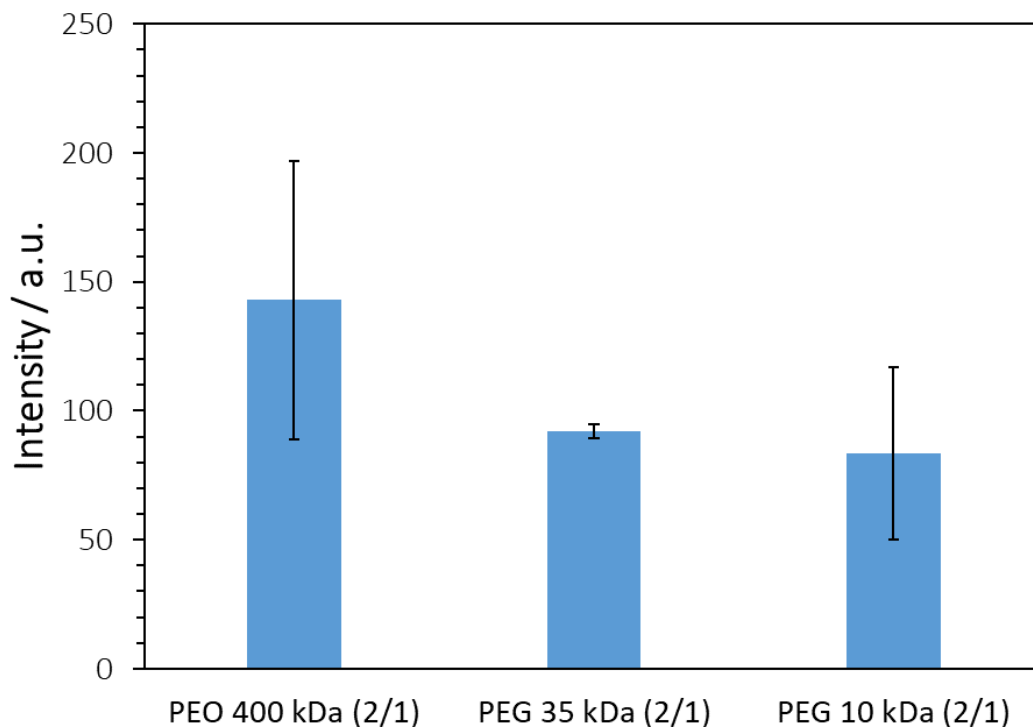
Figure 4.4 *Fluorescence intensity of chitosan blended hydrogels in cuvettes after thermal treatment at 80 °C for 8 h and after incubation with BSA-FITC solution (0.05% w/v) for 2 h. The hydrogel was produced at a mixing ratio of 2/1 % (chitosan /polymer; PEO 400 kDa, PEG 35 kDa and PEG 10 kDa). The reading represents the average of three runs using three blended hydrogels for each condition applied. A one-way ANOVA statistical analysis indicated that there was not significant difference in terms of fluorescence intensity emitted from cuvettes of PEO 400 kDa (2/1), PEG 35 kDa (2/1) and PEG 10 kDa (2/1); as the p-value was at 0.14 (> 0.05).*

The extraction of the blended polymers from the chitosan hydrogel was further investigated under alkaline conditions. The hydrogels were incubated in NaOH solution at 5% (v/v) for about 16 h. This was followed by intensive washing with de-ionised water before incubation with BSA-FITC solution (0.05%) for 2 h. Photographs of the hydrogels after alkaline treatment are shown in table 4.2. As seen previously, a white hydrogel was obtained after treatment with NaOH solution (image (a)). During the BSA-FITC incubation (image (b)), it was clearly seen that the entire volume of the hydrogel was completely immersed in the fluorescent solution and therefore the hydrogel turned yellowish. This was not observed with the hydrogels that had undergone thermal treatment (table 4.1, image (d)), in which the white gel was clearly separated from the surrounding solution. Images from (c) – (h) were taken after incubation with BSA-FITC

solution at various conditions as detailed in table 4.2. It can be seen that all these hydrogels had turned into a colour, indicating the diffusion of BSA molecules and hence an enhancement of the hydrogel's porosity. This was significantly different from what was obtained with thermal treatment where the BSA molecules were only adsorbed at the surface or at edge of the hydrogel (table 4.1). A higher concentration of NaOH (10% v/v) was also investigated for polymer extraction (image (i)); the hydrogel obtained featured an identical colour to that of the previous gel, indicating that using a higher NaOH concentration had no effect. Increasing the incubation time with BSA-FITC to 24 h (image (j)) resulted in a darker colour which could indicate that more BSA molecules had diffused inside the hydrogel. An interesting result was seen from a first control cuvette (image (k)). The hydrogel was made only from the chitosan solution (2%). After alkaline treatment for 16 h and after incubation with BSA-FITC solution for 2 h, the gel clearly took on a colour. This would indicate that BSA molecules diffused into the hydrogel and thus indicated to suitable porosity even without using a porogen. This leads us to say that the alkaline treatment was the most significant factor for the enhancement of the hydrogel's porosity. Image (l) is a second control cuvette in which the chitosan hydrogel (2%) was not blended with polymer and not treated with NaOH. The gel as expected remained transparent after incubation which indicated that the BSA molecules were not diffused.

Table 4.2 Images of chitosan-blended hydrogels in cuvettes under various steps and conditions as stated on each image. The blended hydrogels were obtained after 24 hours of drying at room temperature. Each hydrogel was incubated with NaOH solution (5% w/v) for about 16 hours except images (i) (washed with NaOH (10 %) for about 16 hours) and (l) (second control cuvette where the chitosan hydrogel (2%) was not blended with polymer and not treated with NaOH). All hydrogels were then intensively washed with de-ionised water before incubation with BSA-FITC solution (0.05%) for two hours.

Blended hydrogel obtained after drying at room temperature for 24 h and washing with NaOH (5%) solution for 16 h	During incubation with BSA-FITC (0.05%) solution for 2 h. The gel was totally immersed in the solution.	After BSA-FITC incubation for 2 h and washing with PBS buffer. The mixing ratio was 2/1 (Chitosan/PEG 35 kDa)
After BSA-FITC incubation for 2 h and washing with PBS buffer. The mixing ratio was 1/1 (Chitosan/PEG 35 kDa)	After BSA-FITC incubation for 2 h and washing with PBS buffer. The mixing ratio was 1/2 (Chitosan/PEG 35 kDa)	After BSA-FITC incubation for 2 h and washing with PBS buffer. The mixing ratio was 2/1(Chitosan/PEG 10 kDa)

After BSA-FITC incubation for 2 h and washing with PBS buffer. The mixing ratio was 1/1(Chitosan/PEG 10 kDa)	After BSA-FITC incubation for 2 h and washing with PBS buffer. The mixing ratio was 1/2(Chitosan/PEG 10 kDa)	After washing with NaOH (10%) for 16 h and BSA-FITC incubation for 2 h and washing with PBS buffer. The mixing ratio was 2/1(Chitosan/PEG 35 kDa)
After BSA-FITC incubation for 24 h and washing with PBS buffer. The mixing ratio was 2/1(Chitosan/PEG 35 kDa)	First control cuvette. After washing with NaOH (5%) solution for 16 h and BSA-FITC incubation for 2 h. The hydrogel was only made by 2% of chitosan solution without addition of PEG	Second control cuvette: After BSA-FITC incubation for 2 h. The hydrogel was made by 2% (w/v) of chitosan solution without addition of PEG and without washing with NaOH (5%) solution.
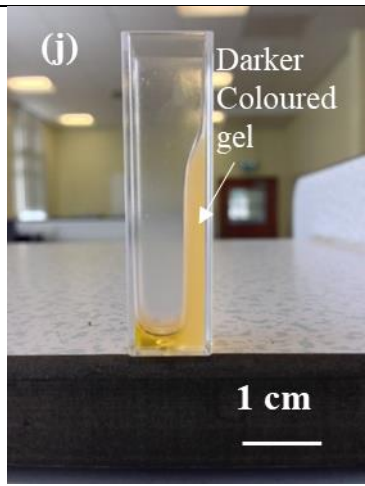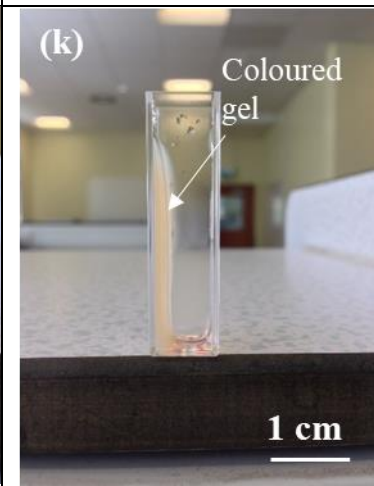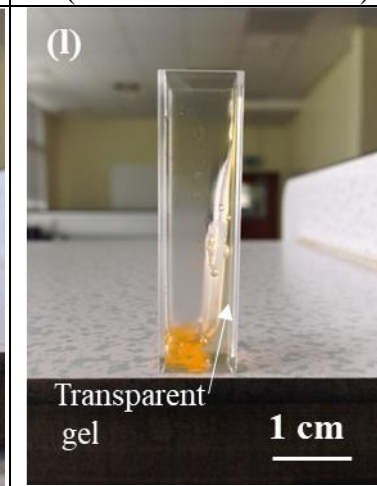
Figure 4.5 shows the fluorescence intensity measured from each cuvette after incubation with BSA-FITC solution (0.05%) and washing with PBS buffer. Each column represents a specific mixing ratio between chitosan and other substances. First, polyethylene glycol (PEG) (Chitosan/PEG (35 kDa) at mixing ratios of 2/1, 1/1 and 1/2 (%) (v/v); and second, Chitosan/PEG (10 kDa) at mixing ratios of 2/1, 1/1 and 1/2 (%) (v/v)). All were given overnight incubation with BSA-FITC solution (condition: Chitosan/PEG 35 kDa hydrogel at mixing ratio of 2/1(%) (v/v)). The first control cuvette (condition: 2% (w/v) of chitosan hydrogel) was prepared without addition of PEG; however, it was treated with NaOH (5 %) for 16 h. A second control cuvette (condition; 2% (w/v) of chitosan hydrogel) was prepared without addition of PEG and without treatment with NaOH solution (5 %). The two control cuvettes are also presented by separate columns. From the figure, it is clear that the intensity of emitted light was almost comparable from all hydrogels that had undergone the alkaline treatment for 16 h. The intensity of emitted lights was about 700 a.u. A significant difference can only be seen from the second control cuvette where the chitosan hydrogel was not blended with a porogen and also not treated with NaOH solution. The intensity of emitted light was lower than 100 a.u. In comparison with a thermal treatment (Figure 4.3), the intensity of emitted light was between 150 a.u and 100 a.u from hydrogels that were blended with a porogen at mixing ratio of 2/1 (%) (v/v) (Chitosan/PEO (400 kDa), Chitosan/PEG (35 kDa) and Chitosan/PEG (10 kDa)) and all had undergone for a thermal treatment for 8 h at 80 °C. This significant difference between alkaline treatment and thermal treatment in terms of intensity of emitted light would indicate a large amount of BSA molecules being diffused into hydrogel after incubation with BSA-FITC solution for 2 h. This would further confirm to a strong enhancement of the hydrogel's porosity using alkaline treatment. This improvement in the porosity was further examined in a spin-coated chitosan waveguide as shown in the following section.
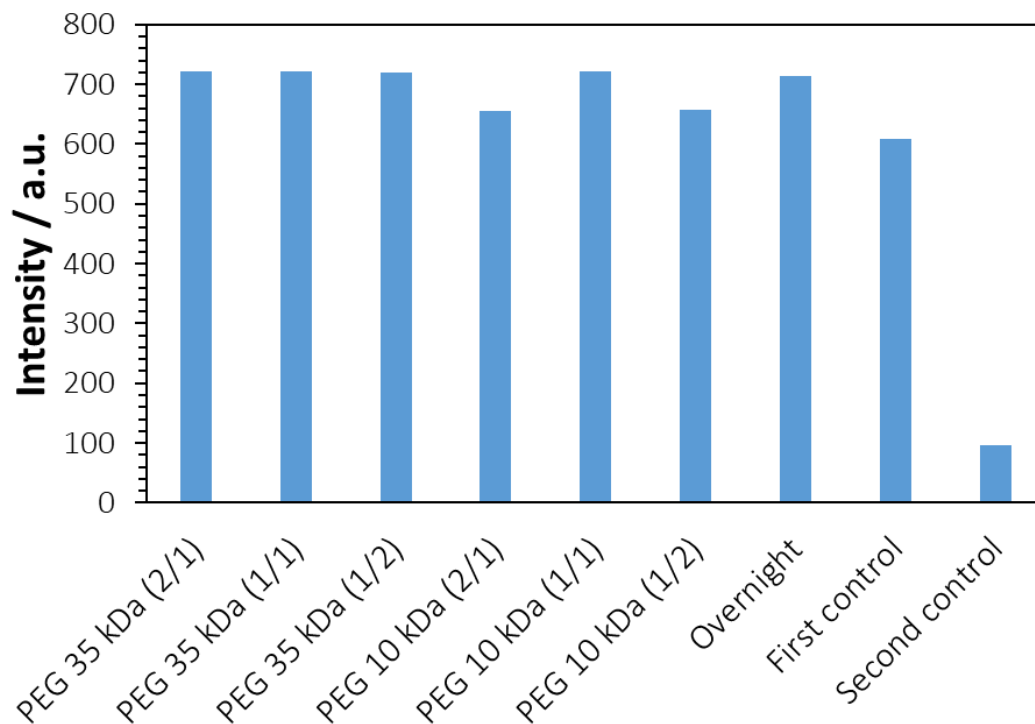
Figure 4.5 *Fluorescence intensity taken from chitosan-blended hydrogels in cuvettes after incubation with BSA-FITC solution (0.05% w/v) for 2 h and subsequently after washing with PBS buffer several times. All cuvettes were initially treated with NaOH (5% w/v) for 16 h to extract polymer component, except the second control cuvette. The hydrogels were produced at specific mixing ratios of chitosan and polyethylene glycol (PEG) (Chitosan/PEG (35 kDa): 2/1, 1/1 and 1/2 (%) (v/v); and Chitosan/PEG (10 kDa) at mixing ratios of 2/1, 1/1 and 1/2 (%) (v/v)).Overnight incubation with BSA-FITC solution (Chitosan/PEG 35 kDa hydrogel at mixing ratio of 2/1(%) (v/v)).The first control cuvette (condition; 2% (w/v) of chitosan hydrogel prepared without addition of PEG) was treated with NaOH (5 %) for 16 h. The second control cuvette (condition; 2% (w/v) of chitosan hydrogel prepared without addition of PEG) was not treated with NaOH solution (5 %). The experiment was performed one time using one separate cuvette for each condition applied.*

4.2.2 Introducing a porogen (PEG) into the chitosan waveguide

The aim of this experiment was to introduce a porogen into a thin chitosan waveguide layer. This was accomplished by mixing the chitosan solution with PEG or PEO polymer before spin coating onto a glass substrate. Upon obtaining the coated film, the polymer component was then extracted from the waveguide using thermal and alkaline treatment.

Here in this section, a thermal treatment was used even though it was not achieved previously. This is because the thickness of the spin coated chitosan film was around 1300 nm (see section 2.5.3) which is much lower than the thickness of the chitosan hydrogel in cuvette that was around 2.5 mm. Therefore, it was thought that using a thermal treatment to extract the polymer component from a thin chitosan film could be achieved.

Chitosan waveguides were prepared at mixing ratios of 2/1 (% (v/v)) (Chitosan/PEO (400 kDa) and Chitosan/PEG (35 kDa) as explained in section 2.7.2. The waveguide prepared with PEG (35 kDa) was placed in a bath of NaOH solution (5% v/v) for 16 h to dissolve the polymer component, while the waveguide made with PEO (400 kDa) was treated in a water bath at 80 °C for 8 h to extract the blended component. Both waveguides were then incubated with RB4 dye (100 µM) for 10 min before insertion into a flow cell and subsequent mounting on a prism. Glycerol and polymer solutions (PEG (10 kDa) and PEG (35 kDa)) made at the same refractive index value (1.3355) in PBS buffer were then sequentially applied to each waveguide at a flow rate of 250 µL min^{-1}.

The shift in resonance angle as a function of time upon introducing glycerol and polymers into chitosan waveguide made at condition of 2/1 (% (v/v)) (Chitosan/PEG (35 kDa) is presented in figure 4.6. The waveguide initially underwent alkaline treatment to extract the polymer component. From the figure, it can be seen that the dip shifted to 0.09° when glycerol solution was introduced. In contrast, the dip only moved by 0.02° when polymer solutions (PEG (10 kDa) and PEG (35 kDa)) were pumped through the waveguide. This was also comparable to what was observed from the second waveguide (Figure 4.7) made under the condition of 2/1 (% (v/v)) (Chitosan/PEO (400 kDa), and being thermally treated to dissolve the polymer component. The shift in resonance angle was at 0.1° with glycerol solution while it was at 0.01° with any of the other polymers applied. This significant difference in terms of shifting in resonance angle upon applying glycerol and polymers (PEG (10 kDa) and PEG (35 kDa)) would indicate that the waveguide's pore size was still not large enough to diffuse large molecules such as PEG (10 kDa and 35 kDa) even though the waveguides were initially treated either thermally or under alkaline condition to dissolve the polymer component.

It should be noticed that the blended chitosan waveguide film was highly affected by thermal and alkaline treatments. The fact is that several blended chitosan waveguides had undergone thermal and alkaline treatments; however, only one substrate out of ten from

each treatment allowed a proper waveguide film to be intact. The experiment could not be repeated three times. Therefore it would be difficult to consider the results from the figures 4.6 and 4.7 show a lack of success in improving the porosity. Many attempts were made to overcome this problem such as reducing the concentration of NaOH, decreasing the temperature of the water bath and finally shortening the time of treatment; but none of these attempts were successful. The film either peeled off the substrate or the waveguide mode no longer existed. Therefore the thermal and alkaline treatments should be considered as inapplicable approaches for the enhancement of the chitosan's porosity in a thin film as compared to a bulk chitosan hydrogel particular with alkaline treatment. Thus, other methodologies needed to be investigated to improve the waveguide's porosity.
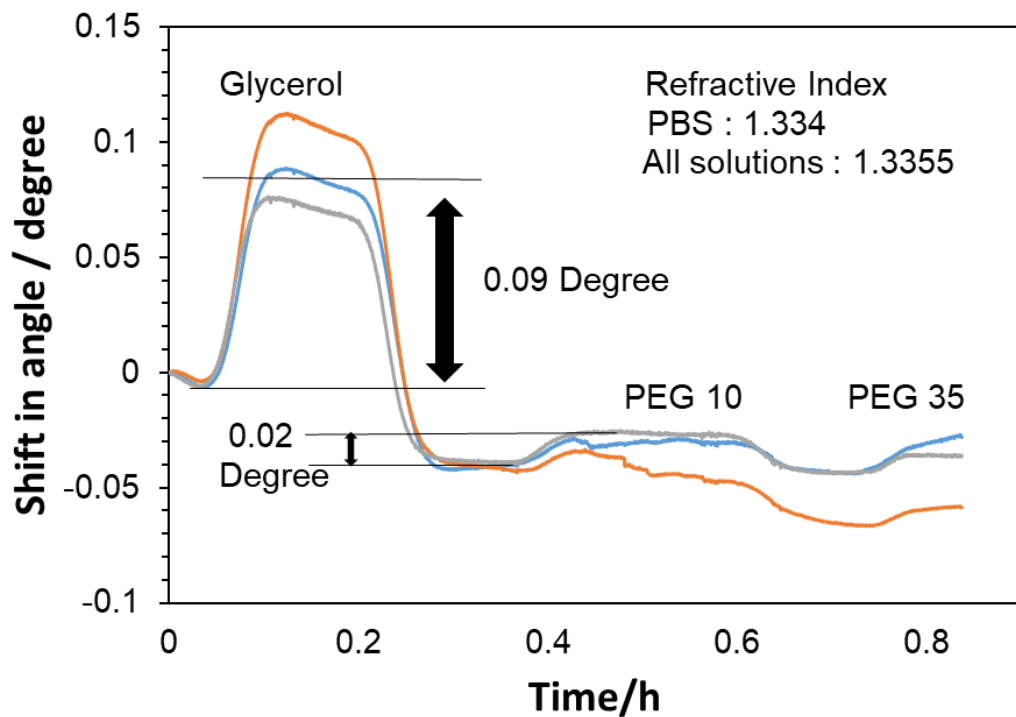
Figure 4.6 *Shift in resonance angle as a function of time on flushing a chitosan waveguide made at condition of 2/1 (% (v/v)) (Chitosan/PEG (35 kDa)) with glycerol and polymer solutions (PEG (10 kDa) and PEG (35 kDa)) at a flow rate of 250 μL min⁻1. The waveguide was initially treated with NaOH (5%) for 16 h to extract the polymer component. All glycerol and polymer solutions were made in the PBS buffer at the same refractive index (1.3355). The experiment was performed one time using one chitosan waveguide.*
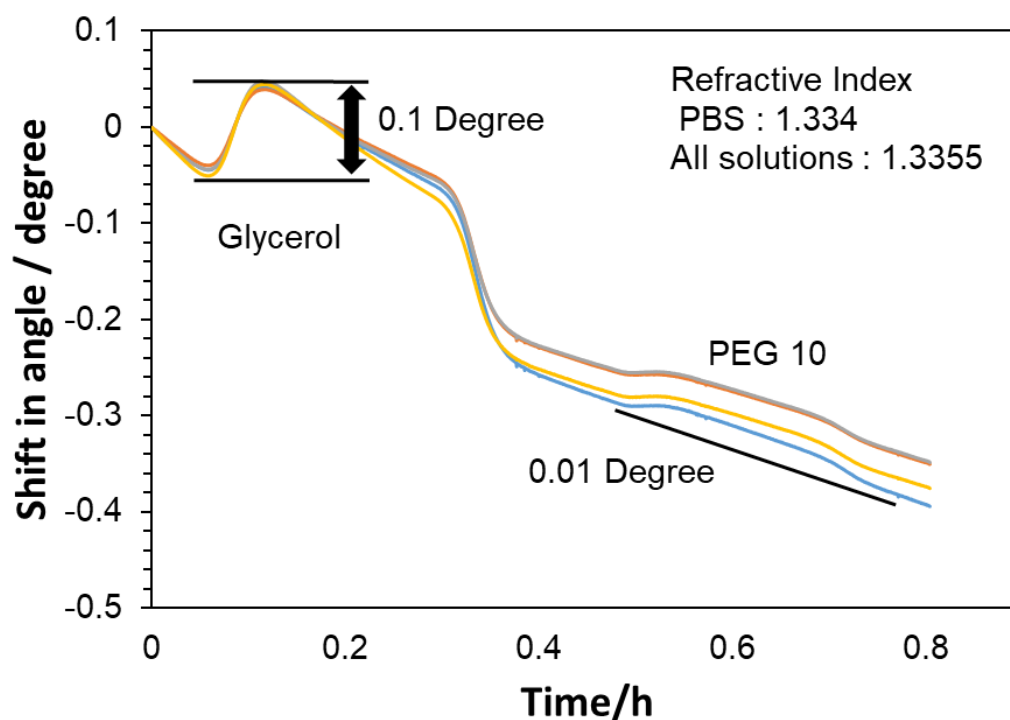
Figure 4.7 *Shift in resonance angle as a function of time upon flushing a chitosan waveguide prepared at condition of 2/1 (% (v/v)) (Chitosan/PEO (400 kDa)) with glycerol and polymer solutions (PEG (10 kDa)) at a flow rate of 250 µL min^{-1}. The waveguide was initially thermally treated in a water bath at 80° C for 8 h to extract the polymer component. All glycerol and polymer solutions were made in the PBS buffer at the same refractive index (1.3355). The experiment was performed one time using one chitosan waveguide.*

4.3 Controlling the drying time of the chitosan film

The chitosan waveguide produced is a fully dried film leading to a rigid and uniform film. However, the wet film is more porous, with the pore size gradually decreasing as the film dried. Furthermore, a higher concentration of chitosan would result in a higher density film which could influence the waveguide's porosity. The next aim was to utilise a lower concentration of chitosan with a controlled drying time for the coated film. This was accomplished by first investigating various lower concentrations of chitosan coated at different spin speeds. The films obtained were then left to dry for different times. The optimum condition was considered upon observing a sharp single dip in reflectivity with a specific condition of concentration, spin speed and drying time. This was followed by investigating the porosity of the new condition by monitoring the shift in resonance angle

(in a real time) as a function of time upon applying glycerol and polymer solutions at the same refractive index.

Chitosan coated films were prepared at lower concentrations (0.5%, 1% and 1.5% w/v) with deposition speeds ranging from 500 to 1500 rpm. Upon coating, the film was left to dry for various times before incubation with the HEPES buffer (100 mM). Each film was then stained with RB4 dye (100 µM) for 5 min before mounting on a prism. This was followed by irradiation of all coated films with a laser light between incident angles of 50° and 75° in order to observe a dip in reflectivity as explained in section 2.7.3.

Reflectivity curves from various chitosan films for different drying times are shown in figure 4.8. Chitosan films prepared at a concentration of 1% (w/v) with deposition speed of 900 rpm, were left to dry at room temperature from 2 min to 10 min. It can be seen that at 2 min of drying no dip was observed and this could be due to the porosity of the film being too high to support a waveguide mode. A single dip in reflectivity started to appear from 3 min and onwards. However, it is obvious that the dip became wider and broader upon increasing the drying time. This could be linked to the density of the film obtained which gradually increased upon drying due to the evaporation of water molecules. This could result in the light being trapped for a longer time inside the waveguide and hence higher absorption occurring for the dye molecules, leading to a wider dip. The sharpest dip was considered to respond to the refractive index value with the highest sensitivity. Thus 3 min of drying was chosen as the optimum time and selected for further investigation. In this, chitosan solution (1% w/v) was deposited at various spin speeds ranging from 500 rpm to 1500 rpm; all films obtained were left to dry for 3min. From figure 4.9 clearly no dip was observed except at a speed of 1100 rpm. However, the dip appeared to be broader than the one seen previously in figure 4.8 where the sharpest dip was seen at a spin speed of 900 rpm. Changing the concentrations of chitosan (0.5% and 1.5% w/v) that were spun at a speed of 900 rpm and dried for 3 min, did not provide a film that could support the waveguide mode and thus no obvious dip were obtained at the resonance angle ($\Theta r = 65°$) as shown in figure 4.10. The experiment was carried out three times using three chitosan-coated substrates for each condition tested. The results were almost comparable to all conditions in figures of 4.8, 4.9 and 4.10. Therefore, chitosan waveguide produced at a concentration of 1% (w/v) with coating speed of 900 rpm and with 3 min of drying time was selected as the optimum condition and was to be used for all following investigations.
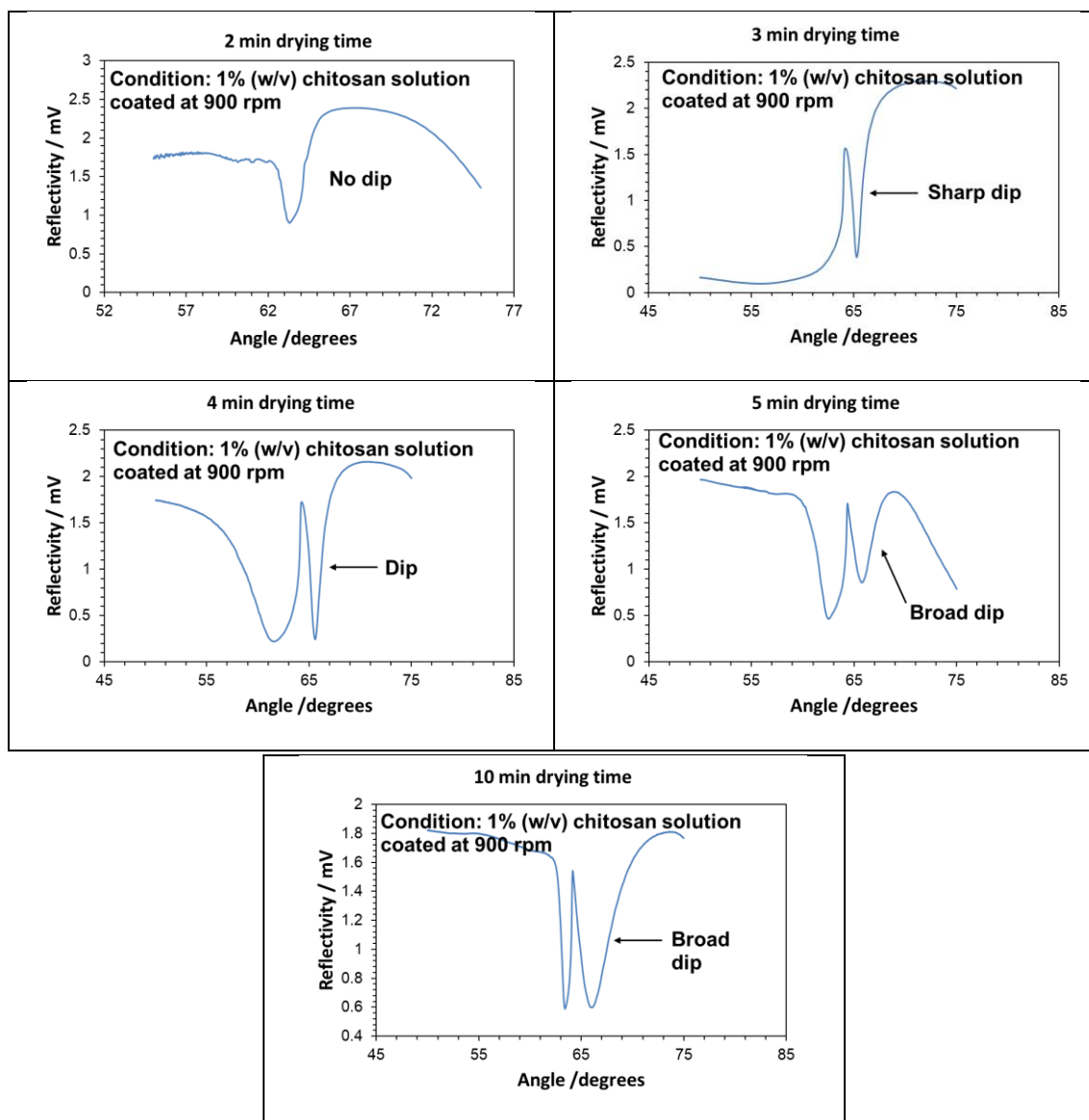
Figure 4.8 *Reflectivity curves as a function of incident angles from various chitosan films and different drying times. All films were obtained from chitosan solution at a concentration of 1% (w/v) with deposition speeds of 900 rpm for 30 seconds. The coated films were then dried at room temperature either for 2, 3, 4, 5 or 10 min before being stained with RB4 (100 µM) for 5 min. The reflectivity from each film was then measured between incident angles of 50° and 75°. The experiment was repeated two times using two separate chitosan coated films for each drying time. The results were comparable to all reflectivity curves in this figure.*
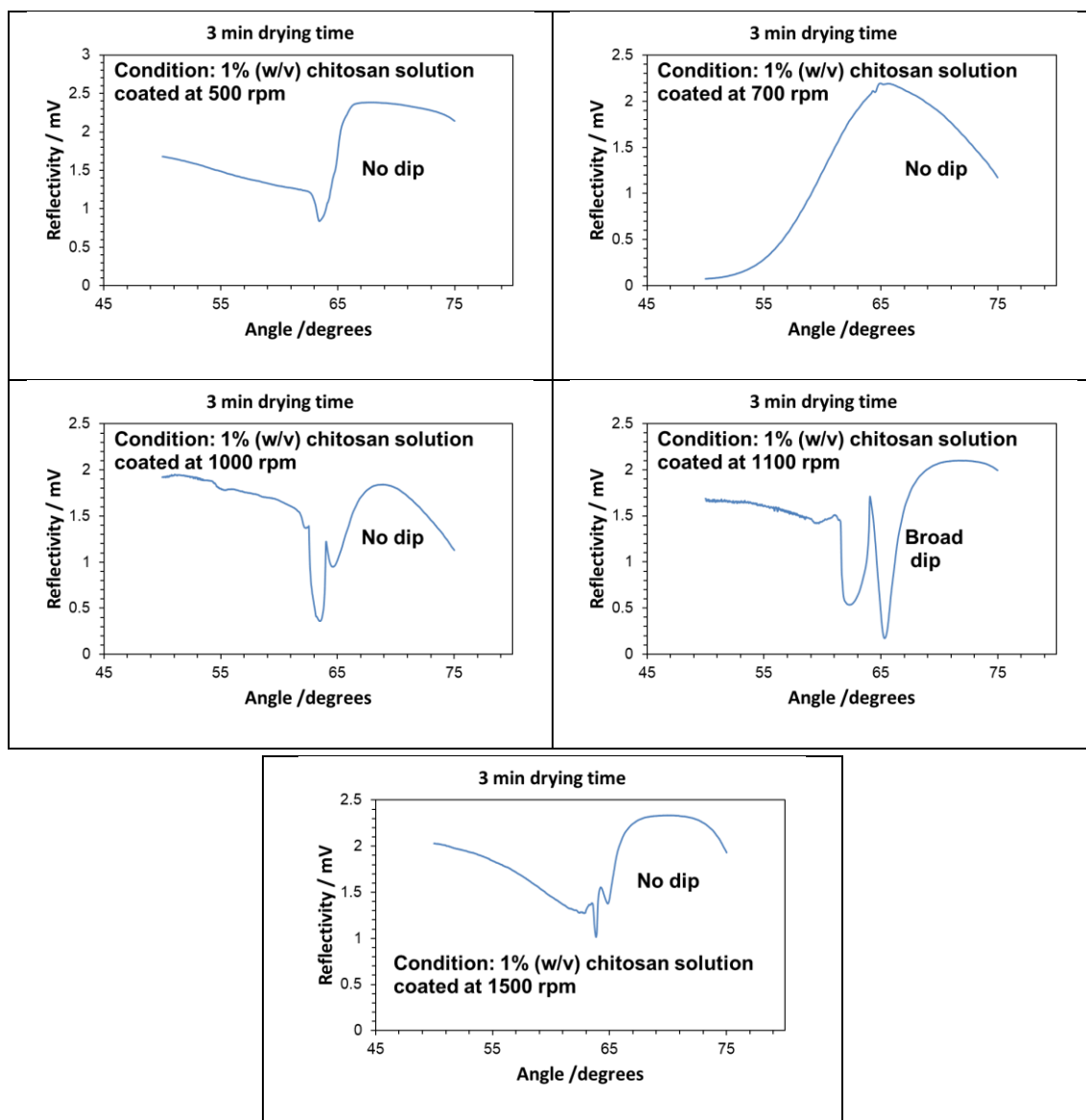
Figure 4.9 *Reflectivity curves as a function of incident angles from various chitosan films. All films were obtained from chitosan solution at a concentration of 1% (w/v) with deposition speeds ranging from 500 to 1500 rpm for 30 seconds. All coated films were then dried at room temperature for 3 min before being stained with RB4 (100 μM) for 5 min. The reflectivity from each film was then measured between incident angles of 50° and 75°. The experiment was repeated two times using two separate chitosan coated films for each deposition speeds. The results were comparable to all reflectivity curves in this figure.*
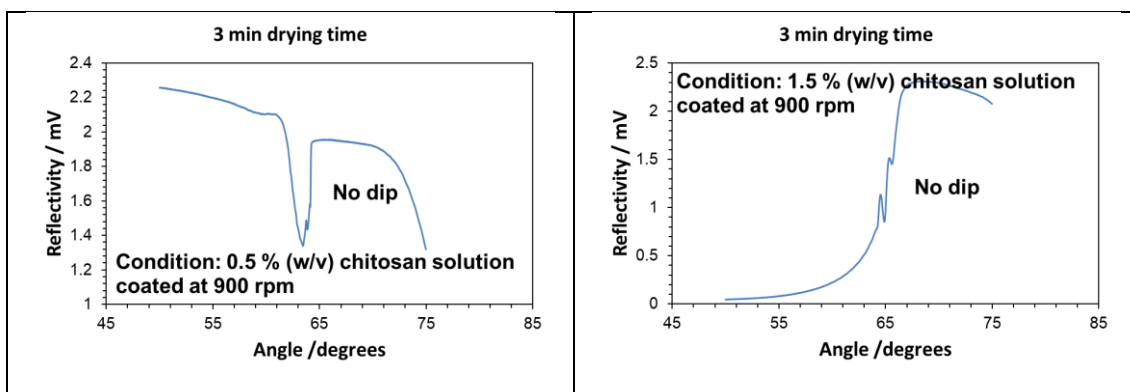
Figure 4.10 *Reflectivity curves as a function of incident angles from two chitosan films.*
The films were prepared from chitosan solution at concentrations of either 0.5 % (w/v)
or 1.5 % (w/v) with deposition speeds of 900 rpm for 30 seconds. All coated films were
then dried at room temperature for 3 min before being stained with RB4 dye (100 μM)
for 5 min. The reflectivity from each film was then measured between incident angles of
50° and 75°. The experiment was repeated two times using two separate chitosan coated
films for each concentration of chitosan used. The results were comparable to all
reflectivity curves in this figure.

4.3.1 Sensitivity of chitosan waveguide to refractive index

The sensitivity of the chitosan waveguide to the refractive index with drying time
condition was examined. This was accomplished by monitoring the shift in resonance
angle in a real-time upon applying glycerol solutions with known refractive index values.
A chitosan waveguide was prepared under the optimum conditions mentioned previously.
Briefly, chitosan solution (1%) was coated on glass substrate at speed of 900 rpm for 30
s. The film obtained was left to dry at room temperature for 3 min before incubation with
RB4 dye (100 μM) for 5 min. A series of concentrations of glycerol solutions were made
in the HEPES buffer (100 mM/ pH 7.4). The refractive index was then measured for each
solution. Finally, all solutions were applied sequentially into the chitosan waveguide at a
flow rate of 250 μL min^{-1} as explained in section 2.8.1.

The shift in resonance angle as a function of time upon introducing glycerol solutions into
the chitosan waveguide (1%) is displayed in figure 4.11. As can be seen from the figure,
the dip shifted to a higher degree once the concentration of applied glycerol increased.
This was because of the change in the refractive index of the waveguide. At a higher
concentration of glycerol (10%), the dip moved by 1.5°, with an increment in the
refractive index value of 0.014: the refractive index of glycerol (10%) (1.351) minus the

refractive index of the running buffer (HEPES buffer) (1.337). This was almost comparable to what has been observed previously when the same concentration of glycerol (10%) was applied into a 2% chitosan waveguide (Figure 3.9). The dip shifted to 1.4° with an increment in the refractive index value of 0.015. This would indicate that the sensitivity of the waveguide to the refractive index with drying time condition did not significantly change. The experiment was carried out three times using three chitosan waveguides (1%). The results are summarised in figure 4.12.
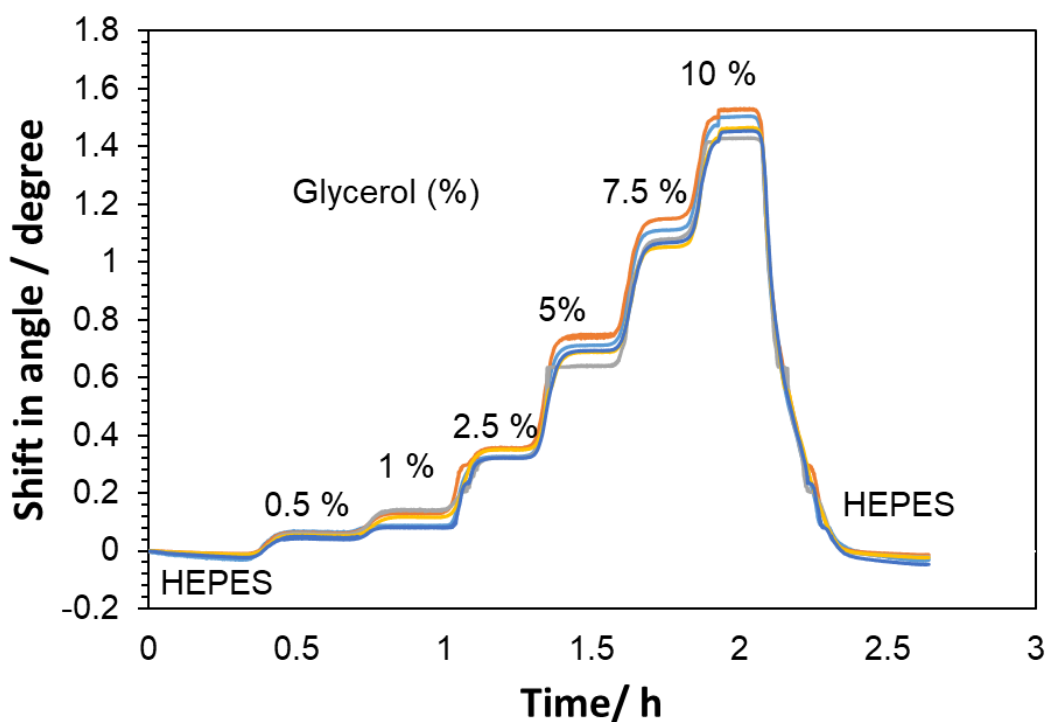
Figure 4.11 *Shift in resonance angle upon applying different concentrations of glycerol into chitosan waveguide (1%) at a flow rate of 250 µL min^{-1}. The waveguide was made at a concentration of 1% (w/v) with deposition speed of 900 rpm and 3 min drying time. All glycerol solutions were made in the HEPES buffer (100 mM/ pH 7.4) at different concentrations ranging from 0.5 % to 10 % (v/v) and were all pumped at the flow rate of 250 µL min^{-1}. Each solution of glycerol had a different refractive index value.*

Figure 4.12 exhibits the average shift in resonance angle from three chitosan waveguides (1%) as a function of refractive index value of glycerol solutions. The shift in resonance angle was directly proportional to the value of refractive index of glycerol leading to a trend line with a slope value of 106.55° RIU^{-1}. This was slightly higher than that observed in the 2% chitosan waveguide where the steepest slope was 100.67° RIU^{-1} (Figure 3.10)

upon introducing glycerol solutions. Therefore, the sensitivity to the refractive index was not significantly changed upon utilising a lower concentration of chitosan (1%) and controlling the drying time of the obtained wet film. This was also confirmed by a two way ANOVA statistical analysis which indicated that there was not significant difference between 1% and 2% chitosan waveguides in terms of shifting in resonance angle upon applying glycerol solutions between 0.5 % to 10%. The p-value was at 0.36 (> 0.05). The chitosan waveguide with drying time condition was further characterised in terms of the waveguide' porosity as shown below.

$$y = 106.55x - 142.44$$
$$R^2 = 0.999$$
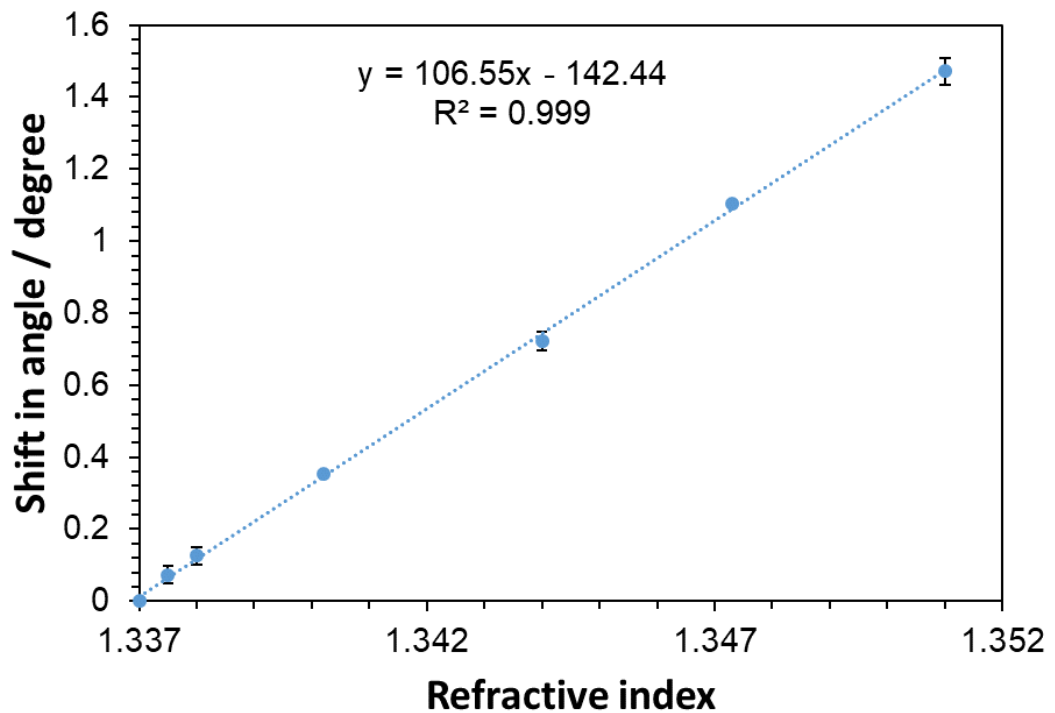
Figure 4.12 Average shift in resonance angle from three chitosan waveguides (1%) as a function of the refractive index value of glycerol solutions. All waveguides were made at the concentration of 1% (w/v) with deposition speed of 900 rpm and with 3 min drying time. All glycerol solutions were made in the HEPES buffer (100 mM/ pH 7.4) at different concentrations ranging from 0.5 % to 10 % (v/v) and all were pumped at a flow rate of 250 μL min^{-1}. Each solution of glycerol had different value of refractive index.

4.3.2 Porosity of chitosan waveguide with drying time

The aim of this experiment was to investigate the porosity of the waveguide with drying time condition. This was performed by monitoring in a real-time the shift in resonance angle as a function of time on introducing small (glycerol) and large molecules (polymers) that were made at the same refractive index.

A chitosan waveguide (1%) was prepared with drying time condition as explained earlier. In order to make a clear comparison with previous condition, chitosan waveguide was also produced at a concentration of 2% (w/v) with deposition speed of 3000 rpm. The film obtained was then left to fully dry at room temperature. Both waveguides were then stained with dye for 5 min before inserting into a flow cell as explained in section 2.8.2. Glycerol and polymers solutions that were made in the HEPES buffer (100 mM/ pH 7.4) at the same refractive index (1.3365) were then sequentially applied to each waveguide at a flow rate of 250 µL min^{-1}.

Figure 4.13 displays the shift in resonance angle as a function of time upon applying glycerol and polymer solutions into the chitosan waveguide (1%). As can be seen from the figure, the dip shifted to 0.075° with the glycerol solution at a refractive index value of 1.3365. Upon applying polymer solutions at different molecular weights (10 kDa, 35 kDa, 40 kDa, 200 kDa and 400 kDa) and at the same refractive index, the dip moved to a higher degree of angles with all polymer solutions. As an example, the dip shifted by 0.05° when 40 kDa polymer solution was applied. In contrast, using a 2% chitosan waveguide, the dip only moved by 0.005° (Figure 4.14) when the same polymer at the same molecular weights (40 kDa) and at the same value of refractive index (1.3365) was introduced. This leads to the conclusion that using a lower concentration of chitosan and controlling the drying time of the coated film has shown a large enhancement in the waveguide's porosity in comparison with the 2% chitosan waveguide. To obtain a reproducible result, the experiment was carried out three times using three different chitosan waveguides (1%). The findings are summarised in figure 4.15.
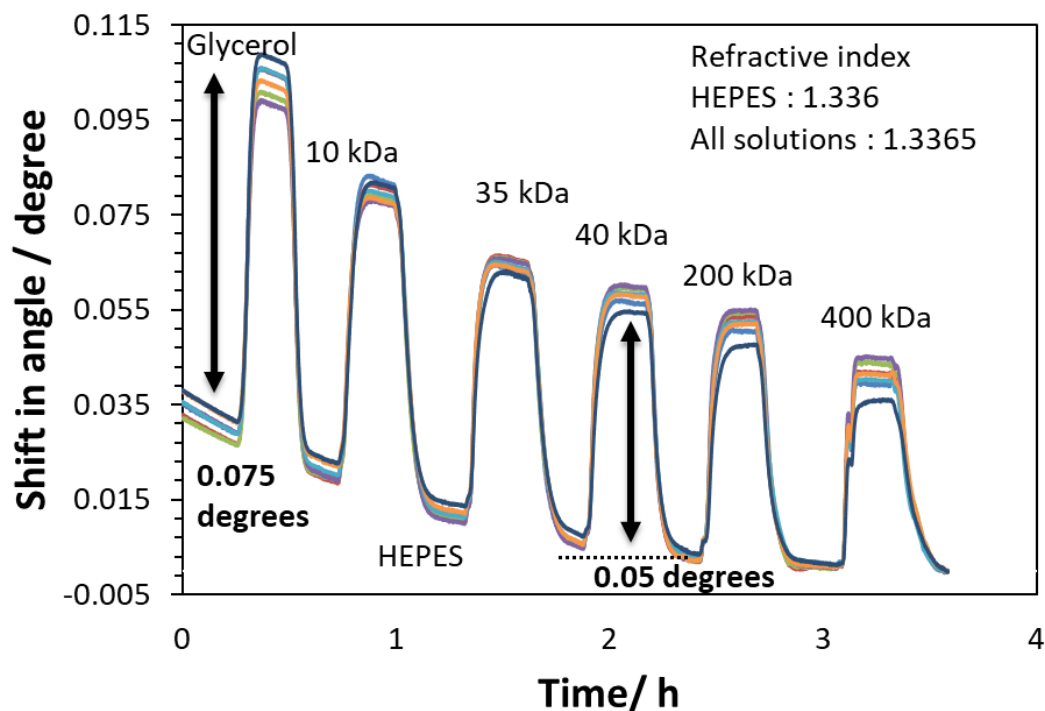
Figure 4.13 *Degree of shift in resonance angle as a function of time upon applying glycerol and polymer solutions (10 kDa, 35 kDa, 40 kDa, 200 kDa and 400 kDa) to the chitosan waveguide (1%) at the flow rate of 250 μL min⁻¹. The waveguide was obtained at a concentration of 1% (w/v) with deposition speed of 900 rpm and with 3 min drying time. All solutions were made in the HEPES buffer (100 mM/ pH 7.4) at the same refractive index (1.3365). The experiment was performed one time using one chitosan waveguide.*
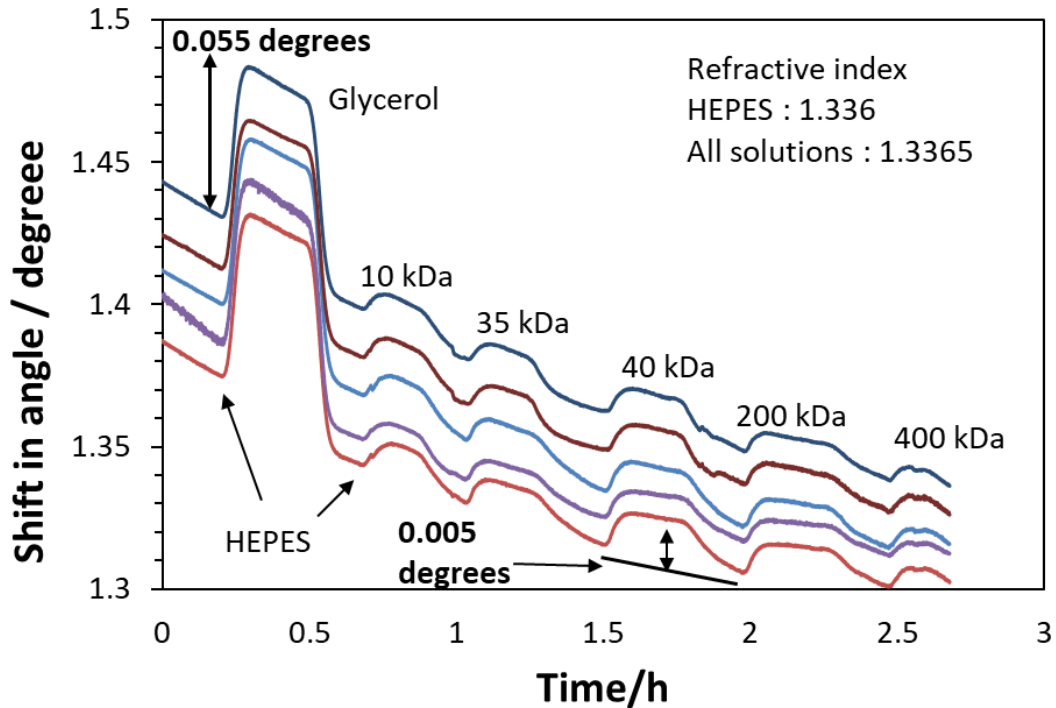
Figure 4.14 *Degree of shift in resonance angle as a function of time upon applying glycerol and polymer solutions (10 kDa, 35 kDa, 40 kDa, 200 kDa and 400 kDa) to the chitosan waveguide (2%) at a flow rate of 250 µL min⁻¹. The waveguide was obtained at a concentration of 2% (w/v) with deposition speed of 3000 rpm and with a fully dried film. All solutions were made in the HEPES buffer (100 mM/ pH 7.4) at the same refractive index (1.3365). The experiment was performed one time using one chitosan waveguide.*

Figure 4.15 shows the average shift in resonance angle upon applying glycerol and polymer solutions (10 kDa, 35 kDa, 40 kDa, 200 kDa and 400 kDa) into three chitosan waveguides (1%) at the same refractive index (1.3365). The shift in resonance angle observed upon applying glycerol and polymers to the 2% chitosan waveguide (Figure 4.14) was added here to show a clear comparison. From the figure, it can be seen that the highest shift in resonance angle was obtained when the glycerol solution was applied; the dip moved by 0.075° as an average of three runs. This level of shift then gradually decreased upon increasing the molecular weights of the polymer applied. At the highest molecular weight (400 kDa), the dip shifted only to 0.04°. This could be related to the porosity of the waveguide (1%) with the drying time where the pores were not large enough to allow larger polymers to diffuse into the same level of glycerol. Therefore, lower shifting was obtained with increasing the molecular weights. This was also indicated by a one way ANOVA statistical analysis in which there was a significant

157

differences in terms of shifting in resonance angle between glycerol and all other polymers solutions when they were applied onto 1% chitosan waveguide (p-value $\leqslant$ 0.001).

The error bars were slightly higher with polymer solutions. This would be linked to the effectiveness of the room temperature and the relative humidity on the wet film obtained. It has been noticed that at a higher temperature the film dried more rapidly before reaching 3 min while at a higher humidity the film was still wet even after 3 min. This variation would have an effect on the porosity of the waveguide as it would increase or decrease the evaporation of water molecules and hence the shrinking of the pore size. Nevertheless, the observed shift with all polymer solutions onto 1% chitosan waveguides was significantly higher than when they were introduced into a 2% chitosan waveguide as shown in figure 4.15. Using a two way ANOVA statistical analysis, it was found that there was a significant difference in terms of shifting in resonance angle when polymer solutions (10 kDa, 35 kDa, 40 kDa, 200 kDa and 400 kDa) were applied onto 1% and 2% chitosan waveguides. For 2% chitosan waveguide, the data was obtained from figure 3.15 as the experiment was run three times. This would further confirm the successful enhancement on the waveguide's porosity using a lower concentration of chitosan and controlling the drying time of the coated film. The porosity of the waveguide was further characterised using different cross-linkers, as described in the following section.
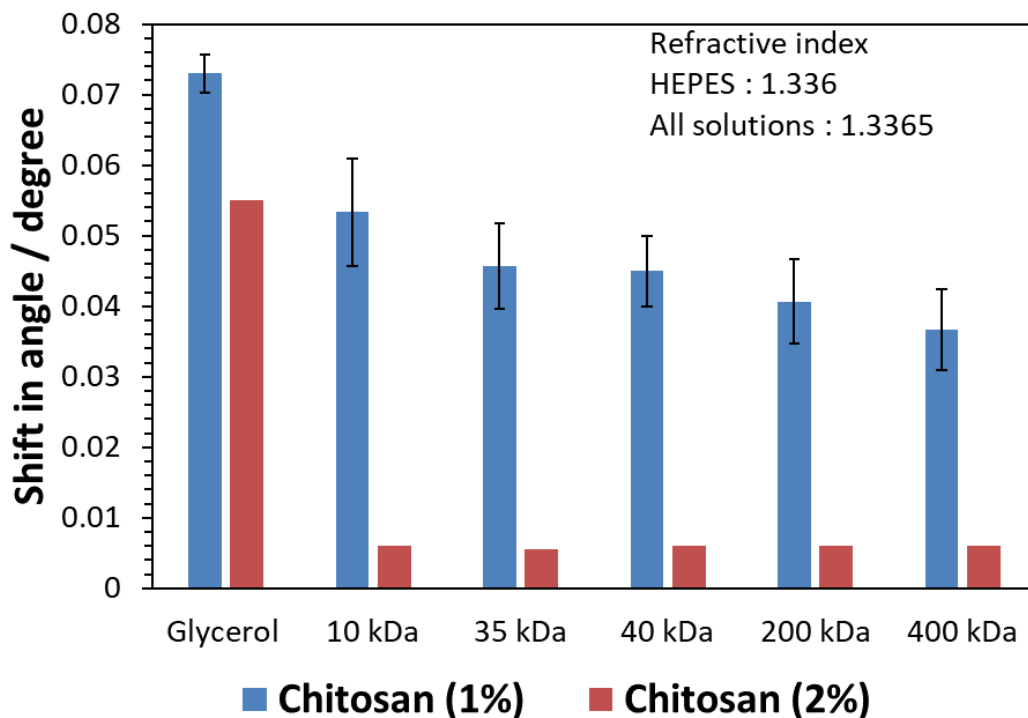
Figure 4.15 *Average shift in resonance angle upon introducing glycerol and polymer solutions (10 kDa, 35 kDa, 40 kDa, 200 kDa and 400 kDa) into three chitosan waveguides (1%) at a flow rate of 250 μL min⁻¹. The waveguides were produced at a concentration of 1% (w/v) with deposition speed of 900 rpm and with 3 min drying time. The figure also includes the shift in resonance angle upon applying glycerol and polymers into a chitosan waveguide that had been prepared at a concentration of 2% (w/v) with deposition speed of 3000 rpm and with a fully dried film. The experiment on 2% chitosan waveguide was performed one time using one separate chitosan waveguide. All solutions applied into both waveguides (1% and 2%) were all made in the HEPES buffer (100 mM/ pH 7.4) at the same refractive index (1.3365). A one way ANOVA statistical analysis indicated that there was a significant differences in terms of shifting in resonance angle between glycerol and all other polymers solutions when they were applied onto 1% chitosan waveguide (p-value ⩽ 0.001).*

4.3.3　Cross-linking chitosan film with drying time

The aim of this experiment was to further investigate the waveguide's porosity by using a cross-linker named NHS-PEG-NHS. The waveguide was cross-linked via NHS ester making amide bonds with two functional amino groups [157] on chitosan polymer as demonstrated in figure 4.16. This in turn leads to an enhancement in the rigidity and the stability of the obtained wet film which could eliminate the effectiveness of the room

temperature and the relative humidity on the waveguide pore size as mentioned previously in figure 4.15. However, using a cross-linker could also lead to increase or decrease the porosity of the waveguide which in turn could influence the diffusion of the large molecule such as bio-recognition element. Therefore, in this experiment, various lengths of the cross-linker presented by different molecular weights (2 kDa, 3 kDa and 10 kDa) were utilised in order to examine its impact on the waveguide's porosity.

Chitosan waveguides (1%) were produced with drying time condition. Upon drying for 3 min, a few droplets of NHS-PEG-NHS (1 mM w/v) solution was then doped on the top of the chitosan film for 5 min followed by incubation with HEPES buffer (100 mM/ pH 7.4) for 10 min and subsequently with RB4 dye (100 µM) for 5 min. Finally, glycerol and polymer solutions at the same refractive index were then applied to each waveguide as explained in section 2.8.3.
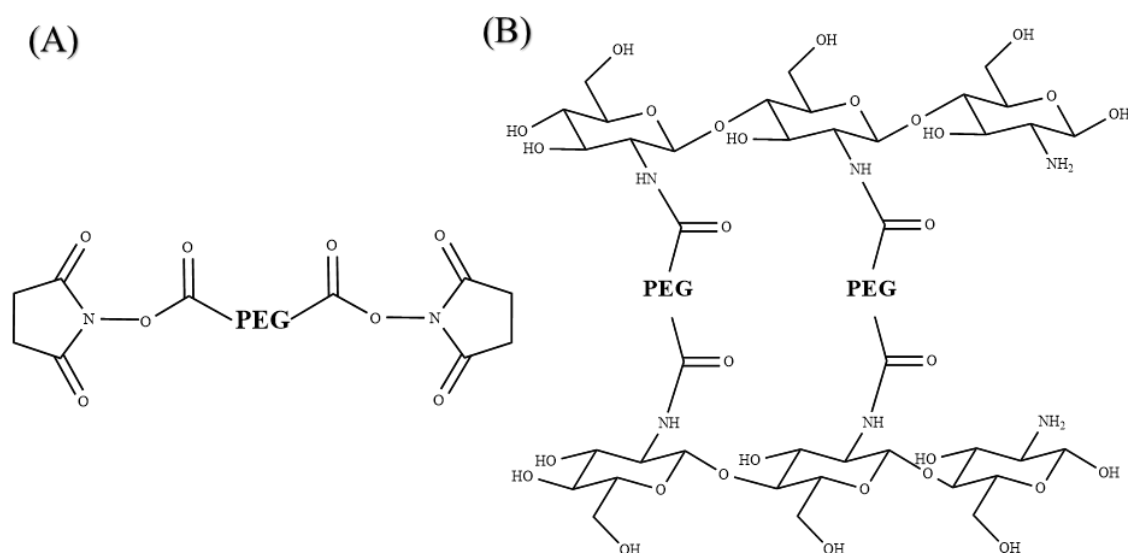
Figure 4.16 (A) *Diagram of NHS-PEG-NHS structure,* (B) *Final stage of cross-linked chitosan polymer with NHS-PEG-NHS.*

Figure 4.17 shows the change in resonance angle upon introducing glycerol and polymers solutions into a chitosan waveguide (1%). The waveguide was initially cross-linked with NHS-PEG-NHS at a molecular weight of 3 kDa. It can clearly be seen that the shift in resonance angle was higher with the glycerol solution, where the dip moved by 0.08°. Upon flushing the surface with polymer solutions, the shift in resonance angle was almost the same, in particular at molecular weights of 10 kDa, 35 kDa and 40 kDa at which the dip moved by 0.046°. This was similar to what was observed when polymer solutions at

the same molecular weights were applied into non-cross linked waveguides (Figure 4.15). However, an obvious reduction in the dip shift was observed at higher molecular weights (200 kDa and 400 kDa). For non-cross linked waveguide, the shift was at 0.04° (Figure 4.15) with the highest molecular weight (400 kDa), while in this experiment it was at 0.028°. This reduction could be related to the molecular weight of the cross-linker used (3 kDa) which influenced the pore size of the chitosan waveguide. In order to further examine this effect, the experiment was carried out three times using three chitosan waveguides (1%). The results are shown in figure 4.18.
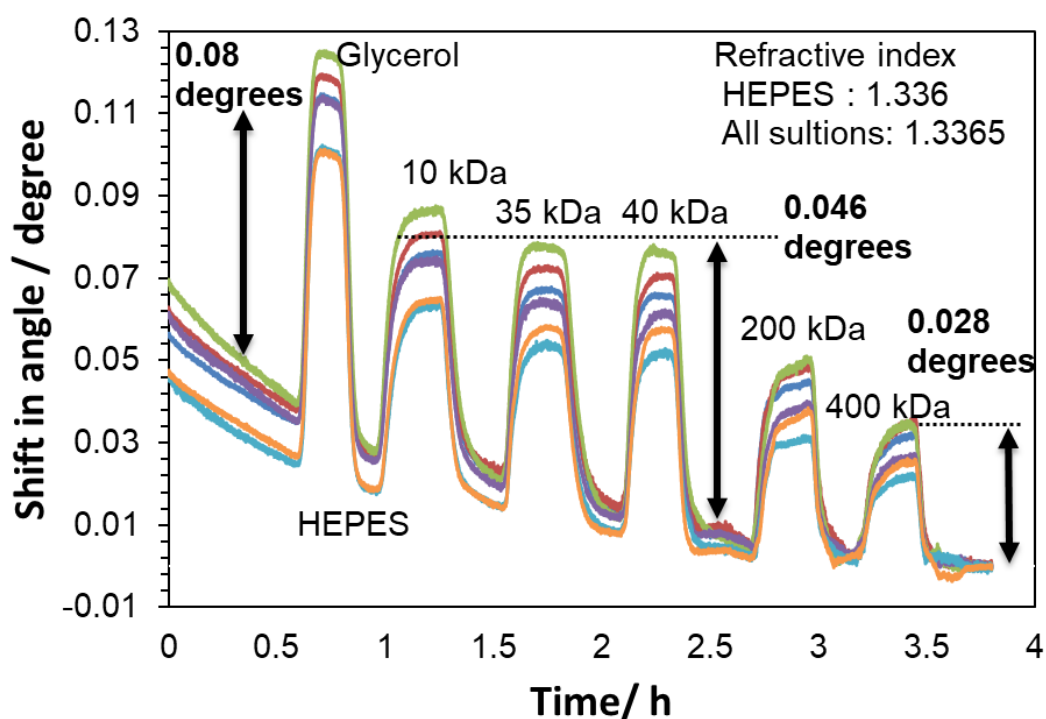
Figure 4.17 *Shift in resonance angle as a function of time upon applying glycerol and polymer solutions (10 kDa, 35 kDa, 40 kDa, 200 kDa and 400 kDa) into a chitosan waveguide (1%) at a flow rate of 250 µL min⁻¹. The chitosan waveguide was produced at a concentration of 1% (w/v) with deposition spin speed of 900 rpm and with 3 min drying time. The waveguide was then cross-linked with NHS-PEG-NHS at a molecular weight of 3 kDa. All solutions were made in the HEPES buffer (100 mM/ pH 7.4) at the same refractive index (1.3365). The experiment was performed one time using one chitosan waveguide.*

Figure 4.18 shows the average shift in resonance angle from three chitosan waveguides (1%) on introducing glycerol and polymer solutions at the same refractive index (1.3365). All waveguides were initially cross-linked with NHS-PEG-NHS at a molecular weight

of 3 kDa. From the figure, it can be seen that the average shift in resonance angle upon applying glycerol solution into three cross-linked chitosan waveguides (1%) was 0.075°. This was also identical when the same solution at the same refractive index was applied into non cross-linked waveguides (1%), showing the shift at 0.075° (Figure 4.15). When polymer solutions were introduced, the degree of shifting gradually decreased as the molecular weights of polymer applied increased, as was noticed previously in figure 4.15. However the reduction in the degree of shift was clearly different insofar as at the highest molecular weight (400 kDa), the dip only moved by 0.02°. In contrast, the dip shifted by 0.04° when the same molecular weight (400 kDa) at the same refractive index was flushed through non cross-linked waveguides (Figure 4.15). This clear difference in terms of shift in resonance angle might be related to the length of the cross-linker used presented by its molecular weight (3 kDa) that reduced the pore size. This was also confirmed by a two way ANOVA statistical analysis in which there was a difference in terms of shifting in resonance angle between cross-linked and non cross-linked chitosan waveguides when 400 kDa polymer solution was applied. The p-value was at 0.011 (<0.05). In order to further clarify this impact, the experiment was repeated using different molecular weights of cross-linker. The findings are summarised in figure 4.19.
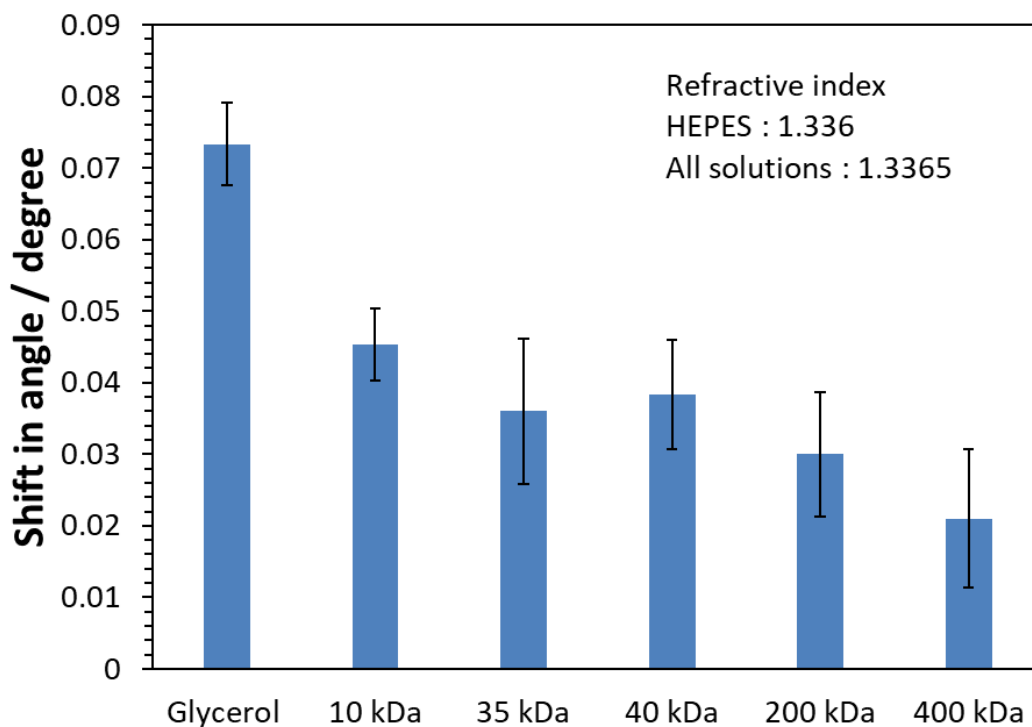
Figure 4.18 *Average shift in resonance angle as a function of introducing glycerol and polymer solutions (10 kDa, 35 kDa, 40 kDa, 200 kDa and 400 kDa) at the flow rate of 250 μL min^{-1}into three chitosan waveguides (1%). The waveguides were produced at a concentration of 1% (w/v) with deposition spin speed of 900 rpm and with 3 min of drying time. All waveguides were then cross-linked with NHS-PEG-NHS at a molecular weight of 3 kDa. A one way ANOVA statistical analysis indicated that there was a significant differences in terms of shifting in resonance angle between glycerol and all other polymer solutions when they were applied onto a cross-linked chitosan waveguide (1%) (p-value ≤ 0.001).*

Figure 4.19 exhibits the shift in resonance angle as a function of applying glycerol and polymer solutions onto two chitosan waveguides (1%). The waveguide was initially cross-linked with NHS-PEG-NHS either at a molecular weight of 2 kDa or 10 kDa as indicated in the figure. The reading represents one run for each cross-linker used. It can be seen from the figure that a similar behaviour was observed in which the shift gradually decreased when a higher molecular weight of polymer was applied. At the highest molecular weight (400 kDa), the dip moved by 0.035° when it was flushed through the 10 kDa cross-linked waveguide while the dip shifted by 0.02° when the same solution was introduced into the 2 kDa cross-linked waveguide. From the previous figure (Figure 4.18), the shift was at 0.021° for the same solution applied into the 3 kDa cross-linked

waveguide. This would lead us to say that using a higher molecular weight of cross-linker (10 kDa) results in a higher pore size for a molecular weight of 400 kDa. However, it was still lower than 0.04° when the same solution at the same refractive index was flushed through non cross-linked waveguides (Figure 4.15). This reduction of the pore size of the waveguide could be due to the influence of using cross-linkers or could be due to the impact of the room temperature and relative humidity on the porosity of the waveguide as mentioned previously in figure 4.15. In order to further investigate the effectiveness of using a cross-linker, various pHs buffers were flushed through cross-linked waveguide. The cross-linked waveguide should be stable and responded well at wide range of pH due to the covalent linkage between chitosan's functional groups. The results are shown in the following section.
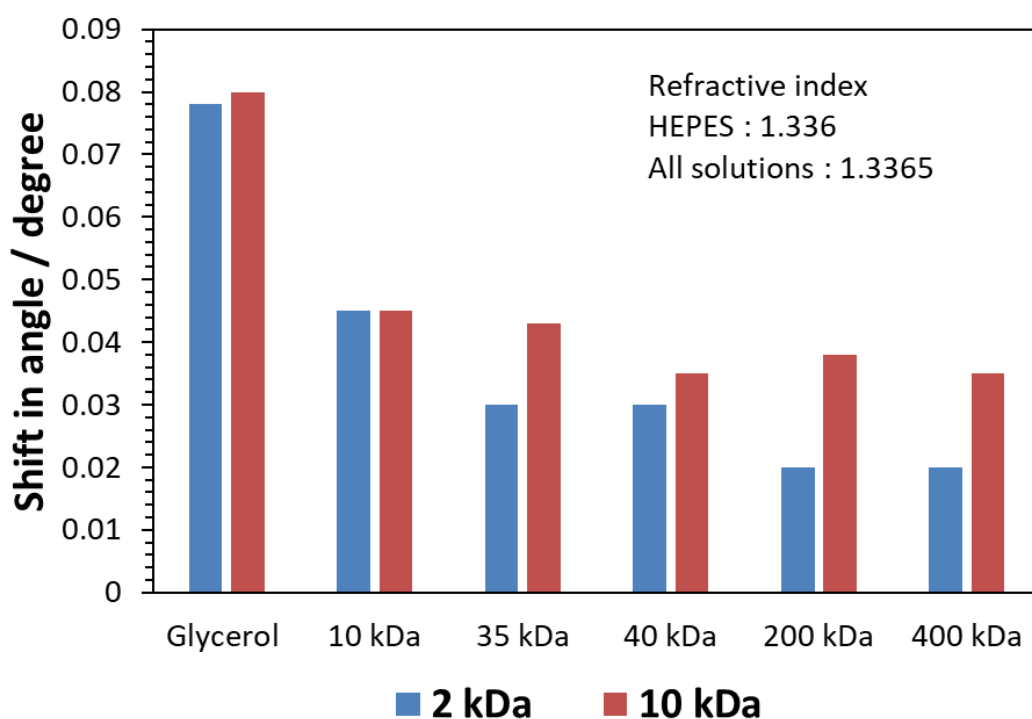
Figure 4.19 Shift in resonance angle upon introducing glycerol and polymer solutions *(10 kDa, 35 kDa, 40 kDa, 200 kDa and 400 kDa) at a flow rate of 250 µL min^{-1}into two chitosan waveguides (1%). The waveguides were produced at 1% (w/v) of chitosan concentration with deposition speed of 900 rpm and with 3 min of drying time. The waveguides were then cross-linked with NHS-PEG-NHS at a molecular weight of either 2 kDa or at 10 kDa as indicated on the figure. All solutions were made in the HEPES buffer (100 mM/ pH 7.4) at the same refractive index (1.3365). The experiment was performed one time using one separate chitosan waveguide for each cross linker used.*

4.3.4   Effect of pH on cross-linked and non cross-linked waveguide

The effect of pH on cross-linked and non cross-linked waveguides was investigated. Two chitosan waveguides (1%) were produced. One of the waveguides was cross-linked with NHS-PEG-NHS at a molecular weight of 3 kDa as described in section 2.8.4. HEPES buffer (100 mM) at various pH from 8.5 to 4.5 was introduced sequentially into both waveguides. Between each buffer, HEPES at pH 7.5 was flushed through the surface.

The change in resonance angle upon applying various pH buffers onto a non cross-linked waveguide (1%) is shown in figure 4.20. As can be seen from the figure, a significant reduction in the resonance angle was observed when the surface was flushed with HEPES buffer at pH 8.5. The dip shifted to a lower resonance angle by 0.075°. This is attributed to deprotonation of the amino groups ($-NH_2$) at higher pH which would lead to a reduction in electrostatic repulsion between the positive charge amino groups ($-NH_3^+$). Consequently, a change in the thickness of the waveguide occurred and hence a shift in the resonance angle (θr) was obtained [142]. The dip remained at the same resonance angle even when the HEPES buffer at pH 7.4 was flushed again. This could be due to irreversible shrinking of the thickness of the waveguide. Upon introducing a buffer of lower pH, the dip moved slightly to a higher degree with pH 6.5 and 5.5 and then returned back to the same level with pH 7.4. At pH 4.4, a reduction on the resonance angle immediately occurred. This significant reduction occurred because the waveguide mode no longer existed at pH 4.4 and hence the dip totally disappeared. This would be attributed to the pKa value of chitosan polymer that is about 6.5[146]. At lower pH, the amino group is positively charged and hence chitosan is soluble. In contrast, it is insoluble at neutral and basic pH conditions due to the deprotonation of amino groups. This would lead us to say that at pH 4.4, the chitosan film was totally affected by the high protonation of the amino groups on the surface and hence the waveguide mode totally collapsed and the dip therefore disappeared. Although the pKa value of chitosan polymer is about 6.5, the waveguide mode operated at pH 6.4 and at 5.4, allowing the possibility of bioassay measurement at various pH.
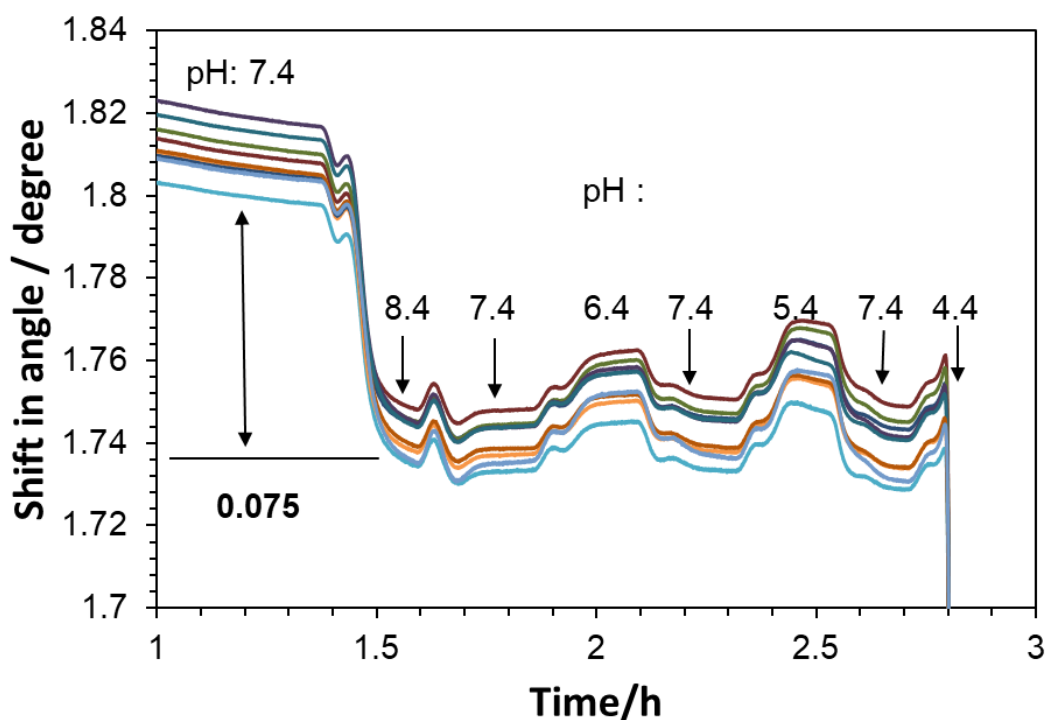
Figure 4.20 *Shift in resonance angle as a function of time upon applying HEPES buffer (100 mM) under various pH (8.4, 7.4, 6.5, 5.4 and 4.4) into a non cross-linked chitosan waveguide (1%). The buffers were sequentially pumped at a flow rate of 250 µL min^{-1}. The waveguide was produced at a concentration of 1% (w/v) with coating spin speed of 900 rpm and with 3 min drying time. The experiment was performed one time using one chitosan waveguide.*

Figure 4.21 shows the same experiment performed on a cross-linked waveguide (3 kDa). Similar behaviour was observed where a reduction in the resonance angle was seen at higher pH. Using a cross-linker should result in a lower degree of shrinking or swelling of the chitosan waveguide due to the covalent linkage between its functional amino groups. However, in this experiment, the reduction in the resonance angle from pH 7.4 to 8.4 was at 0.07° which was almost identical to that of the non cross-linked waveguide (0.075° /Figure 4.20). Furthermore, using a cross-linker should eliminate the dissolving of the waveguide at lower pH (lower than the pKa value) due to the covalent linkage between amino functional groups. This was confirmed when glutaraldehyde was utilised as a cross-linker on 2% chitosan waveguide (chapter three). The waveguide mode operated successfully even at pH 4 (Figure 3.3). Here in this experiment, at pH 4.4 an immediate drop in the resonance angle was observed, indicating the dissolving of the chitosan waveguide as it had been obtained previously in the non cross-linked waveguide

(Figure 4.20). This was also confirmed by an image from a CMOS camera where the dip at pH 4.4 had totally disappeared as shown in figure 4.22. This leads to the conclusion that using NHS-PEG-NHS as a cross-linker was not effective as the waveguide mode was totally dissolved at lower pH.
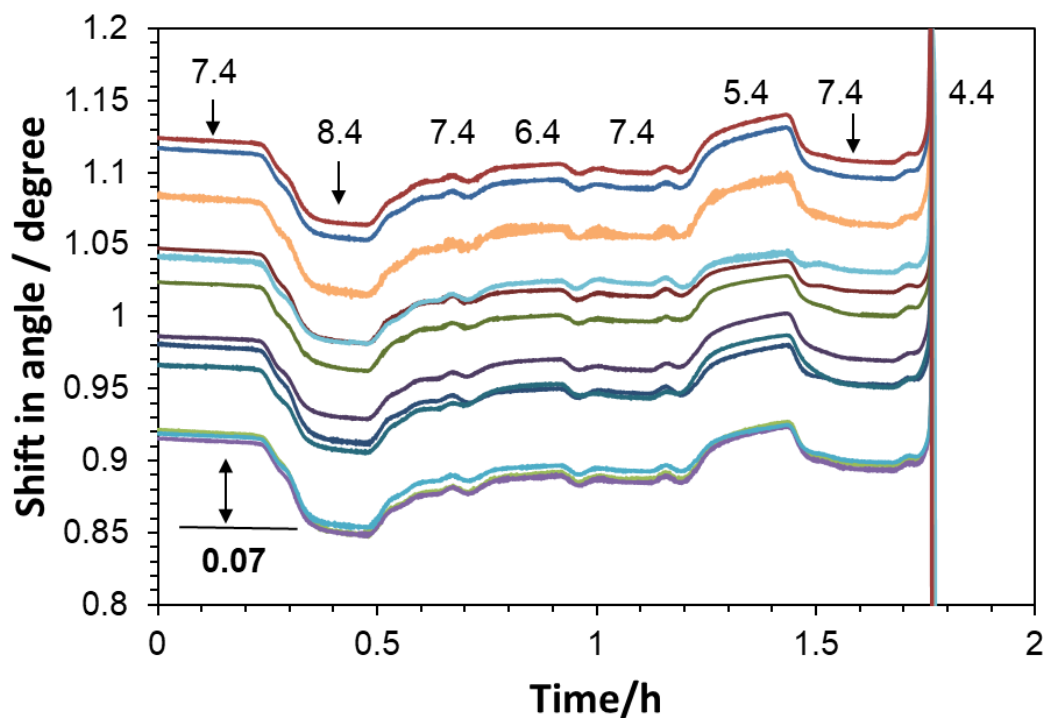
Figure 4.21 *Shift in resonance angle as a function of time upon applying HEPES buffer (100 mM) at various pH values (8.4, 7.4, 6.5, 5.4 and 4.4) into a cross-linked chitosan waveguide (1%). The buffers were sequentially pumped at a flow rate of 250 μL min⁻¹. The waveguide was produced at a concentration of 1% (w/v) with coating spin speed of 900 rpm and with 3 min of drying time. The film was then cross-linked with NHS-PEG-NHS at a molecular weight of 3 kDa. The experiment was performed one time using one chitosan waveguide.*
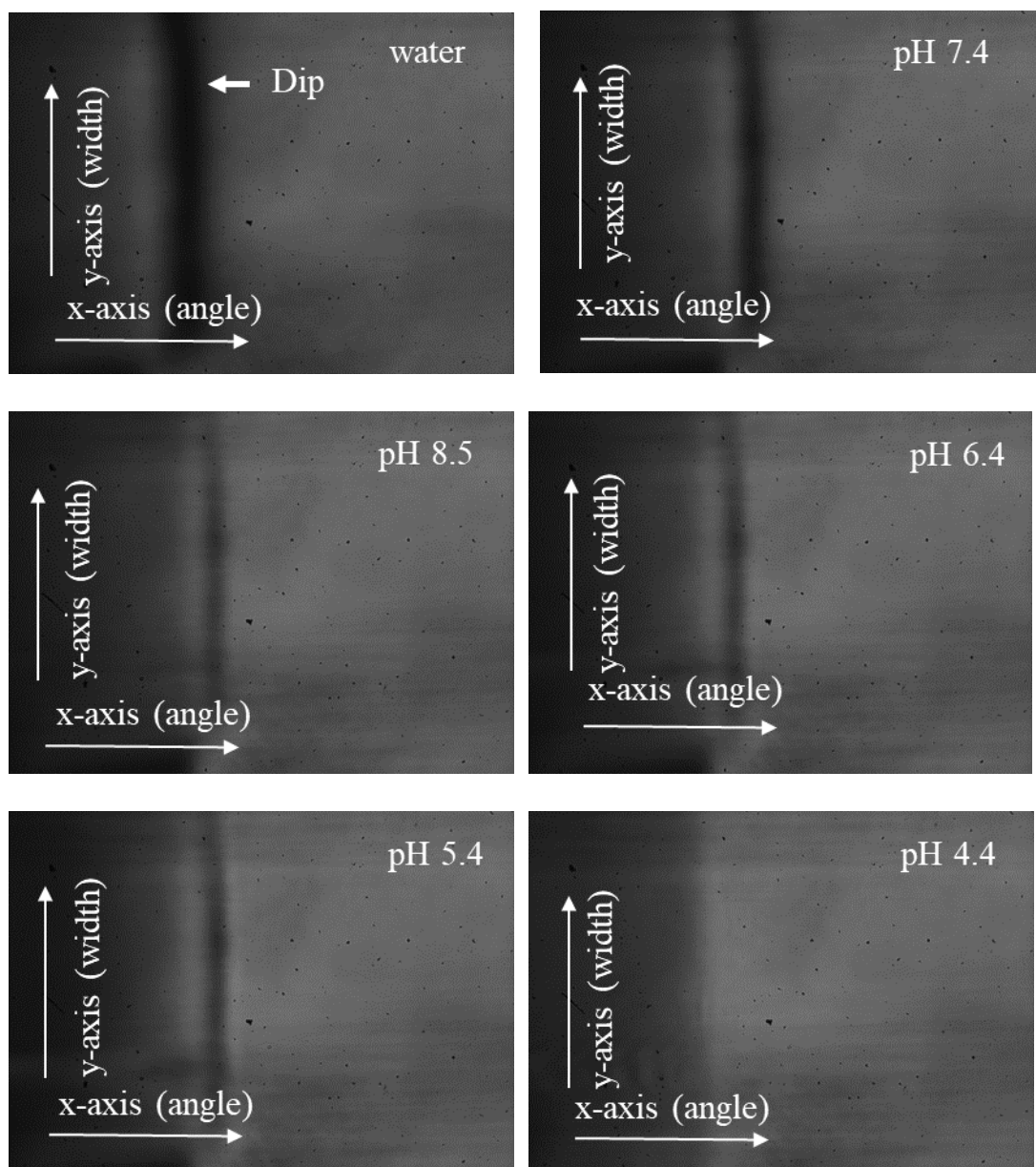
Figure 4.22 *photographs of the dip taken by CMOS camera from a cross-linked chitosan waveguide (1%) (NHS-PEG-NHS / 3 kDa) upon applying HEPES buffer at various pH values (8.4, 7.4, 6.4, 5.4 and 4.4). The dip was totally removed from the image at pH 4.4 indicating the dissolving of the chitosan waveguide (1%).*

The pore size with drying time condition using non cross-linked waveguide was significantly enhanced by comparison with 2% chitosan waveguide. At a molecular weight of 40 kDa which is higher than the molecular weight of the target analytes in this project (Thrombin (37 kDa) and Prostate specific antigen (34 kDa)), the shift in the resonance angle was on average 0.05° (Figure 4.15). In contrast, the shift in the resonance angle was at 0.005° when the same molecular weight (40 kDa) at the same refractive

index was applied on 2% chitosan waveguide. This was also confirmed by a two way ANOVA statistical analysis in which there was a significant difference in terms of shifting in resonance angle between 1% and 2% chitosan waveguides upon applying polymer solutions (p-value ≤ 0.001). This would lead us to say that the waveguide prepared with drying time condition and without using any cross-linker showed a large enhancement in terms of the porosity and therefore it was selected as the optimum condition for all following experiments.

4.3.5 Effect of ionic buffer on chitosan waveguide

The aim of this experiment was to investigate the effectiveness of using a high ionic strength buffer on a chitosan waveguide (1%). The pKa value of chitosan is 6.5, in which at neutral pH most amino groups ($-NH_2$) are deprotonated. However, full deprotonation of amino groups ($-NH_2$) would occur at the basic condition. Therefore a chitosan waveguide prepared at pH 7.4 would possess a few positively charged ($-NH_3^+$). The positive charge could influence the bioassay measurement as this would enhance the nonspecific binding of molecules. Using a high ionic strength buffer could eliminate or reduce this binding by shielding the charges on molecules. Therefore, an experiment was conducted to examine the impact of using HEPES buffer (pH 7.4 and pH 8), HEPES salt buffer (pH 7.4) and Tris salt buffer (pH 7.4) (table 2.4). The addition of this type of salt to the running buffers is required. They are usually utilised for aptamer immobilisation and also for the subsequent reaction with analyte [158, 159]. Oligonucleotide (Oligo 1 / table 2.2) and bovine serum albumin (BSA), both possessing a negative charge at pH 7.4 [160, 161], were made at a concentration of 0.5µM (v/v) and 0.5% (w/v) respectively, in various buffers as explained in section 2.8.5. Chitosan waveguides (1%) were first flushed with buffer solutions followed by introduction of either oligo 1 or BSA in the same running buffer at a flow rate of 118 µL min^{-1}.

Figure 4.23 shows the shift in resonance angle as a function of time upon introducing oligo 1 solutions (0.5 µM) into a chitosan waveguide (1%). Oligo 1 solutions were prepared in the HEPES buffer (pH 7.4) and the Tris salts (pH 7.4) buffer, and each buffer was used in a separate waveguide. From the figure, it can be seen that the dip moved by 1.3° upon applying the oligo1 solution that had been made up in the HEPES buffer (pH 7.4). After reaching a saturation level, the dip remained at almost the same level even when the running buffer (HEPES buffer (pH 7.4)) was flushed again through the surface. This would indicate the binding of oligo 1 to the chitosan waveguide via a positive-

negative interaction [161]. This would also confirm that chitosan waveguide (1%) featured a positive charge at pH 7.4. In contrast, the dip shifted only by 0.04° when oligo1 solution was flushed in the Tris salts (pH 7.4) buffer. This significant differences in terms of shift in the resonance angle between oligo 1 solutions (1.3°/0.04°) would be linked to the ionic strength of the running buffer. The Tris salts (pH 7.4) buffer was made by adding NaCl, KCl, $MgCl_2$ and $CaCl_2$ while the HEPES buffer (pH 7.4) was prepared without adding any salt. Therefore, adding salts into the running buffer leads to the shielding of the majority of the positive and negative charges on chitosan and DNA molecules and hence lower nonspecific binding occurred. This behaviour, in which the charge shielding in solution was raised with an increase in the solution ionic strength, has been reported previously. This resulted in an attenuation of interaction between DNA and chitosan molecules [162]. The effect of an ionic buffer on a chitosan waveguide (1%) was further investigated using bovine serum albumin (BSA) as shown in figure 4.24.
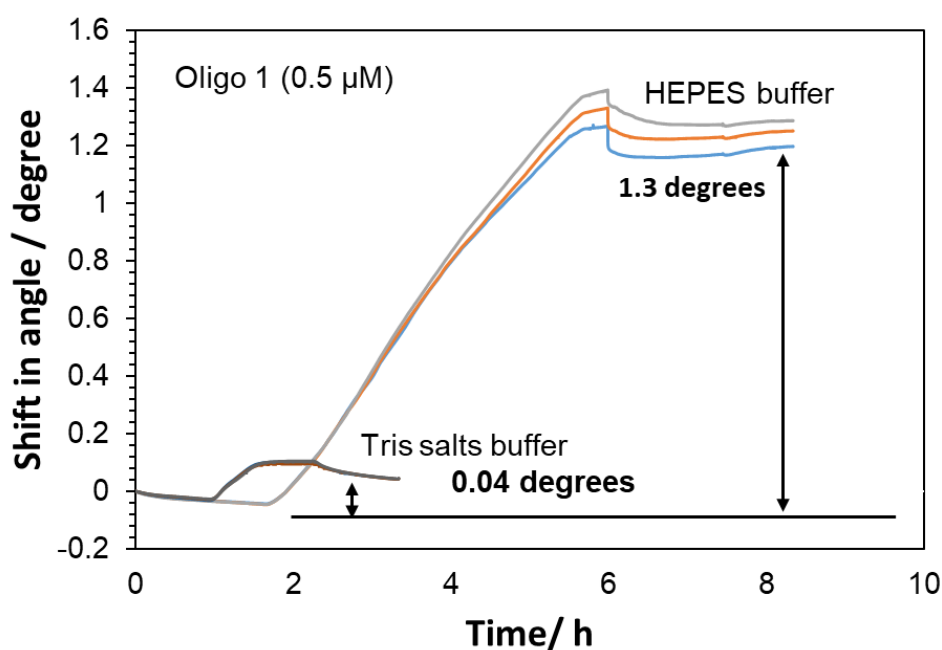
Figure 4.23 *Shift in resonance angle upon applying two oligo 1 (0.5 µM) solutions into two chitosan waveguides (1%) at a flow rate of 118 µL min⁻¹. The waveguides were produced at a concentration of 1% (w/v) with deposition spin speed of 900 rpm and with 3 min drying time. The oligo solutions were made 1) in the HEPES buffer (100 mM/ pH 7.4), and 2) in the Tris salts buffer (Tris-HCl (20 mM), NaCl (100 mM), KCl (5 mM), $MgCl_2$ (2 mM) and $CaCl_2$ (1 mM) pH 7.4). The experiment was performed one time using one separate chitosan waveguide for each buffer applied.*

Figure 4.24 displays the change in resonance angle as a function of time upon flushing the chitosan waveguide (1%) with BSA solutions (0.5%) made in the HEPES buffer (pH 7.4) and HEPES salts buffer (pH 7.4) (table 2.4). Each buffer was applied to a separate chitosan waveguide. As can be seen, a clear difference is observable upon applying BSA solution (0.5%) in the HEPES buffer. The dip reached saturation level at 0.8° and subsequently stabilised at 0.6° when the running buffer (HEPES buffer) was reapplied. This was totally different to the BSA in HEPES salts buffer where the saturation level was at 0.05° and the dip afterwards returned back to the original baseline with running buffer (HEPES salts buffer). From this , it could be concludes that the BSA in the HEPES buffer was bound to the chitosan waveguide, while this binding was eliminated in the HEPES salt buffer. BSA was successfully adsorbed on chitosan microsphere at various pH while the reaction at pH ≤ 6.5 was attributed to electrostatic interactions and the reaction at pH ≥ 6.5 was suggested to be linked to van der Walls interactions[163]. However, figure 4.25 shows the change in resonance angle upon introducing BSA (0.5 %) solution made in the HEPES buffer at pH 8 and without adding any salts. It can be clear that BSA molecules did not interact with the chitosan waveguide (1%) at pH 8 as the dip returned back to the original baseline with running buffer (HEPES buffer pH 8). The isoelectric point (pI) of BSA is 4.8 [160] so it possesses negative charge at pH 8 while the pKa value of chitosan is at 6.5 [146] in which the amino group would be almost neutral at pH 8. This would confirm that the reaction between BSA and chitosan waveguide was also eliminated using a higher pH of the HEPES buffer. This was because of the deprotonation of all amino groups (-NH2) on the chitosan waveguide at pH 8. This also confirms that the reaction between BSA and chitosan observed in figure 4.24 at pH 7.4 was linked to the negative-positive attraction. To obtain a reproducible result, the experiment was carried out three times using three chitosan waveguides (1%) for each buffer used. The results are summarised in figure 4.26.
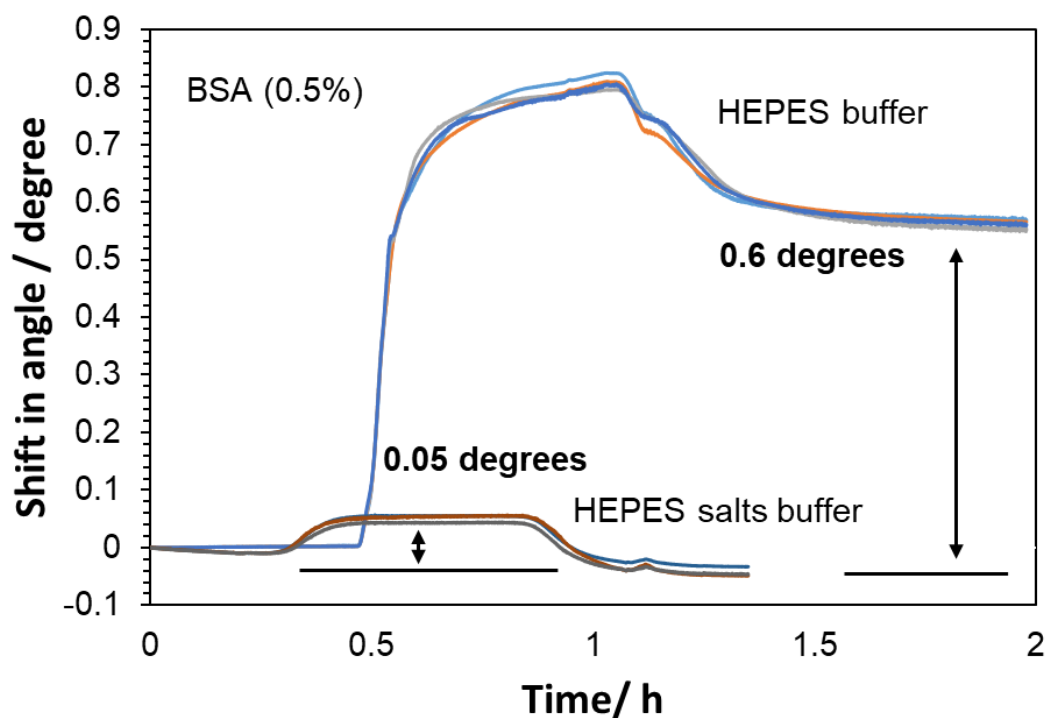
Figure 4.24 *Shift in resonance angle as a function of time upon applying BSA (0.5%) solutions into two chitosan waveguides (1%) at a flow rate of 118 μL min⁻¹. The waveguide was produced at a concentration of 1% (w/v), with deposition spin speed of 900 rpm and with 3 min drying time. The BSA solutions were made in the HEPES buffer (100 mM/ pH 7.4) and in the HEPES salts buffer (HEPES (100 Mm), NaCl (100 mM), KCl (5 mM), MgCl$_2$ (2 mM) and CaCl$_2$ (1 mM) pH 7.4). The experiment was run one time using one separate chitosan waveguide for each buffer used.*
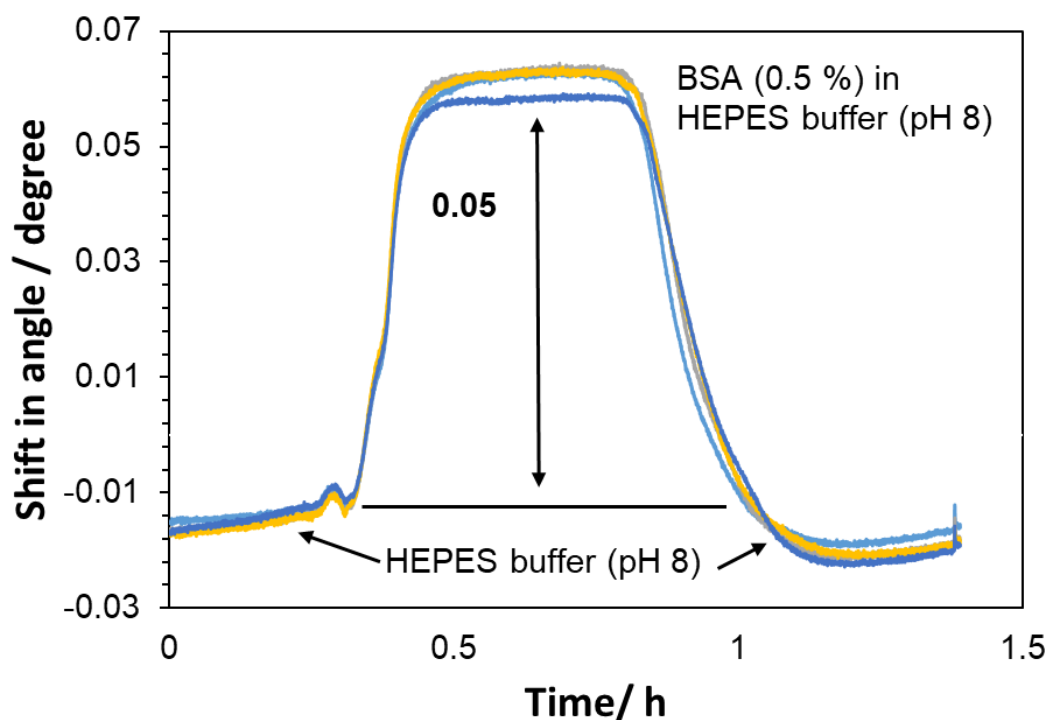
Figure 4.25 *Change in resonance angle upon applying BSA (0.5%) solution prepared in the HEPES buffer (100 mM) at pH 8 into chitosan waveguides (1%) at a flow rate of 118 μL min⁻¹. The waveguide was produced at a concentration of 1% (w/v) with deposition spin speed of 900 rpm and with 3 min drying time. The experiment was run one time using one separate chitosan waveguide.*

The average shift in resonance angle for BSA binding into three chitosan waveguides (1%) using HEPES buffer at pH 7.4, HEPES buffer at pH 8 and HEPES salts buffer at pH 7.4 is shown in figure 4.26. The figure shows that BSA was easily attached onto three separate chitosan waveguides (1%) using HEPES buffer at pH 7.4 while this attachment was significantly reduced upon adding various types of salts in the running buffer or using a buffer of higher pH (pH 8). This would confirm that the chitosan waveguide featured a positive charge at neutral pH (pH 7.4) which would facilitate nonspecific binding upon immobilisation of recognition molecules and target analytes. This binding can be easily eliminated or reduced by using a buffer of high ionic strength at pH 7.4 to shield the charges on molecules or using a buffer of higher pH (pH 8) to deprotonate amino groups (-NH$_2$) on the chitosan waveguide. This was also confirmed by one way ANOVA statistical analysis which indicated that there was a significant difference in terms of shifting in resonance angle when BSA solution was applied in HEPES buffer at pH 7.4 by comparison to other buffers used (p-value ⩽ 0.001).
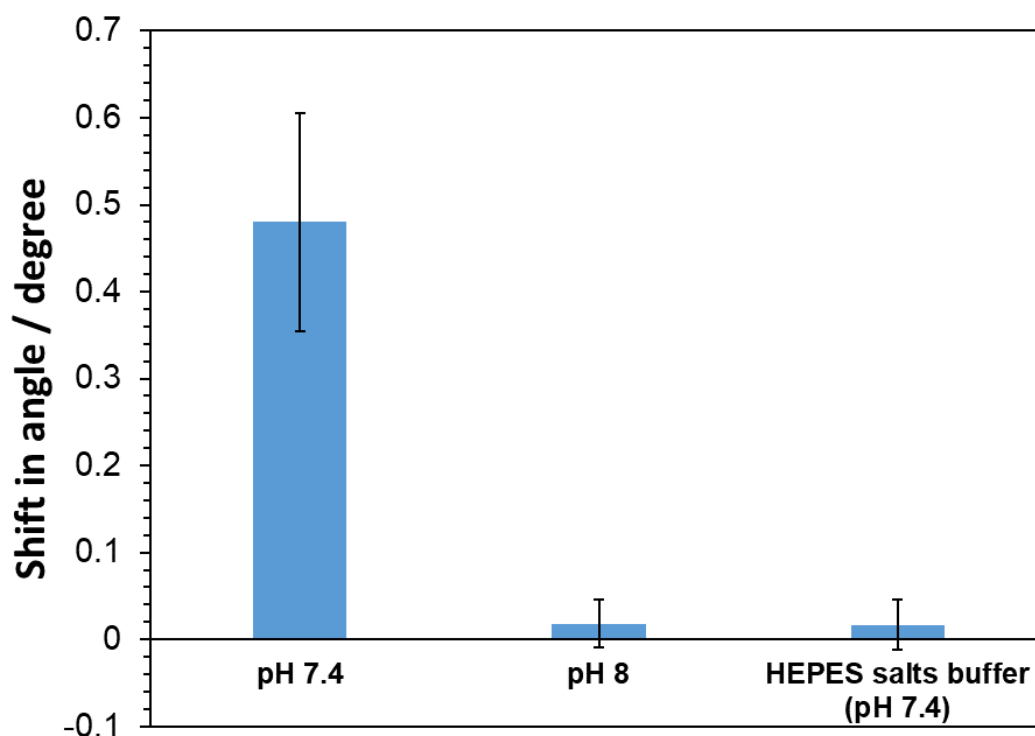
Figure 4.26 Average shift in resonance angle as a function of introducing BSA solutions (0.5%) made in the HEPES buffer at pH 7.4, in the HEPES buffer at pH 8, and in the HEPES salts buffer at pH 7.4. The waveguides were produced at a concentration of 1% (w/v) with deposition spin speed of 900 rpm and with 3 min of drying time. The reading represents the average of three runs using three separate chitosan waveguides (1%) for each buffer applied. The p-value ($\leqslant$ 0.001) indicated that there was a significant difference in terms of shifting in resonance angle when BSA solution was applied in the HEPES buffer at pH 7.4, in the HEPES buffer at pH 8, and in the HEPES salts buffer at pH 7.4.

4.3.6 Scanning electron microscope (SEM) images of the film

A scan electron microscope (SEM) (Model EVO 60, Carl Zeiss) was utilised to further characterise the chitosan film. First various films of chitosan were produced at a concentration of 1% (w/v) with a deposition spin speed of 900 rpm as explained in section 2.8.6. The films obtained were then dried at room temperature between 1 and 10 min before incubation with HEPES buffer (100 mM / pH 7.4). This was followed by transferring all coated films to a different building on campus for SEM measurement.

Figure 4.27 displays SEM images of the dried chitosan film taken randomly from various locations at a magnification of 10 k. Upon scanning various chitosan films under different drying times, it was noticed that the film was not totally uniform: raised areas were seen

at different locations particularly at the edges of the substrate. This was clearly pronounced at lower drying times, especially at 1 min, 2 min and 3 min as shown in figure 4.27. This could be related to the time of drying which was not sufficient to gain a fully smooth uniform film, as was seen with 4 min, 5 min and 10 min. Furthermore, all films were significantly affected by an incident electron beam particular at higher magnification. This led to evaporation of some part of the film and hence changed the morphology.
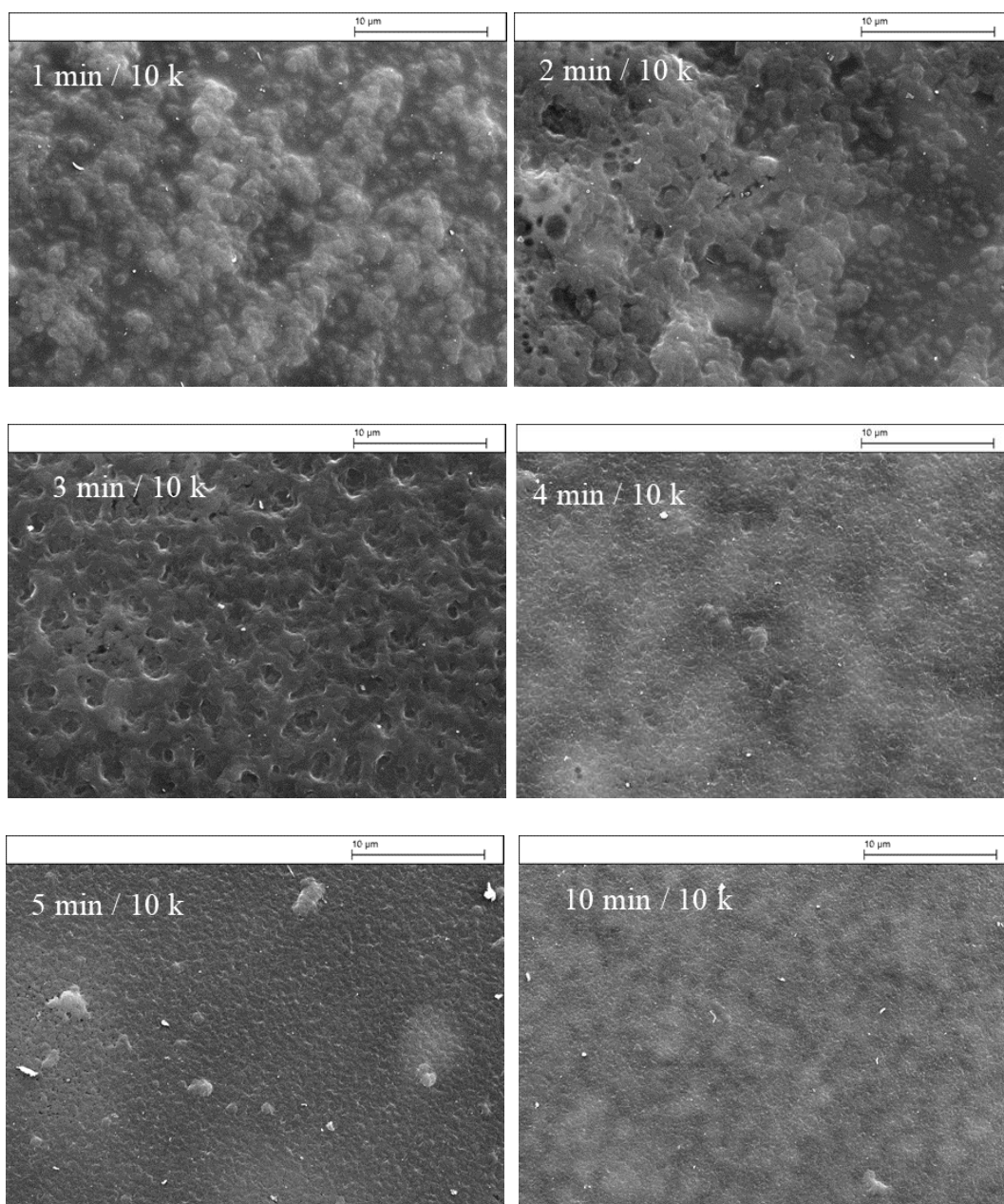
Figure 4.27 *SEM images of chitosan films with drying times taken randomly from different locations at a magnification of 10k. All films were produced at a concentration of 1% (w/v) with deposition spin speed of 900 rpm.*

4.3.7   Confocal microscopy

A confocal microscope was used in order to shine the surface of the chitosan film after drying for 3 min. This was accomplished using fluorescein isothiocyanate isomer I (FITC). The molecular weight of FITC is 390 Da which is closer to the molecular weight of glycerol (92 g mol^{-1}) and hence can be easily diffused through the pore size of the waveguide. The reaction is based on the covalent linkage between the isothiocyanate group on the FITC molecule and the amino group on the chitosan film[145]. Chitosan

solutions (1%) were coated on cover slips at a spin speed of 900 rpm. Upon drying for 3 min, the films were incubated with FITC solution (3 µM) for 2 h and then the fluorescence was measured with the confocal microscope as explained in section 2.8.3. Figure 4.28 shows the images taken from different locations on the chitosan films as indicated in each image. As can be seen in the images, the film was not uniform, particularly at the edges of the substrate, showing unclear porosity due to the roughness of the film. At the centre of the substrate, a smooth porous film was observed where the pore size was estimated to be in the range of 1-5µm.
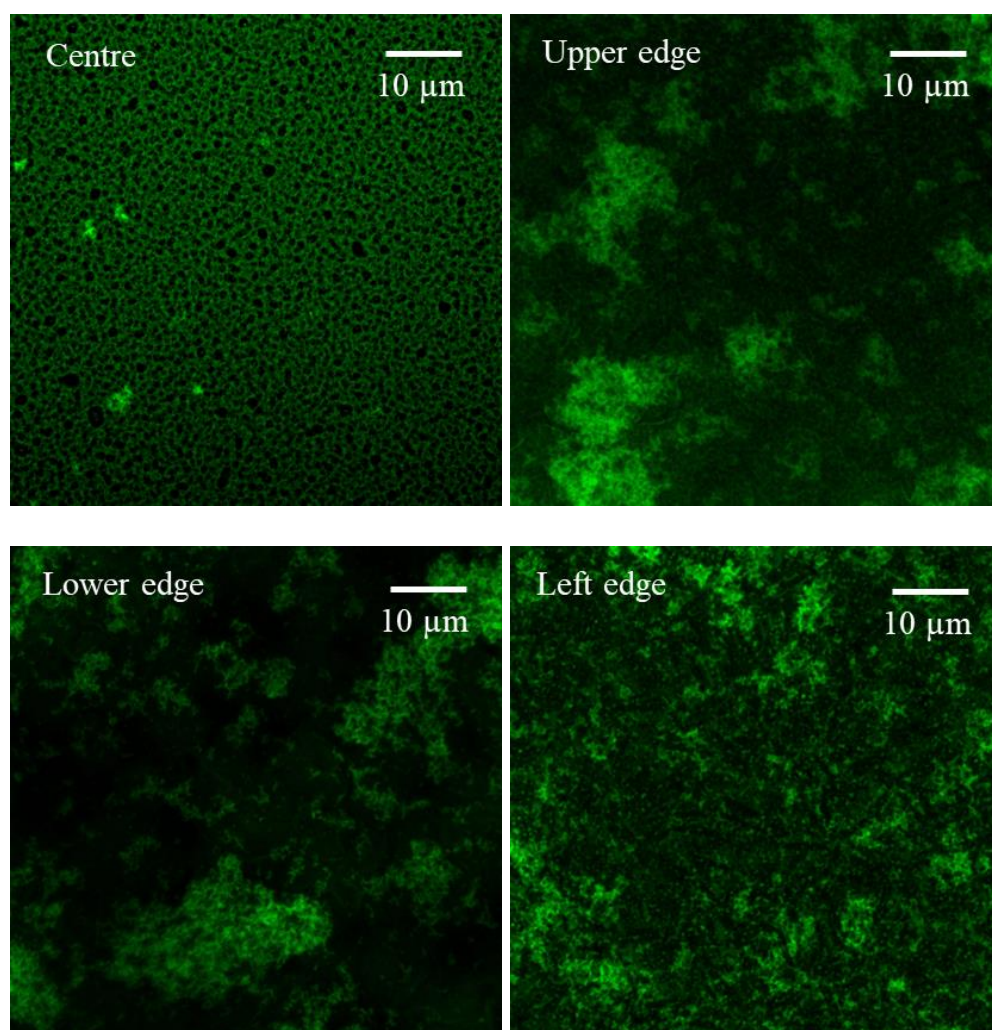
Figure 4.28 *Confocal microscope images of chitosan film (1%) from different locations. The film was deposited on a cover slip at a spin speed of 900 rpm followed by drying at room temperature for 3 min. Upon drying, the film was incubated with FITC solution (3 µM) for two hours before the fluorescence measurement was taken.*

4.4 Summary

The porosity of the waveguide plays a major role in the sensitivity of the DDLW device as it influences the diffusion of the biorecognition molecules into the waveguide. In the previous chapter, the straightforward chitosan waveguide was shown to be impermeable to large molecules such as BSA, PEG and PEO. Therefore, various methods were investigated to improve the porosity of the waveguide.

The effect of the amount of cross-linker on the pore size was investigated by reducing the concentration of glutaraldehyde from 25% to 0%. However, the waveguide was still impermeable to large molecules even when no glutaraldehyde was used. Blending chitosan with a porogen in order to obtain a microporous hydrogel was examined in bulk using the coloured and fluorescent BSA-FITC molecule as an indicator of diffusion. Porogens PEG and PEO were mixed with the chitosan hydrogel at various ratios followed by dissolution in a water bath at 80 °C for 8 h. However, the diffusion of BSA-FITC molecule into bulk chitosan was not successful. It was thought that the blended components were not fully extracted from the chitosan hydrogel and hence the porosity was not enhanced. A significant enhancement on the hydrogel's porosity was however observed upon washing the hydrogel with NaOH solution (5% w/v) for 16 h. BSA-FITC clearly penetrated into the gel as shown by the high fluorescence intensity compared to the thermal treatment. Nevertheless, neither alkaline nor thermal treatment was applicable to the chitosan waveguide as the film was easily collapsed or removed from the substrate.

The wet chitosan film was considered porous and it was thought that the pore size shrank upon drying. It was thought that a film of lower density would facilitate the enhancement of the porosity compared with highly dense film. Thus an investigation was carried out using a lower concentration of chitosan followed by controlling the drying time of the wet film. Upon optimisation, the sharpest dip in reflectivity was seen at a concentration of 1% (w/v) with a deposition spin speed of 900 rpm and with 3 min of drying time. The sensitivity to the value of refractive index using a small molecule (glycerol) was found to be comparable to that of the 2% (w/v) chitosan waveguide (chapter 3) in which the slope values were at 106° RIU^{-1} and at 100° RIU^{-1} respectively. The waveguide's porosity was investigated using polyethylene glycol (PEG) and polyethylene oxide (PEO) at various molecular weights. The shift in resonance angle was at 0.05° with polymer solutions while it was at less than 0.005° when the same solutions at the same refractive index were applied on the plain 2% (w/v) chitosan waveguide. This indicated high improvement in

the porosity of the waveguide on utilising a lower concentration of chitosan and controlling the drying time of the obtained wet film. Cross-linking the chitosan waveguide with NHS-PEG-NHS at various lengths was confirmed not to be effective as the waveguide mode was clearly dissolved at pH 4.4. However, the waveguide was still well operated at pH 6.4 and pH 5.4 using non cross-linked waveguides. This would allow the possibility of bioassay measurement at various pH.

The waveguide obtained with drying time condition (1%) was found to possess a positive charge at pH 7.4 which enhanced the nonspecific binding of oligo and BSA leading to a high shift in resonance angle. However, this binding was shown to be eliminated or reduced either by shielding all charges on all molecules using a buffer of high ionic strength at pH 7.4 or by deprotonating the amino groups on chitosan waveguide using a buffer at higher pH. The coated film at optimum condition did not appear to be uniform particularly at the edges of the substrate as shown in SEM and confocal microscopy images. This can be related to the time of drying which was not sufficient to gain a fully smooth and uniform film. The pore size was estimated to be in the range of 1-5 µM.

Although the film obtained was not uniform across the substrate, the porosity of the waveguide has been significantly enhanced by comparison to the previous condition (2% chitosan waveguide). Therefore this would be considered as a large enhancement in the waveguide's porosity and would be enough to proceed further. The next chapter will discuss in detail the immobilisation of streptavidin molecules on the chitosan waveguide under various approaches.

CHAPTER 5

Immobilisation of streptavidin onto chitosan
waveguide

5 Immobilisation of streptavidin onto chitosan waveguide

The streptavidin-biotin complex has been considered the strongest non-covalent interaction with a dissociation constant (K_d) of around 10^{-14} M. The reaction is very rapid and once formed, it is resistant to extreme pH, enzymatic degradation and denaturing agents, and it has high thermostability up to 112°C [164]. Furthermore, streptavidin is a tetrameric protein that can bind up to four biotinylated molecules such as antibodies and DNA with a minimal impact on the biological activity of the attached molecules [114]. Therefore, the streptavidin-biotin complex was selected in the present research as a cross-linker for immobilisation of the aptamer onto the chitosan waveguide. The immobilisation of streptavidin molecules was performed with various approaches such as covalent attachment using glutaraldehyde, non-covalent attachment via electrostatic interaction and physical adsorption based on biotin-streptavidin affinity. All these approaches are described in depth below. In this chapter, all waveguides were prepared with drying time as optimised in the previous chapter. Briefly; 1% (w/v) of chitosan solution was deposited at spin speed of 900 rpm for 30 s. The film obtained was then left for 3 min to dry at room temperature. This was followed by incubation with the HEPES buffer (pH 7.4) and subsequently with RB4 dye (100 µM) for 5 min before being inserted into a flow cell. These conditions held in all following experiments, unless otherwise stated.

5.1 Covalent attachment (Glutaraldehyde)

In previous chapter (chapter four), it was shown that there was not any impact on the waveguide's porosity upon using glutaraldehyde as a cross linker. Therefore, in this chapter, glutaraldehyde was utilised as a cross linker for protein immobilisation. Immobilisation of streptavidin molecules onto an amino functionalised surface by glutaraldehyde has been performed before[165, 166]. Glutaraldehyde is a bifunctional molecule that contains a short alkyl chain with an aldehyde group at each end (Figure 5.1 a). The attachment is based on reacting an aldehyde group from one end with an amine group on the surface forming an imine bond and hence yielding an aldehyde functionalized surface. Lysine residues in the streptavidin molecule contain free amino groups which then form an imine bond with an aldehyde group at the other end (Figure 5.1 b).
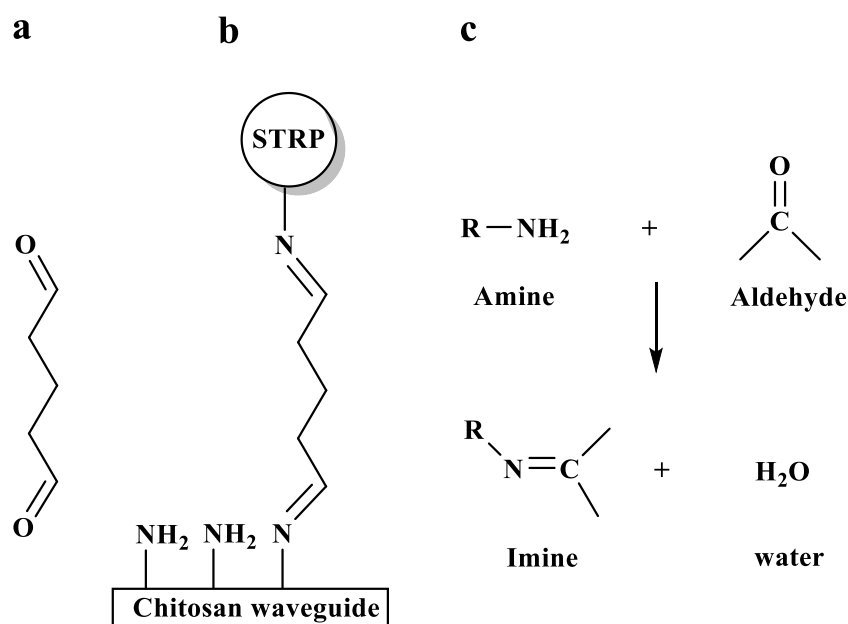
***Figure 5.1* a** *Chemical structure of glutaraldehyde,* **b** *after reacting one aldehyde group with an amine group on chitosan surface and subsequently after an attachment of streptavidin molecules via an aldehyde group at the other end yielding streptavidin functionalized chitosan waveguide.* **c** *Reaction mechanism between amine and aldehyde group yielding an imine bond known as Schiff bases (compounds having a C=N function)[167].*

5.1.1   Immobilisation of BSA onto chitosan waveguide

Bovine serum albumin (BSA) was utilised as a model protein for immobilisation onto a chitosan waveguide via glutaraldehyde. This would validate the effectiveness of using glutaraldehyde as a coupling agent for streptavidin. The reaction between glutaraldehyde and BSA has been investigated under various concentrations[168] while the attachment of BSA onto chitosan polymer via glutaraldehyde was previously performed for fabrication as a biosensor[169]. Here a buffer of high ionic strength was used in order to eliminate non-specific binding between BSA molecules (negative charge) and chitosan surface (positive charge), as was shown in figure 4.22 (chapter four). Chitosan waveguide (1%) was flushed sequentially with BSA (0.5%), glutaraldehyde (0.6%) and again with BSA (0.5%) as explained in section 2.9.1. All solutions were made in HEPES salts buffer (table 2.4) and were pumped at a flow rate of 118 µL min^{-1}.

Figure 5.2 displays the shift in resonance angle as a function of time on introducing BSA (0.5%), glutaraldehyde (0.6%) and again BSA (0.5%) onto the chitosan waveguide (1%). The BSA (0.5%) solution was first applied into the waveguide in order to examine the

binding of BSA molecules into the chitosan waveguide before introducing glutaraldehyde. The dip moved by 0.1° when BSA (0.5%) solution was introduced. However, it returned to the original baseline upon flushing the surface with HEPES salts buffer which indicated that the BSA molecules were not adsorbed into the surface. This was expected because using a buffer of high ionic strength (HEPES salts buffer) would eliminate the non-specific binding as was earlier shown in figure 4.22. Upon applying glutaraldehyde solution (0.6%), a significant shift was observed where the dip moved by 0.4° and subsequently stabilised at 0.3° with running buffer. This shows that the attachment of glutaraldehyde onto the chitosan waveguide was achieved via an imine bond as the dip did not return to the previous baseline. A further shift was seen upon re-applying BSA (0.5%) solution when the dip further increased by 0.25° and remained almost at the same level with the running buffer. From this one can conclude that BSA molecules were successfully conjugated to the chitosan waveguide via glutaraldehyde. To measure the reproducibility of the results, the experiment was performed three times using three chitosan waveguides (1%). The results are summarised in figure 5.3.
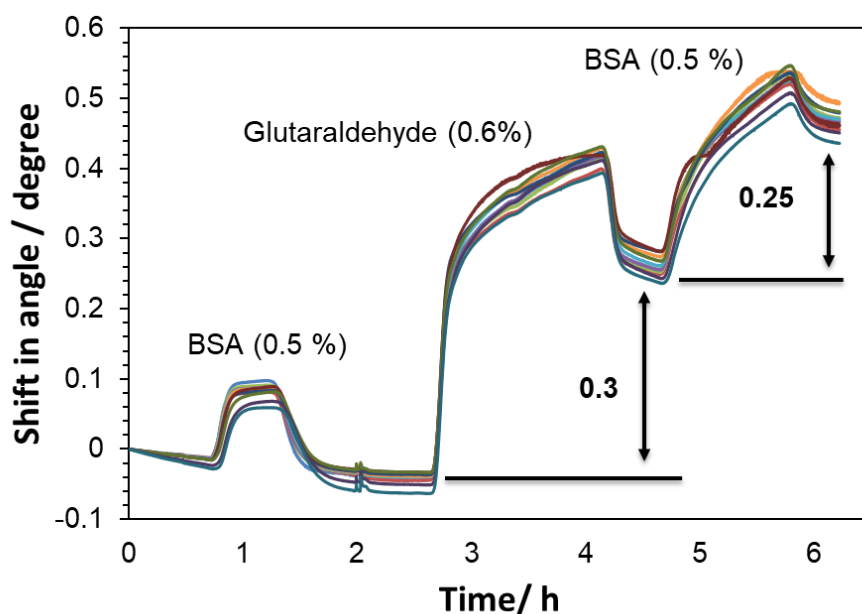
Figure 5.2 *Change in resonance angle as a function of time on introducing BSA (0.5%), glutaraldehyde (0.6%) and again BSA (0.5%) solutions at a flow rate of 118 µL min⁻¹. All solutions were made in HEPES salts buffer (table 2.4) which was flushed through the surface between each solution applied. The chitosan waveguide was produced at a concentration of 1% (w/v) with a deposition spin speed of 900 rpm and with 3 min of drying time. The experiment was run one time using one chitosan waveguide.*

Figure 5.3 exhibits the shift in resonance angle upon applying glutaraldehyde (0.6%) and subsequently BSA (0.5%) solutions into three chitosan waveguides (1%). As can be seen, the amount of glutaraldehyde attached on the first two runs was almost the same leading to a similar degree of shift in resonance angle, while it was slightly higher for the third run. It has been reported that glutaraldehyde tends to self-polymerise leading to glutaraldehyde oligomers rather than reacting with free amino groups on the BSA molecules[168]. This phenomenon was clearly pronounced when a glutaraldehyde solution (0.25%) was added in one go while it was negligible when it was introduced slowly in small amounts. Therefore, the difference between the first two runs and the third run could be due to the polymerisation of glutaraldehyde molecule as the concentration was clearly higher (0.6%) than the one seen in the study (0.25%)[168]. The amount of BSA conjugated to the chitosan waveguide via an immobilised glutaraldehyde was identical in the first two runs while it was higher in the third run. This could be attributed to the availability of free aldehyde groups on the surface where the two aldehyde groups on the glutaraldehyde could prefer to react with two free amino groups on the chitosan waveguide rather than with the BSA molecules. Although this is a slight variation, the effectiveness of using glutaraldehyde as a coupling agent for a protein such as BSA was clearly demonstrated as it was shown over three runs. The immobilisation of streptavidin molecules via glutaraldehyde is shown in the following section.
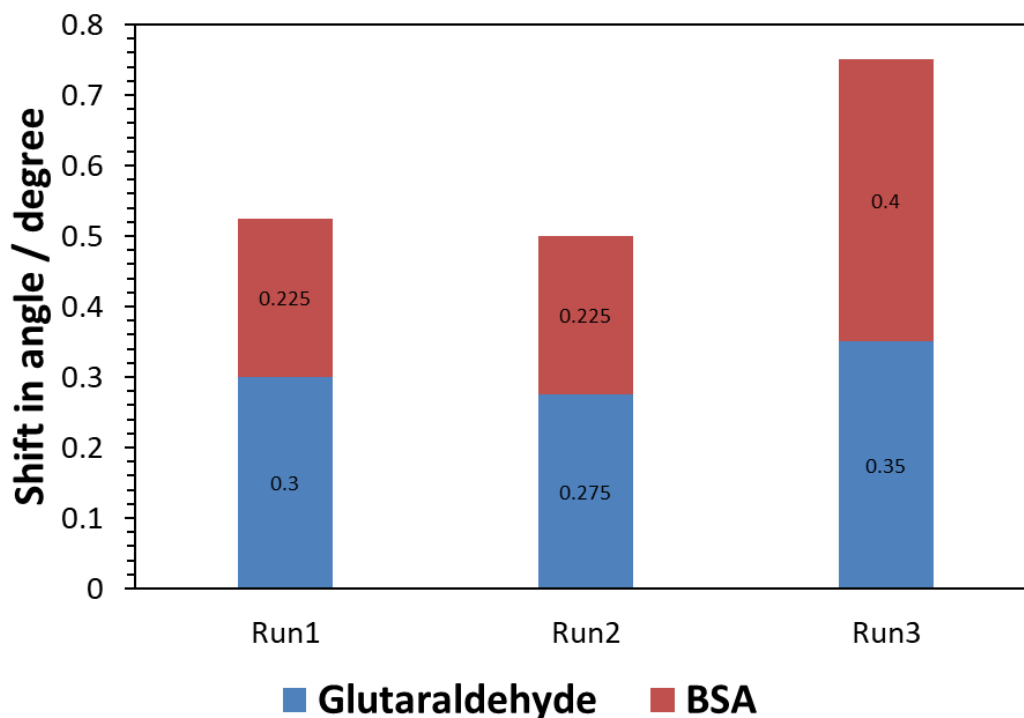
Figure 5.3 *Shift in resonance angle upon attachment of glutaraldehyde molecules (0.6%) into three chitosan waveguides (1%) (three runs) and the subsequent binding of BSA molecules (0.5%) to the immobilised glutaraldehyde. The number shown inside each box represents the degree of shifting in resonance angle for a specific solution as indicated in the figure.*

5.1.2   Immobilisation of streptavidin onto chitosan waveguide

The aim of this experiment was to immobilise streptavidin molecule on the chitosan waveguide (1%) using glutaraldehyde as a cross-linker. Biotinylated bovine serum albumin (Biotin-BSA) and biotinylated aptamer (oligo 2 / table 2.2) were utilised in order to verify the binding of streptavidin molecules onto the chitosan waveguide. Bovine serum albumin (BSA) was also used as a blocking molecule. Chitosan waveguides (1%) were first flushed with glutaraldehyde (0.6%) and subsequently with streptavidin (1.6μM/83μM). Both solutions were made in the HEPES buffer (100 Mm/pH 7.4). This was followed by sequentially applying BSA (0.5%) and biotinylated aptamer (0.75 μM/4μM/10μM) or biotinylated BSA (10 µg/mL). These solutions were all prepared in HEPES salt buffer (table 2.4) as explained in section 2.9.1.

Figure 5.4 (a) exhibits a full shift in resonance angle as a function of time upon sequentially introducing glutaraldehyde (0.6%), streptavidin (1.6 µM) and biotinylated aptamer (0.75 µM) into the chitosan waveguide (1%). The running buffer, either HEPES

buffer (100 mM/pH 7.4) or HEPES salts buffer, was flushed through the surface before and after each solution applied. It can be seen that a significant shift was observed when glutaraldehyde solution (0.6%) was introduced. The dip finally stabilised at 0.3° when the running buffer (HEPES buffer) was flushed again through the waveguide. This would indicate an attachment of glutaraldehyde molecules into the waveguide. Figure 5.4 (b) displays the introduction of streptavidin and biotinylated aptamer. As can be seen, the dip continuously shifted for two hours when streptavidin solution (1.6 µM) was applied until the dip stabilised at the degree that was slightly higher than the previous baseline. The shift in resonance angle was at 0.03°. The dip remained at the same level even when the running buffer (HEPES buffer) was introduced. This would indicate a successful conjugation of streptavidin molecules onto the surface. Upon introducing HEPES salts buffer, a shift in resonance angle was clearly observed and that was due to the change in the waveguide's refractive index. This was followed by a slightly further shift upon applying biotinylated aptamer solution (0.75 µM) showing a shift in resonance angle by 0.03°. This shift could be due to the successful binding of biotinylated aptamer onto the immobilised streptavidin or could be as a result of the reaction between the free amino groups on the aptamer molecules (oligonucleotide's bases) and the remaining aldehyde group on the surface. To verify this impact, the experiment was repeated using BSA solution (0.5%) to block any remaining aldehyde group on the surface before applying biotinylated aptamer. The result is shown in figure 5.5.
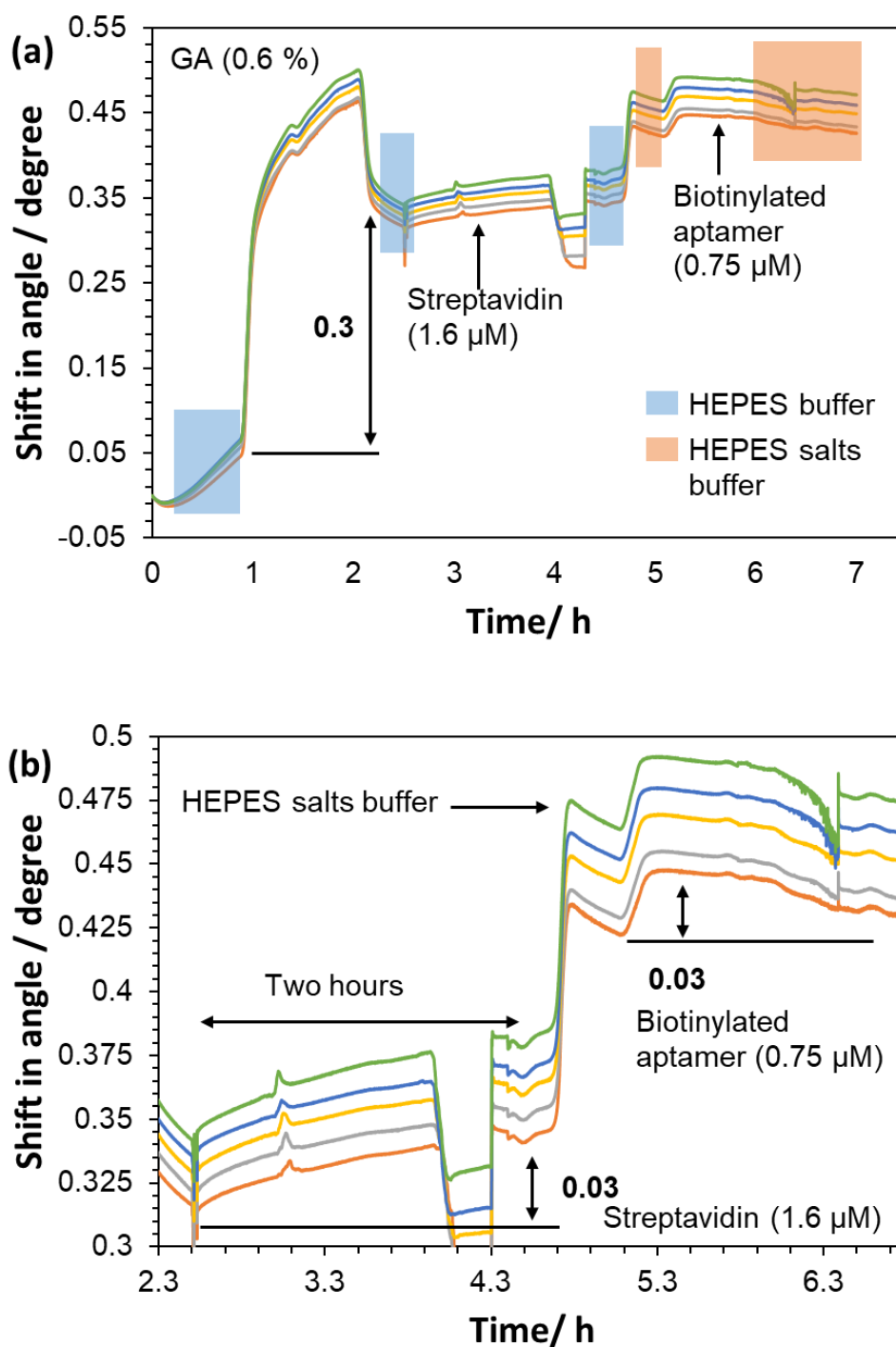
Figure 5.4 *(a) A full shift in resonance angle upon flushing the chitosan waveguide (1%)*
sequentially with glutaraldehyde (0.6%), streptavidin (1.6 μM) and biotinylated aptamer
(oligo 2/0.75 μM) at a flow rate of 118 μL min⁻¹. Glutaraldehyde and streptavidin
solutions were both made in the HEPES buffer (100 mM/pH 7.4) while biotinylated
aptamer was prepared in HEPES salts buffer. (b) Enlargement of the section showing the
application of streptavidin and biotinylated aptamer solutions. The experiment was run
one time using one chitosan waveguide.

The shift in resonance angle upon introducing blocking molecules (BSA/0.5%) into the chitosan waveguide (1%) is shown in figure 5.5. The waveguide was first treated with glutaraldehyde (0.6%) solution for one hour and subsequently with streptavidin (1.6 µM) solution for two hours. As can be seen, the dip reached a higher degree of angle with the glutaraldehyde solution (0.6 %) followed by a gradual shift back with running buffer. The dip remained at the lower angle until injection of the streptavidin solution (1.6 µM) where the dip immediately stabilised at a certain level. This would confirm the attachment of streptavidin molecules onto the chitosan waveguide which resulted in change in the refractive index of the waveguide. A significant shift was seen when blocking molecules (BSA/0.5%) in HEPES salts buffer was applied leading to a shift in resonance angle by 0.2°. This would indicate a large number of BSA molecules being conjugated onto the surface via the remaining available aldehyde group. This is because BSA molecules would not be adsorbed onto the surface while using a buffer of high ionic strength. Therefore, this would confirm that using 0.6% (v/v) of glutaraldehyde solution to attach 1.6 µM of the streptavidin molecules would lead to a large number of unreacted aldehyde groups remaining. Thus, this might also confirm that the shift obtained upon applying aptamer solution in figure 5.4 (b) can be a result of reacting with free available aldehyde groups on the surface. Upon introducing biotinylated aptamer into this experiment at higher concentration (4 µM), the dip shifted by 0.03° which was identical with the same shift observed in the previous experiment when a lower concentration of aptamer (0.75µM) was applied. This would indicate the poor attachment of aptamer in this experiment. This could be due to the large number of BSA molecules attached hiding the binding sites on the streptavidin molecules. Therefore, a high concentration of streptavidin (83 µM) was utilised in the following experiment in order to first block all the remaining aldehyde groups and second to enhance the binding sites of the aptamer.
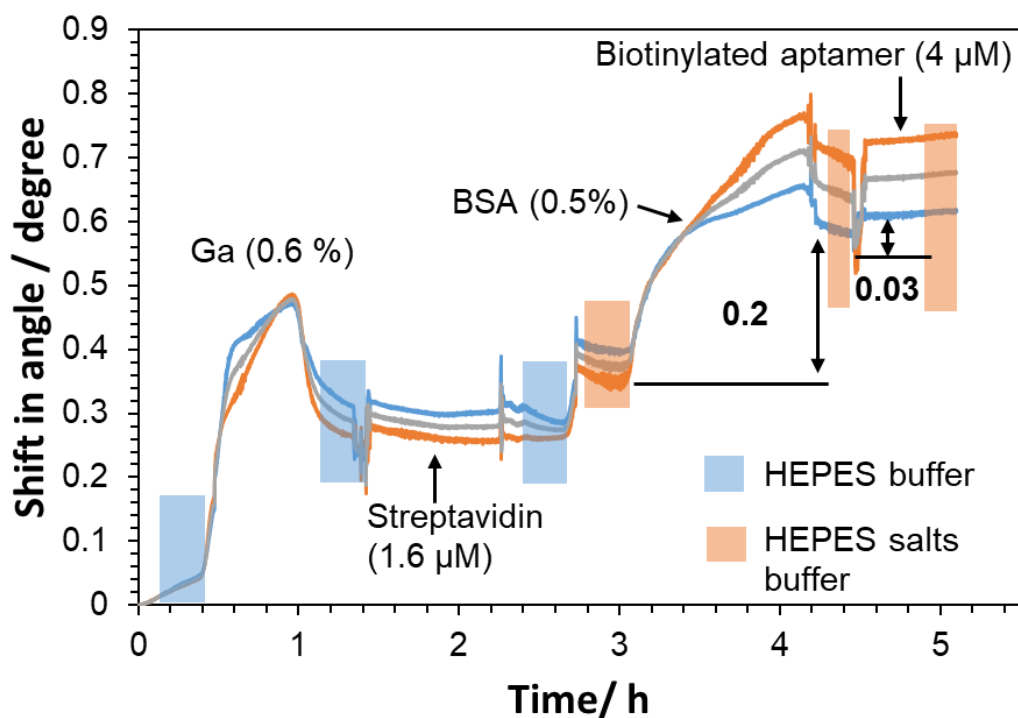
***Figure* 5.5** *Shift in resonance angle as a function of time upon flushing the chitosan waveguide (1%) sequentially with glutaraldehyde (Ga) (0.6%), streptavidin (1.6 µM), blocking molecules (BSA/0.5%) and biotinylated aptamer (oligo 2 / 4 µM) at a flow rate of 118 µL min⁻¹. Glutaraldehyde and streptavidin were made in the HEPES buffer (100 mM/pH 7.4) while blocking molecules and biotinylated aptamer were prepared in HEPES salts buffer. The experiment was run one time using one chitosan waveguide.*

Figure 5.6 displays the shift in resonance angle upon introducing a high concentration of streptavidin (83 µM) into the chitosan waveguide (1%) that had been initially treated with glutaraldehyde solution (0.6%). As shown in the figure, a significant shift was observed upon injection streptavidin solution (83 µM) leading to a large change in the resonance angle, by 1°. Upon applying blocking molecules (BSA/0.5%) in HEPES salts buffer, the dip shifted slightly to a higher resonance angle, however, it totally returned to the previous baseline with running buffer (HEPES salts buffer). This would confirm that all aldehyde groups on the surface were successfully blocked by streptavidin molecules as all the BSA molecules were removed by the running buffer. A further large shift was seen upon applying a high concentration of biotinylated aptamer (10µM) where the dip rapidly moved by 0.4° and stabilised at the same level. First, this would confirm the successful attachment of biotinylated aptamer onto the immobilised streptavidin. Second, the degree of shifting (0.4°) is significantly higher than any previous shifts in the resonance angle

cause upon immobilisation of aptamer either at a concentration of 4 µM or at 0.75 µM where the dip only moved by 0.03° (Figure 5.4 and 5.5). This would indicate the large amount of aptamer being bound. To verify this binding of aptamer, the experiment was repeated without using streptavidin molecules. BSA molecules at the same concentration of streptavidin (83µM) immobilised instead as shown in figure 5.7.
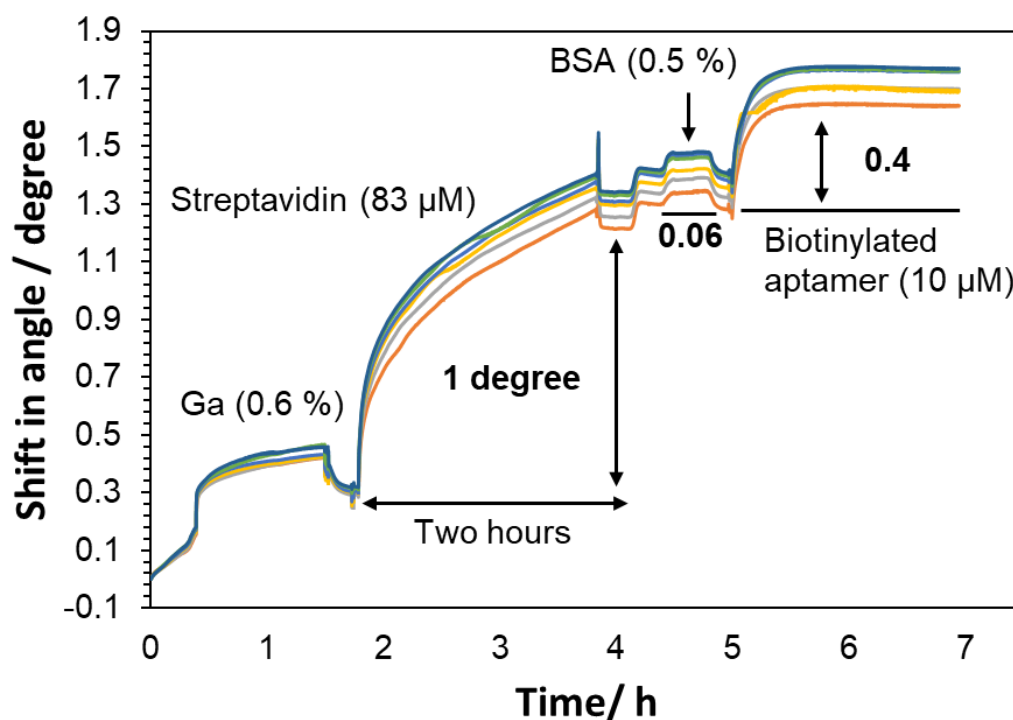
Figure 5.6 *Shift in resonance angle as a function of time upon flushing the chitosan waveguide (1%) sequentially with glutaraldehyde (0.6%), high concentration of streptavidin (83 µM), blocking molecules (BSA/0.5%) and high concentration of biotinylated aptamer (oligo 2/10 µM) at a flow rate of 118 µL min^{-1}. Glutaraldehyde and streptavidin were made in the HEPES buffer (100 mM/pH 7.4) while blocking molecules and biotinylated aptamer were prepared in HEPES salts buffer. The experiment was run one time using one chitosan waveguide.*

The change in resonance angle as a function of time upon immobilisation of BSA (83µM) instead of streptavidin is shown in figure 5.7. The waveguide (1%) was first treated with glutaraldehyde solution (0.6 %) for one hour and subsequently with BSA solution (83µM) for two hours. As can be seen, the dip shifted by 0.1° with glutaraldehyde solution (0.6 %) while it was further increased by 0.17° when BSA solution (83µM) was applied. This would confirm the attachment of BSA molecules onto chitosan waveguide via the

immobilised aldehyde groups. The degree of shifting with BSA solution (0.17°) was significantly lower than had been seen previously (Figure 5.6) upon the introduction of streptavidin solution (1°) at the same concentration (83µM). This could be related to the amount of glutaraldehyde attached to the surface. In this experiment, the amount of glutaraldehyde conjugated led to shift in resonance angle by 0.1°, while it was at 0.3° when the same concentration of glutaraldehyde (0.6%) was applied in all previous experiments (Figures 5.4, 5.5 and 5.6). This would lead one to say that the amount of glutaraldehyde attached was clearly lower by comparison to all other runs and hence a lower amount of BSA was bound. Upon introducing blocking molecules (BSA/0.5%) in HEPES salts buffer, the dip moved to the higher resonance angle, however, it returned to the original baseline with running buffer. This would indicate that all immobilised aldehyde groups being blocked by immobilised BSA (83µM) as all blocking molecules were removed by the running buffer. Biotinylated aptamer at the same concentration (10 µM) as in the previous experiment (Figure 5.6) and for the same incubation time (two hours) followed. The dip slightly decreased to a lower degree of angle, however, it returned to the original baseline upon re-applying the running buffer. This would indicate that the aptamer molecules were not bound into the surface. Therefore, this would further confirm that the shift observed upon applying aptamer solution (10 µM) in the previous experiment (Figure 5.6) represented the successful attachment of aptamer molecules to the immobilised streptavidin. In order to further verify the binding of biotinylated molecule into the immobilised streptavidin, biotinylated bovine serum albumin (Biotin-BSA) was applied under the same condition as shown in figure 5.8.
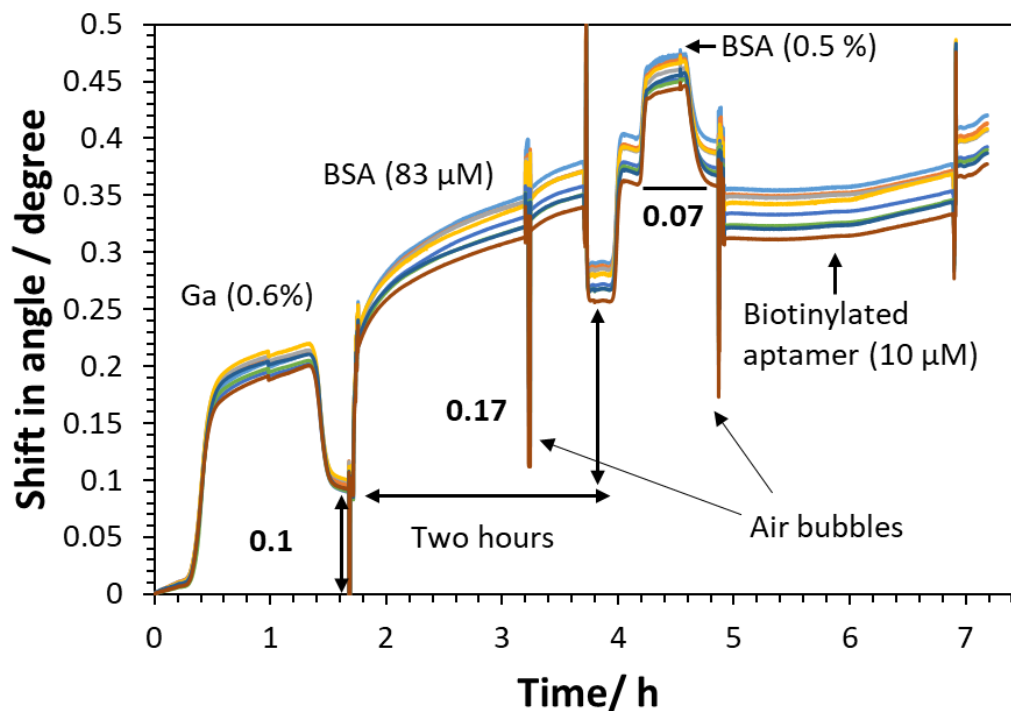
Figure 5.7 *Shift in resonance angle on flushing the chitosan waveguide (1%) sequentially with glutaraldehyde (0.6%), high concentration of BSA (83 μM), blocking molecules (BSA/0.5%) and high concentration of biotinylated aptamer (oligo 2/10 μM) at a flow rate of 118 μL min[1]. Glutaraldehyde and BSA (83 μM) were made in the HEPES buffer (100 mM/pH 7.4) while blocking molecules and biotinylated aptamer were prepared in HEPES salts buffer. The experiment was run one time using one chitosan waveguide.*

Further confirmation on the successful attachment of biotinylated molecule into the immobilised streptavidin is shown in figure 5.8. The waveguide (1%) was initially flushed with glutaraldehyde solution (0.6 %) for one hour and subsequently with streptavidin solution (83 μM) for two hours. Upon applying blocking molecules (BSA/0.5%) in HEPES salts buffer, a shift in resonance angle was observed by 0.06° while the dip shifted back to the original baseline with running buffer. This would indicate that all blocking molecules were removed from the surface with running buffer. This would also indicate that the majority of the immobilised aldehyde groups were blocked by streptavidin molecules. A large shift in resonance angle was seen upon introducing biotinylated BSA (10 μg/mL ≈150 nM) into the HEPES salts buffer. The dip moved by 0.5°. This would confirm a successful conjugation of biotinylated BSA onto the immobilised streptavidin leading to change in the refractive index of the waveguide. This is because the dip remained at a higher level even when the running buffer was re-applied. This would lead

to the conclusion that the immobilisation of biotinylated molecules, either biotinylated BSA or biotinylated aptamer, onto the immobilised streptavidin was achieved and was successfully detected by the DDLW device. The amount of glutaraldehyde attached would affect the amount of streptavidin immobilised. Therefore various concentrations of glutaraldehyde were investigated as shown in the flowing section.
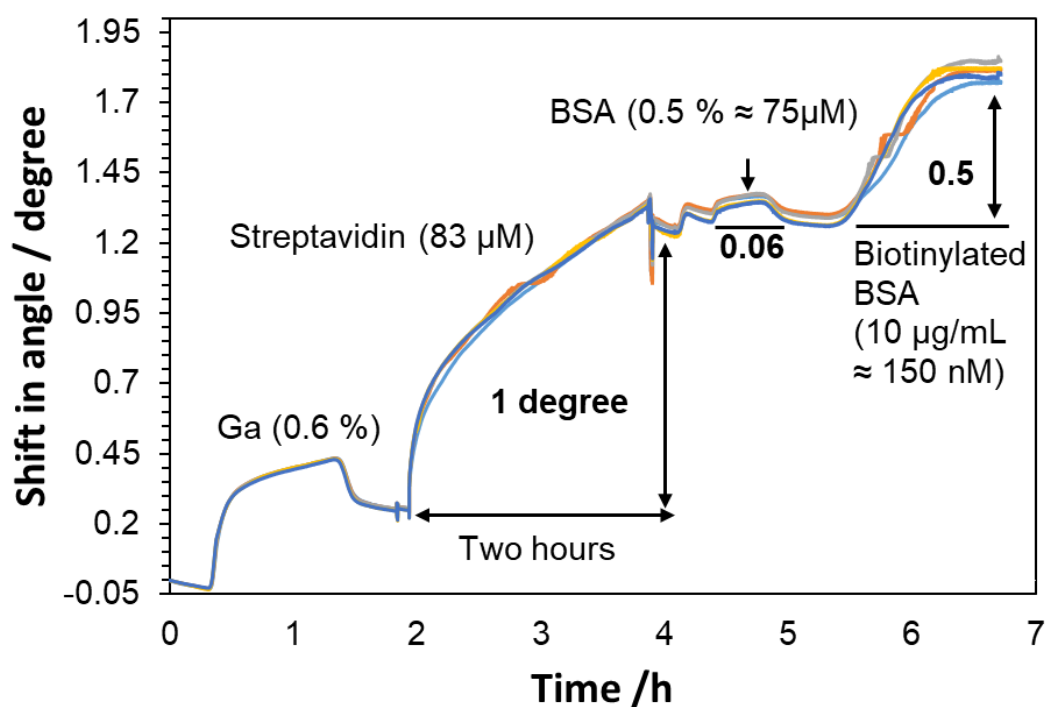
Figure 5.8 *Shift in resonance angle as a function of time upon immobilisation of biotinylated BSA (10 µg/mL ≈150 nM) onto the chitosan waveguide (1%). The waveguide (1%) was sequentially flushed with glutaraldehyde (0.6%), streptavidin (83 µM), blocking molecules (BSA/0.5%) and finally with biotinylated BSA (10 µg/mL ≈150 nM) at a flow rate of 118 µL min⁻¹. Glutaraldehyde and streptavidin were made in the HEPES buffer (100 mM/pH 7.4) while blocking molecules and biotinylated BSA were prepared in HEPES salts buffer. The experiment was run one time using one chitosan waveguide.*

5.1.2.1 Optimisation of glutaraldehyde concentration

Various concentrations of glutaraldehyde were used in order to optimise the amount of streptavidin attached and consequently the amount of biotinylated molecules bound. A chitosan waveguide (1%) was first flushed with various concentrations of glutaraldehyde ranging from 0.2% to 1.4 % (v/v) for one hour. This was followed by introducing streptavidin solution (83µM) for two hours. Finally, biotinylated BSA solution (10 µg/mL)

was then applied as explained in section 2.8.1. Measurement for each concentration of glutaraldehyde was performed on a separate chitosan waveguide.

Figure 5.9 displays the shift in resonance angle upon sequentially attachment of glutaraldehyde, streptavidin and biotinylated BSA molecules onto five chitosan waveguides (1%). Each waveguide was treated with glutaraldehyde either at concentration of 0.2%, 0.4%, 0.6%, 0.8% or 1.4% (v/v). Streptavidin and biotinylated BSA solutions were then sequentially applied at constant concentrations of 83µM and 10 µg/mL respectively. It can be seen from the figure that the degree of shift in resonance angle was almost similar upon applying 0.6% and 0.8 % of glutaraldehyde solutions, while it was higher when lower and higher concentrations of glutaraldehyde (0.2%, 0.4% and 1.4 %) were introduced. This would indicate that the shift in resonance angle was not directly proportional to the concentrations of glutaraldehyde applied. This would be highly linked to the polymerisation of glutaraldehyde which leads to forming the oligomers rather than reacting with free amino groups on the surface [168]. Further fluctuations were seen upon introducing streptavidin solution (83µM). The dip shifted between 1° and 0.5° from two chitosan waveguides (1%) that exhibited an identical amount of glutaraldehyde attached (0.25° and 0.25°). This would confirm that the amounts of streptavidin attached were also not directly proportional to the amount of glutaraldehyde immobilised. This might be linked to the number of free aldehyde groups on the surface. The reaction between chitosan and glutaraldehyde is proposed to involve formation of either one or two Schiff bases. Thus using both aldehyde groups of the glutaraldehyde molecule could have occurred[148]. In contrast, the amount of biotinylated BSA bound was seen to be related to the amount of conjugated streptavidin. At the highest (0.65°) and the lowest (0.35°) amount of biotinylated BSA bound were shown to be proportional to the amount of streptavidin attached; 1.3° and 0.5° respectively. From the data presented, it can be concluded that the amount of streptavidin immobilised was effected by the polymerisation of glutaraldehyde molecules and also by the availability of aldehyde groups on the surface. In order to enhance the immobilisation of streptavidin on the chitosan waveguide, other methods were investigated such as non-covalent attachment via electrostatic interaction and physical adsorption based on biotin-streptavidin affinity as shown in the following section.
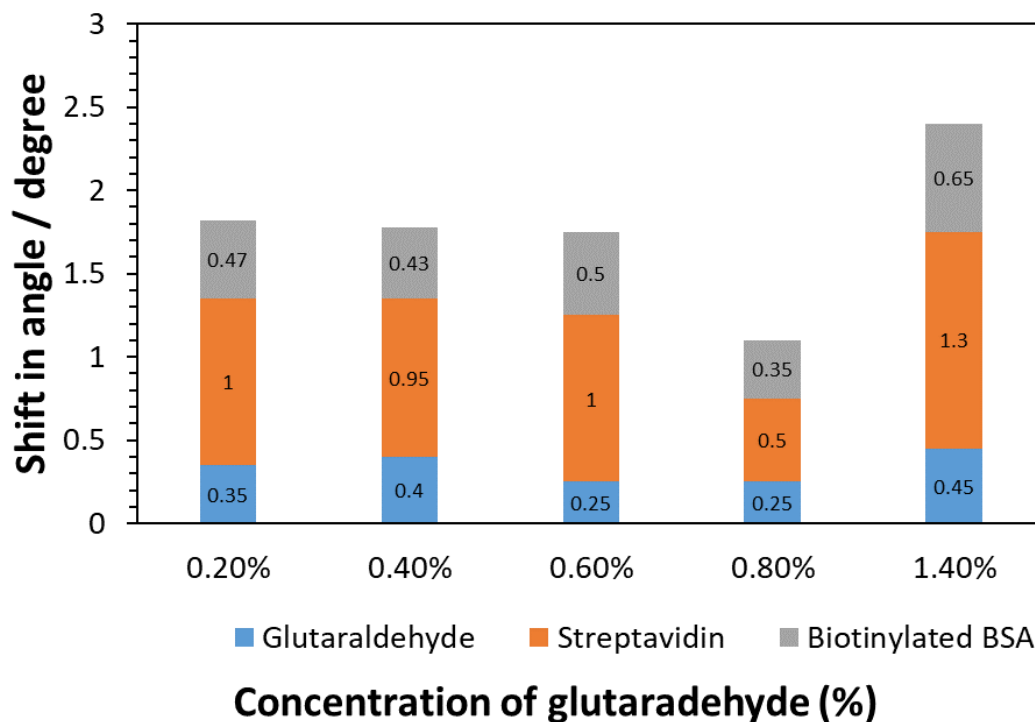
Figure 5.9 *Shift in resonance angle upon sequentially attachment of glutaraldehyde, streptavidin and biotinylated BSA molecules onto five chitosan waveguides (1%). Glutaraldehyde was applied into each waveguide either at concentration of 0.2%, 0.4%, 0.6%, 0.8% or 1.4% (v/v) as indicated in the figure. This was followed by immobilisation of streptavidin at a concentration of 83μM and subsequent binding of biotinylated BSA at a concentration of 10 μg/mL. The number shown inside each box represents the degree of shifting in resonance angle for a specific solution as indicated in the figure. The experiment was run one time using one separate chitosan waveguide for each concentration of glutaraldehyde used.*

5.2 Non-covalent attachment via electrostatic interaction

The aim of this experiment was to enhance the immobilisation of streptavidin on the chitosan waveguide without using glutaraldehyde. The isoelectric point of streptavidin molecule is between 5 and 6 which would lead to a negatively charged protein at neutral pH [165] [170]. Therefore, streptavidin can be immobilised via an electrostatic interaction as the chitosan waveguide possesses an opposite charge (Figure 5.10). The immobilisation of streptavidin has been achieved via electrostatic interaction onto protonated chitin film at pH 6 while the attachment was successfully verified using biotinylated molecules [170]. Here the concentration of streptavidin (83 μM) and the concentration of biotinylated aptamer (oligo 2/10 μM) and the incubation time (two hours) for both solutions were all

kept constant in order to make a clear comparison with the glutaraldehyde method. Chitosan waveguides (1%) were first treated with streptavidin solution (83 µM) in the HEPES buffer for two hours and then with biotinylated aptamer (oligo 2/10 µM) in HEPES salts buffer for two hours as explained in section 2.9.2.
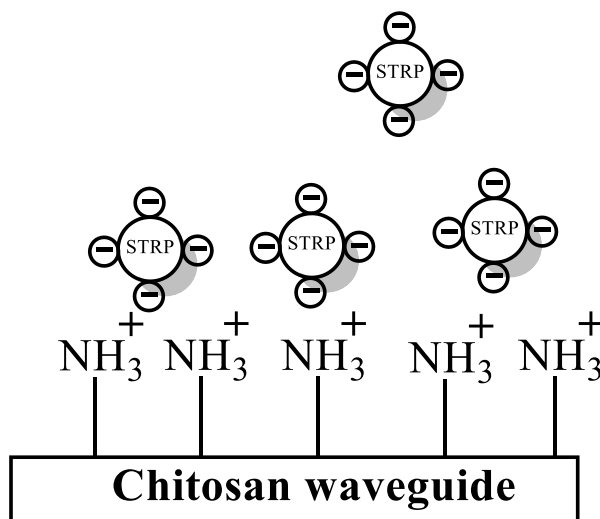
Figure 5.10 *Schematic for immobilisation of streptavidin on chitosan waveguide via an electrostatic interaction.*

As shown in figure 5.11, the dip rapidly moved by 0.45° upon injection of streptavidin solution (83 µM) and reached 0.55° after two hours of incubation. However, upon introducing the running buffer (HEPES Buffer), a clear reduction was observed where the dip finally stabilised at 0.17°. This would indicate a poor attachment of streptavidin molecules via electrostatic interaction as the shift in resonance angle at the same concentration of streptavidin was between 0.5° and 1.3° (Figure 5.9) using glutaraldehyde. Upon introducing the biotinylated aptamer (10 µM), a slightly lower shift in angle was seen during the incubation for two hours. However, the dip returned to the original baseline with running buffer. This would suggest that the aptamer molecules were not attached to an immobilised streptavidin as the dip totally returned to the previous baseline and therefore, the refractive index of the waveguide had not changed. The experiment was carried out three times using three chitosan waveguides (1%) and the results are summarised in figure 5.12.
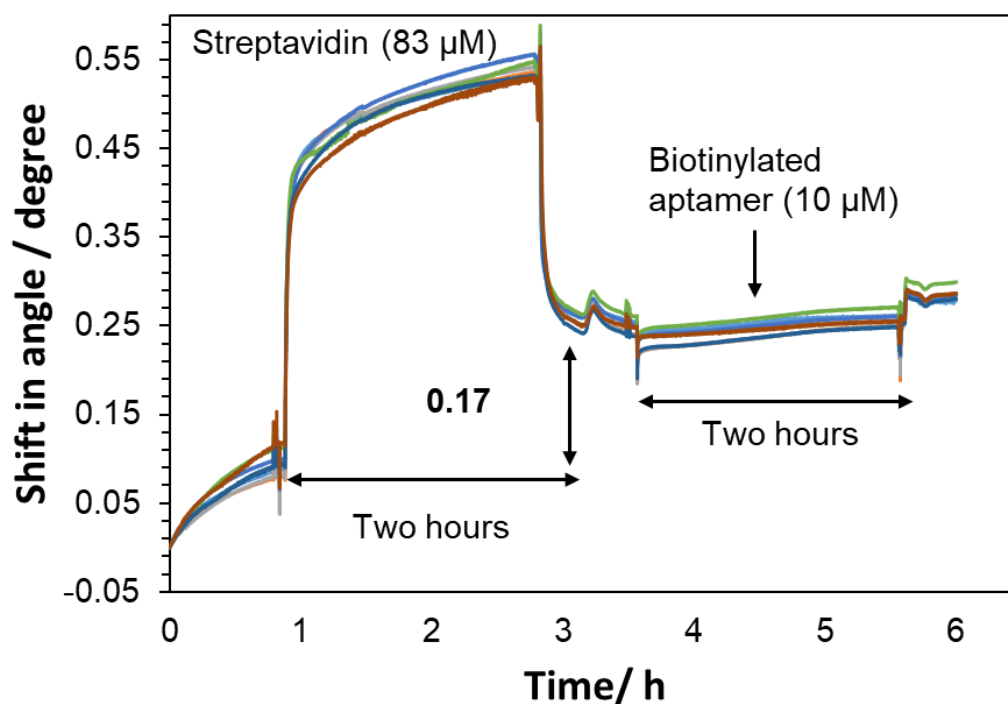
Figure 5.11 *Shift in resonance angle as a function of time upon immobilisation of streptavidin (83 μM) into chitosan waveguide (1%) via electrostatic interaction for two hours. This was followed by applying biotinylated aptamer (10 μM) for two hours. Streptavidin was made in the HEPES buffer (100 mM/ pH 7.4) while biotinylated aptamer was prepared in HEPES salts buffer. The experiment was run one time using one chitosan waveguide.*

Figure 5.12 shows the shift in resonance angle upon attachment of streptavidin molecules (83 μM) and the subsequent binding of biotinylated aptamer (10μM) onto three chitosan waveguides (1%). A variation in the amount of streptavidin adsorbed was observed showing an increase in the resonance angle between 0.1° and 0.17°. Despite this slight variation between each run, the attachment of streptavidin was still significantly lower than with the glutaraldehyde method where the dip shifted between 0.5° and 1.3° (Figure 5.9). For the subsequent binding, the dip slightly shifted between 0.02° and 0.06° upon applying biotinylated aptamer (10μM) onto three chitosan waveguides (1%). By comparison with the glutaraldehyde method, the amount of aptamer attached that was applied at the same concentration (10μM) was significantly higher. The dip rapidly moved by 0.4° and remained at the same level even when the running buffer was flushed again (Figure 5.6). This points to the conclusion that immobilisation of streptavidin via an electrostatic interaction cannot be considered as an alternative approach to the

glutaraldehyde method as the attachment of streptavidin and the subsequent binding of aptamer molecules were significantly poorer. Therefore, a further protocol was utilised in order to enhance the attachment of streptavidin and the binding of aptamer as shown in the following section.
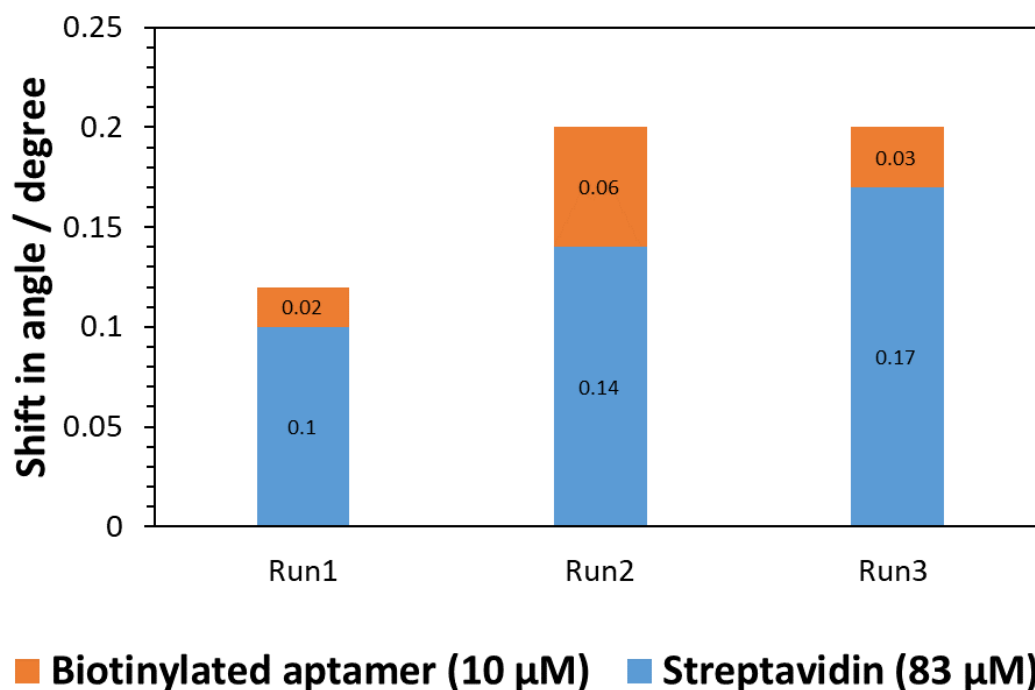
Figure 5.12 *Shift in resonance angle upon attachment of streptavidin molecules (83 µM) into three chitosan waveguides (1%) via electrostatic interaction and the subsequent binding of biotinylated aptamer (10 µM) into the immobilised streptavidin. The number shown inside each box represents the degree of shifting in resonance angle for a specific solution as indicated in the figure. Each run was performed in a separate chitosan waveguide.*

5.3 Physical adsorption based on biotin-streptavidin affinity

Based on the high affinity between biotin and streptavidin, the immobilisation of streptavidin on the chitosan waveguide can be enhanced by functionalising the surface with biotin molecules. Upon immobilisation of streptavidin onto biotinylated chitosan waveguide, one or two binding sites on the streptavidin molecule would be occupied while the remaining sites would be used for the subsequent binding of biotinylated aptamer. Biotinylated chitosan polymer has been previously reported in which the conjugation of the biotin molecule was performed either by N-hydroxysuccinimide ester (NHS) [171] [172] or EDC [173]. Here, biotin 3-sulfo-N-hydroxysuccinimide ester sodium salt

(Sulfo-NHS-Biotin) was utilised as a coupling reagent in order to facilitate the biotinylation of chitosan waveguide. The attachment of Sulfo-NHS-Biotin is performed via NHS ester making an amide bond with chitosan's functional amino group as demonstrated in figure 5.13.
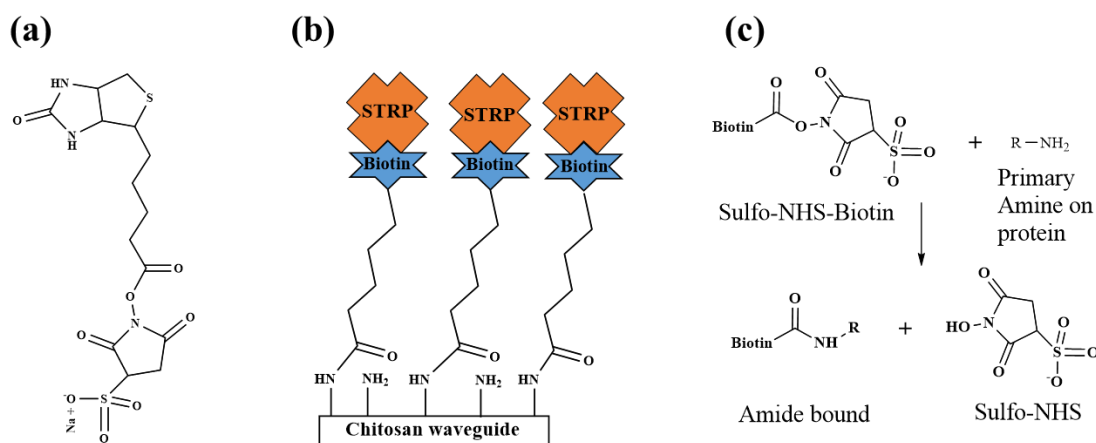
Figure 5.13 **(a)** *Chemical structure of Sulfo-NHS-Biotin,* **(b)** *after reaction of Sulfo-NHS-Biotin with chitosan waveguide via NHS ester making an amide bond and after immobilisation of streptavidin molecules onto biotinylated chitosan waveguide.* **(c)** *Reaction mechanism between Sulfo-NHS-Biotin and amine group yielding a stable conjugate amide bond.*

Sulfo-NHS-Biotin solution (1 mM/ w/v) in HEPES buffer was first flushed through the chitosan waveguide (1%) at various times ranging from 1 min to 50 min at the flow rate of 118 µL min^{-1}. This was followed by manual injection of streptavidin solution (83µM) in the HEPES buffer. Biotinylated aptamer (1 µM/ oligo 3/table 2.2) in HEPES salts buffer was then applied to verify the binding of streptavidin as explained in section 2.9.3

In the glutaraldehyde method, the binding of streptavidin onto the immobilised aldehyde group was verified using oligo 2 solutions at a concentration of 10 µM (known as non-specific biotinylated aptamer (table 2.2)). In this section oligo 3 solution at a concentration of 1µM (known as anti-thrombin biotinylated aptamer (table 2.2)) was utilised instead. The molecular weights of oligo 2 and oligo 3 are 12 kDa and 6 kDa respectively (table 2.2). As they are different in size, the shift in resonance angle upon immobilisation aptamer molecules would also be different. Therefore, in order to make a clear comparison between the physical adsorption method and the glutaraldehyde method, oligo 3 solution (1µM) was first applied into a chitosan waveguide (1%) initially treated

with glutaraldehyde for one hour (0.2 %) and subsequently with streptavidin (83 µM) for two hours. As shown in figure 5.14, the dip rapidly moved by 0.25° upon introducing biotinylated aptamer (oligo 3/ 1 µM) in HEPES salts buffer. The dip remained at the same level even when the running buffer was re-applied. This would indicate the successful attachment of aptamer molecules to the immobilised streptavidin. The immobilisation of streptavidin onto the chitosan waveguide (1%) based on physical adsorption, biotin-streptavidin affinity and using biotinylated aptamer (oligo 3/ 1 µM) to verify the binding is shown in figure 5.15.
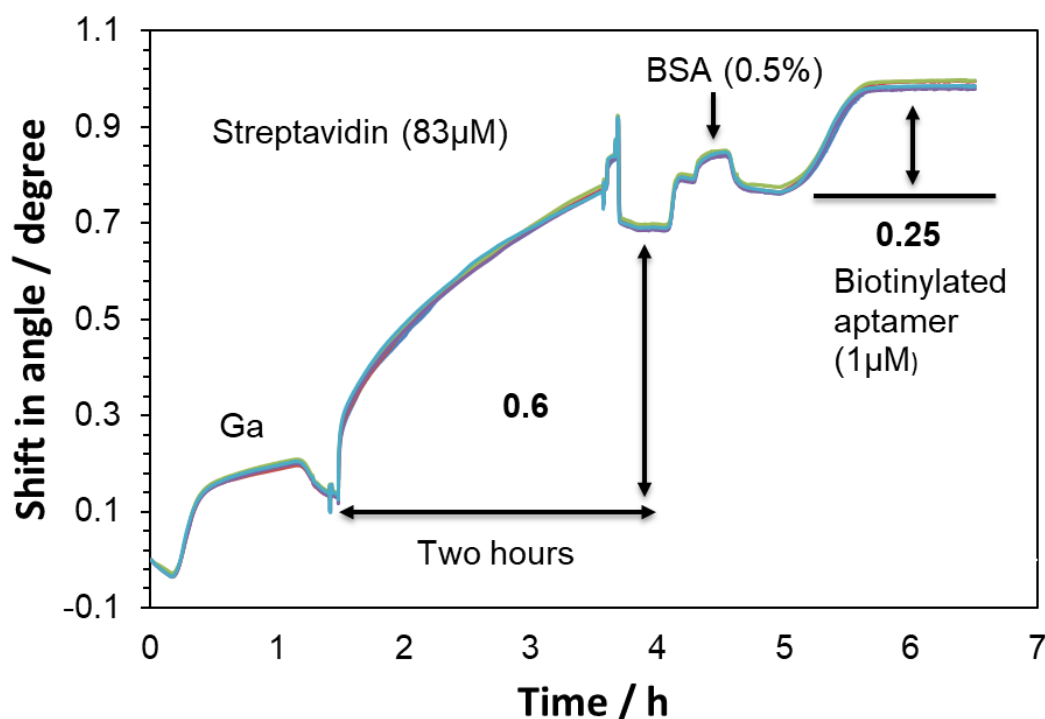
Figure 5.14 *Shift in resonance angle as a function of time on immobilisation of biotinylated aptamer (oligo 3/1 µM) on a chitosan waveguide (1%) that was initially treated with glutaraldehyde solution (0.2%) for one hour and subsequently with streptavidin solution (83µM) for two hours. Glutaraldehyde (0.2%) and streptavidin (83µM) were made in HEPES buffer (100 mM/ pH 7.4) while blocking molecules (BSA/0.5 %) and biotinylated aptamer (oligo 3/1 µM) were prepared in HEPES salts buffer. All solutions were flushed at a flow rate of 118 µL min^{-1} except streptavidin solution, which was manually injected. The experiment was run one time using one chitosan waveguide.*

Figure 5.15 displays the shift in resonance angle upon flushing the chitosan waveguide (1%) with Sulfo-NHS-Biotin solution (1mM) for 1, 5, 10, 30 and 50 min. Each incubation time of the solution was applied to a separate chitosan waveguide (1%). It can be seen that the dip shifted to a higher resonance angle upon increasing the flushing time of Sulfo-NHS-Biotin solution. After introducing the running buffer, the dip clearly stabilised at 0.015° and 0.02° for flushing time of 30 min and 50 min respectively. This would first indicate that the biotin molecules were successfully conjugated onto the surface, as the dip did not shift back to the original baseline with running buffer. Second, the degree of shifting was clearly proportional to the flushing time of Sulfo-NHS-Biotin solution which indicates that higher incubation times corresponded to higher amounts of biotin molecules bound. Although the degree of shifting in resonance angle was clearly low (0.015° and 0.02°), the amount of biotin molecules attached to the waveguide would be expected to be high. This is because Sulfo-NHS-Biotin is a small molecule (443.43 Da) which would not lead to a significant change in the refractive index of the waveguide upon binding.
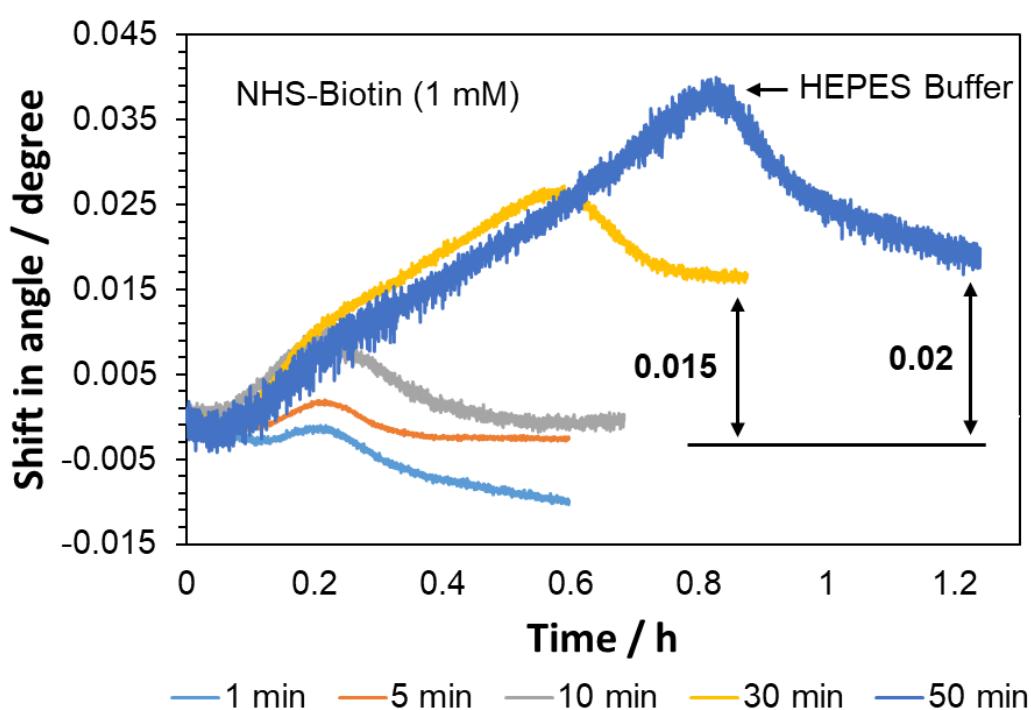
Figure 5.15 *Shift in resonance angle upon flushing various chitosan waveguides (1%) with Sulfo-NHS-Biotin solution (1mM) for various times (1, 5, 10, 30 and 50 min) at a flow rate of 118 µL min⁻¹ as indicated on the legend of the figure. Each flushing time was performed one time using one separate chitosan waveguide (1%). Sulfo-NHS-Biotin solution was made in the HEPES buffer (100 mM/ pH 7.4).*

Figure 5.16 exhibits the immobilisation of streptavidin solution (83µM) following Sulfo-NHS-biotin treatment. After flushing the waveguide with Sulfo-NHS-biotin for 50 min and after injection of streptavidin solution (83µM), the dip finally stabilised at 2.1° with running buffer. This was considered to give the highest amount of streptavidin immobilised onto chitosan waveguide by comparison with all previous protocols. The degree of stabilisation gradually reduced upon reducing the flushing time of Sulfo-NHS-biotin solution showing 1.5°, 0.7°, 0.1° and 0.05° for the flushing time of 30 min, 10 min, 5 min and 1 min respectively. This suggests that the amount of streptavidin attached was clearly proportional to the time of treatment with Sulfo-NHS-biotin solution. Moreover, after introducing streptavidin solution (83µM) onto all waveguides, the dip reached saturation level within 10 min due to the high affinity between the streptavidin molecules and biotinylated chitosan waveguide. After 20 min as a total of 10 min of Sulfo-NHS-biotin treatment and 10 min of introducing streptavidin solution (83µM), a shift in resonance angle was seen at 0.95°. In comparison with the glutaraldehyde method, a similar shift was observed (1° (Figures 5.6 and 5.8)), although after three hours of treatment, one hour for the glutaraldehyde attachment and two hours for the streptavidin conjugation (83µM). Therefore, this would indicate a good enhancement of the immobilisation of streptavidin onto biotinylated chitosan waveguide. This also has been previously confirmed where the adsorption of streptavidin onto biotinylated surface reached saturation level within a few minutes, while a longer time was required when it was immobilised using a covalent attachment[174]. In the previous section where streptavidin (83µM) was immobilised by electrostatic interaction, the stabilised level was between 0.1° and 0.17° (Figure 5.12). Here, lower than this (0.1° and 0.17°) was observed when the waveguide was initially flushed with Sulfo-NHS-biotin solution (1mM) for 1 min followed by introducing streptavidin solution (83 µM). The stabilised level was seen at 0.05°. This would be attributed to the availability of the positive charge on the surface which was reduced upon the biotinylation process. This behaviour has also been reported, where the electrostatic forces between DNA (negative charge) and chitosan (positive charge) were attenuated upon increasing the biotinylation process of chitosan [172].
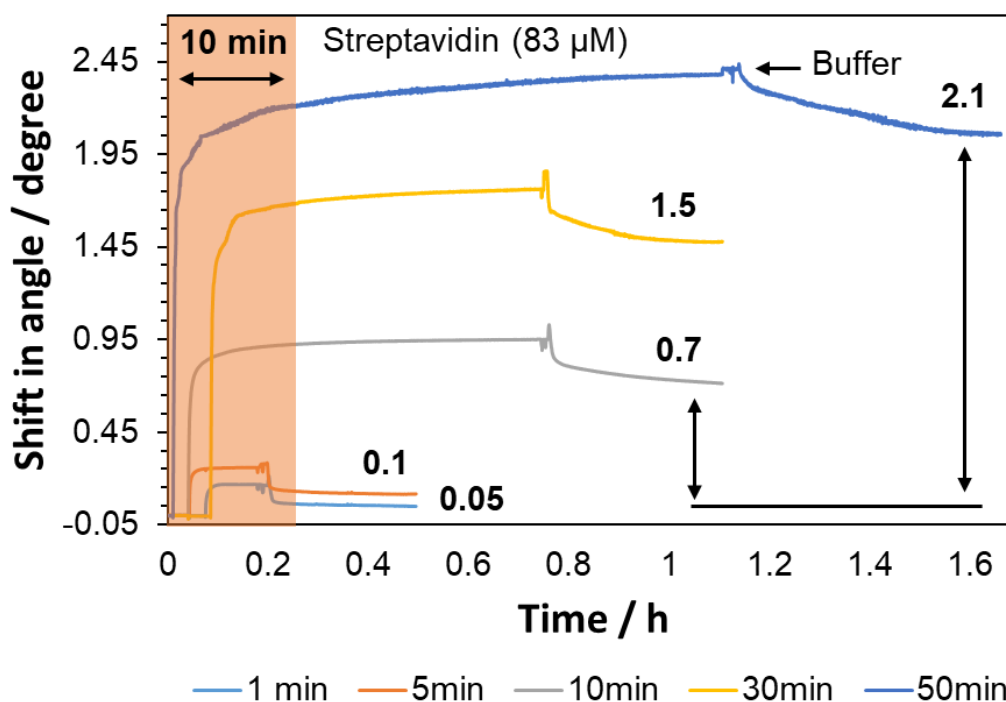
Figure 5.16 *Shift in resonance angle as a function of time on introducing streptavidin solutions (83 μM) into various chitosan waveguides (1%) that were all initially flushed with Sulfo-NHS-biotin solution (1mM) in the HEPES buffer (100 mM/ pH 7.4) for 1, 5, 10, 30, and 50 min at the flow rate of 118 μL min⁻¹ as indicated on the legend of the figure. The immobilisation of streptavidin was performed manually. The experiment was performed one time using one separate chitosan waveguide for each flushing time.*

Figures 5.17; (a), (b), (c), (d) and (e) show the subsequent binding of biotinylated aptamer (oligo 3/1 μM) after streptavidin immobilisation. The amount of streptavidin that was initially immobilised on the waveguide (Figure 5.16) is shown in the legend of this figure presented by the shift in resonance angle (degree). HEPES salts buffer was flushed through the surface before and after introducing the aptamer solution as indicated in the figure. It can be seen that the dip shifted to a higher resonance angle when the biotinylated aptamer solutions (1μM) were applied onto the majority of chitosan waveguides. The highest shift was observed when the waveguide was initially functionalised with streptavidin molecules. Here, the shift was by 0.7°, leading to a shift with the aptamer solution (1μM) by 0.05° (Figure 5.17 c). The second shift was seen at the highest and the lowest amount of streptavidin attached (2.1° and 0.05° respectively) leading to a shift in resonance angle with the aptamer solution (1μM) by 0.03° (Figure 5.17 a and e). The third shift was seen at the amount of streptavidin attached (0.1°) leading to a shift in

resonance angle with the aptamer solution (1µM) by 0.015° (Figure 5.17 d). However, these observed shifts cannot be considered as a successful attachment of aptamer molecules as the shift in resonance angle was clearly not related to the amount of streptavidin attached. At the lowest amount of streptavidin attached (0.05°) (Figure 5.17 e), the shift with aptamer solution was identically (0.03°) to the shift observed at the highest amount of streptavidin conjugated (2.1°) (Figure 5.17 a). Furthermore, no stabilised shift was obtained when aptamer solution was applied onto the chitosan waveguide that shows an amount of streptavidin attached at 1.5°.

Moreover, by comparison to the glutaraldehyde method using the same aptamer solution (oligo 3) at the same concentration (1µM) (Figure 5.14), the dip rapidly moved by 0.25° and remained at the same level. This degree of shifting (0.25°) was clearly higher than those obtained in this experiment (0.05°, 0.03°and 0.015°). Therefore, this leads to the conclusion that the attachment of aptamer molecules were not successful even though the immobilisation of streptavidin onto biotinylated chitosan waveguide was significantly high (Figure 5.16). The immobilisation of streptavidin molecules onto biotinylated surface was considered to be in an ordered arrangement with only two available binding sites per streptavidin facing the solution. In contrast, the molecules are supposed to be randomly orientated when they are covalently attached with the greater number of binding sites per streptavidin. Furthermore, the immobilisation of biotinylated DNA onto an ordered arrangement of streptavidin had not resulted in occupation of the two remaining binding sites. This was attributed to the distance between the two available biotin binding sites, which is near to the hydrodynamic diameter of DNA. This led to an electrostatic repulsion and steric hindrance, hence preventing the binding of two DNA molecules per streptavidin [174-176]. All these findings could be linked to the poor attachment of aptamer molecules in this section.
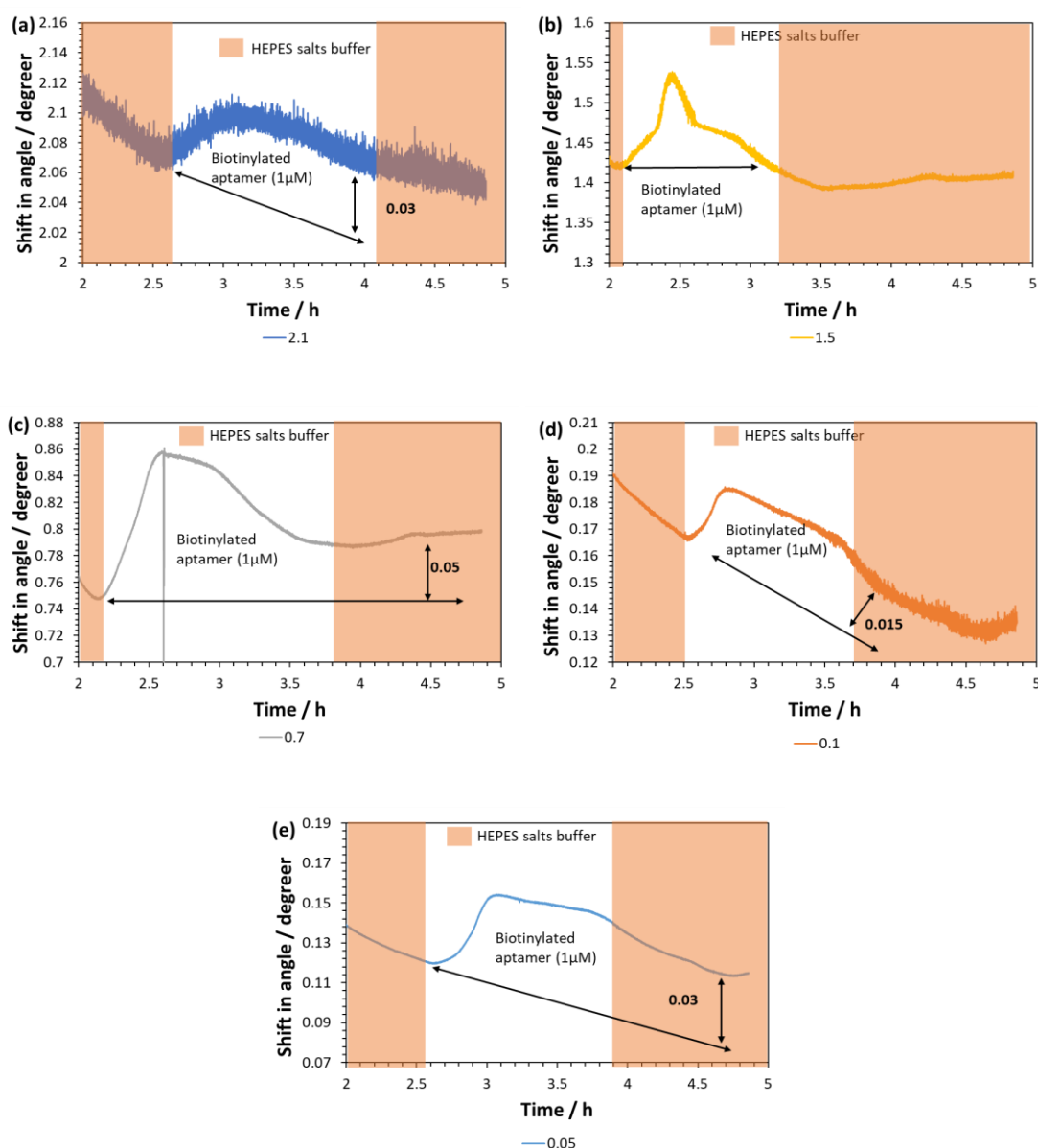
Figure 5.17 *Shift in resonance angle on introduction of biotinylated aptamer solutions (oligo 3/1 μM) into five chitosan waveguides (1%); (a), (b), (c), (d) and (e); at a flow rate of 118 μL min^{-1}. Each waveguide was initially flushed with Sulfo-NHS-biotin solution (1mM) for 50 min (a), 30 min (b), 10 min (c), 5 min (d) and 1 min (e) at the flow rate of 118 μL min^{-1}. This was followed by manually applying streptavidin solution (83μM) into each waveguide. The amount of streptavidin attached on each waveguide is shown in the legend of the figures which presented by the shift in resonance angle (degrees); (a) 2.1, (b) 1.5, (c) 0.7, (d) 0.1, and (e) 0.05. The aptamer solution was made in HEPES salts buffer. The experiment was run one time using one separate chitosan waveguide for each condition.*

Further examination of the attachment of aptamer molecule was carried out. Here, the conjugation of biotin molecules into the chitosan waveguide (1%) via Sulfo-NHS-biotin was performed in a buffer of high ionic strength in order to reduce the non-specific binding. Sulfo-NHS ester carries a negative charge on its structure (Figure 5.13) which therefore would enhance the non-specific binding of biotin onto the chitosan waveguide. This in turn would lead to non-stable conjugation of the biotin molecule which would have an effect on the immobilisation of streptavidin and hence on the subsequent binding of aptamer. Sulfo-NHS-biotin solution (1mM) was made in HEPES salts buffer before flushing through the waveguide at various times. As shown in figure 5.18 , the dip, as expected, shifted to a higher resonance angle upon increasing the flushing time. However, it stabilised with running buffer at a lower degree than previously observed. The stabilised level after flushing the surface with Sulfo-NHS-biotin solution in HEPES salts buffer for 50 min and 30 min was seen at $0.009°$ and $0.003°$ respectively. In contrast, the dip stabilised at $0.02°$ and $0.015°$ when the same solution was flushed in the HEPES buffer (Figure 5.15) for 50 min and 30 min respectively. This would show an obvious reduction in the amount of biotin conjugated on the waveguide using HEPES salts buffer. Therefore, it can be concluded that the majority of biotin molecules that were attached previously to the chitosan waveguide (Figure 5.15) were based on an electrostatic attraction.
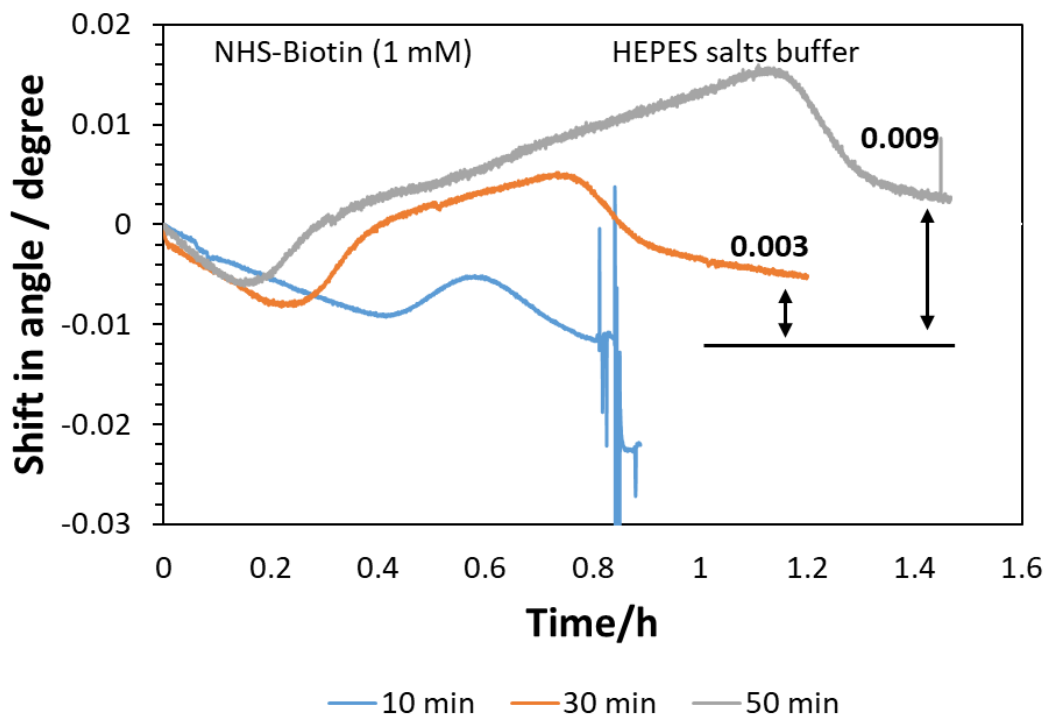
Figure 5.18 *Shift in resonance angle upon flushing three chitosan waveguides (1%) with Sulfo-NHS-Biotin solution (1mM) for various times (10, 30 and 50 min) at a flow rate of 118 μL min⁻¹ as indicated on the legend of the figure. Each flushing time was performed one time using one separate chitosan waveguide (1%). Sulfo-NHS-Biotin solution was made in HEPES salts buffer.*

Further confirmation can be seen in figure 5.19 when streptavidin solution (83 μM) was then applied. The dip stabilised with running buffer at 1°, 0.6° and 0.1° for the waveguides that were initially flushed with Sulfo-NHS-biotin solution in HEPES salts buffer for 50 min, 30 min and 10 min respectively. In contrast, using the HEPES buffer and for the same flushing time, 50 min, 30 min and 10 min, a stabilised level with running buffer and after applying streptavidin solution (83 μM) was at 2.1°, 1.5° and 0.6° respectively (Figure 5.16). This would indicate a clear reduction in the amount of streptavidin immobilised which confirm the reduction in the amount of biotin conjugated on the waveguide when HEPES salts buffer was used.
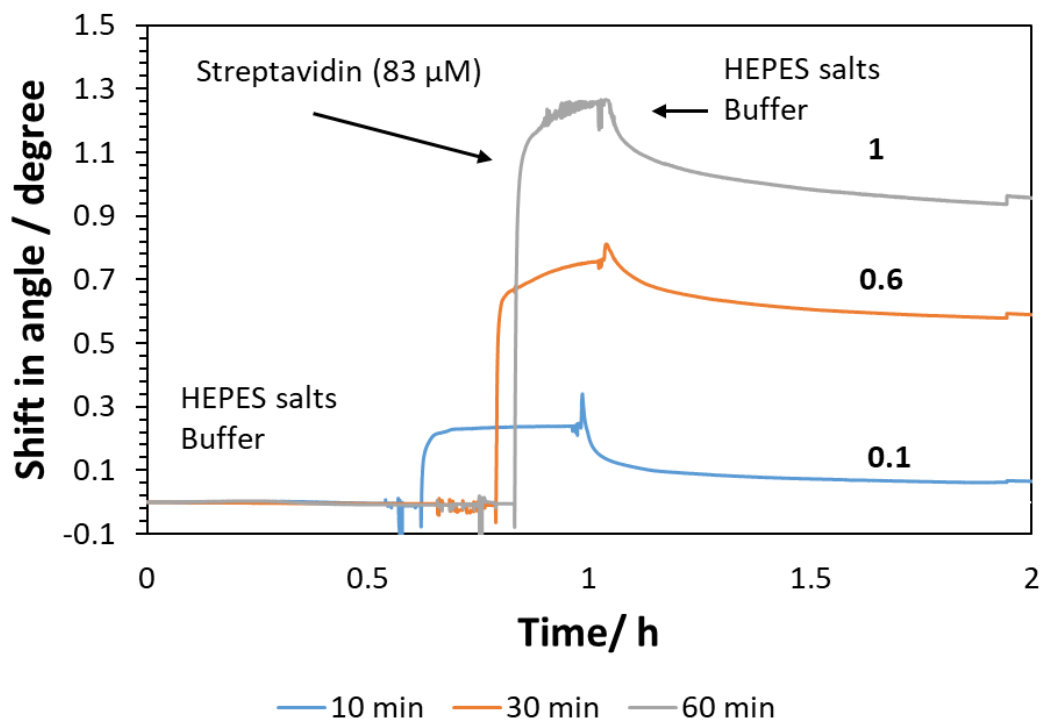
Figure 5.19 *Shift in resonance angle as a function of time on introducing streptavidin solutions (83 µM) into three chitosan waveguides (1%) that were all initially flushed with Sulfo-NHS-biotin solution (1mM) in the HEPES salts buffer for 10, 30, and 50 min at the flow rate of 118 µL min^{-1} as indicated on the legend of the figure. The immobilisation of streptavidin was performed manually. The experiment was performed one time using one separate chitosan waveguide for each flushing time.*

Upon introducing biotinylated aptamer solutions (oligo 3/1 µM), a shift in resonance angle was seen on all waveguides (Figure 5.20 a, b and c). However, the amount of aptamers bound were clearly not proportional to the amount of streptavidin immobilised. At the highest amount of streptavidin attached (1° (Figure 5.20 a)), the observed shift upon applying aptamer solution was seen at 0.05° (Figure 5.20 a) while a higher shift in resonance angle was obtained (0.1° (Figure 5.20 b)) when the aptamer solution was introduced into the waveguide that showed a lower amount of streptavidin conjugated (0.6° (Figure 5.20 b)). Furthermore, the amount of aptamer bound (0.1° (Figure 5.20 b)) was still clearly lower than in the glutaraldehyde method when the same solution of aptamer was introduced (0.25° (Figure 5.14).

Moreover, by comparison with the previous condition when Sulfo-NHS-biotin solution was applied in HEPES buffer and subsequently the waveguide was functionalised with

streptavidin showing a shift in resonance angle by 0.7°. The amount of aptamer bound was seen at 0.05° (Figure 5.17 c). Here in this experiment the amount of aptamer bound was seen at 0.1° (Figure 5.20 b) which is clearly higher than 0.05° even though both waveguides had almost the same amount of streptavidin attached (0.7°/0.6°, Figure 5.17 (c) and 5.20 (b) respectively) and the aptamer solutions were constant at a concentration of 1 µM.

From this, it can be concluded that a fluctuation in the amount of aptamer bound can be easily obtained even when the amount of streptavidin immobilised was identical. Therefore, the attachment of the biotinylated aptamer onto the streptavidin that was initially immobilised onto the biotinylated chitosan waveguide should not be considered a reliable and reproducible method and hence cannot be used as an alternative method to the glutaraldehyde.

In the glutaraldehyde method and upon optimising the concentration of glutaraldehyde (Figure 5.9) it was found that higher concentration of glutaraldehyde can easily affect the stability of the chitosan film, which led to the removal of the dip from the CMOS camera. This resulted in repeating the experiment more than one time with each concentration of glutaraldehyde in order to complete the optimisation. This impact was significantly reduced when lower concentrations of glutaraldehyde were utilised particularly at 0.2 % (v/v). Therefore 0.2 % (v/v) of glutaraldehyde was considered as the optimum concentration and would be used in all following experiments.
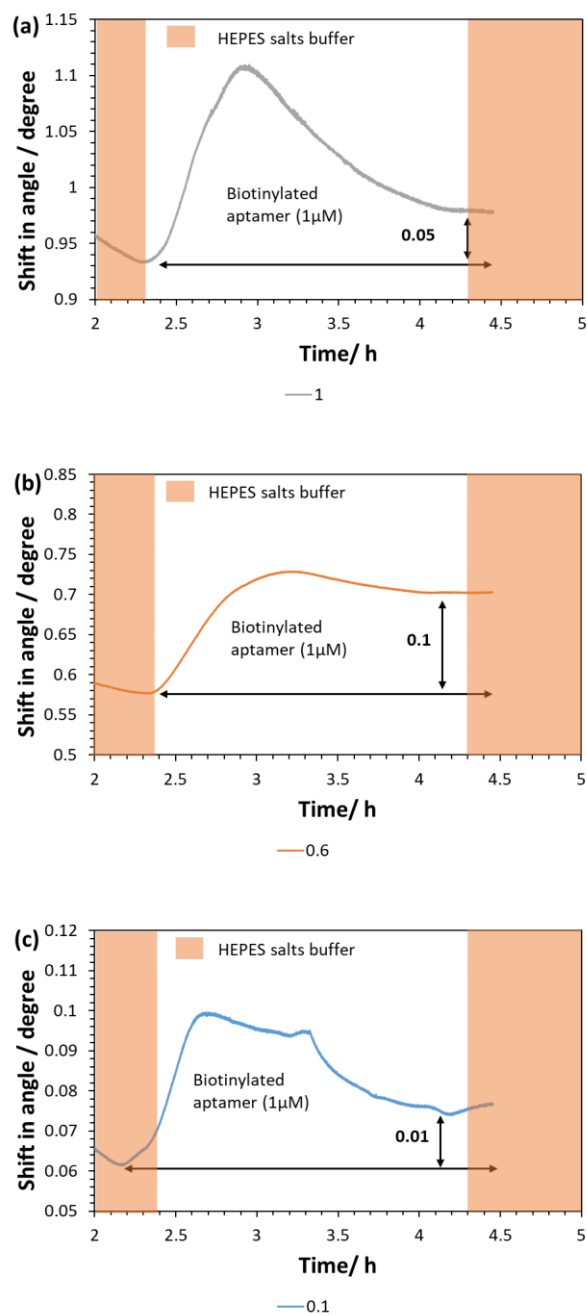
Figure 5.20 *Shift in resonance angle on introduction of biotinylated aptamer solutions (oligo 3/1 μM) into three chitosan waveguides (1%); (a), (b) and (c); at a flow rate of 118 μL min⁻¹. Each waveguide was initially flushed with Sulfo-NHS-biotin solution in HEPES salts buffer (1mM) for 50 min (a), 30 min (b) and 10 min (c) at the flow rate of 118 μL min⁻¹. This was followed by manually applying streptavidin solution (83μM) into each waveguide. The amount of streptavidin attached on each waveguide is shown in the legend of the figures which presented by the shift in resonance angle (degrees); (a) 1, (b) 0.6 and (c) 0.1. The aptamer solution was made in HEPES salts buffer. The experiment was run one time using one separate chitosan waveguide for each condition.*

5.4 Summary

Due to the high affinity between streptavidin and biotin, the complex has been selected as a cross-linker for immobilisation of the aptamer molecule onto the chitosan waveguide. The immobilisation of streptavidin was investigated using various approaches while the binding was verified using biotinylated aptamer and biotinylated BSA.

For covalent attachment, the effectiveness of using glutaraldehyde (0.6 %) as a coupling agent was successfully demonstrated by conjugation of BSA molecules (0.5% ≈ 75µM) onto the chitosan waveguide (1%). Upon immobilisation of streptavidin (1.6 µM), a slight shift in resonance angle was detected which indicated an attachment of streptavidin. However, the amount of unreacted aldehyde group on the surface was extremely high which resulted in large numbers of blocking molecules being conjugated into the surface. Consequently, the binding sites on streptavidin were hidden and a poor attachment of aptamer was obtained. A large improvement was gained when the high concentration of streptavidin (83µM) was used which served as a blocking molecule and also as a binding site. The amount of streptavidin immobilised was significantly higher leading to a shift in resonance angle by 1°. This resulted in a greater enhancement of the aptamer attachment (oligo 2/(10µM)) giving a further rapid shift by 0.4°. Further confirmation of the successful binding of streptavidin was also observed upon applying biotinylated BSA solution (10 µg/mL) leading to a shift in resonance angle by 0.5°. The glutaraldehyde concentration was then investigated to find out the optimum concentrations that were measured by monitoring the amount of streptavidin (83 µM) immobilised. It was found that the amount of streptavidin attached was indeed not related to the amount of glutaraldehyde bound leading to a clear variation over different runs. This was attributed to the polymerisation of the glutaraldehyde which led to forming oligomers rather than reacting with free amino groups. Therefore further investigation in the immobilisation of streptavidin was carried on in order to overcome this impact.

Immobilisation via electrostatic interaction showed a slight variation in the amount of streptavidin (83 µM) attached over three runs (between 0.1° and 0.17°). However, it was significantly lower than in the glutaraldehyde method where the dip moved between 0.5° and 1.3°. For the subsequent binding of the biotinylated aptamer (10 µM), the dip shifted between 0.02° and 0.05° which was also significantly lower than the amount of aptamer (10 µM) bound in the glutaraldehyde protocol (0.4°). Furthermore, the shift obtained with the aptamer solution was found to be not related to the amount of streptavidin adsorbed.

It was concluded that aptamer molecules were not bound to the immobilised streptavidin and hence the immobilisation via an electrostatic interaction cannot be considered as an alternative approach to the glutaraldehyde method.

Immobilisation of the streptavidin (83 µM) was further enhanced when it was adsorbed onto a biotinylated chitosan waveguide. The stabilised level was seen at 2.1° on the waveguide that had been initially flushed with Sulfo-NHS-biotin solution (1 mM) for 50 min. This was considered to be the highest amount of streptavidin to be immobilised among all the previous protocols. Furthermore, the saturation level was obtained in the first 10 min of introducing the streptavidin solution (83 µM) showing a shift in resonance angle by 0.95° from the waveguide that had been initially flushed with Sulfo-NHS-biotin solution (1 mM) for 10 min. In contrast, three hours were required to reach the same level (0.95°) using the glutaraldehyde method.

Nevertheless, for the subsequent binding, the amount of aptamer attached was significantly poorer by comparison with the glutaraldehyde protocol using the same oligo solution (oligo 3) and at the same concentration (1µM). This could be linked firstly to the availability of the biotin binding sites because of one or two sites being already occupied upon the immobilisation of the streptavidin and secondly to electrostatic repulsion and steric hindrance which prevents the aptamer binding on the two close remaining biotin binding sites. Conjugation of the biotin molecules onto the chitosan waveguide using a buffer of high ionic strength was shown to reduce the amount of streptavidin immobilised. For the subsequent binding, the amount of aptamer bound (0.1°) was still clearly lower than that observed in the glutaraldehyde method (0.25°) using the same oligo solution (oligo 3/1µM). Furthermore, a clear fluctuation in the amount of aptamer attached was observed from various waveguides that exhibited the same amount of streptavidin immobilised. Therefore, the attachment of aptamer molecule onto streptavidin that was immobilised on the biotinylated chitosan waveguide was considered as a not reliable and not reproducible binding. By comparing the all protocols utilised for streptavidin immobilisation and for the subsequent binding of biotinylated aptamer, it can be said that the glutaraldehyde method still was the optimum condition. The following chapter will discuss the immobilisation of anti-thrombin biotinylated aptamer using the glutaraldehyde protocol for detection of thrombin.

CHAPTER 6

Detection of Thrombin

6 Detection of Thrombin

Thrombin binding to its aptamer has been the most commonly used model system as a proof of principle for an assay based on aptamer affinity [177]. Therefore, this system has been selected to validate the effectiveness of using a DDLW as a biosensor device with an aptamer as the bio-recognition element. Two aptamers have been reported to bind thrombin at different binding sites. The first aptamer was described by Bock *et al.* in 1992. It consisted of 15 mer of DNA oligonucleotide (5'GGT TGG TGT GGT TGG'3) [178]. This 15-mer aptamer was found to interact with human α-thrombin at one anion site; the fibrinogen-recognition exosite; with a dissociation constant (Kd) of ≈100 nM. The second aptamer was reported by Tasset and Kubik in 1997. It consisted of 29-mer of DNA oligonucleotide (5'AGT CCGTGG TAG GGC AGG TTG GGG TGA CT'3) [121]. This 29-mer aptamer was bound to thrombin at the second anion site; heparin-binding exosite; with a higher binding affinity (Kd≈ 0.5 nM). However, the binding affinity (Kd) has later been reported to be varied for the second aptamer (29-mer) particular between 11.9 nM [179] and 255 nM [180] while it was observed to be at a higher affinity for the first aptamer (15-mer) (1.2 nM) [179]. Comparing the two aptamers, the first aptamer (15-mer) has been extensively and widely used for detection of thrombin under various techniques such as surface plasmon resonance (SPR)[131, 181, 182] and electrochemical aptasensors[183, 184]. Therefore, it was selected for thrombin detection in this project. The immobilisation of the aptamer onto chitosan waveguide was performed via the streptavidin-biotin complex using the glutaraldehyde method (Figure 6.1) found to be optimum in chapter 5. The detection of thrombin was performed in an aqueous buffer and in a commercial human serum sample.
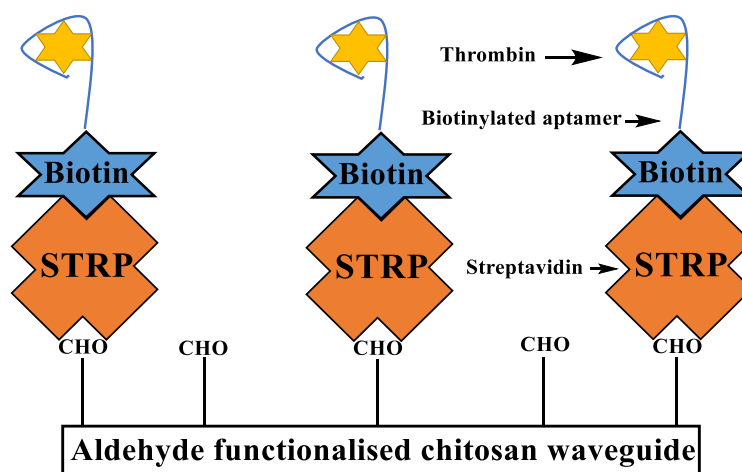
Figure 6.1 *Schematic diagram of thrombin binding to its aptamer that had been initially immobilised onto a chitosan waveguide via streptavidin-biotin complex. Streptavidin was attached to the chitosan waveguide via glutaraldehyde.*

6.1 Detection of thrombin in aqueous buffer

The immobilisation of the anti-thrombin aptamer (oligo 3 / table 2.2) onto the chitosan waveguide (1%) followed by detection of thrombin molecules were both performed in the HEPES salts buffer at pH 7.4 (table 2.4). This buffer was made up with various salts and was almost the same as the composition of the running buffer utilised previously for thrombin detection[158, 185]. The chitosan waveguide (1%) was first flushed with the glutaraldehyde (0.2%) solution for 1 h and subsequently with the streptavidin (83µM) solution for 2 h as explained in section 2.10.1. Both solutions were made in the HEPES buffer (100 mM/pH 7.4). The anti-thrombin biotinylated aptamer (oligo 3/1µM) and thrombin solution (1µM), both made in HEPES salts buffer, were then sequentially introduced at a flow rate of 118 µL min^{-1}.

Figure 6.2 displays the shift in resonance angle as a function of time on applying various solutions into the chitosan waveguide (1%). The running buffer, either HEPES buffer (100 mM/pH 7.4) or HEPES salts buffer, was introduced through the surface before and after each solution was applied in order to gain a new baseline. It can be seen that the dip shifted by 0.25° upon introducing glutaraldehyde solution (0.2 %) for 1 h. This was followed by a further shift in resonance angle by 0.6° when streptavidin solution (83µM) was injected for 2 h. This indicates the attachment of the streptavidin molecules onto the immobilised glutaraldehyde. Upon introducing the anti-thrombin biotinylated aptamer (oligo 3/1µM), the dip moved by 0.25° which confirmed the conjugation of aptamer molecules via the streptavidin–biotin complex. Thrombin solution (1µM) was then

followed for 15 min which led to a rapid shift in resonance angle by 0.18 °. The dip remained at the same level even when the running buffer (HEPES salts buffer) was re-applied. This would lead us to say that thrombin molecules were successfully bound to the immobilised aptamer. In order to validate this binding, a control run was conducted by repeating the same experiment under the same conditions, however, without using anti-thrombin biotinylated aptamer. Non-specific biotinylated aptamer (oligo 2/1µM) was utilised instead as shown in figure 6.3.
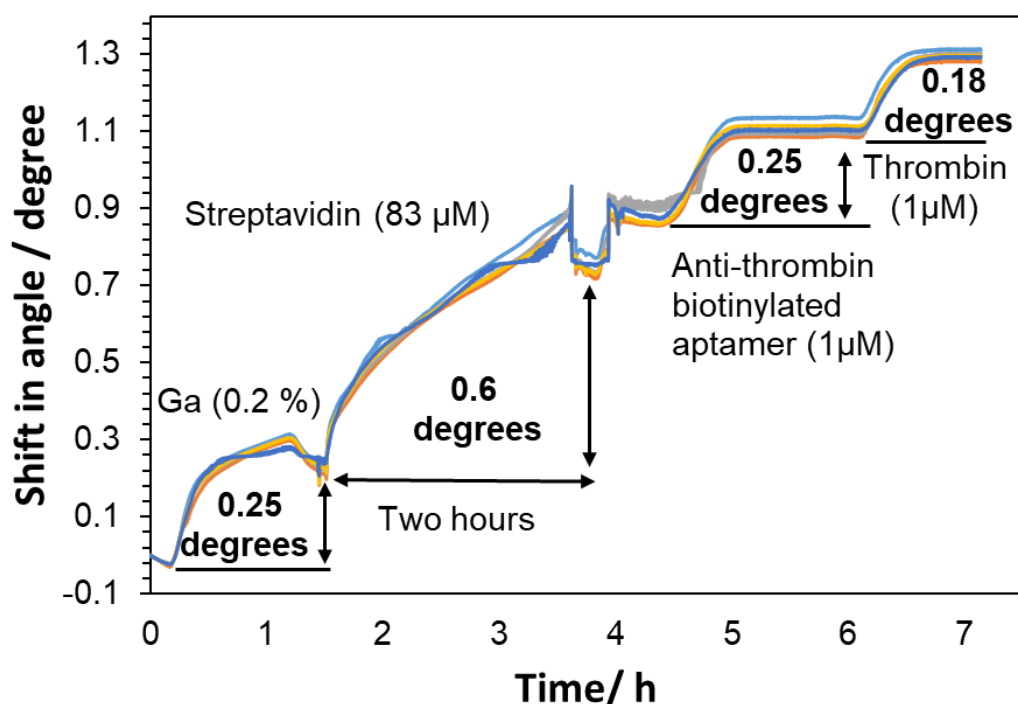
Figure 6.2 *Shift in resonance angle as a function of time on applying glutaraldehyde (Ga) (0.2 %), streptavidin (83 µM), anti-thrombin biotinylated aptamer (oligo 3/1µM) and thrombin (1µM) solutions onto the chitosan waveguide (1%). Glutaraldehyde and streptavidin solutions were made in the HEPES buffer (100 mM/pH 7.4) while anti-thrombin biotinylated aptamer and thrombin solutions were prepared in HEPES salts buffer. Thrombin solution (1µM) was applied for 15 min. All solutions were flushed at a flow rate of 118 µL min^{-1} except streptavidin, which was manually injected. The experiment was run one time using one chitosan waveguide.*

Figure 6.3 exhibits the immobilisation of a non-specific biotinylated aptamer (oligo 2/1µM) onto the chitosan waveguide (1%) for detection of thrombin. Upon immobilisation of the streptavidin molecules, the dip shifted by 0.6° which was identical to the shift observed in figure 6.2. This would indicate that streptavidin was immobilised

onto both waveguides by almost the same amount. A further rapid shift in resonance angle was obtained when a non-specific sequences biotinylated aptamer (oligo 2 /1μM) was applied. The dip shifted by 0.45°. This shift was clearly higher than the 0.25° obtained previously when anti-thrombin biotinylated aptamer (oligo 3/1μM) was immobilised (Figure 6.2). Both aptamers solutions were prepared in the same buffer (HEPES salts buffer) at the same concentration (1μM) and were both immobilised onto the chitosan waveguides that had been initially functionalised with the same amount of streptavidin. This clearly shows differences in the degree of shift between the two aptamer solutions (0.25° and 0.45°). This is attributed to the size of each aptamer. This is because the change in the refractive index of the waveguide and hence the shift in resonance angle is directly proportional to the molecular mass. The molecular weights of oligo 2 and oligo 3 are ≈ 12 kDa and ≈ 6 kDa (table 2.2) respectively. Upon introducing thrombin solution (1μM) for 15 min, a slight shift in resonance angle was observed. However, it immediately dropped down to the original baseline upon flushing the surface with running buffer (HEPES salts buffer). This indicates unbound thrombin molecules on the immobilised non-specific aptamer. The slight shift obtained at the beginning was due to the refractive index of the solution. This would therefore further confirm the successful detection of thrombin molecules that was observed in figure 6.2. This would also validate the effectiveness of using the DDLW as a biosensor device. In order to investigate the detection sensitivity of the sensor, the experiment was repeated, applying a lower concentration of thrombin as shown in figure 6.4.
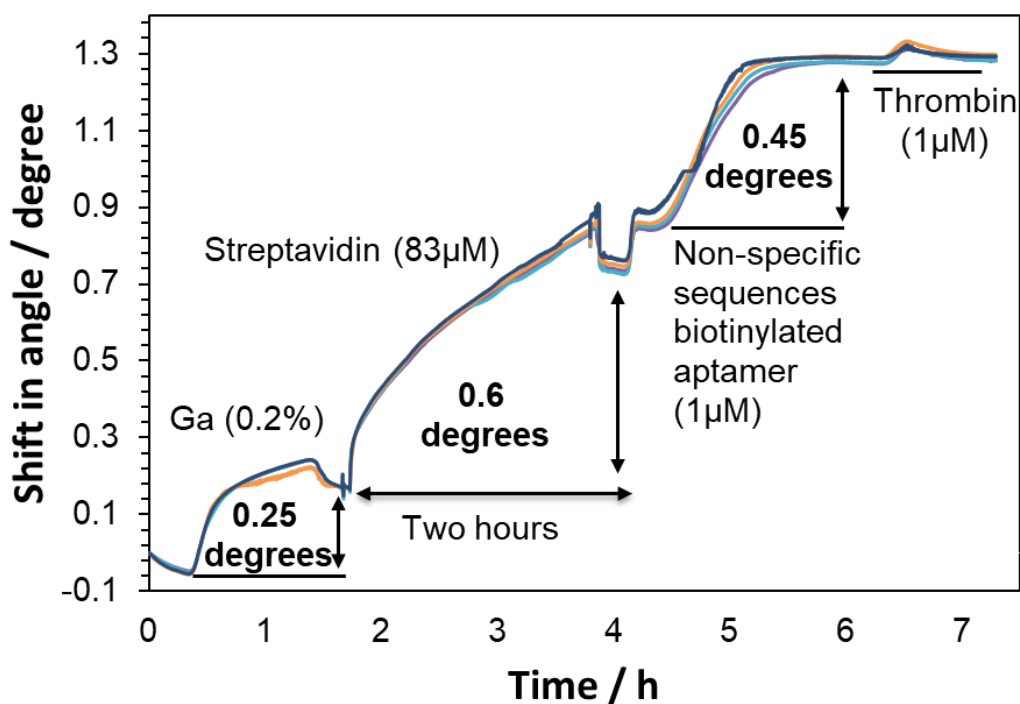
Figure 6.3 *Shift in resonance angle as a function of time on immobilisation of a non-specific biotinylated aptamer (oligo 2/1µM) onto the chitosan waveguide (1%) for thrombin detection. The waveguide was first treated with glutaraldehyde solution (0.2%) for 1 h and subsequently with streptavidin (83µM) for 2 h. Both solutions were made in the HEPES buffer (100 mM/pH 7.4). A non-specific biotinylated aptamer (oligo 2/1µM) was then applied followed by thrombin solution (1µM) for 15 min. Both solutions were introduced in HEPES salts buffer. The experiment was run one time using one chitosan waveguide.*

Figure 6.4 shows the immobilisation of anti-thrombin biotinylated aptamer (oligo 3/1µM) onto the chitosan waveguide (1%) for the detection of thrombin at lower concentrations. From the figure, the dip shifted by 0.225° upon immobilisation of the aptamer molecules. A series of concentrations of thrombin were then sequentially applied to the chitosan waveguide starting from 1 nM to 1 µM. Each solution was flushed for 15 min at a flow rate of 118 µL min^{-1} before applying the next thrombin solution. At the end, HEPES salts buffer was introduced to obtain a new baseline. As can be seen, the dip remained at the same level of the baseline even when 1 nM and 10 nM of thrombin solutions were applied. A shift in resonance angle was begun to be seen at a concentration of 100 nM while a significant shift was seen at a concentration of 1 µM. This was expected because at a higher concentration, a higher amount of thrombin is bound to the immobilised aptamer

and consequently a significant change in the refractive index of the waveguide occurs. The dip remained at the same level even when HEPES salts buffer was applied at the end. This would indicate the successful detection of a series of concentrations of thrombin in a real-time measurement. After flushing the surface with a series of concentrations of thrombin, the dip stabilised by 0.3°. This shift was clearly higher than the 0.18° obtained previously when 1 µM of thrombin solution was measured (Figure 6.2). This would confirm that in this experiment a large amount of thrombin molecules were bound after flushing the surface with a series of concentrations of thrombin. However, a clear shift was only seen when higher concentrations of thrombin (100 nM and 1µM) were applied which indicated the poor detection sensitivity of the DDLW device. In order to enhance the sensitivity of the sensor, a thrombin solution was continuously flushed over the surface for about 14 hours as shown in figure 6.5.
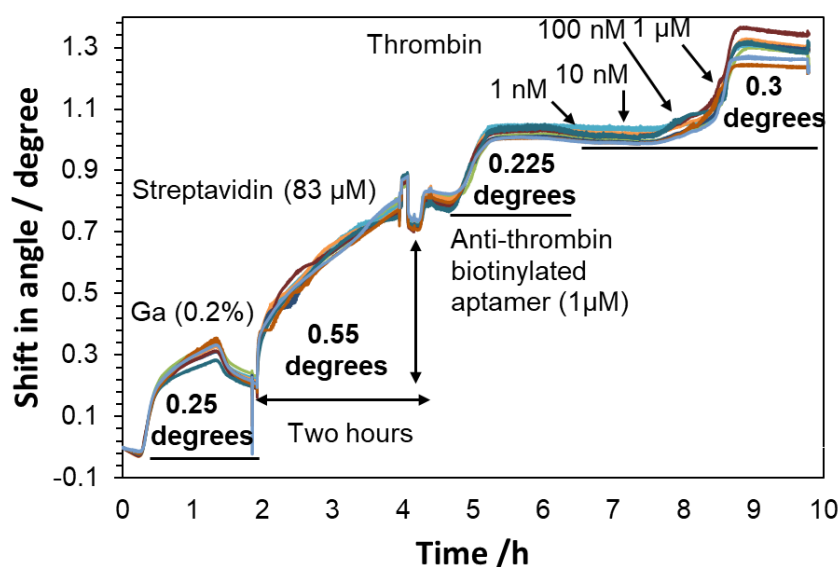
Figure 6.4 *Shift in resonance angle as a function of time upon immobilisation of anti-thrombin biotinylated aptamer (oligo 3/1µM) for detection of thrombin at lower concentrations. A chitosan waveguide (1%) was first treated with glutaraldehyde solution (0.2%) for 1 h and subsequently with streptavidin solution (83µM) for 2 h. Both solutions were made in the HEPES buffer (100 mM/ pH 7.4). Anti-thrombin biotinylated aptamer (oligo 3/1µM) was then applied followed by sequentially introducing thrombin solutions starting from 1 nM to 1 µM. Each solution was flushed for 15 min before applying the next thrombin solution. HEPES salts buffer was introduced at the end of the experiment. The experiment was run one time using one chitosan waveguide.*

Figure 6.5 shows the shift in resonance angle upon continuously flushing the chitosan waveguide (1%) with 100 nM of thrombin solution for about 14 hours. Upon introducing anti-thrombin biotinylated aptamer (oligo 3/ 1µM), the dip moved by 0.22° indicating the attachment of the aptamer molecules to the immobilised streptavidin. A further large shift in resonance angle was seen upon applying the thrombin solution (100 nM) for about 14 hours. The saturation level was gained after four hours of reaction shown a shift in resonance angle by 0.65°. This shift is significantly higher than the 0.18° observed when 1µM of thrombin solution was measured (Figure 6.2). Furthermore, it is also clearly higher than the 0.3° obtained when the series concentrations of thrombin ranging from 1 nM until 1µM were sequentially measured (Figure 6.4). Therefore, this would indicate the enhancement of the detection of thrombin upon increasing the flushing time. In order to further validate the binding between thrombin and its aptamer that was observed upon flushing the surface with thrombin solution (100 nM) for about 14 hours, the experiment was repeated under the same condition, however, without using thrombin solution. Bovine serum albumin (BSA/ 100 nM) was flushed instead as shown in figure 6.6.
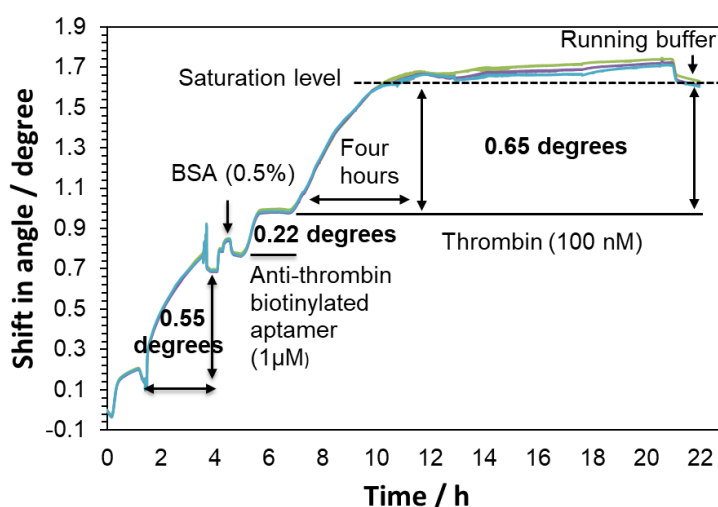
Figure 6.5 *Shift in resonance angle as a function of time upon continuously flushing the chitosan waveguide (1%) with thrombin solution (100 nM) for about 14 hours. The waveguide was initially treated with glutaraldehyde solution (0.2%) for 1 h and subsequently with streptavidin solution (83 µM) for 2 h. Both solutions were made in the HEPES buffer (100 mM/ pH 7.4). Blocking molecules (BSA/ 0.5%) and anti-thrombin biotinylated aptamer (oligo 3/ 1µM) were then sequentially applied. Finally, thrombin solution (100 nM) was introduced for about 14 hours. The experiment was run one time using one chitosan waveguide.*

Figure 6.6 displays the scope for introducing the BSA solution (100 nM) for about 14 hours onto the chitosan waveguide (1%) that was initially treated with 1 µM of anti-thrombin biotinylated aptamer. The shift in resonance angle observed upon introducing the thrombin solution (100 nM) for about 14 hours in the previous experiment (Figure 6.5) was also added here in order to make a clear comparison. From the figure, it can be seen that the dip remained at almost the same level as the running buffer (HEPES salts buffer) when the BSA solution (100 nM) was applied during the first four hours. After this period, a gradual shift in resonance angle was observed reaching 0.1° after 10 hours of incubation. However, the dip totally shifted back to the original baseline when the running buffer (HEPES salts buffer) was flushed through the surface at the end. This would confirm that the BSA molecules did not bind to the immobilised anti-thrombin aptamer. This would further confirm that the observed shift upon introducing thrombin solution (100 nM) for about 14 hours in the previous experiment (Figure 6.5) (also it is added in this figure) represented the successful binding to the immobilised anti-thrombin aptamer as it was not seen when the BSA solution (100 nM) was applied for the same period.
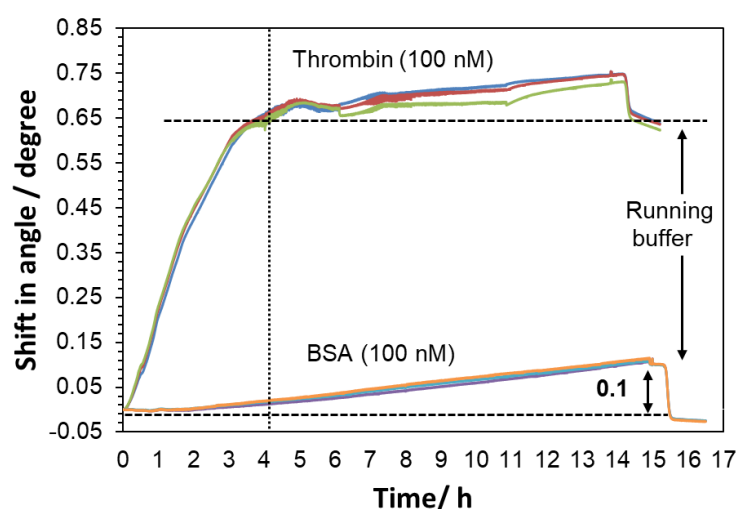
Figure 6.6 Shift in resonance angle as a function of time upon introducing the BSA solution (100 nM) and the thrombin solution (100 nM) onto two separate chitosan waveguides (1%) for about 14 hours. Both waveguides were initially treated with glutaraldehyde solution (0.2%) for 1 h and subsequently with streptavidin solution (83 µM) for 2 h. Both solutions were made in the HEPES buffer (100 mM/ pH 7.4). This was followed by applying blocking molecules (BSA/0.5%) and subsequently anti-thrombin biotinylated aptamer (oligo 3/ 1µM) onto both waveguides.

Further confirmation can be seen in figure 6.7 which shows images of the dip taken from two chitosan waveguides which were utilised for thrombin (100 nM) and BSA (100 nM) detection. The images were taken at three different steps: at the beginning of the experiment with the HEPES buffer; after anti-thrombin aptamer immobilisation; and after flushing the surface with thrombin (100 nM) and BSA (100 nM) solutions for about 14 hours. It can be seen that the dip clearly shifted upon immobilisation of the anti-thrombin biotinylated aptamer (1µM) onto both chitosan waveguides (image **(c)** and **(d)**). A further obvious shift was observed when the thrombin solution (100 nM) was applied for about 14 hours (image **(e)**) which confirmed the binding of thrombin molecules. In contrast, upon introducing BSA solution (100 nM) for the same period of time, the dip remained at the same position (image **(f)**) which indicated unbound BSA molecules. This would further confirm the achievement of detection of thrombin molecules by the DDLW device. In order to investigate the best level of aptamer immobilised for detection of thrombin, a series of concentrations of aptamers were introduced onto various chitosan waveguides to detect 100 nM of thrombin. The results are shown in figures 6.8 and 6.9.

It has been noticed that after reaching the saturation level which was after four hours of introducing thrombin solution (100 nM) (Figure 6.5), the dip was appeared to be shifted again to higher degree of angles during the incubation that was last for 14 hours. This was also observed when BSA solution (100 nM) was applied to the chitosan waveguide that was initially functionalised with 1 µM of anti-thrombin biotinylated aptamer (Figure 6.6). However, in both waveguides when the running buffer was applied at the end, the dip was totally returned to the previous stabilised level. This would be linked to the non-specific binding of protein to surface leading to change in the waveguide's refractive index. In order to avoid this impact, thrombin solution in all flowing experiments was only applied for four hours.
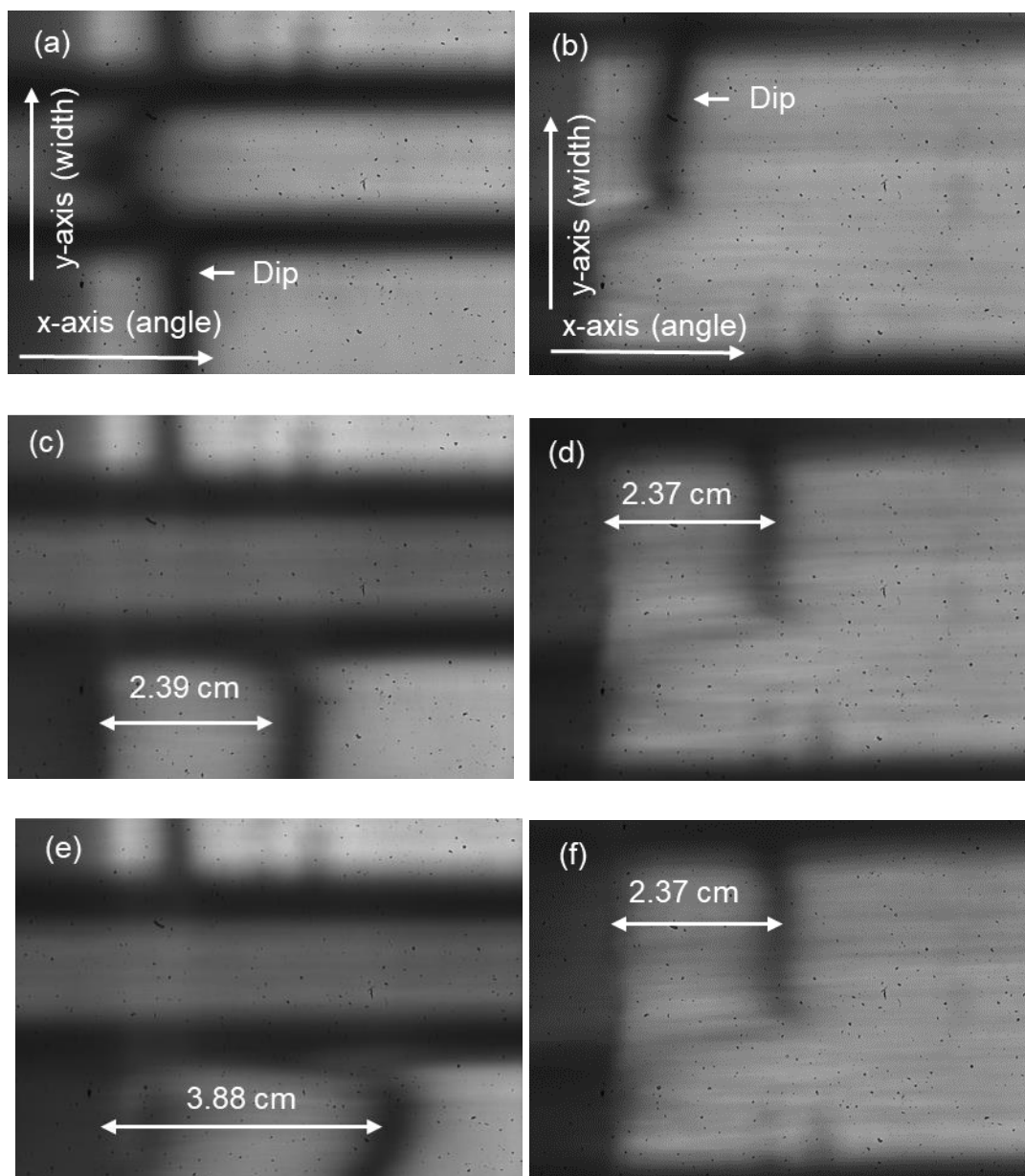
Figure 6.7 *Images of the dip taken by CMOS camera from two chitosan waveguides (1%)*
under different steps. **(a)** *and* **(b)** *after flushing both waveguides (1%) at the beginning of*
the experiment with the HEPES buffer. **(c)** *and* **(d)** *after the immobilisation of anti-*
thrombin biotinylated aptamer (1µM) onto both waveguides (1%). **(e)** *after flushing the*
waveguide with thrombin solution (100 nM). **(f)** *after flushing the waveguide with BSA*
(100 nM) solution.

Figure 6.8 shows the immobilisation of a higher concentration of anti-thrombin
biotinylated aptamer (1.5 µM) for detection of 100 nM of thrombin. From the figure, the
dip shifted by 0.52° upon introducing the thrombin solution (100 nM) for about 4 hours.
This would confirm the binding of thrombin to the immobilised aptamer. Although a

higher concentration of aptamer (1.5 µM) was used in this experiment, the degree of shift with the thrombin solution (0.52°) was lower than the 0.65 ° obtained previously when the same concentration of thrombin (100 nM) was applied onto the chitosan waveguide (1%) functionalised with 1 µM of aptamer (Figure 6.5). This difference in the degree of shift would indicate the differences on the amount of thrombin bound into both waveguides. This could be linked to the steric hindrance effect in which a higher concentration of aptamer could result in a lower amount of thrombin bound. To further investigate this impact, various concentrations of anti-thrombin aptamer were used to detect 100 nM of thrombin. The results are summarised in figure 6.9.
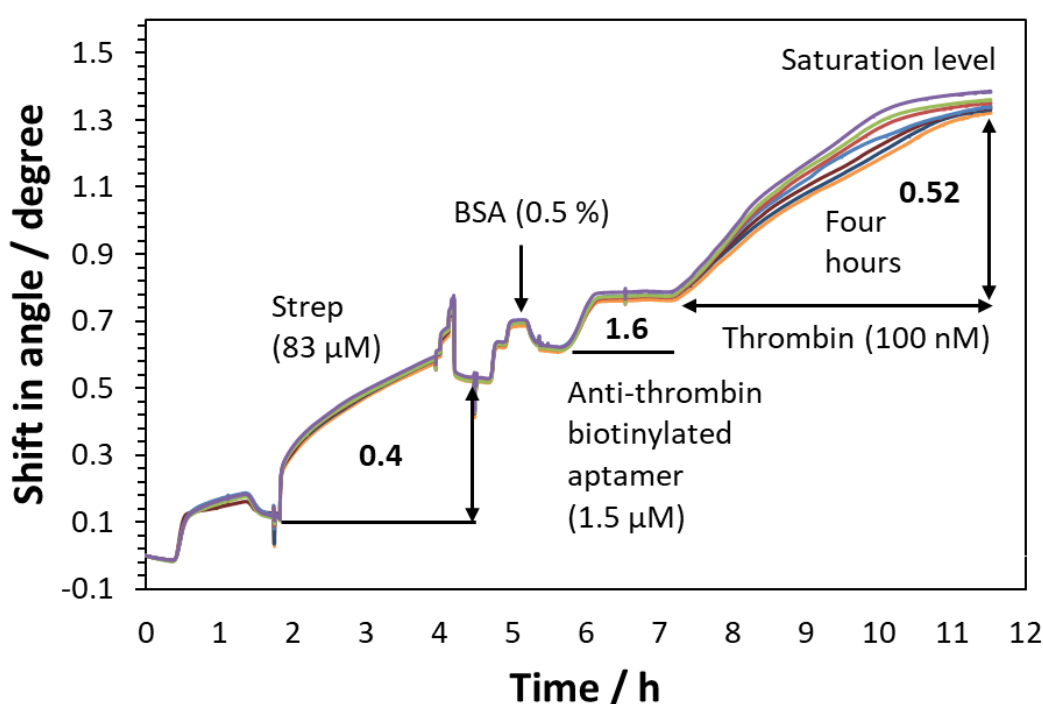
Figure 6.8 *Shift in resonance angle as a function of time upon immobilisation of a higher concentration of anti-thrombin biotinylated aptamer (oligo 3/ 1.5 µM) for detection of 100 nM of thrombin. The waveguide was initially treated with glutaraldehyde solution (0.2%) for 1 h and subsequently with streptavidin solution (83 µM) for 2 h. Both solutions were made in the HEPES buffer (100 mM/ pH 7.4). Blocking molecules (BSA/0.5%) and anti-thrombin biotinylated aptamer (oligo 3/ 1.5µM) were then sequentially applied followed by thrombin solution (100 nM) for about 4 hours. The experiment was run one time using one chitosan waveguide.*

Figure 6.9 **(a)** shows the shift in resonance angle upon sequentially attachment of glutaraldehyde (0.2%), streptavidin (83 µM) and various concentrations of anti-thrombin aptamer to five chitosan waveguides (1%). Each waveguide was functionalised either with 0.1 µM, 0.5 µM, 1 µM or 2 µM of anti-thrombin biotinylated aptamer while the concentrations of glutaraldehyde and streptavidin were kept constant as indicated on the legend of the figure. As can be seen from the figure, the amount of glutaraldehyde bound was very similar between different chitosan waveguides while it varied slightly between different runs for the amount of the streptavidin immobilised. Upon introducing the aptamer solutions at different concentrations, the highest shift in resonance angle was seen when 1µM of aptamer solution was used. The dip shifted by 0.22°. Lower and higher concentrations of aptamers (0.5 µM, 1.5 µM, and 2 µM) were also shown a closer shift that were between 0.11° and 0.16°. The lowest shift was seen when 0.1 µM of aptamer solution was used leading to the shift by 0.02°.

Figure 6.9 **(b)** displays the shift in resonance angle after flushing each chitosan waveguide with 100 nM of thrombin for the first four hours. From the figure, it can be seen that the shift in resonance angle gradually increased upon increasing the flushing time of the thrombin solution (100 nM). This was expected because for a longer flushing time a higher amount of thrombin molecules were bound to the immobilised aptamer and hence a higher change in the refractive index occurred. This was observed for all chitosan waveguides (1%). It can be seen from the figure that the highest amount of thrombin bound was clearly observed for the waveguide that was initially functionalised with 1µM of aptamer solution. Therefore, 1µM was selected as the optimum concentration for this research.
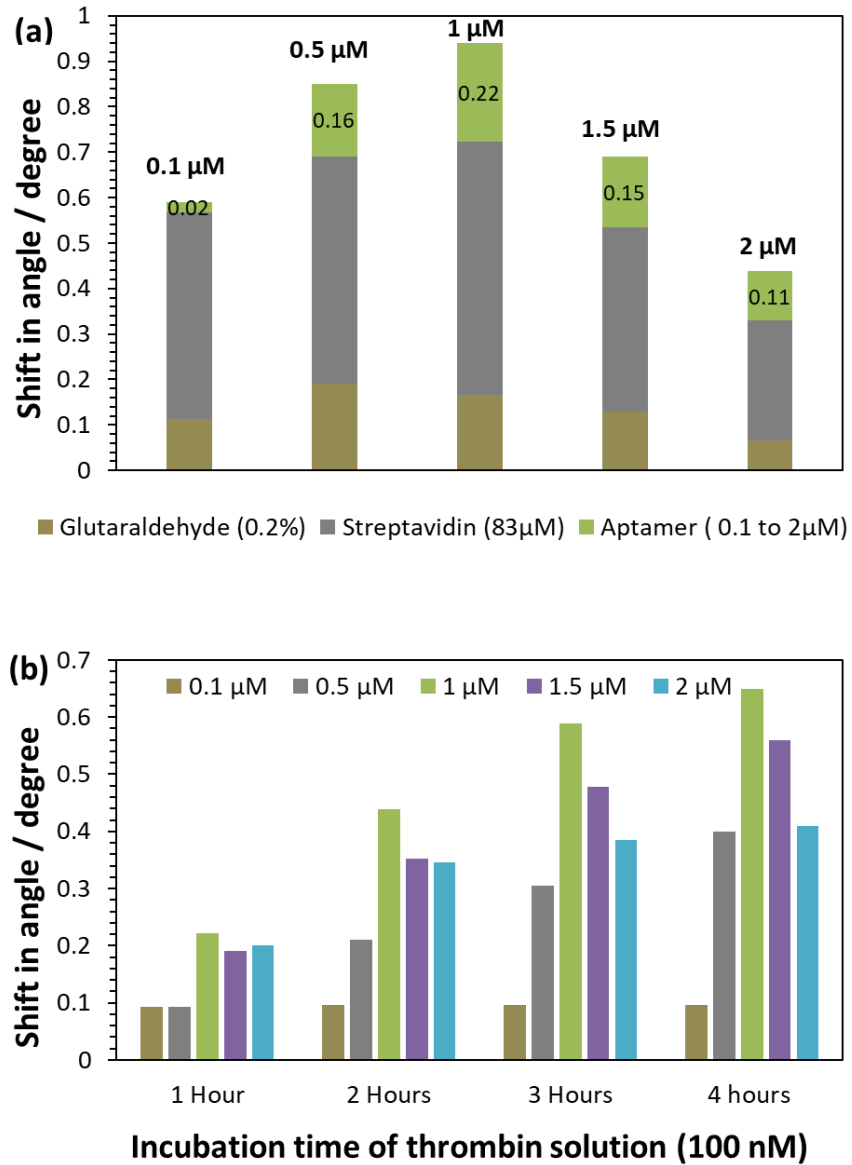
Figure 6.9 **(a)** *Shift in resonance angle upon attachment of glutaraldehyde (0.2%), streptavidin (83 μM) and anti-thrombin aptamer to five chitosan waveguides (1%). Each waveguide was functionalised either with 0.1 μM, 0.5 μM, 1 μM or 2 μM of anti-thrombin aptamer as indicated on the figure. The number shown inside each box represents the degree of shifting in resonance angle for each concentration of aptamer.* **(b)** *Shows the shift in resonance angle after introducing thrombin solution (100 nM) to five chitosan waveguides for the first four hours. The experiment was run one time using one separate chitosan waveguide for each concentration of aptamer used.*

6.1.1 Calibration and limit of detection of the DDLW device

In order to calculate the limit of detection (LOD) of the DDLW device, a calibration curve for different solutions of thrombin was prepared. This was accomplished by applying different concentrations of thrombin ranging from 1 nM to 100 nM, including the blank, to various chitosan waveguides (1%). Each concentration including the blank was measured on a separate waveguide. In order to examine the reproducibility, the measurement was repeated three times using three separate chitosan waveguides (1%) for each concentration of thrombin including the blank. On all waveguides, the surface was initially functionalised with anti-thrombin biotinylated aptamer at a concentration of 1µM as explained in section 2.10.1. Upon obtaining the calibration curve, the limit of detection (LOD) was calculated based on equation 6.1.

$$LOD = 3 * \text{standard deviation} / \text{slope} \hspace{2cm} \textit{Equation 6.1}$$

Figure 6.10 shows the detection of thrombin at a concentration of 75 nM. It can be seen that the dip shifted by 0.45° when the thrombin solution (75 nM) was introduced for about 4 hours to obtain a saturation level. The dip remained at the same level with running buffer which confirmed the binding of thrombin to the immobilised aptamer. This shift was clearly lower than the 0.65° observed when 100 nM of thrombin was measured (Figure 6.5). This would be expected because at a lower concentration, a lower amount of thrombin was bound to the immobilised aptamer and hence a lower shift in resonance angle occurred.
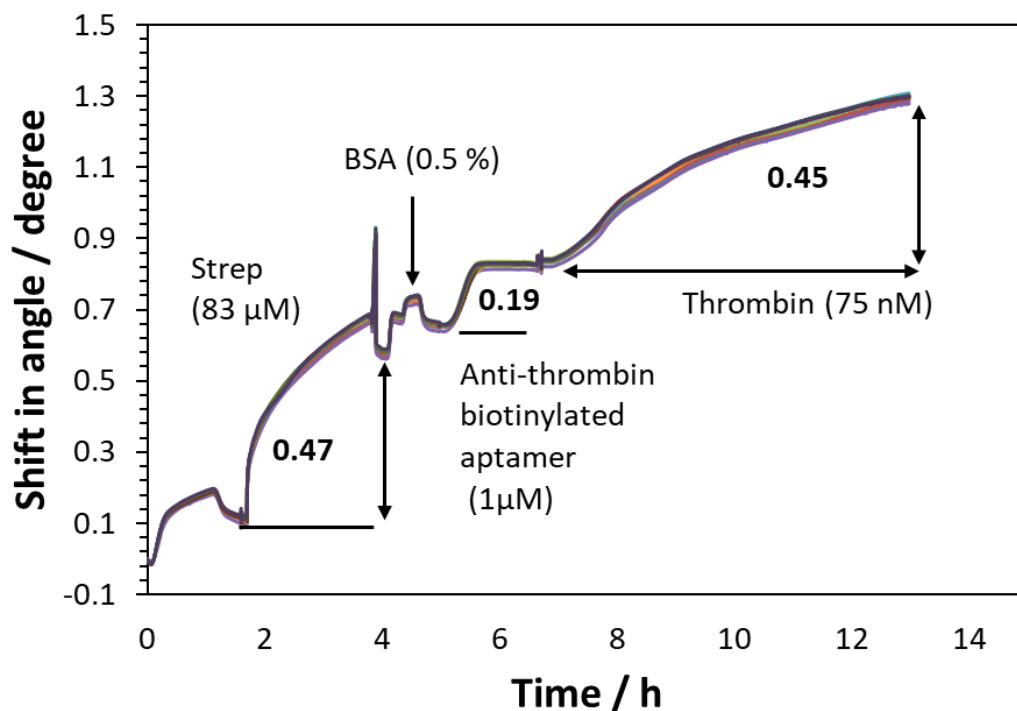
Figure 6.10 *Shift in resonance angle as a function of time upon detection of thrombin at a concentration of 75 nM. The waveguide was initially treated with glutaraldehyde solution (0.2%) for 1 h and subsequently with streptavidin solution (83 μM) for 2 h. Both solutions were made in the HEPES buffer (100 mM/ pH 7.4). Blocking molecules (BSA/ 0.5%) and anti-thrombin biotinylated aptamer (oligo 3/ 1μM) were then applied sequentially. Thrombin solution (75 nM) was then followed for about 6 hours to obtain a saturation level. The experiment was run one time using one chitosan waveguide.*

Figure 6.11 displays the shift in resonance angle for the first four hours of introducing different concentrations of thrombin ranging from 1 nM to 100 nM including a blank onto separate chitosan waveguides (1%). From the figure, the dip shifted with a degree proportional to the concentration of thrombin applied during the first four hours of the reaction. This would be expected as at higher concentration; a larger number of thrombin molecules were bound to the immobilised aptamer and hence a larger change in the refractive index of the waveguide occurred. Upon introducing the lowest concentration of thrombin (1nM), the dip remained at the same level as the blank sample for the first two hours. A slight shift in resonance angle was then seen with thrombin solution (1 nM) and it was clearly higher than the blank sample. This would indicate the successful detection of thrombin at a concentration of 1 nM.
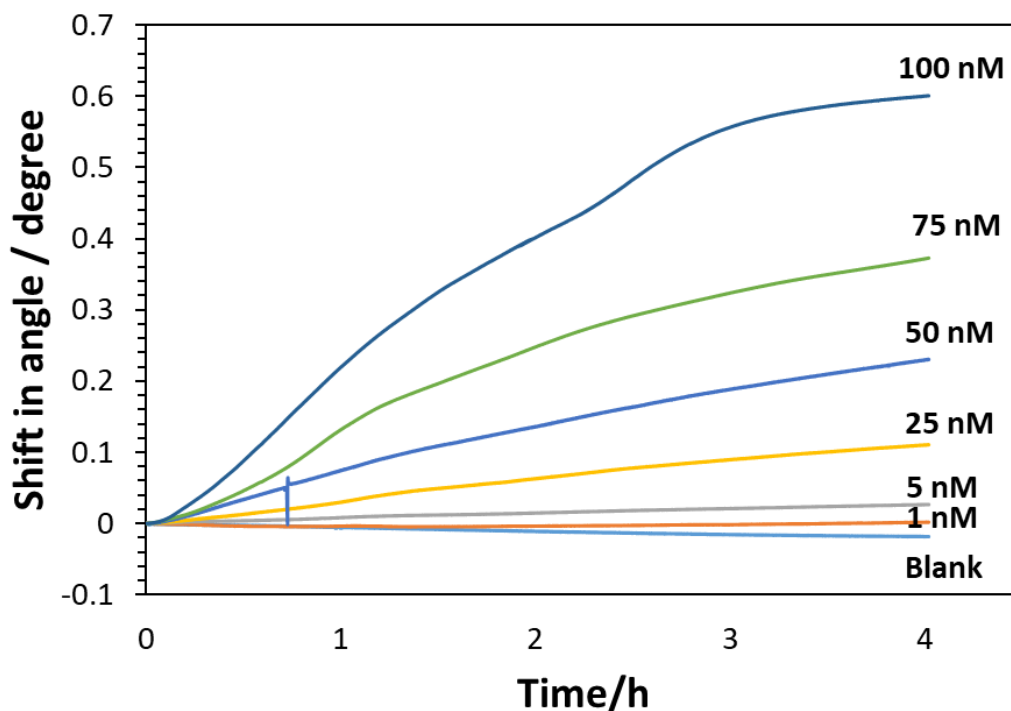
Figure 6.11 *Shift in resonance angle as a function of time upon introducing thrombin solutions at different concentrations (1 nM, 5 nM, 25 nM, 50 nM, 75 nM and 100 nM) including a blank onto a separate chitosan waveguide (1%). All waveguides were initially treated with glutaraldehyde solution (0.2%) for 1 h and subsequently with streptavidin solution (83 μM) for 2 h. This was followed by applying blocking molecules (BSA/0.5%) and subsequently anti-thrombin biotinylated aptamer (oligo 3/ 1μM). The experiment was run one time using one separate chitosan waveguide for each concentration of thrombin used including the blank.*

In order to obtain a reproducible result for the thrombin detection, the measurement was repeated three times using three separate chitosan waveguides (1%). Figure 6.12 shows the average shift in resonance angle upon attachment of glutaraldehyde (0.2%), streptavidin (83 μM) and anti-thrombin aptamer (1μM) onto 21 chitosan waveguides (1%). All these 21 chitosan waveguides (1%) were used for detection of thrombin. Three waveguides were utilised for each concentration of thrombin including the blank. The readings represent the average of three runs. From the figure, the average amount of glutaraldehyde (0.2%) bound into the majority of the chitosan waveguides (1%) was very similar showing the shift between 0.15° and 0.18°. For the subsequent binding of streptavidin (83μM), the shift in resonance angle was between 0.3° and 0.6°, while upon applying the aptamer solution, the dip shifted between 1.5° and 2°. A one way ANOVA

statistical analysis indicated that there was not significant difference in terms of shifting in resonance between glutaraldehyde (0.2%) solutions and also between streptavidin (83μM) solutions and between anti-thrombin aptamer (1μM) solutions upon applying onto those 21 chitosan waveguides. The p-value were at 0.31, 0.25 and 0.28 ($\geqslant$ 0.05) for glutaraldehyde, streptavidin and aptamer solutions respectively.
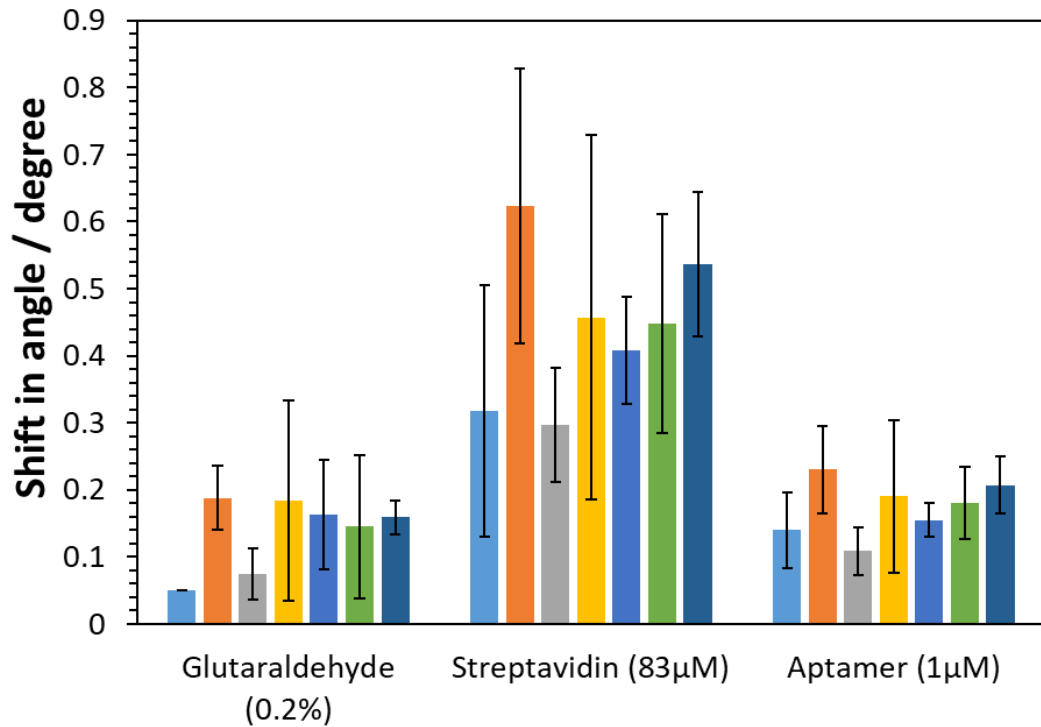
Figure 6.12 Average shift in resonance angle upon attachment of glutaraldehyde (0.2%), streptavidin (83 μM) and anti-thrombin biotinylated aptamer (oligo 3/ 1μM) into 21 chitosan waveguides (1%). Each coloured column represents an average of three runs that were performed for measurement one concentration of thrombin as shown in the flowing figure. A one way ANOVA statistical analysis indicated that there was not significant difference in terms of shifting in resonance between glutaraldehyde (0.2%) solutions and also between streptavidin (83μM) solutions and between anti-thrombin aptamer (1μM) solutions upon applying onto those 21 chitosan waveguides. The p-value were at 0.31, 0.25 and 0.28 ($\geqslant$ 0.05) for glutaraldehyde, streptavidin and aptamer solutions respectively.

Figure 6.13 displays the average shift in resonance angle on binding thrombin molecules at different concentrations (1nM to 100 nM), including the blank, onto those prepared 21 chitosan waveguides (1%). The figure shows the shift for the first four hours of incubation

of thrombin solution. It can be seen that the shift in resonance angle was directly proportional to the concentration of thrombin applied at all the incubation times. This was expected because at higher concentration, a higher amount of thrombin was bound to the immobilised aptamer and consequently a greater change in the refractive index of the waveguide occurred. Upon applying the blank sample onto three chitosan waveguides, the dip gradually and slightly shifted to a lower degree of angle particularly from -0.004° to -0.013° during the first four hours of incubation as shown in the blue box inside the figure. This could be due to some aptamer molecules that were not initially bound into the immobilised streptavidin, being slightly and gradually eluted from the surface when the blank sample was applied. Upon introducing 1 nM of thrombin to three chitosan waveguides, the average shift in resonance angle for the first one hour was at -0.002° which was slightly higher than the blank sample (-0.004°). However, upon increasing the incubation time, the differences to the blank sample started to rise. For the second, third and four hours of incubation, the shift for 1 nM of thrombin was at -0.0004°, 0.004° and 0.006° respectively while it was at -0.009°, -0.011° and -0.013° respectively, for the blank sample. This would further confirm the successful detection of thrombin at a concentration of 1 nM particular after two hours of incubation as the differences in the shift of the blank sample can be easily observed. A two way ANOVA statistical analysis indicated that there was a significant difference in terms of shifting in resonance angle upon applying various concentrations of thrombin including the blank into various chitosan waveguides. The p-value was at < 0.001.
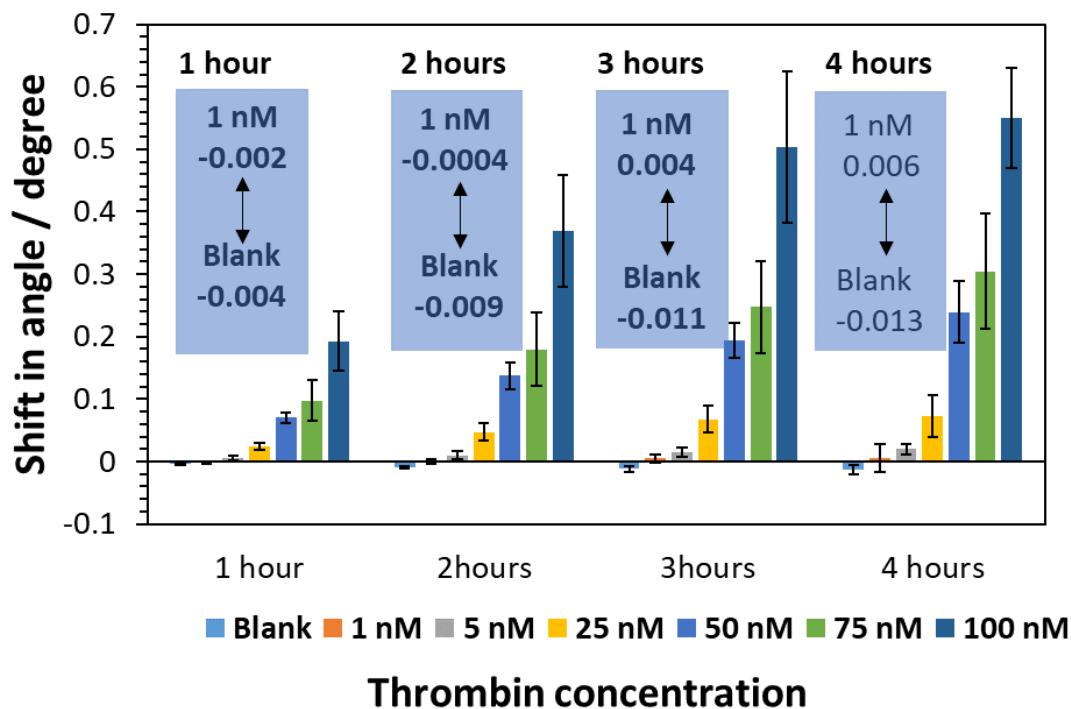
Figure 6.1*3 Average shift in resonance angle for the first four hours of introducing different concentrations of thrombin including the blank into various chitosan waveguides. All waveguides were initially treated with glutaraldehyde solution (0.2%) for 1 h and subsequently with streptavidin solution (83 μM) for 2 h. This was followed by applying blocking molecules (BSA/0.5%) and subsequently anti-thrombin biotinylated aptamer (oligo 3/ 1μM). The number inside the blue box shows the average shift in resonance angle upon applying 1 nM of thrombin solution and the blank for the first fours of introducing. The experiment was run three times using three separate chitosan waveguides for each concentration of thrombin measured including the blank. A two way ANOVA statistical analysis indicated that there was a significant difference in terms of shifting in resonance angle upon applying various concentrations of thrombin including the blank into various chitosan waveguides. The p-value was at < 0.001.*

Figure 6.14 shows a calibration curve for thrombin solutions between concentrations of 0 nM (blank sample) and 75 nM under different incubation times. From the figure, the best trend line was observed for the first hour of incubation shown by the R^2 value of 0.992 while it was slightly lower for the second, third and four hours of incubation which gave the R^2 value of 0.986, 0.982 and 0.977 respectively. As would be expected, the sensitivity of the sensor was at its highest value at the highest incubation time giving slope values of $0.0043°$ RIU^{-1}, $0.0035°$ RIU^{-1}, $0.0026°$ RIU^{-1} and $0.0014°$ RIU^{-1} for the

incubation time of four hours, three hours, two hours and one hour respectively. Based on equation 6.1 and on the straight line equation (Figure 6.14), the limit of detection (LOD) of the DDLW device for the first hour of incubation was found to be $\approx$ 3.7 nM.
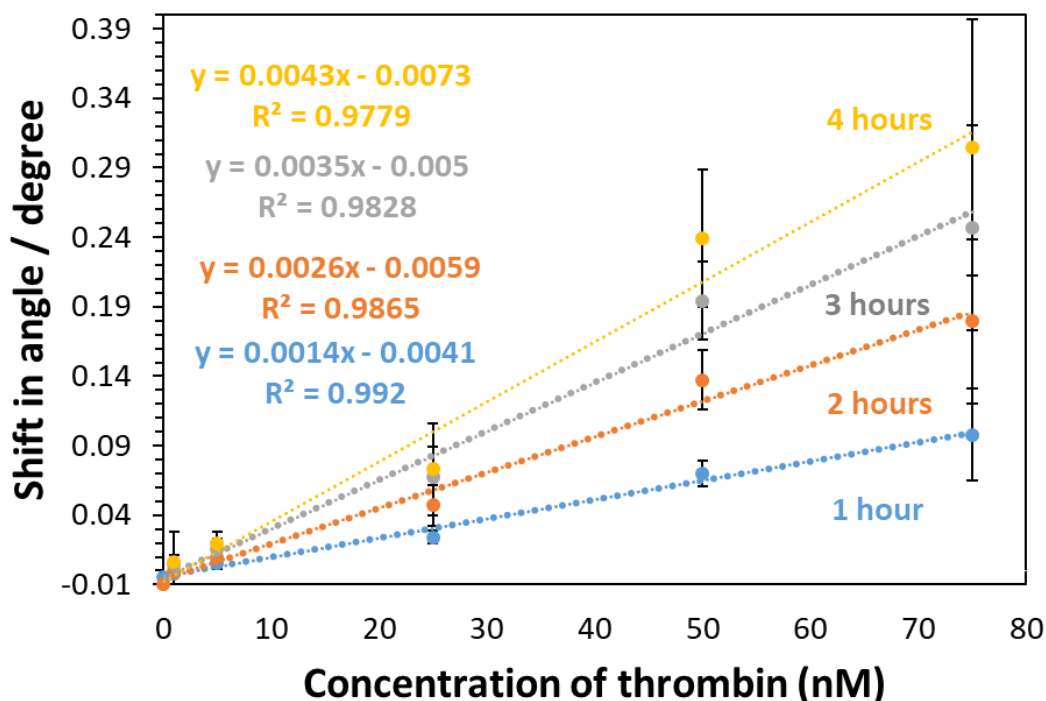
Figure 6.14 *Calibration curves for various concentrations of thrombin ranging from 0 nM (blank) until 75 nM under different incubation times (1 hour, 2 hours,3 hours and 4 hours).*

The typical range of thrombin in blood under normal conditions and during coagulation is between high pM and low µM[117], while lower than high pM is known to be associated with disease[186]. This would indicate that the DDLW device can almost detect the normal range of thrombin. Furthermore, this limit of detection ($\approx$ 3.7 nM) was comparable to those reported for detection of thrombin in an aqueous buffer as shown in table 6.1. However, the fabricated DDLW device offers several advantages over other techniques such as low cost, easy fabrication, affordable read-out instrumentation, label-free detection and real-time measurement. Furthermore, the DDLW aptasensor was shown to be suitable to measure the concentration of thrombin up to 1 µM which indicated to a dynamic range.

Table 6.1 The limit of detection (LOD) of thrombin in an aqueous buffer by different techniques.

Detection method	Limit of Detection (LOD) of Thrombin	Reference
Quartz crystals microbalance (QCM)	10 nM	40
Surface acoustic wave (SAW)	7.5 pM	43
Chemiluminescence (CL)	1.5 nM	
Surface plasmon resonance (SPR)	5 nM	131_187
Fiber-Optic Interferometric	100 nM	188
Electrochemical	10 pM	189

6.2 Detection of thrombin in a commercial human serum sample

The fabricated DDLW device was evaluated for measurement of thrombin in a clinically relevant sample. After immobilisation of anti-thrombin aptamer (oligo 3/ 1µM), the chitosan waveguide (1%) was flushed with undiluted commercial human serum sample at a flow rate of 118 µL min^{-1}. This was followed by introducing thrombin solution that was spiked at a concentration of 50 nM as explained in section 2.10.2.

As can be seen in figure 6.15, a significant shift in resonance angle was observed upon introducing undiluted human serum sample to the prepared chitosan waveguide (1%). The dip shifted by 1.4° and remained at the same level. This high shift should be attributed to the non-specific adsorption of serum proteins onto the waveguide leading to a large change in the waveguide's refractive index. This is because the human serum sample was applied without dilution in a high ionic strength buffer. Therefore, in this case chitosan waveguide possesses a positive charge at pH 7.4 which enhanced the binding of negatively charged protein in the serum. Upon applying thrombin solution (50 nM) spiked in the serum sample, the dip further shifted by 0.4°. This would indicate the further change in the waveguide's refractive index which could be due to the binding of thrombin to the immobilised aptamer. Figure 6.16 **(a)** shows the introduction of the spiked thrombin

solution (50 nM) into the waveguide. From the figure, it can be seen that the dip reached saturation level with undiluted human serum sample and before applying the spiked thrombin solution. However, figure 6.16 **(b)** exhibits the last part of the experiment when undiluted human serum sample was re-applied. The dip shifted further to a higher resonance angle. This would lead us to say that using undiluted human serum sample would result in further adsorption of serum proteins which could affect the detection of thrombin. Therefore, further investigation was carried out by diluting the human serum sample in HEPES salts buffer to the concentration of 10% (v/v). The result is shown in figure 6.17.
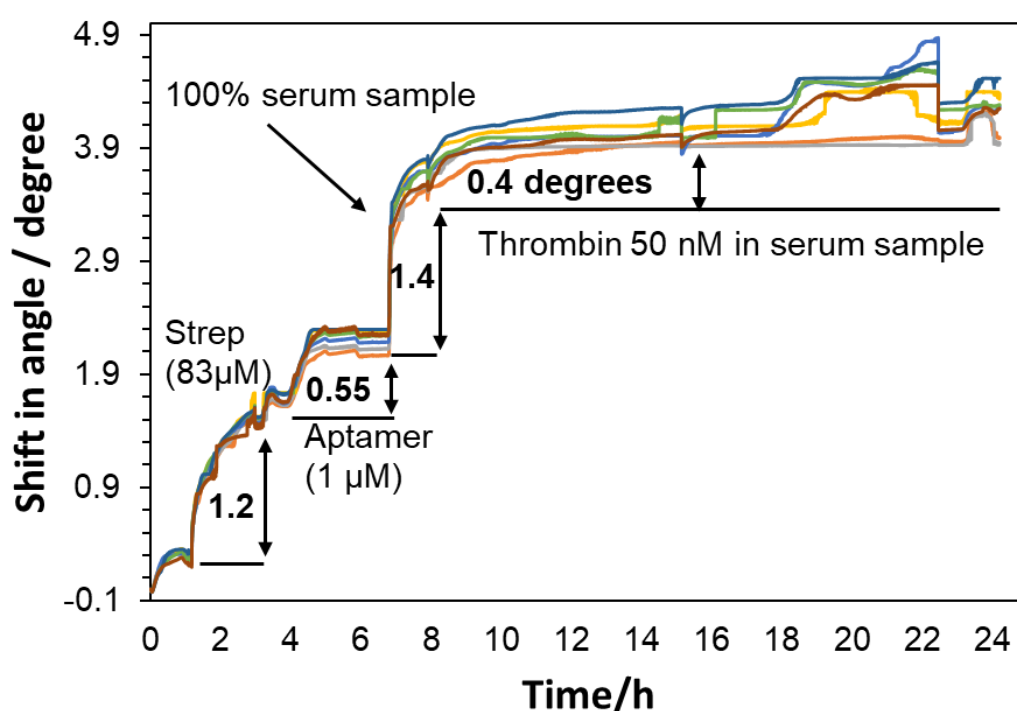
Figure 6.15 *Shift in resonance angle upon detection of 50 nM of thrombin spiked into undiluted commercial human serum sample. The waveguide was first treated with glutaraldehyde solution (0.2%) for 1 h and subsequently with streptavidin solution (83 µM) for 2 h. Both solutions were flushed in the HEPES buffer (100 mM/ pH 7.4). This was followed by applying blocking molecules (BSA/ 0.5%) and then anti-thrombin biotinylated aptamer (oligo 3/ 1 µM) in HEPES salts buffer. Undiluted commercial human serum sample was then introduced until saturation level was observed. The experiment was run one time using one chitosan waveguide.*
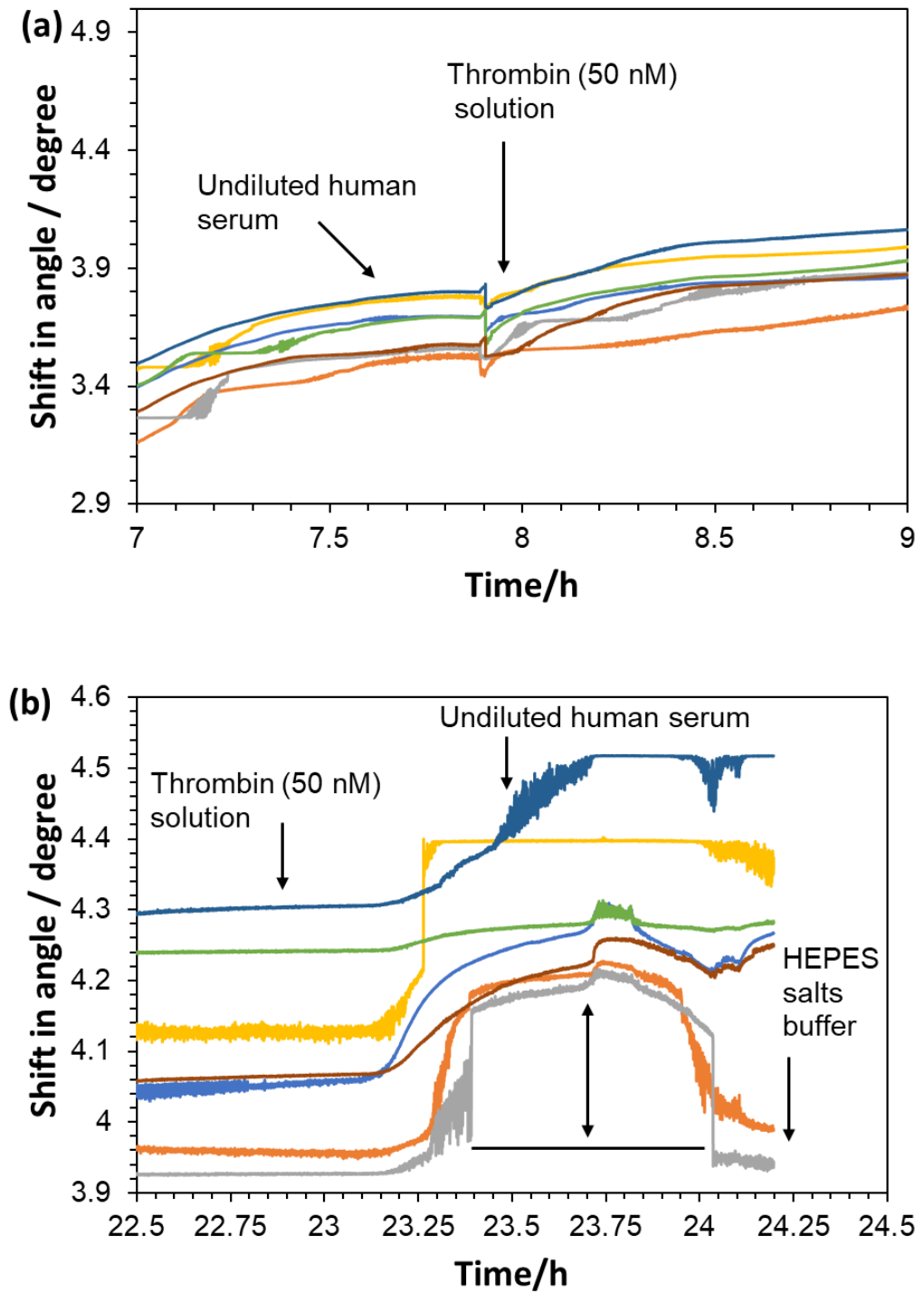
Figure 6.16 **(a)** *Shows the introduction of the spiked thrombin solution (50 nM) into the chitosan waveguide (1%) and after flushing the surface with undiluted human serum sample.* **(b)** *displays the last part of the experiment when the waveguide was flushed sequentially with undiluted human serum sample and with HEPES salts buffer.*

Figure 6.17 shows the detection of the thrombin solution (50 nM) in a serum sample that was diluted with HEPES salts buffer to the concentration of 10 % (v/v). The waveguide was flushed with diluted human serum sample (10%) before and after applying the spiked thrombin solution (50 nM). As can be seen from the figure, the dip shifted by 0.2° upon applying the diluted serum sample (10%). This shift was clearly lower than the 1.4° observed when undiluted serum was utilised (Figure 6.15). This would be expected because at a higher dilution factor, there was a lower concentration of serum proteins and hence, lower non-specific binding occurred. Upon introducing the thrombin solution (50 nM), the dip gradually moved to a higher resonance angle until stabilised at 0.15°. This shift was clearly lower than the 0.4° seen previously when thrombin solution (50 nM) was detected in undiluted human serum sample (Figure 6.15). This could be attributed to the large interferences observed when an undiluted serum sample was used. Upon flushing the surface with a diluted serum (10%) at the end, the dip remained at the same level. This would suggest that the thrombin molecules were bound to the immobilised aptamer as the dip did not shift back to the previous baseline.
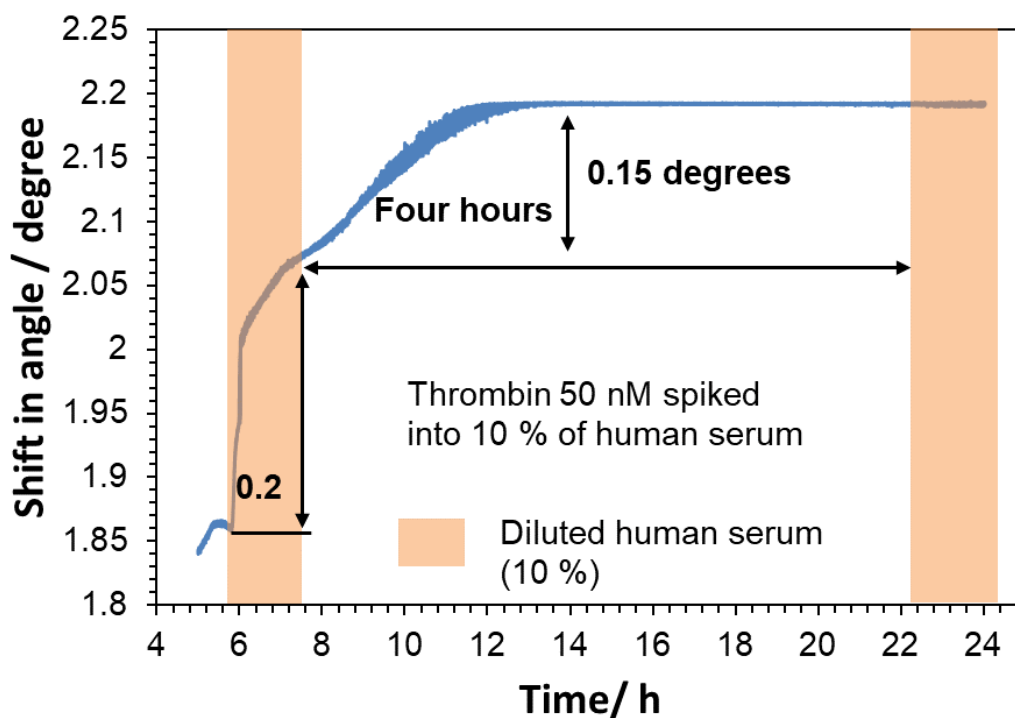
Figure 6.17 *Shows the introduction of a diluted human serum sample (10 %) and a spiked thrombin solution (50 nM) into the chitosan waveguide (1%). The waveguide was initially functionalised with anti-thrombin biotinylated aptamer (1 µM) in the same procedure as shown previously. The serum was diluted in HEPES salts buffer at the concentration of 10% before flushing into the waveguide. Thrombin solution was spiked at a concentration of 50 nM in 10 % of the serum sample. The experiment was run one time using one chitosan waveguide.*

Figure 6.18 shows the comparison in terms of the shift in resonance angle upon detection of 50 nM of thrombin in aqueous buffer and 50 nM of thrombin in 10% of human serum sample. It can be seen that the dip shifted upon applying thrombin solution (50 nM) in 10% of human serum sample with a degree being closer to the shift observed when thrombin solution (50 nM) was measured in aqueous buffer. The dip shifted by 0.04°, 0.07° and 0.13° in 10% of human serum sample for the first, second and third hours of intubation respectively. In contrast, the shift was at 0.06°, 0.13° and 0.19° for the same incubation time using an aqueous buffer. This would lead to the conclusion that the observed shift in diluted human serum sample was in the same range as that seen in the aqueous buffer. Therefore, this would confirm the successful detection of thrombin molecules in 10 % of human serum sample. This would make the DDLW device highly attractive in the field of healthcare monitoring and point of care diagnostics.
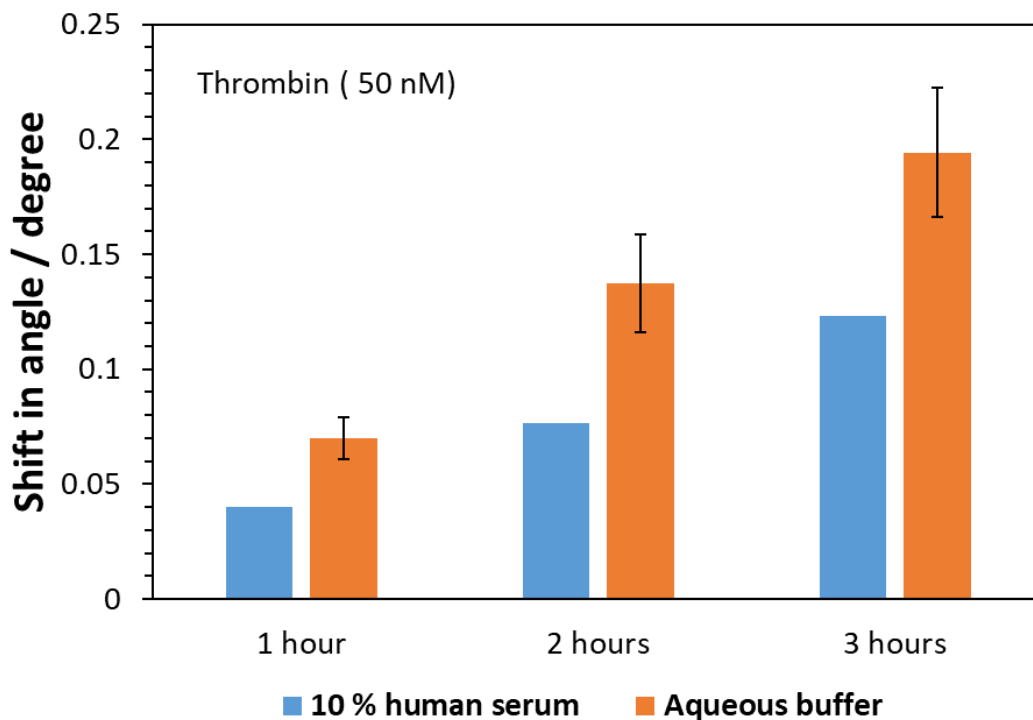
Figure 6.17 *Shows the comparison in terms of shifting in resonance angle when applying thrombin solution (50 nM) in aqueous buffer and in 10% of a human serum sample for the first three hours of incubation. The experiment was rune three times using three separate chitosan waveguide for measurement of the thrombin (50 nM) in aqueous buffer while it was run one time using one chitosan waveguide for measurement of the thrombin (50 nM) in diluted human serum sample.*

6.3 Summary

Thrombin was selected as a model compound to validate the effectiveness of using the DDLW as a biosensor device with an aptamer as a bio-recognition element. Two aptamers have been reported to bind to thrombin at two different sites. The aptamer with a 15-mer of oligonucleotides has been extensively and widely used under various approaches by comparison to the aptamer with 29-mer of oligonucleotides. Therefore, it was chosen in this project.

For detection of thrombin, anti-thrombin aptamer was first immobilised onto the chitosan waveguide via streptavidin-biotin complex as optimised in chapter 5. Therefore, the waveguide was first treated with glutaraldehyde solution (0.2%) for 1 h and subsequently with streptavidin solution (83 µM) for 2 h. Anti-thrombin biotinylated aptamer was then applied until saturation level was reached. The detection of thrombin was achieved via observing a rapid shift in resonance angle upon applying 1 µM of thrombin solution for

15 min. The successful detection of thrombin by DDLW device was confirmed by conducting a control experiment with a non-specific sequence aptamer. Upon applying thrombin solution (1 µM) for 15 min with this aptamer, the dip remained at the same level, which indicated that the thrombin molecules had not bound to the non-specific sequence. The sensitivity of the DDLW to detect lower concentrations of thrombin was significantly enhanced by increasing the incubation time of thrombin solution. This dip moved by 0.65° upon flushing the surface with 100 nM of thrombin solution for four hours. In contrast, the dip only shifted by 0.18° when the waveguide was flushed with a higher concentration of thrombin (1µM) for 15 min. This would indicate that at a higher incubation time, a larger number of thrombin molecules were bound to the aptamer and hence a higher shift in resonance angle occurred. A series of concentrations of anti-thrombin aptamer were then investigated for detection of 100 nM of thrombin. 1µM of biotinylated aptamer gave a higher amount of thrombin bound into the chitosan waveguide for all incubation times compared to other concentrations of aptamer ranging from 0.1µM to 2µM. Thus, 1µM was selected as the optimum concentration.

For investigation of the limit of detection (LOD) of the DDLW device, a series of concentrations of thrombin ranging from 1 nM to 100 nM, including a blank, were applied into various chitosan waveguides until obtaining the saturation level. In order to obtain a reproducible result, the run was repeated three times using three chitosan waveguides for each concentration applied. On all waveguides, the dip shifted to a higher resonance angle with the degree being proportional to the concentration of thrombin introduced. This was expected because at a higher concentration, a higher amount of thrombin bound to the immobilised aptamer and therefore a larger shift in resonance angle obtained. A calibration curve was then obtained between 0 nM (blank sample) and 75 nM for the first four hours of incubation. The R^2 value was seen at 0.992 by comparison to the value of 0.986, 0.982 and 0.972 for the second, third and four hours of incubation respectively. The limit of detection (LOD) was found to be $\approx$ 3.7 nM for the first hour of incubation. The typical range of thrombin during the coagulation process is between nM and µM. The fabricated DDLW device can cover this range. Furthermore, the limit of detection (LOD) was comparable to those were previously reported for detection of thrombin using different techniques. However, the DDLW device has several advantages over SPR such as low cost, easy fabrication, affordable read-out instrumentation, label-free detection and real time measurement.

The applicability of using the DDLW device for the measurement of the thrombin in a clinically relevant sample was evaluated. A significant shift in resonance angle was obtained when undiluted commercial human serum sample was flushed through the waveguide before and after introducing a spiked thrombin solution (50 nM). Therefore, it was concluded that the detection of thrombin in undiluted serum sample can be easily affected by the non-specific adsorption of serum proteins.

Further dilution of the serum sample to the concentration of 10% (v/v) was investigated. The dip shifted by 0.2° using 10 % of human serum which indicates a large reduction in the amount of serum proteins adsorbed. This is because the dip moved by 1.4° when undiluted serum sample was used. Upon introducing spiked thrombin solution (50 nM) in 10% serum sample, the observed shift for the first three hours of incubation was closer to the shift obtained when 50 nM of thrombin was measured in aqueous buffer. Therefore, it was concluded that the thrombin was successfully detected in a clinically relevant sample. This would make the fabricated DDLW device highly attractive in the field of healthcare monitoring and point of care diagnostics. The next chapter will investigate the validation of using the fabricated DDLW device to detect another target molecule namely prostate specific antigen (PSA), using an aptamer as a bio-recognition element.

CHAPTER 7

Detection of prostate specific antigen (PSA)

7 Detection of prostate specific antigen (PSA)

Prostate cancer is considered to be the most common cancer in men in USA and is the second leading cause of deaths among men aged 80 and older[190]. Prostate specific antigen (PSA) is the most validated biomarker in the serum for early detection of prostate and breast cancers[191]. A PSA level of 4ng/mL in human serum is usually considered to be a potential sign of tumours in the prostate[191]. Therefore, this protein has been selected as the second target to be detected with the DDLW device using an aptamer as the recognition element. Two aptamers have been reported to recognise prostate specific antigen (PSA). The first aptamer was an RNA aptamer consisting of 90 mer of nucleotides[192]. However, few studies have selected this aptamer for PSA detection, probably due to the long length of the sequence which results in difficulties for commercially synthesising this aptamer[126]. The second aptamer was a DNA aptamer consisting of 32 mer of nucleotides. The aptamer was identified by Savory and co-workers in 2010 and has a dissociation constant (KD) in the range of several tens of nM[193]. Using this aptamer, PSA has been successful measured using various different approaches including an electrochemical aptasensor[191, 194, 195] and a fluorescence aptasensor[196, 197]. This aptamer was therefore chosen for detection of PSA in this project. The immobilisation of PSA aptamer was performed using the same procedure utilised in the previous chapter with the streptavidin-biotin complex.

7.1 Detection of PSA in an aqueous buffer

The immobilisation of anti-PSA aptamer followed by detection of PSA molecules were both performed in a PSA buffer. The buffer was prepared with the HEPES buffer (100 mM/pH 7.4) including NaCl (150 mM), $MgCl_2$ (5 mM) and KCl (5mM). The composition of this buffer was almost identical with that of the buffer utilised previously for PSA detection[193, 196]. A chitosan waveguide (1%) was first flushed with glutaraldehyde solution (0.2%) for 1 h and subsequently with streptavidin solution (83 µM) for 2 h. Both solutions were made in the HEPES buffer (100 mM/pH 7.4). Blocking molecules (BSA 0.5%), anti-PSA biotinylated aptamer (1 µM), both prepared in PSA running buffer, were then sequentially introduced. Finally, PSA solution (75 nM) was then applied for about 4 hours as explained in section 2.11. All solutions were pumped at a flow rate of 118 µL min^{-1}.

Figure 7.1 displays the shift in resonance angle as a function of time upon detection of PSA at a concentration of 75 nM. From the figure, the dip shifted by 0.25° upon immobilisation of anti-PSA biotinylated aptamer (1 µM) which confirmed the attachment of aptamer molecules to the prepared chitosan waveguide (1%). Upon the introduction of PSA solution (75nM) for about 4 hours, the dip gradually moved by 0.075° and remained at the same level. This would indicate the successful detection of PSA at a concentration of 75 nM.
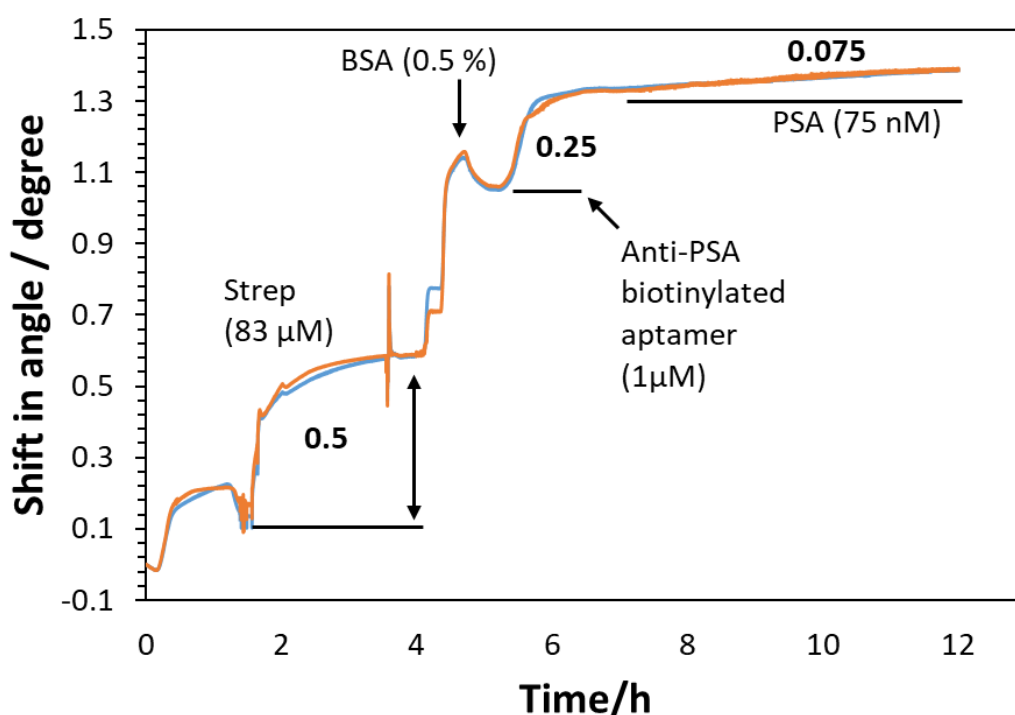
Figure 7.1 *Shift in resonance angle as a function of time upon sequentially applying glutaraldehyde (0.2%), streptavidin (83µM), blocking molecules (BSA 0.5%), anti-biotinylated PSA aptamer (1 µM) and finally PSA solution (75 nM) into a chitosan waveguide (1%). Glutaraldehyde and streptavidin were prepared in the HEPES buffer (100 mM/pH 7.4) while all other solutions were made in PSA running buffer. All solutions were flushed at a flow rate of 118 µLmin^{-1}. The experiment was run one time using one chitosan waveguide.*

In order to make a clear comparison in terms of detection sensitivity between PSA and thrombin, figure 7.2 shows the shift in resonance angle for the first four hours of detection of PSA and thrombin at the same concentration (75 nM). Each molecule was measured in a separate chitosan waveguide (1%) that had been initially functionalised with aptamer,

either anti-thrombin aptamer (1µM) or anti-PSA aptamer (1µM). The measurement of PSA was carried out twice. The result of thrombin was shown in chapter 6 and is added here just for a clear comparison. From the figure, the dip shifted by 0.03° for the first run and 0.01° for the second run during the first four hours of introducing the PSA solution (75 nM). In contrast, the dip moved by 0.3° when thrombin solution (75nM) was applied for the first four hours (as an average of three runs using three different chitosan waveguides). From this it can be concluded that the amount of thrombin bound was significantly higher than the amount of PSA. In order to enhance the binding of PSA, thermal treatment for the anti-PSA aptamer was performed before immobilisation onto chitosan waveguide. The aim of this was to unfold aptamer molecules which could enhance the binding of the target analyte. The results are shown in figure 7.3.
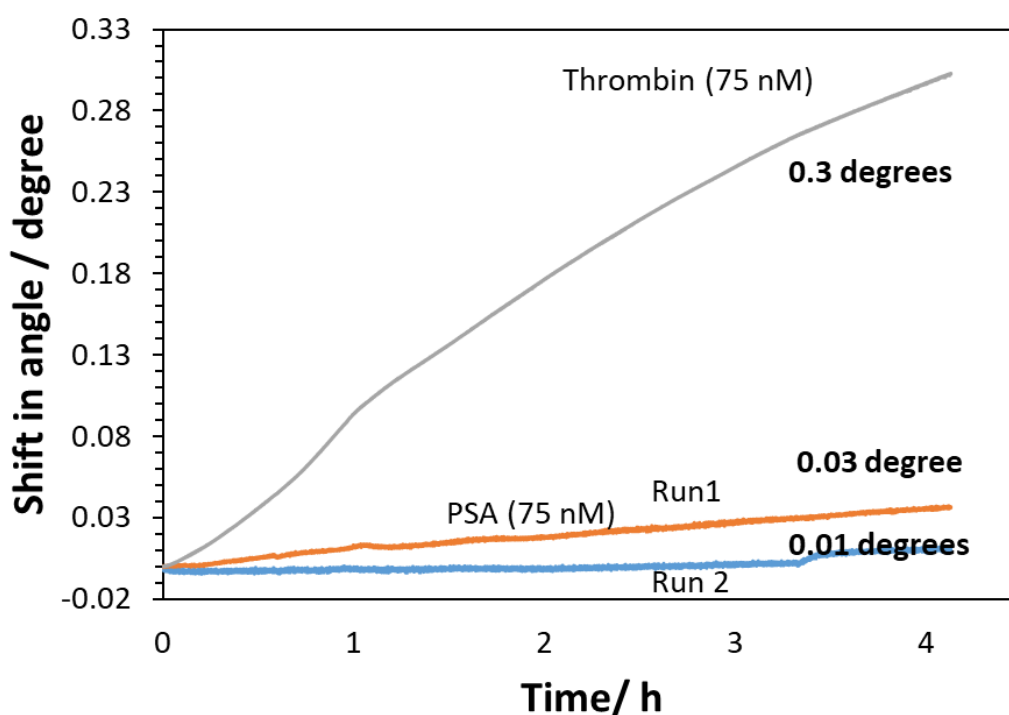
Figure 7.2 *Shift in resonance angle as a function of time upon introducing thrombin and PSA solutions (75 nM) into separate chitosan waveguides (1%). The waveguides were initially functionalised either with anti-thrombin aptamer (1µM) or with anti-PSA aptamer (1µM). The results for thrombin were an average of three runs using three separate chitosan waveguides. For PSA measurement, it was performed two times(run1 and run2) using two separate chitosan waveguides.*

Figure 7.3 shows the immobilisation of anti-PSA aptamer (1μM) onto the chitosan waveguide (1%). Before immobilisation, the aptamer was thermally treated at 95° C for 10 min followed by a gradual reduction in the temperature to 25° C for 30 min as previously reported[193]. After flushing the surface with glutaraldehyde (0.2%), streptavidin (83 μM) and blocking molecules (BSA 0.5%), the dip shifted by 0.3° when aptamer solution (1μM) was applied, which confirmed the binding to the immobilised streptavidin. Upon introducing PSA solution (75 nM), a clear shift in resonance angle was observed in which the dip shifted by 0.25° during the incubation of PSA solution for about 4 hours. This shift was significantly higher than the 0.075° seen when PSA solution was introduced at the same concentration (75 nM) and at the same period of time (Figure 7.1). This would indicate the enhancement on the amount of PSA bound into an immobilised aptamer which could be due to the initial thermal treatment of aptamer molecules. Further investigation was carried out by repeating the experiment under the same conditions, however using a lower concentration of PSA.
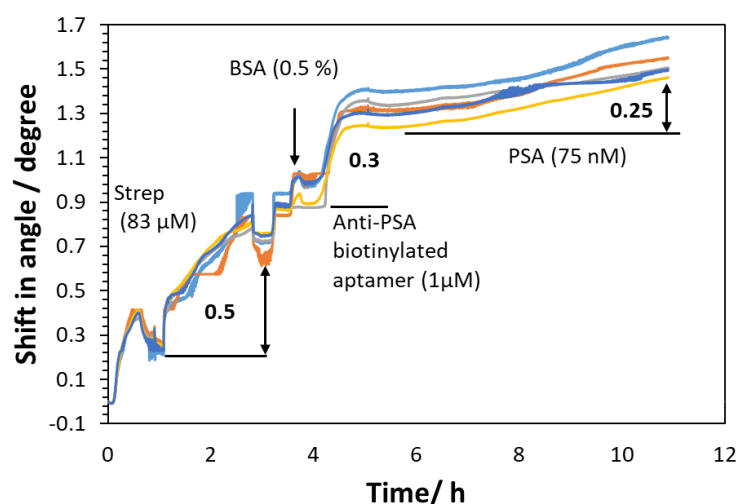
Figure 7.3 Shift in resonance angle as a function of time upon immobilisation of anti-PSA aptamer onto the chitosan waveguide (1%) for detection of PSA at a concentration of 75 nM. Before immobilisation, aptamer molecules were thermally treated at 95 ° C for 10 min followed by a gradual reduction in the temperature to 25 ° C for 30 min. The waveguide was initially treated with glutaraldehyde (0.2%) for 1 h and subsequently with streptavidin (83μM) for 2 h. Both solutions were made in the HEPES buffer (100 mM/pH 7.4). Blocking molecules (BSA 0.5%), anti-PSA aptamer (1 μM) and PSA solution (75 nM) were then sequentially applied in PSA buffer. The experiment was run one time using one chitosan waveguide.

Figure 7.4 shows the shift in resonance angle upon detection of PSA at a concentration of 50 nM. Aptamer molecule was thermally treated before immobilisation as explained previously. Upon applying PSA solution (50 nM) for about 4 hours, the dip gradually shifted by 0.1° and remained at almost at the same level . This would indicate the binding of PSA molecules to the immobilised aptamer.
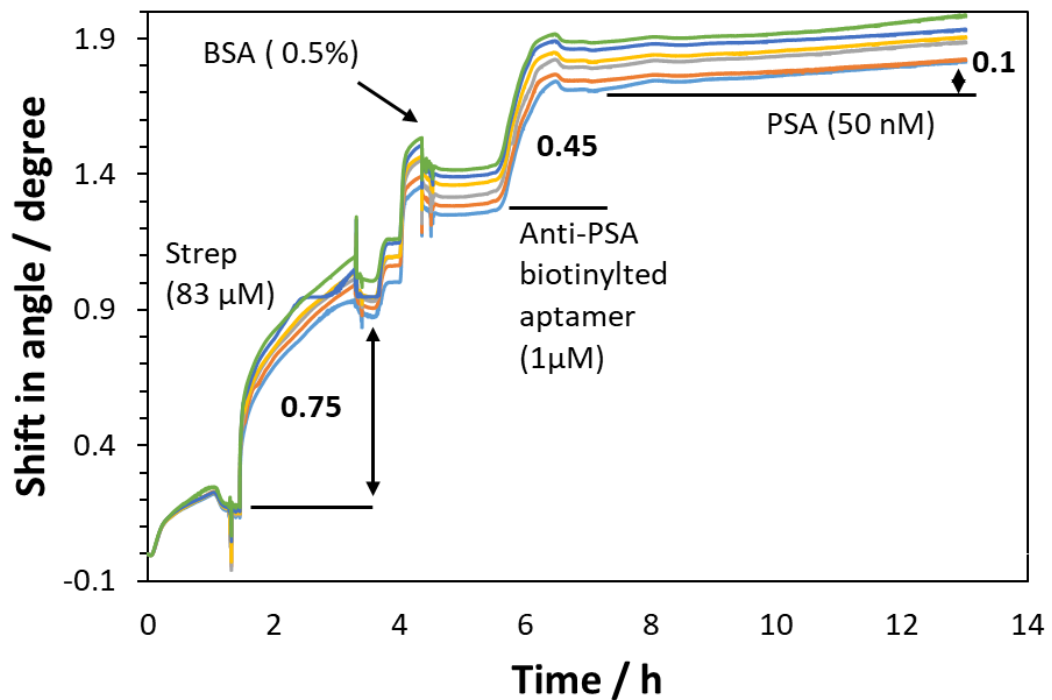
Figure 7.4 *Shift in resonance angle as a function of time upon detection of PSA at a concentration of 50 nM for about 4 hours. The waveguide was initially treated with glutaraldehyde solution (0.2%) for 1 h and subsequently with streptavidin solution (83μM) for 2 h. Both solutions were made in the HEPES buffer (100 mM/pH 7.4). Blocking molecules (BSA 0.5%), anti-biotinylated PSA aptamer (1 μM) and PSA solution (50 nM) were then sequentially applied in PSA buffer. Aptamer was thermally treated before immobilisation as explained previously. The experiment was run one time using one chitosan waveguide.*

Figure 7.5 shows the shift in resonance angle for the first four hours of detection of PSA at concentrations of 25 nM, 50 nM and 75 nM. Each measurement of PSA was performed in a separate chitosan waveguide that had been initially functionalised with anti-PSA biotinylated aptamer (1μM). A control experiment was added to the figure to prove the detection of PSA. The control run was conducted using a nonspecific sequence

biotinylated aptamer (oligo 2, 1 µM) that was thermally treated with the same procedure on anti-PSA aptamer. PSA solution (50 nM) was then applied on a control run for about 4 hours. From the figure, it can be seen that the dip shifted to a higher resonance angle with the degree being proportional to the concentration of PSA applied. This would be expected because at higher concentrations, a higher amount of PSA bound into the immobilised aptamer and hence a higher change in the waveguide's refractive index would be seen. Upon introducing PSA solution (50 nM) in a control experiment, the dip gradually shifted to a lower angle until reaching a stabilised level that was clearly lower than the levels for PSA solution. This distinguishable difference between the control experiment and other experiments further confirmed the achievement of detection of PSA molecule via a fabricated DDLW device.
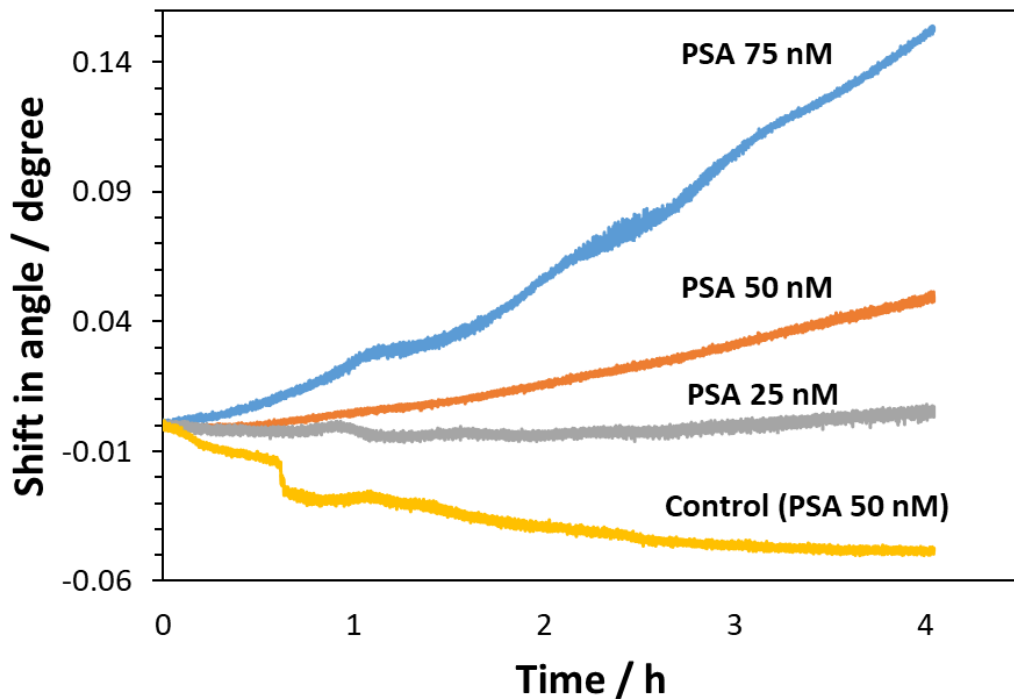
Figure 7.5 *Shows the shift in resonance angle for the first four hours of detection of PSA at concentrations of 25 nM, 50 nM and 75 nM. Each measurement was performed in a separate chitosan waveguide (1%) that had been initially functionalised with 1 µM of anti-PSA biotinylated aptamer. A control run was added to prove the detection of PSA. The control run was carried out using nonspecific sequence biotinylated aptamer (oligo 21 µM) that was thermally treated with the same procedure the anti-PSA aptamer.*

Figure 7.6 shows the average shift in resonance angle upon applying PSA solutions at concentrations of 25 nM, 50 nM and 75 nM including a control run to the chitosan waveguide (1%) for the first four hours of incubation. Each measurement including the control run was carried out three times using three separate chitosan waveguides (1%). The control experiment was performed using non-specific sequence aptamer (oligo 2/1μM) followed by flushing the surface with PSA solution at a concentration of 50 nM. From the figure, it can be seen that the dip shifted to a higher resonance angle with a degree proportional to the time of incubation of the PSA solutions. This would be due to the fact that at a higher incubation time, a larger amount of PSA bound to the immobilised aptamer and therefore a larger change in the waveguide's refractive index occurred. For the control experiment, the dip gradually shifted to a lower angle during the incubation of PSA solution (50 nM) for about 4 hours. This would confirm that the PSA molecules were not bound to the non-specific sequence aptamer as the dip shifted to a lower degree of angle. Using anti-PSA aptamer, the dip moved to a higher resonance angle when each concentration of PSA (25 nM or 50 nM or 75 nM) was applied in three separate chitosan waveguides (1%). Therefore this would further confirm the successful detection of PSA molecules by the fabricated DDLW device. Further confirmation was obtained by a two way ANOVA statistical analysis which indicated that there was a significant difference in terms of shifting in resonance angle between PSA solutions (25 nM or 50 nM or 75 nM) including the control run when they were applied into chitosan waveguide. The p-value was at <0.001.

The detection of PSA has been reported by different techniques such as fluorescence [196, 197] and electrochemical sensor[191, 194]. The major drawback was that a fluorescence label dye was required in order to allow the measurement of PSA. This would increase the cost and the time of the assay with possibility of producing a pollutant or toxic waste during the measurement. For the electrochemical sensor, expensive various electrodes such as working and reference electrode were required to perform the assay while the measurement was not conducted in a real-time form. SPR instrument has been utilised for PSA detection in a label-free and a real-time form. Apart from the instrument being extremally expensive, the assay was carried out with using the most expensive recognition element (Antibody)[198, 199]. PSA was measured by the SPR technique with using an aptamer as a recognition element. However, the surface of the SPR was modified with various complex materials such as gold nanoparticles and quantum dots in order to

improve the SPR signal[200]. Here in this project, the detection of PSA was achieved with using a simple, easy and inexpensive materials for fabrication the DDLW device by comparison to other techniques. Furthermore, the measurement was performed in a real-time form and without using any label.
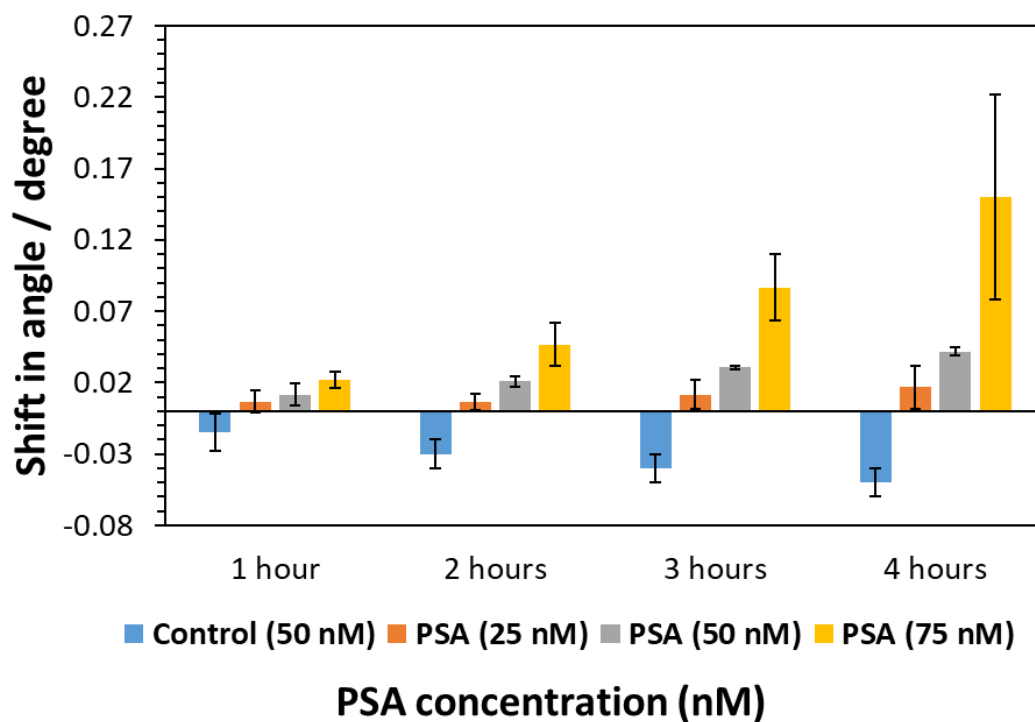
Figure 7.6 *Average shift in resonance angle upon introducing PSA solutions at concentrations of 25 nM, 50 nM and 75 nM including a control run (PSA 50 nM) into chitosan waveguides (1%) for the first four hours of incubation. Each measurement including the control run was carried out three times using three separate chitosan waveguides (1%). The control experiment was conducted using non-specific sequence aptamer (oligo 2 /1 µM) followed by flushing the surface with 50 nM of PSA solution for 4 hours. A two way ANOVA statistical analysis indicated that there was a significant difference in terms of shifting in resonance angle between PSA solutions (25 nM or 50 nM or 75 nM) including the control run when they were applied into chitosan waveguide. The p-value was at < 0.001.*

7.2 Summary

Prostate specific antigen (PSA) has been considered the most validated biomarker for earlier detection of prostate cancer disease. Therefore, this protein was selected as a target analyte and its measurement would further validate the effectiveness of using a DDLW biosensor device with an aptamer as a recognition element. Although two aptamers have been reported to recognise PSA, the DNA aptamer has been extensively utilised under various approaches for PSA detection. Thus it was selected in this project.

The immobilisation of anti-PSA aptamer onto a chitosan waveguide (1%) was performed with the same procedure as was used in chapter 6. Thus the waveguide was first treated with glutaraldehyde (0.2%) solution for 1 h and subsequently with streptavidin solution (83 µM) for 2 h. Blocking molecules (BSA 0.5%) and anti-PSA biotinylated aptamer (1 µM) sequentially followed, in PSA buffer. Upon introducing PSA solution at a concentration of 75 nM for about 4 hours, the dip shifted slightly to a higher resonance angle which was significantly lower than that obtained upon detection of thrombin at the same concentration (75 nM). This indicated poor binding of the PSA molecule. One of the suggestions for the enhancement of the PSA binding was based on thermal treatment of aptamer molecules prior to immobilisation. This was thought to prevent the folding of aptamer molecules and hence improve the binding of PSA. When this process was carried out, the shift in resonance angle obtained upon applying PSA solution (75 nM) for about 4 hours showed an enhancement in the amount of PSA bound. Under the same conditions, lower concentrations of PSA (25 nM and 50 nM) were then applied leading to a shift in resonance angle proportional to the concentration of PSA introduced. Confirmation of the successful detection of PSA by DDLW device was provided on conducting a control experiment using a nonspecific sequence aptamer. Upon applying PSA solution (50 nM) in a control run, the dip clearly shifted to a lower resonance angle which confirmed that the PSA molecules had not been attached. It was concluded that PSA was successfully measured by the DDLW device and thus it was proved that the DDLW device can be applied to any other applications with using an aptamer as a recognition element.

CHAPTER 8

Conclusion, Future work and Appendix

8 Conclusion, Future work and Appendix
8.1 Conclusion

The objective of this research project was to develop a label-free optical aptasensor based on a dye-doped leaky waveguide (DDLW) for biomarker detection. The DDLW device constitutes a waveguide with a leaky optical mode that features a lower index porous waveguide material, such as a hydrogel. This is beneficial for the sensitivity of the sensor as the analytes can diffuse into the waveguide material and hence interact with all light present in the waveguide. The device could be easily prepared with inexpensive materials and its sensitivity was found to be very similar to that of the more complex and expensive metal clad leaky waveguide (MCLW)[86] and for that reason DDLW detection was chosen for the feasibility of developing a biosensor device for biomarker detection. The aim was to investigate a new inexpensive porous hydrogel for the waveguide layer and to utilise it in a biosensor device. Chitosan also features functional amino groups and is thus amenable for tethering of bio-recognition elements. In this research an aptamer was chosen as a recognition element as aptamers have high stability a high affinity and a good selectivity and are low cost compared to more commonly used antibodies[11, 20]. This was the first time the possibility of using an aptamer as bio-receptor in a 3D network leaky waveguide containing chitosan porous hydrogel on glass substrate was investigated. Thrombin was selected as a first target analyte, because its binding to its aptamer was considered the most commonly used model system to demonstrate the proof-of-concept of aptamer-based affinity assays[117]. Prostate-specific antigen (PSA) has been identified as the most validated biomarker in serum for early detection of prostate and breast cancer[191]. Thus, PSA has been chosen as the second target analyte in this project.

Chapter three described the development and characterisation of a DDLW device using chitosan as a waveguide layer. A single-mode waveguide was successfully achieved at condition of 2% (w/v) of chitosan solution coated at speed of 3,000 rpm. The waveguide obtained operated at a wide range of pH, ranging from 4 to 10, which would allow a variety of conditions of the DDLW sensor to be used for the bioassay measurement. The number of moles of amino groups on the waveguide was found to be 6.8×10^{-13} mol for each volume of 1.5×10^{-11} m^3 on the 2% chitosan waveguide. This information could be used as a guide choice for the immobilisation of bio-recognition element. Reactive blue 4 dye was used in order to visualise the resonance angle (Θ). However, the dye concentration was found to affect the shape of the dip in reflectivity, which would

influence how the dip moved with a change in the refractive index and therefore, an optimisation was performed. Incubation of the waveguide with RB4 dye (100 µM) for 10 min resulted in the highest sensitivity for the change in refractive index compared to 30 min and 60 min. The slope value was at 100.6° RIU^{-1}, 93° RIU^{-1} and 62° RIU^{-1} for incubation times of 10 min, 30 min and 60 min, respectively. The sensitivity was not significantly changed when different buffers were used; for example, PBS and HEPES produced results almost identical to water.

The sensitivity of the fabricated sensors was further investigated based on the porosity of the waveguide. This was accomplished by monitoring the shift in the dip upon applying small and large molecules that were all prepared to have the same refractive index value. A significant shift in resonance angle was only observed when glycerol solution was applied. Other larger molecules such as PEG and PEO, applied at various molecular weights, only showed a small shift in resonance angle. The dip shifted by 1.4° with glycerol solution, while it shifted by 0.02° with other polymer solutions. This confirmed that the 2% chitosan waveguide featured a small pore size, and thus, large molecules could not diffuse into the waveguide. Further confirmation was obtained when chitosan was prepared as a bulk hydrogel in a cuvette. The hydrogel remained transparent before, during and after incubation with BSA-FITC solution, which indicated that the BSA molecule was not entering the hydrogel. In contrast, the hydrogel became coloured during and after incubation with FITC solution, indicating penetration of FITC molecules. This was expected because of the small size of the FITC molecule compared to BSA-FITC molecule. Therefore, 2% of chitosan as a hydrogel or as a waveguide proved to be impermeable to large molecules such as BSA, PEG and PEO. This would affect the immobilisation of recognition elements, such as an aptamer, and the detection sensitivity of the DDLW sensor.

In chapter four, the aim was to enhance the waveguide's porosity. Different methodologies were investigated to improve the porosity. Using a glutaraldehyde as a cross-linker could impact the waveguide's porosity as it reduced the pore size of the chitosan membrane[149]. Nevertheless, reducing the amount of the cross-linker from 25% to 0% did not show improvement, as the waveguide was still impermeable to large molecules. This was seen when the dip shifted with PEG and PEO solutions, with a degree being significantly lower than the glycerol solution. Further investigations were carried out by blending the chitosan bulk hydrogel in cuvette with porogens such as PEG or PEO.

The blended components were then dissolved in a water bath at 80°C for 8 h, which should lead to a microporous hydrogel structure as previously reported[134, 151]. The improvement was then monitored via application of a BSA-FITC solution. However, the BSA-FITC molecule did not penetrate into the hydrogel, and this was thought to be related to lack of time to extract all blended components. In contrast, an enhancement on the hydrogel's porosity was been obtained when the blended component was extracted in NaOH solution (5% w/v) for 16 h. With this approach the BSA-FITC molecules were clearly seen to diffuse into the hydrogel as it became coloured and to a significant emission of fluorescent light from cuvettes was seen compared to the thermal treatment. Nevertheless, neither alkaline nor thermal treatment was applicable to the chitosan waveguide as the alkaline solution degraded the film leading to collapse or removal from the substrate.

Controlling the drying time of the wet chitosan film was then performed using lower concentration of chitosan. The sharpest dip in reflectivity was seen with 1% (w/v) of chitosan solution coated at spin speed of 900 rpm, with the wet film then being left to dry for 3 min. The sensitivity to refractive index was investigated, given a slope of $106° \text{ RIU}^{-1}$, which was comparable to $100° \text{ RIU}^{-1}$ when the 2% chitosan waveguide was used (previous condition). Using this method of preparation the dip shifted by 0.05° when PEG and PEO polymer solutions at various molecular weights and at same refractive index value were applied, this is compared with a dip shifted by 0.005° when the previous 2% chitosan waveguide was utilised. This indicated a high improvement in the porosity of the waveguide when using a lower concentration of chitosan and controlling the drying time of wet film. The waveguide was investigated under different pH and was found to be well operated between pH 5.4 and pH 8.4. At pH values lower than this the waveguide dissolved due to the high protonation of the amino group. The chitosan waveguide had a positive charge at pH 7.4 due to the protonation of the amino group. This enhanced the nonspecific binding of the negative charge molecule, which affects the bioassay measurement. Nevertheless, using a high ionic strength buffer, this binding was eliminated or reduced by shielding all charges on all molecules. The non specific binding was also eliminated when a higher pH buffer (pH 8) was used, leading to deprotonating the amino groups on the chitosan waveguide. Due to the significant enhancement of the waveguide's porosity by comparison to 2% chitosan waveguide, the condition obtained at 1% (w/v) of chitosan solution coated at 900 rpm with 3 min of drying time, was selected for immobilisation of the bio-recognition element.

Due to the high affinity between streptavidin and biotin, this complex was selected as a cross-linker for immobilisation of the aptamer molecule. In chapter five, the immobilisation of the streptavidin molecule onto chitosan waveguide was optimised. At a concentration of 1.6 µM, streptavidin successfully attached onto the chitosan waveguide using 0.6% of glutaraldehyde. However, the amount of unreacted aldehyde group on the surface was extremely high, resulting in a large number of blocking molecules being conjugated into the surface. Consequently, the binding sites on streptavidin were hidden, and a poor attachment of aptamer was obtained. A significant enhancement in the amount of aptamer conjugated was observed when a higher concentration of streptavidin (83 µM) was used, which served as a blocking molecule and also as a binding site for aptamer. Thus, 83 µM was considered an optimum concentration. The glutaraldehyde concentration (ranging from 0.2% to 1.4%) was then optimised based on the amount of streptavidin (83µM) attached. It was found that the amount of streptavidin (83 µM) attached varied, and that was attributed to the polymerisation of the glutaraldehyde leading forming oligomers rather than reacting with free amino groups on streptavidin.

Streptavidin (83 µM) was immobilised via electrostatic interaction. However, the amount of streptavidin attached was significantly lower than the amount from the glutaraldehyde method. The dip shifted by 0.15° as an average of three runs when streptavidin (83 µM) was immobilised by electrostatic interaction, while it shifted between 0.5° and 1° when the glutaraldehyde method was used. Therefore, the immobilisation via an electrostatic interaction cannot be considered as an alternative approach to the glutaraldehyde method. The amount of streptavidin (83 µM) immobilised was significantly enhanced when it was adsorbed onto a biotinylated chitosan waveguide. As a comparison to glutaraldehyde method, the dip shifted by 0.95° within 10 min of introducing streptavidin (83 µM) while reaching the same level (0.95°) after two hours of immobilisation of streptavidin (83 µM) by the glutaraldehyde method. Nevertheless, for subsequent binding, the amount of biotinylated aptamer attached was significantly poor by comparison to the glutaraldehyde method using the same oligo solution (oligo 3) at the same concentration (1 µM). This could be linked firstly to the availability of the biotin binding sites, because one or two sites were already occupied upon the immobilisation of the streptavidin onto biotinylated chitosan waveguide; and secondly, to the electrostatic repulsion and steric hindrance which prevents the aptamer binding on the two close remaining biotin binding sites. By comparing all protocols utilised for streptavidin immobilisation and for the subsequent

binding of the biotinylated aptamer, the glutaraldehyde method still was the optimum condition.

In chapter six, the aim was to detect a thrombin molecule in an aqueous buffer and in a commercial human serum sample. An anti-thrombin aptamer was immobilised onto the chitosan waveguide via the streptavidin-biotin complex. In the aqueous buffer, the detection of thrombin was achieved by observing a rapid shift in resonance angle upon applying 1 µM of thrombin solution for 15 min. The successful detection of thrombin by DDLW device was confirmed by conducting a control experiment with a non-specific sequence aptamer. Upon applying the thrombin solution (1 µM) for 15 min with this aptamer, the dip remained at the same level, indicating that the thrombin molecules had not bound to the non-specific sequence. The sensitivity of the DDLW to detect lower concentrations of thrombin was significantly enhanced by increasing the incubation time of thrombin solution. The dip moved by 0.65° upon flushing the surface with 100 nM of thrombin solution for four hours. In contrast, the dip only shifted by 0.18° when the waveguide was flushed with a higher concentration of thrombin (1 µM) for 15 min. This would indicate that at a higher incubation time, a larger number of thrombin molecules were bound to the aptamer and hence a higher shift in resonance angle occurred. A series of concentrations of anti-thrombin aptamer were then investigated for detection of 100 nM of thrombin. 1 µM of biotinylated aptamer resulted in a higher amount of thrombin bound to the chitosan waveguide for all incubation times compared to other concentrations of aptamer ranging from 0.1 µM to 2 µM. Thus, 1 µM was selected as the optimum concentration.

For investigation of the limit of detection (LOD) of the DDLW device, a series of concentrations of thrombin ranging from 1 nM to 100 nM, including a blank, was applied into various chitosan waveguides for about 4 hours. In order to obtain a reproducible result, the run was repeated three times using three chitosan waveguides for each concentration applied. For all waveguides, the dip shifted to a higher resonance angle with the degree being proportional to the concentration of thrombin introduced. This was expected because at a higher concentration, a higher amount of thrombin was bound to the immobilised aptamer, and therefore, a larger shift in resonance angle was obtained. A calibration curve was then obtained, and the limit of detection (LOD) was calculated based on three times the standard deviation divided by the slope of the calibration curve. It was found to be $\approx$ 3.7 nM for the first hour of incubation. The typical range of thrombin

during the coagulation process is between high pM and low µM; therefore, the fabricated DDLW device can almost cover this range[117]. Many different types of thrombin aptasensor have been described such as chemiluminescence (CL)[55], Quartz crystals microbalance (QCM)[40] and electrochemical[189]. The limit of detection (LOD) was comparable to what was obtained by DDLW device. The most drawback of these techniques was that either a label dye or an expensive electrode was required in order to perform the detection while the measurement in most of these sensors was not carried out in a real-time form. SPR instrument has been utilised to measure thrombin in a label-free and in a real-time detection[130, 131].However, the instrument was expensive. Here in this project the fabricated DDLW device offers several advantages over other techniques such as low cost, easy fabrication, affordable read-out instrumentation, label-free detection, real-time measurement and a large dynamic range up to 1µM.

The applicability of using the fabricated DDLW device for the measurement of the thrombin in a clinically relevant sample was evaluated. The detection of thrombin in undiluted commercial human serum sample was found to be affected by the non-specific adsorption of serum proteins. Therefore, further dilution of the human serum to the concentration of 10% (v/v) was performed. The dip shifted by 0.2° using 10% of the human serum, which indicates a large reduction in the amount of serum proteins adsorbed. This is because the dip moved by 1.4° when the undiluted serum sample was used. Upon introducing the spiked thrombin solution (50 nM) in the 10% serum sample, the observed shift was closer to the shift obtained when 50 nM of thrombin was measured in an aqueous buffer during the first four hours of incubation. Therefore, it was concluded that thrombin was successfully detected in a diluted serum sample.

In chapter seven, the detection of prostate-specific antigen (PSA) was carried out. Upon introducing the PSA solution at a concentration of 75 nM for about 4 hours, the dip shifted slightly to a higher resonance angle, which was significantly lower than that obtained upon detection of thrombin at the same concentration (75 nM). This indicated poor binding of the PSA molecule. To enhance the binding, a thermal treatment of the aptamer molecules was carried out prior to immobilisation. This was thought to prevent the folding of aptamer molecules and hence improve the binding of PSA. An enhancement in the amount of PSA bound was obtained when the thermal treatment was carried out. Under the same conditions, lower concentrations of PSA (25 nM and 50 nM) were then applied, leading to a shift in resonance angle proportional to the concentration of PSA introduced.

Confirmation of the successful detection of PSA by the DDLW device was provided using a control experiment with a nonspecific sequence aptamer. Upon applying PSA solution (50 nM) in a control run, the dip clearly shifted to a lower resonance angle which confirmed that the PSA molecules had not been attached. This would confirm the successful detection of PSA in an aqueous buffer by the DDLW device. PSA has been detected by SPR instrument but with using the most expensive recognition element (Antibody)[198, 199]. Using an aptamer for detection of PSA in SPR has been reported, however, apart from the instruments high cost, the SPR chip was fabricated with complex materials such as gold nanoparticles and quantum dots in order to enhance the SPR signal[200]. In this research, PSA was directly detected by the DDLW device that is featuring an easy, cost effective, affordable read-out instrumentation, label-free, real-time measurement and inexpensive hydrogel material utilised as a waveguide layer. The fabricated DDLW device therefore can be used to other applications using an aptamer as a recognition element.

For the applicability of the sensor to be used in a real sample, further investigations still need to be performed in order to eliminate the non-specific binding of serum proteins into the waveguide.

8.2 Future work

Dye-doped leaky waveguide (DDLW) has been successfully utilised as a biosensor for detection of biomarker such as thrombin and prostate-specific antigen (PSA). The measurement was achieved in an aqueous buffer and for the thrombin in a 10% (v/v) diluted serum sample.

In order to translate this device into practical use, various challenges need to be investigated and optimised. Thrombin solution was flushed into the waveguide at least for one hour in order to obtain a high shift in angle and hence a high limit of detection (3.7 nM). This was considered as a low response time which is not ideal for practical applications. Introducing thrombin solution only for a shorter time would result in a loss of sensitivity of DDLW. The LOD for thrombin can be improved by three orders of magnitude using integrated isoelectric focusing at a pH step as shown by our group[201]. The preconcentration of analytes before detection not only improves the LOD, but also reduces the assay time. DDLW is a completely dielectric structure and hence its integration with electrokinetic sample processing is much easier than other label-free biosensors with continuous metal layers such as surface plasmon resonance (SPR) and

metal-clad leaky waveguide (MCLW). Further challenge can be seen by changing in the bulk refractive index of the waveguide when switching from buffer to sample. This can be significantly reduced by internal referencing using a stacked waveguide sensor where one waveguide layer responds to the analyte and the other acts as a reference[202].

Furthermore, the non-specific binding of serum proteins needs to be highly reduced in order not to interface with actual measurement. This can be done by synthesis the chitosan hydrogel polymer with lower number of positively charge amino groups. Other method can be seen by covalently blocking all remaining positively charge amino groups before introducing the undiluted serum sample.

Moreover, the shelf life of the DDLW chip needs to be examined. This can be obtained by storage various chitosan coated slides under different days at room temperature. This is then followed by comparing the sensitivity of measuring the biomarker such as thrombin between each coated slides.

The reusability of the chitosan coated slide also needs to be characterised. This could be accomplished by using a high concertation of salt solution such as NaCl which works as a regeneration of the surface. This would lead to elute all captured analyte leaving unreacted immobilised aptamer. The target analyte is then reapplied to the waveguide and the sensitivity of the sensor is then compared between the first and the second measurement.

Finally, to further improve the potential of DDLW biosensor for practical use, our group have been developing a 3D printed instrument with dimensions and weight of $\sim 16 \times 13 \times 11$ cm and ~ 800 g respectively. Future work will focus on testing the DDLW aptasensor using the portable 3D printed instrument to facilitate practical analysis.

8.3 Appendix

Publication

<u>Nasser A. Alamrani</u>, Gillian M. Greenway, Nicole Pamme, Nicholas J. Goddard and Ruchi Gupta (A feasibility study of a leaky waveguide aptasensor for thrombin)[203].

Ruchi Gupta, **<u>Nasser A. Alamrani</u>**, Gillian M. Greenway, Nicole Pamme, and Nicholas J. Goddard (Method for Determining Average Iron Content of Ferritin by Measuring its Optical Dispersion)[66].

Oral Presentation

<u>Nasser A Alamrani</u>, Nicole Pamme, Gillian M. Greenway , Ruchi Gupta (Development of a Label-Free Aptasensor based on dye-doped leaky waveguides (DDLW) for protein detection) RSC 5th Analytical Biosciences Early Career Researcher Meeting 2018, York.

<u>Nasser A Alamrani</u>, Nicole Pamme, Gillian M. Greenway , Ruchi Gupta, (Development of a Label-Free Optical Sensor for Detection of Chloramphenicol). PhD experience conference, University of Hull, 2017.

Poster Presentation

<u>Nasser A Alamrani</u>, Nicole Pamme, Gillian M. Greenway Ruchi Gupta. (An optical label-free aptasensor based on dye doped leaky waveguide (DDLW) for biomarker detection). International Conference on Miniaturized Systems for Chemistry and Life Sciences (MicroTAS 2018), Taiwan.

Rana Al-Shemary, Leigh Madden, **<u>Nasser Alamrani,</u>** Nicole Pamme, Gillian M. Greenway, Ruchi Gupta. (An optical label-free biosensor based on dye-doped leaky waveguide (DDLW) for tissue factor analysis). International Conference on Miniaturized Systems for Chemistry and Life Sciences (MicroTAS 2018), Taiwan.

<u>Nasser A. Alamrani</u>, Gillian M. Greenway, Nicholas J. Goddard and Ruchi Gupta. (A Label-Free Optical Sensor for Chloramphenicol Measurement). EUROPT(R)ODE XIII - Conference on Optical Chemical Sensors and Biosensors - Austria, Graz, March, 2016.

<u>Nasser A. Alamrani</u>, Gillian M. Greenway, Nicholas J. Goddard and Ruchi Gupta. (A Label-Free Optical Sensor for Chloramphenicol Measurement). The 9th Saudi Students Conference, Birmingham (UK), February 2016.

Nasser A. Alamrani, Gillian M. Greenway, Nicholas J. Goddard and Ruchi Gupta. (A Label-Free Optical Sensor for Chloramphenicol Measurement). International Women's Day Career Symposium, Hull (UK), March 2016.

9   References

1.   Mascini, M.; Tombelli, S., Biosensors for biomarkers in medical diagnostics. *Biomarkers* **2008,** *13* (7-8), 637-657.
2.   Szunerits, S.; Boukherroub, R., Graphene-based biosensors. *Interface Focus* **2018,** *8* (3), 8.
3.   Metkar, S. K.; Girigoswami, K., Diagnostic biosensors in medicine - A review. *Biocatal. Agric. Biotechnol.* **2019,** *17*, 271-283.
4.   Gerard, M.; Chaubey, A.; Malhotra, B., Application of conducting polymers to biosensors. *Biosensors and bioelectronics* **2002,** *17* (5), 345-359.
5.   Thevenot, D. R.; Toth, K.; Durst, R. A.; Wilson, G. S., Electrochemical biosensors: recommended definitions and classification. *Pure and applied chemistry* **1999,** *71* (12), 2333-2348.
6.   Ricci, F.; Volpe, G.; Micheli, L.; Palleschi, G., A review on novel developments and applications of immunosensors in food analysis. *Anal. Chim. Acta* **2007,** *605* (2), 111-129.
7.   Jarczewska, M.; Górski, Ł.; Malinowska, E., Electrochemical aptamer-based biosensors as potential tools for clinical diagnostics. *Analytical Methods* **2016,** *8* (19), 3861-3877.
8.   Thévenot, D. R.; Toth, K.; Durst, R. A.; Wilson, G. S., Electrochemical biosensors: recommended definitions and classification. *Analytical Letters* **2001,** *34* (5), 635-659.
9.   Clark Jr, L. C.; Lyons, C., Electrode systems for continuous monitoring in cardiovascular surgery. *Annals of the New York Academy of sciences* **1962,** *102* (1), 29-45.
10.   Borisov, S. M.; Wolfbeis, O. S., Optical biosensors. *Chemical reviews* **2008,** *108* (2), 423-461.
11.   Wu, S.; Zhang, H.; Shi, Z.; Duan, N.; Fang, C.; Dai, S.; Wang, Z., Aptamer-based fluorescence biosensor for chloramphenicol determination using upconversion nanoparticles. *Food Control* **2015,** *50*, 597-604.
12.   Jayasena, S. D., Aptamers: an emerging class of molecules that rival antibodies in diagnostics. *Clinical chemistry* **1999,** *45* (9), 1628-1650.
13.   Mehta, J.; Van Dorst, B.; Rouah-Martin, E.; Herrebout, W.; Scippo, M.-L.; Blust, R.; Robbens, J., In vitro selection and characterization of DNA aptamers recognizing chloramphenicol. *Journal of Biotechnology* **2011,** *155* (4), 361-369.
14.   Ellington, A. D.; Szostak, J. W., In vitro selection of RNA molecules that bind specific ligands. *Nature* **1990,** *346* (6287), 818.
15.   Stoltenburg, R.; Reinemann, C.; Strehlitz, B., SELEX—a (r) evolutionary method to generate high-affinity nucleic acid ligands. *Biomolecular engineering* **2007,** *24* (4), 381-403.
16.   Alizadeh, N.; Memar, M. Y.; Moaddab, S. R.; Kafil, H. S., Aptamer-assisted novel technologies for detecting bacterial pathogens. *Biomedicine & Pharmacotherapy* **2017,** *93*, 737-745.
17.   Wang, W.; Chen, C.; Qian, M. X.; Zhao, X. S., Aptamer biosensor for protein detection based on guanine-quenching. *Sensors and Actuators B: Chemical* **2008,** *129* (1), 211-217.
18.   O'Sullivan, C. K., Aptasensors–the future of biosensing? *Anal. Bioanal. Chem.* **2002,** *372* (1), 44-48.
19.   Pilehvar, S.; Mehta, J.; Dardenne, F.; Robbens, J.; Blust, R.; De Wael, K., Aptasensing of chloramphenicol in the presence of its analogues: reaching the maximum residue limit. *Anal. Chem.* **2012,** *84* (15), 6753-6758.

20.   Han, K.; Liang, Z.; Zhou, N., Design strategies for aptamer-based biosensors. *Sensors* **2010,** *10* (5), 4541-4557.

21.   Potyrailo, R. A.; Conrad, R. C.; Ellington, A. D.; Hieftje, G. M., Adapting selected nucleic acid ligands (aptamers) to biosensors. *Anal. Chem.* **1998,** *70* (16), 3419-3425.

22.   Lee, M.; Walt, D. R., A fiber-optic microarray biosensor using aptamers as receptors. *Analytical Biochemistry* **2000,** *282* (1), 142-146.

23.   Abnous, K.; Danesh, N. M.; Emrani, A. S.; Ramezani, M.; Taghdisi, S. M., A novel fluorescent aptasensor based on silica nanoparticles, PicoGreen and exonuclease III as a signal amplification method for ultrasensitive detection of myoglobin. *Anal. Chim. Acta* **2016,** *917*, 71-78.

24.   Freeman, R.; Girsh, J.; Fang-ju Jou, A.; Ho, J.-a. A.; Hug, T.; Dernedde, J.; Willner, I., Optical aptasensors for the analysis of the vascular endothelial growth factor (VEGF). *Anal. Chem.* **2012,** *84* (14), 6192-6198.

25.   Hilton, J. P.; Nguyen, T. H.; Pei, R.; Stojanovic, M.; Lin, Q., A microfluidic affinity sensor for the detection of cocaine. *Sensors and Actuators A: Physical* **2011,** *166* (2), 241-246.

26.   Huang, L.; Yang, X.; Qi, C.; Niu, X.; Zhao, C.; Zhao, X.; Shangguan, D.; Yang, Y., A label-free electrochemical biosensor based on a DNA aptamer against codeine. *Anal. Chim. Acta* **2013,** *787*, 203-210.

27.   Guo, X. D.; Wen, F.; Zheng, N.; Luo, Q. J.; Wang, H. W.; Wang, H.; Li, S. L.; Wang, J. Q., Development of an ultrasensitive aptasensor for the detection of aflatoxin B-1. *Biosens. Bioelectron.* **2014,** *56*, 340-344.

28.   Song, K. M.; Jeong, E.; Jeon, W.; Cho, M.; Ban, C., Aptasensor for ampicillin using gold nanoparticle based dual fluorescence-colorimetric methods. *Anal. Bioanal. Chem.* **2012,** *402* (6), 2153-2161.

29.   Ye, B.-F.; Zhao, Y.-J.; Cheng, Y.; Li, T.-T.; Xie, Z.-Y.; Zhao, X.-W.; Gu, Z.-Z., Colorimetric photonic hydrogel aptasensor for the screening of heavy metal ions. *Nanoscale* **2012,** *4* (19), 5998-6003.

30.   Cui, L.; Wu, J.; Ju, H., Label-free signal-on aptasensor for sensitive electrochemical detection of arsenite. *Biosensors and Bioelectronics* **2016,** *79*, 861-865.

31.   Perumal, V.; Hashim, U., Advances in biosensors: Principle, architecture and applications. *Journal of applied biomedicine* **2014,** *12* (1), 1-15.

32.   Wang, Y.; Xu, H.; Zhang, J.; Li, G., Electrochemical sensors for clinic analysis. *Sensors* **2008,** *8* (4), 2043-2081.

33.   Feyzizarnagh, H.; Park, B.-W.; Sharma, L.; Patania, M. M.; Kim, D.-S., Amperometric mediatorless hydrogen peroxide sensor with horseradish peroxidase encapsulated in peptide nanotubes. *Sensing and bio-sensing research* **2016,** *7*, 38-41.

34.   Paniagua, G.; Villalonga, A.; Eguílaz, M.; Vegas, B.; Parrado, C.; Rivas, G.; Díez, P.; Villalonga, R., Amperometric aptasensor for carcinoembryonic antigen based on the use of bifunctionalized Janus nanoparticles as biorecognition-signaling element. *Anal. Chim. Acta* **2019**.

35.   Ding, J.; Lei, J.; Ma, X.; Gong, J.; Qin, W., Potentiometric aptasensing of Listeria monocytogenes using protamine as an indicator. *Anal. Chem.* **2014,** *86* (19), 9412-9416.

36.   Guo, L.; Lu, Q., Potentials of piezoelectric and thermoelectric technologies for harvesting energy from pavements. *Renewable and Sustainable Energy Reviews* **2017,** *72*, 761-773.

37.   Ranjan, R.; Esimbekova, E. N.; Kratasyuk, V. A., Rapid biosensing tools for cancer biomarkers. *Biosensors and Bioelectronics* **2017,** *87*, 918-930.

38.   Jiang, P.; Wang, Y.; Zhao, L.; Ji, C.; Chen, D.; Nie, L., Applications of gold nanoparticles in non-optical biosensors. *Nanomaterials* **2018,** *8* (12), 977.

39.   Pohanka, M., The Piezoelectric Biosensors: Principles and Applications. *Int. J. Electrochem. Sci* **2017,** *12*, 496-506.

40.		Chen, Q.; Tang, W.; Wang, D.; Wu, X.; Li, N.; Liu, F., Amplified QCM-D biosensor for protein based on aptamer-functionalized gold nanoparticles. *Biosensors and Bioelectronics* **2010,** *26* (2), 575-579.

41.		Mujahid, A.; Dickert, F., Surface acoustic wave (SAW) for chemical sensing applications of recognition layers. *Sensors* **2017,** *17* (12), 2716.

42.		Gronewold, T. M., Surface acoustic wave sensors in the bioanalytical field: Recent trends and challenges. *Anal. Chim. Acta* **2007,** *603* (2), 119-128.

43.		Horiguchi, Y.; Miyachi, S.; Nagasaki, Y., High-performance surface acoustic wave immunosensing system on a PEG/aptamer hybridized surface. *Langmuir* **2013,** *29* (24), 7369-7376.

44.		Damborský, P.; Švitel, J.; Katrlík, J., Optical biosensors. *Essays in biochemistry* **2016,** *60* (1), 91-100.

45.		Tereshchenko, A.; Bechelany, M.; Viter, R.; Khranovskyy, V.; Smyntyna, V.; Starodub, N.; Yakimova, R., Optical biosensors based on ZnO nanostructures: advantages and perspectives. A review. *Sensors and Actuators B: Chemical* **2016,** *229*, 664-677.

46.		Pazos, E.; Vazquez, O.; Mascarenas, J. L.; Vazquez, M. E., Peptide-based fluorescent biosensors. *Chemical Society Reviews* **2009,** *38* (12), 3348-3359.

47.		Nawrot, W.; Drzozga, K.; Baluta, S.; Cabaj, J.; Malecha, K., A fluorescent biosensors for detection vital body fluids' agents. *Sensors* **2018,** *18* (8), 2357.

48.		Liu, D.; Lu, X.; Yang, Y.; Zhai, Y.; Zhang, J.; Li, L., A novel fluorescent aptasensor for the highly sensitive and selective detection of cardiac troponin I based on a graphene oxide platform. *Anal. Bioanal. Chem.* **2018,** *410* (18), 4285-4291.

49.		Chen, Z.; Berciaud, S.; Nuckolls, C.; Heinz, T. F.; Brus, L. E., Energy transfer from individual semiconductor nanocrystals to graphene. *ACS nano* **2010,** *4* (5), 2964-2968.

50.		Kasry, A.; Ardakani, A. A.; Tulevski, G. S.; Menges, B.; Copel, M.; Vyklicky, L., Highly efficient fluorescence quenching with graphene. *The Journal of Physical Chemistry C* **2012,** *116* (4), 2858-2862.

51.		Benito-Pena, E.; Valdes, M. G.; Glahn-Martinez, B.; Moreno-Bondi, M. C., Fluorescence based fiber optic and planar waveguide biosensors. A review. *Anal. Chim. Acta* **2016,** *943*, 17-40.

52.		Sang, S.; Wang, Y.; Feng, Q.; Wei, Y.; Ji, J.; Zhang, W., Progress of new label-free techniques for biosensors: a review. *Critical reviews in biotechnology* **2016,** *36* (3), 465-481.

53.		Sun, Y.; Lu, J., Chemiluminescence‐based aptasensors for various target analytes. *Luminescence* **2018,** *33* (8), 1298-1305.

54.		Pires, N.; Dong, T.; Hanke, U.; Hoivik, N., Recent developments in optical detection technologies in lab-on-a-chip devices for biosensing applications. *Sensors* **2014,** *14* (8), 15458-15479.

55.		Sun, Y.; Wang, Y.; Li, J.; Ding, C.; Lin, Y.; Sun, W.; Luo, C., An ultrasensitive chemiluminescence aptasensor for thrombin detection based on iron porphyrin catalyzing luminescence desorbed from chitosan modified magnetic oxide graphene composite. *Talanta* **2017,** *174*, 809-818.

56.		Daniels, J. S.; Pourmand, N., Label‐free impedance biosensors: Opportunities and challenges. *Electroanalysis: An International Journal Devoted to Fundamental and Practical Aspects of Electroanalysis* **2007,** *19* (12), 1239-1257.

57.		Fan, X.; White, I. M.; Shopova, S. I.; Zhu, H.; Suter, J. D.; Sun, Y., Sensitive optical biosensors for unlabeled targets: A review. *Anal. Chim. Acta* **2008,** *620* (1-2), 8-26.

58.		Hashemi, P.; Abolghasemi, M. M., Preparation of a novel optical sensor for low pH values using agarose membranes as support. *Sensors and Actuators B: Chemical* **2006,** *115* (1), 49-53.

59.		Milosevic, M., Internal reflection and ATR spectroscopy. *Applied Spectroscopy Reviews* **2004,** *39* (3), 365-384.

60.   Garland, P. B., Optical evanescent wave methods for the study of biomolecular interactions. *Quarterly reviews of biophysics* **1996,** *29* (1), 91-117.

61.   Schmitt, K.; Oehse, K.; Sulz, G.; Hoffmann, C., Evanescent field sensors based on tantalum pentoxide waveguides–a review. *Sensors* **2008,** *8* (2), 711-738.

62.   Olaru, A.; Bala, C.; Jaffrezic-Renault, N.; Aboul-Enein, H. Y., Surface plasmon resonance (SPR) biosensors in pharmaceutical analysis. *Critical reviews in analytical chemistry* **2015,** *45* (2), 97-105.

63.   Rusnati, M.; Presta, M., Angiogenic growth factors interactome and drug discovery: The contribution of surface plasmon resonance. *Cytokine & growth factor reviews* **2015,** *26* (3), 293-310.

64.   Nguyen, H.; Park, J.; Kang, S.; Kim, M., Surface plasmon resonance: a versatile technique for biosensor applications. *Sensors* **2015,** *15* (5), 10481-10510.

65.   Gupta, R.; Goddard, N. J., Optical waveguide for common path simultaneous refractive index and broadband absorption measurements in small volumes. *Sens. Actuator B-Chem.* **2016,** *237*, 1066-1075.

66.   Gupta, R.; Alamrani, N.; Greenway, G.; Pamme, N.; Goddard, N., A Method for Determining Average Iron Content of Ferritin by Measuring its Optical Dispersion. *Anal. Chem.* **2019**.

67.   Kozma, P.; Kehl, F.; Ehrentreich-Förster, E.; Stamm, C.; Bier, F. F., Integrated planar optical waveguide interferometer biosensors: A comparative review. *Biosensors and Bioelectronics* **2014,** *58*, 287-307.

68.   Gopinath, S. C.; Awazu, K.; Fujimaki, M., Waveguide-mode sensors as aptasensors. *Sensors* **2012,** *12* (2), 2136-2151.

69.   Mukundan, H.; Anderson, A.; Grace, W. K.; Grace, K.; Hartman, N.; Martinez, J.; Swanson, B., Waveguide-based biosensors for pathogen detection. *Sensors* **2009,** *9* (7), 5783-5809.

70.   Lukosz, W., Integrated optical chemical and direct biochemical sensors. *Sensors and Actuators B: Chemical* **1995,** *29* (1-3), 37-50.

71.   Li, B.; Ju, H., Label-free optical biosensors based on a planar optical waveguide. *BioChip Journal* **2013,** *7* (4), 295-318.

72.   Tien, P.; Ulrich, R.; Martin, R., Modes of propagating light waves in thin deposited semiconductor films. *Appl. Phys. Lett.* **1969,** *14* (9), 291-294.

73.   Yuan, D.; Dong, Y.; Liu, Y.; Li, T., Mach-zehnder interferometer biochemical sensor based on silicon-on-insulator rib waveguide with large cross section. *Sensors* **2015,** *15* (9), 21500-21517.

74.   Ymeti, A.; Subramaniam, V.; Beumer, T. A.; Kanger, J. S., An ultrasensitive Young interferometer handheld sensor for rapid virus detection. *Expert review of medical devices* **2007,** *4* (4), 447-454.

75.   Goddard, N. J.; Singh, K.; Holmes, R. J.; Bastani, B., Resonant grating sensors using frustrated total-internal reflection. *Sensors and Actuators B: Chemical* **1998,** *51* (1-3), 131-136.

76.   Buckle, P.; Davies, R.; Kinning, T.; Yeung, D.; Edwards, P.; Pollard-Knight, D.; Lowe, C., The resonant mirror: a novel optical sensor for direct sensing of biomolecular interactions part II: applications. *Biosensors and Bioelectronics* **1993,** *8* (7-8), 355-363.

77.   Cush, R.; Cronin, J.; Stewart, W.; Maule, C.; Molloy, J.; Goddard, N., The resonant mirror: a novel optical biosensor for direct sensing of biomolecular interactions Part I: Principle of operation and associated instrumentation. *Biosensors and Bioelectronics* **1993,** *8* (7-8), 347-354.

78.   Daghestani, H. N.; Day, B. W., Theory and applications of surface plasmon resonance, resonant mirror, resonant waveguide grating, and dual polarization interferometry biosensors. *Sensors* **2010,** *10* (11), 9630-9646.

79.   Goddard, N. J.; Singh, K.; Hulme, J. P.; Malins, C.; Holmes, R. J., Internally-referenced Resonant Mirror devices for dispersion compensation in chemical sensing and biosensing applications. *Sensors and Actuators A: Physical* **2002,** *100* (1), 1-9.

80.   Horvath, R.; Pedersen, H. C.; Larsen, N. B., Demonstration of reverse symmetry waveguide sensing in aqueous solutions. *Appl. Phys. Lett.* **2002,** *81* (12), 2166-2168.

81.   Horvath, R.; Lindvold, L. R.; Larsen, N. B., Reverse-symmetry waveguides: theory and fabrication. *Applied Physics B* **2002,** *74* (4-5), 383-393.

82.   Taya, S. A.; El-Agez, T. M., A reverse symmetry optical waveguide sensor using a plasma substrate. *Journal of Optics* **2011,** *13* (7), 075701.

83.   Horváth, R.; Pedersen, H. C.; Skivesen, N.; Selmeczi, D.; Larsen, N. B., Optical waveguide sensor for on-line monitoring of bacteria. *Optics letters* **2003,** *28* (14), 1233-1235.

84.   Duguay, M.; Kokubun, Y.; Koch, T. L.; Pfeiffer, L., Antiresonant reflecting optical waveguides in SiO2‐Si multilayer structures. *Appl. Phys. Lett.* **1986,** *49* (1), 13-15.

85.   Goddard, N. J.; Singh, K.; Bounaira, F.; Holmes, R. J.; Baldock, S. J.; Pickering, L. W.; Fielden, P. R.; Snook, R. D. In *Anti-Resonant Reflecting Optical Waveguides (ARROWS) as Optimal Optical Detectors for μTAS Applications*, Micro Total Analysis Systems' 98, Springer: 1998; pp 97-100.

86.   Gupta, R.; Goddard, N. J., Optical waveguide for common path simultaneous refractive index and broadband absorption measurements in small volumes. *Sensors and Actuators B: Chemical* **2016,** *237*, 1066-1075.

87.   Hulme, J. P.; An, S. S. A., The application of leaky anti-resonant reflecting optical waveguides as optical sensors (L-ARROW). *Sensors and Actuators B: Chemical* **2009,** *138* (1), 42-47.

88.   Archambault, J.-L.; Black, R. J.; Lacroix, S.; Bures, J., Loss calculations for antiresonant waveguides. *Journal of Lightwave Technology* **1993,** *11* (3), 416-423.

89.   Carvalho, D.; Alayo, M., a-SiC: H anti-resonant layer ARROW waveguides. *Journal of Optics A: Pure and Applied Optics* **2008,** *10* (10), 104002.

90.   Prieto, F.; Sepúlveda, B.; Calle, A.; Llobera, A.; Domınguez, C.; Lechuga, L. M., Integrated Mach–Zehnder interferometer based on ARROW structures for biosensor applications. *Sensors and actuators B: Chemical* **2003,** *92* (1-2), 151-158.

91.   Bernini, R.; Campopiano, S.; Zeni, L.; Sarro, P. M., ARROW optical waveguides based sensors. *Sensors and Actuators B: Chemical* **2004,** *100* (1-2), 143-146.

92.   Swalen, J., Optical wave spectroscopy of molecules at surfaces. *Journal of Physical Chemistry* **1979,** *83* (11), 1438-1445.

93.   Gupta, R.; Goddard, N. J., A novel leaky waveguide grating (LWG) device for evanescent wave broadband absorption spectroscopy in microfluidic flow cells. *Analyst* **2013,** *138* (6), 1803-1811.

94.   Skivesen, N.; Horvath, R.; Thinggaard, S.; Larsen, N. B.; Pedersen, H. C., Deep-probe metal-clad waveguide biosensors. *Biosensors and Bioelectronics* **2007,** *22* (7), 1282-1288.

95.   Skivesen, N.; Horvath, R.; Pedersen, H., Optimization of metal-clad waveguide sensors. *Sensors and Actuators B: Chemical* **2005,** *106* (2), 668-676.

96.   Zourob, M.; Mohr, S.; Fielden, P. R.; Goddard, N. J., Small-volume refractive index and fluorescence sensor for micro total analytical system (μ-TAS) applications. *Sensors and Actuators B: Chemical* **2003,** *94* (3), 304-312.

97.   Zourob, M.; Mohr, S.; Brown, B. J. T.; Fielden, P. R.; McDonnell, M. B.; Goddard, N. J., Bacteria detection using disposable optical leaky waveguide sensors. *Biosensors and Bioelectronics* **2005,** *21* (2), 293-302.

98.   Gupta, R.; Goddard, N. J., A proof-of-principle study for performing enzyme bioassays using substrates immobilized in a leaky optical waveguide. *Sensors and Actuators B: Chemical* **2017,** *244*, 549-558.

99.   Luppa, P. B.; Sokoll, L. J.; Chan, D. W., Immunosensors—principles and applications to clinical chemistry. *Clinica chimica acta* **2001,** *314* (1-2), 1-26.

100.   Gupta, R.; Goddard, N. J., Broadband absorption spectroscopy for rapid pH measurement in small volumes using an integrated porous waveguide. *Analyst* **2017,** *142* (1), 169-176.

101.   Lee, K. J.; Wawro, D.; Priambodo, P. S.; Magnusson, R., Agarose-gel based guided-mode resonance humidity sensor. *IEEE Sensors Journal* **2007,** *7* (3), 409-414.

102.   Elsabee, M. Z.; Abdou, E. S., Chitosan based edible films and coatings: A review. *Materials Science and Engineering: C* **2013,** *33* (4), 1819-1841.

103.   Koev, S.; Dykstra, P.; Luo, X.; Rubloff, G.; Bentley, W.; Payne, G.; Ghodssi, R., Chitosan: an integrative biomaterial for lab-on-a-chip devices. *Lab Chip* **2010,** *10* (22), 3026-3042.

104.   Voznesenskiy, S.; Sergeev, A.; Mironenko, A. Y.; Bratskaya, S. Y.; Kulchin, Y. N., Integrated-optical sensors based on chitosan waveguide films for relative humidity measurements. *Sensors and Actuators B: Chemical* **2013,** *188*, 482-487.

105.   Sergeev, A.; Voznesenskiy, S., Specific features of chitosan waveguides optical response formation to changes in the values of relative humidity. *Optical Materials* **2015,** *43*, 33-35.

106.   Vakili, M.; Rafatullah, M.; Ibrahim, M. H.; Abdullah, A. Z.; Salamatinia, B.; Gholami, Z., Chitosan hydrogel beads impregnated with hexadecylamine for improved reactive blue 4 adsorption. *Carbohydr. Polym.* **2016,** *137*, 139-146.

107.   Vakili, M.; Rafatullah, M.; Salamatinia, B.; Ibrahim, M. H.; Abdullah, A. Z., Elimination of reactive blue 4 from aqueous solutions using 3-aminopropyl triethoxysilane modified chitosan beads. *Carbohydr. Polym.* **2015,** *132*, 89-96.

108.   Arica, M. Y.; Bayramoglu, G., Purification of lysozyme from egg white by Reactive Blue 4 and Reactive Red 120 dye-ligands immobilised composite membranes. *Process Biochem.* **2005,** *40* (3-4), 1433-1442.

109.   Su, S. N.; Nie, H. L.; Zhu, L. M.; Chen, T. X., Optimization of adsorption conditions of papain on dye affinity membrane using response surface methodology. *Bioresour. Technol.* **2009,** *100* (8), 2336-2340.

110.   Su, S. N.; Zhou, Y. T.; Nie, H. L.; Zhu, L. M.; Branford-White, C. J.; Ieee, *Isotherm, kinetic and thermodynamic analysis of bromelain adsorption on Reactive Blue 4 inmmobilized composite membranes*. Ieee: New York, 2009; p 979-+.

111.   Citartan, M.; Ch'ng, E.-S.; Rozhdestvensky, T. S.; Tang, T.-H., Aptamers as the 'capturing'agents in aptamer-based capture assays. *Microchemical Journal* **2016,** *128*, 187-197.

112.   Balamurugan, S.; Obubuafo, A.; Soper, S. A.; Spivak, D. A., Surface immobilization methods for aptamer diagnostic applications. *Anal. Bioanal. Chem.* **2008,** *390* (4), 1009-1021.

113.   Xia, N.; Xing, Y.; Wang, G.; Feng, Q.; Chen, Q.; Feng, H.; Sun, X.; Liu, L., Probing of EDC/NHSS-mediated covalent coupling reaction by the immobilization of electrochemically active biomolecules. *Int. J. Electrochem. Sci* **2013,** *8*, 2459-2467.

114.   Haes, A. J.; Van Duyne, R. P., A nanoscale optical biosensor: sensitivity and selectivity of an approach based on the localized surface plasmon resonance spectroscopy of triangular silver nanoparticles. *Journal of the American Chemical Society* **2002,** *124* (35), 10596-10604.

115.   Meirinho, S. G.; Dias, L. G.; Peres, A. M.; Rodrigues, L. R., Voltammetric aptasensors for protein disease biomarkers detection: A review. *Biotechnology advances* **2016,** *34* (5), 941-953.

116.   Holmberg, A.; Blomstergren, A.; Nord, O.; Lukacs, M.; Lundeberg, J.; Uhlén, M., The biotin‐streptavidin interaction can be reversibly broken using water at elevated temperatures. *Electrophoresis* **2005,** *26* (3), 501-510.

117.   Deng, B.; Lin, Y.; Wang, C.; Li, F.; Wang, Z.; Zhang, H.; Li, X.-F.; Le, X. C., Aptamer binding assays for proteins: the thrombin example—a review. *Anal. Chim. Acta* **2014,** *837*, 1-15.

118.   Sokolova, E.; Reiser, G., Prothrombin/thrombin and the thrombin receptors PAR-1 and PAR-4 in the brain: localization, expression and participation in neurodegenerative diseases. *Thrombosis and haemostasis* **2008,** *100* (10), 576-581.

119.   Bock, L. C.; Griffin, L. C.; Latham, J. A.; Vermaas, E. H.; Toole, J. J., Selection of single-stranded DNA molecules that bind and inhibit human thrombin. *Nature* **1992,** *355* (6360), 564.

120.   Macaya, R. F.; Schultze, P.; Smith, F. W.; Roe, J. A.; Feigon, J., Thrombin-binding DNA aptamer forms a unimolecular quadruplex structure in solution. *Proceedings of the National Academy of Sciences* **1993,** *90* (8), 3745-3749.

121.   Tasset, D. M.; Kubik, M. F.; Steiner, W., Oligonucleotide inhibitors of human thrombin that bind distinct epitopes. *J. Mol. Biol.* **1997,** *272* (5), 688-698.

122.   Damborska, D.; Bertok, T.; Dosekova, E.; Holazova, A.; Lorencova, L.; Kasak, P.; Tkac, J., Nanomaterial-based biosensors for detection of prostate specific antigen. *Microchimica acta* **2017,** *184* (9), 3049-3067.

123.   Jolly, P.; Tamboli, V.; Harniman, R. L.; Estrela, P.; Allender, C. J.; Bowen, J. L., Aptamer–MIP hybrid receptor for highly sensitive electrochemical detection of prostate specific antigen. *Biosensors and Bioelectronics* **2016,** *75*, 188-195.

124.   Souada, M.; Piro, B.; Reisberg, S.; Anquetin, G.; Noël, V.; Pham, M., Label-free electrochemical detection of prostate-specific antigen based on nucleic acid aptamer. *Biosensors and Bioelectronics* **2015,** *68*, 49-54.

125.   Jeong, S.; Han, S. R.; Lee, Y. J.; Lee, S.-W., Selection of RNA aptamers specific to active prostate-specific antigen. *Biotechnol. Lett.* **2010,** *32* (3), 379-385.

126.   Jolly, P.; Formisano, N.; Estrela, P., DNA aptamer-based detection of prostate cancer. *Chem. Pap.* **2015,** *69* (1), 77-89.

127.   Savory, N.; Abe, K.; Sode, K.; Ikebukuro, K., Selection of DNA aptamer against prostate specific antigen using a genetic algorithm and application to sensing. *Biosensors and Bioelectronics* **2010,** *26* (4), 1386-1391.

128.   Alamrani, N.; Greenway, G. M.; Pamme, N.; Goddard, N.; Gupta, R., A Feasibility Study of a Leaky Waveguide Aptasensor for Thrombin. *Analyst* **2019**.

129.   https://www.zeiss.com/microscopy/int/products/microscope-software/zen-lite.html.

130.   Bai, Y.; Feng, F.; Zhao, L.; Wang, C.; Wang, H.; Tian, M.; Qin, J.; Duan, Y.; He, X., Aptamer/thrombin/aptamer-AuNPs sandwich enhanced surface plasmon resonance sensor for the detection of subnanomolar thrombin. *Biosensors and Bioelectronics* **2013,** *47*, 265-270.

131.   Polonschii, C.; David, S.; Tombelli, S.; Mascini, M.; Gheorghiu, M., A novel low-cost and easy to develop functionalization platform. Case study: Aptamer-based detection of thrombin by surface plasmon resonance. *Talanta* **2010,** *80* (5), 2157-2164.

132.   Padron, I., *Recent interferometry applications in topography and astronomy*. BoD–Books on Demand: 2012.

133.   Park, J.; Kim, J.-A.; Ahn, H.; Bae, J.; Jin, J., A review of thickness measurements of thick transparent layers using optical interferometry. *International Journal of Precision Engineering and Manufacturing* **2019,** *20* (3), 463-477.

134.   Zeng, M.; Fang, Z.; Xu, C., Novel method of preparing microporous membrane by selective dissolution of chitosan/polyethylene glycol blend membrane. *J. Appl. Polym. Sci.* **2004,** *91* (5), 2840-2847.

135.   Zeng, M.; Zhang, X.; Qi, C., Microporous composites prepared by coagulation of a CS/PEG Solution in NaOH. *Int. J. Polym. Mater.* **2010,** *60* (3), 213-222.

136.   Motion Control Tips. https://www.motioncontroltips.com/what-is-an-lvdt-linear-variable-differential-transformer/ (accessed 14/07/2019

).

137.   Page, D.; Burrows, L.; Kowalski, C.; Valencia, J., Dektak 8 advanced development profiler manual. *Veeco Instruments Inc., Tucson, Arizona* **2004**.

138.   W. W. U. Scientific technical services, Scanning Electron Microscope principles,. https://wwuphoto.files.wordpress.com/2014/01/sem-training-2.pdf (accessed 14/07/2019).

139.   Claxton, N. S.; Fellers, T. J.; Davidson, M. W., Laser scanning confocal microscopy. *Department of Optical Microscopy and Digital Imaging, Florida State University, Tallahassee, http://www*. olympusconfocal. com/theory/LSCMIntro. pdf **2006**.

140.   Sampath, U.; Ching, Y. C.; Chuah, C. H.; Singh, R.; Lin, P. C., Preparation and characterization of nanocellulose reinforced semi-interpenetrating polymer network of chitosan hydrogel. *Cellulose* **2017,** *24* (5), 2215-2228.

141.   He, G. H.; Kong, Y. H.; Zheng, H.; Ke, W. W.; Chen, X.; Yin, Y. H.; Yi, Y., Preparation and Properties of Poly(amidoamine) Dendrimer/Quaternary Ammonium Chitosan Hydrogels. *J. Wuhan Univ. Technol.-Mat. Sci. Edit.* **2018,** *33* (3), 736-743.

142.   Wang, Y.; Huang, C. J.; Jonas, U.; Wei, T. X.; Dostalek, J.; Knoll, W., Biosensor based on hydrogel optical waveguide spectroscopy. *Biosens. Bioelectron.* **2010,** *25* (7), 1663-1668.

143.   Verma, R.; Gupta, B. D., Detection of heavy metal ions in contaminated water by surface plasmon resonance based optical fibre sensor using conducting polymer and chitosan. *Food Chem.* **2015,** *166*, 568-575.

144.   Semwal, V.; Shrivastav, A. M.; Gupta, B. D., Surface plasmon resonance based fiber optic trichloroacetic acid sensor utilizing layer of silver nanoparticles and chitosan doped hydrogel. *Nanotechnology* **2017,** *28* (6), 11.

145.   Ge, Y. Q.; Zhang, Y.; He, S. Y.; Nie, F.; Teng, G. J.; Gu, N., Fluorescence Modified Chitosan-Coated Magnetic Nanoparticles for High-Efficient Cellular Imaging. *Nanoscale Res. Lett.* **2009,** *4* (4), 287-295.

146.   Koev, S. T.; Dykstra, P. H.; Luo, X.; Rubloff, G. W.; Bentley, W. E.; Payne, G. F.; Ghodssi, R., Chitosan: an integrative biomaterial for lab-on-a-chip devices. *Lab Chip* **2010,** *10* (22), 3026-3042.

147.   Kildeeva, N. R.; Perminov, P. A.; Vladimirov, L. V.; Novikov, V. V.; Mikhailov, S. N., About mechanism of chitosan cross-linking with glutaraldehyde. *Russ. J. Bioorg. Chem.* **2009,** *35* (3), 360-369.

148.   Monteiro, O. A. C.; Airoldi, C., Some studies of crosslinking chitosan-glutaraldehyde interaction in a homogeneous system. *Int. J. Biol. Macromol.* **1999,** *26* (2-3), 119-128.

149.   Krajewska, B., Diffusional properties of chitosan hydrogel membranes. *J. Chem. Technol. Biotechnol.* **2001,** *76* (6), 636-642.

150.   Zeng, M. F.; Fang, Z. P.; Xu, C. W., Novel method of preparing microporous membrane by selective dissolution of chitosan/polyethylene glycol blend membrane. *J. Appl. Polym. Sci.* **2004,** *91* (5), 2840-2847.

151.   Zeng, M. F.; Fang, Z. P.; Xu, C. W., Effect of compatibility on the structure of the microporous membrane prepared by selective dissolution of chitosan/synthetic polymer blend membrane. *J. Membr. Sci.* **2004,** *230* (1-2), 175-181.

152.   Zeng, M. F.; Fang, Z. P., Preparation of sub-micrometer porous membrane from chitosan/polyethylene glycol semi-IPN. *J. Membr. Sci.* **2004,** *245* (1-2), 95-102.

153.   Reiad, N. A.; Abdelsalam, O. E.; Abadir, E. F.; Harraz, F. A., Preparation, Characterization and Application of Chitosan/Polyethylene Glycol Blend Film for Removal of Iron from Water. *International journal of Sustainable Water and Environmental Systems2013* **2013,** *5* (1), 43-49.

154.   Zeng, M. F.; Zhang, X.; Qi, C. Z., Microporous Composites Prepared by Coagulation of a CS/PEG Solution in NaOH. *Int. J. Polym. Mater.* **2011,** *60* (3), 213-222.

155.   Zeng, X. F.; Ruckenstein, E., Supported chitosan-dye affinity membranes and their protein adsorption. *J. Membr. Sci.* **1996,** *117* (1-2), 271-278.

156.   Zhang, M.; Li, X. H.; Gong, Y. D.; Zhao, N. M.; Zhang, X. F., Properties and biocompatibility of chitosan films modified by blending with PEG. *Biomaterials* **2002,** *23* (13), 2641-2648.

157.   Malhotra, M.; Tomaro-Duchesneau, C.; Saha, S.; Kahouli, I.; Prakash, S., Development and characterization of chitosan-PEG-TAT nanoparticles for the intracellular delivery of siRNA. *Int. J. Nanomed.* **2013,** *8*, 12.

158.   Hianik, T.; Ostatna, V.; Zajacova, Z.; Stoikova, E.; Evtugyn, G., Detection of aptamer-protein interactions using QCM and electrochemical indicator methods. *Bioorg. Med. Chem. Lett.* **2005,** *15* (2), 291-295.

159.   Daniel, C.; Melaine, F.; Roupioz, Y.; Livache, T.; Buhot, A., Real time monitoring of thrombin interactions with its aptamers: Insights into the sandwich complex formation. *Biosens. Bioelectron.* **2013,** *40* (1), 186-192.

160.   Fologea, D.; Ledden, B.; McNabb, D. S.; Li, J. L., Electrical characterization of protein molecules by a solid-state nanopore. *Appl. Phys. Lett.* **2007,** *91* (5), 3.

161.   Bravo-Anaya, L. M.; Soltero, J. F. A.; Rinaudo, M., DNA/chitosan electrostatic complex. *Int. J. Biol. Macromol.* **2016,** *88*, 345-353.

162.   Vorob'ev, E.; Nechipurenko, Y. D.; Salyanov, V.; Evdokimov, Y. M., Description of chitosan binding to DNA at varied ionic strength within the framework of ion condensation and adsorption theories. *Biophysics* **2007,** *52* (4), 383-388.

163.   Torres, M. A.; Beppu, M. M.; Santana, C. C., Characterization of chemically modified chitosan microspheres as adsorbents using standard proteins (bovine serum albumin and lysozyme). *Braz. J. Chem. Eng.* **2007,** *24* (3), 325-336.

164.   Dundas, C. M.; Demonte, D.; Park, S., Streptavidin-biotin technology: improvements and innovations in chemical and biological applications. *Appl. Microbiol. Biotechnol.* **2013,** *97* (21), 9343-9353.

165.   Gong, P. J.; Peng, Z. Y.; Wang, Y.; Qiao, R.; Mao, W. X.; Qian, H. S.; Zhang, M. Y.; Li, C. C.; Shi, S. Y., Synthesis of streptavidin-conjugated magnetic nanoparticles for DNA detection. *J. Nanopart. Res.* **2013,** *15* (4), 11.

166.   Ducker, R. E.; Montague, M. T.; Leggett, G. J., A comparative investigation of methods for protein immobilization on self-assembled monolayers using glutaraldehyde, carbodiimide, and anhydride reagents. *Biointerphases* **2008,** *3* (3), 59-65.

167.   Sprung, M. A., A Summary of the Reactions of Aldehydes with Amines. *Chemical Reviews* **1940,** *26* (3), 297-338.

168.   Silva, C. J.; Sousa, F.; Gübitz, G.; Cavaco-Paulo, A., Chemical modifications on proteins using glutaraldehyde. *Food Technology and Biotechnology* **2004,** *42* (1), 51-56.

169.   Fatoni, A.; Numnuam, A.; Kanatharana, P.; Limbut, W.; Thammakhet, C.; Thavarungkul, P., A highly stable oxygen-independent glucose biosensor based on a chitosan-albumin cryogel incorporated with carbon nanotubes and ferrocene. *Sens. Actuator B-Chem.* **2013,** *185*, 725-734.

170.   Sugawara, K.; Hirabayashi, G.; Kamiya, N.; Kuramitz, H.; Tanaka, S., Evaluation of binding between electroactive biotin derivative and streptavidin immobilized on chitin film. *Electroanalysis: An International Journal Devoted to Fundamental and Practical Aspects of Electroanalysis* **2005,** *17* (18), 1659-1664.

171.   Shi, X. W.; Liu, Y.; Lewandowski, A. T.; Wu, L. Q.; Wu, H. C.; Ghodssi, R.; Rubloff, G. W.; Bentley, W. E.; Payne, G. F., Chitosan biotinylation and electrodeposition for selective protein assembly. *Macromol. Biosci.* **2008,** *8* (5), 451-457.

172.   Hu, W. W.; Syu, W. J.; Chen, W. Y.; Ruaan, R. C.; Cheng, Y. C.; Chien, C. C.; Li, C.; Chung, C. A.; Tsao, C. W., Use of Biotinylated Chitosan for Substrate-Mediated Gene Delivery. *Bioconjugate Chem.* **2012,** *23* (8), 1587-1599.

173.   Darvishi, M. H.; Nomani, A.; Amini, M.; Shokrgozar, M. A.; Dinarvand, R., Novel biotinylated chitosan-graft-polyethyleneimine copolymer as a targeted non-viral vector for anti-EGF receptor siRNA delivery in cancer cells. *Int. J. Pharm.* **2013,** *456* (2), 408-416.

174.   Su, X. D.; Wu, Y. J.; Robelek, R.; Knoll, W., Surface plasmon resonance spectroscopy and quartz crystal microbalance study of streptavidin film structure effects on biotinylated DNA assembly and target DNA hybridization. *Langmuir* **2005,** *21* (1), 348-353.

175.   Yang, N.; Su, X. D.; Tjong, V.; Knoll, W., Evaluation of two- and three-dimensional streptavidin binding platforms for surface plasmon resonance spectroscopy studies of DNA hybridization and protein-DNA binding. *Biosens. Bioelectron.* **2007,** *22* (11), 2700-2706.

176.   Larsson, C.; Rodahl, M.; Hook, F., Characterization of DNA immobilization and subsequent hybridization on a 2D arrangement of streptavidin on a biotin-modified lipid bilayer supported on SiO2. *Anal. Chem.* **2003,** *75* (19), 5080-5087.

177.   Deng, B.; Lin, Y. W.; Wang, C.; Li, F.; Wang, Z. X.; Zhang, H. Q.; Li, X. F.; Le, X. C., Aptamer binding assays for proteins: The thrombin example-A review. *Anal. Chim. Acta* **2014,** *837*, 1-15.

178.   Bock, L. C.; Griffin, L. C.; Latham, J. A.; Vermaas, E. H.; Toole, J. J., SELECTION OF SINGLE-STRANDED-DNA MOLECULES THAT BIND AND INHIBIT HUMAN THROMBIN. *Nature* **1992,** *355* (6360), 564-566.

179.   Ahmad, K. M.; Oh, S. S.; Kim, S.; McClellen, F. M.; Xiao, Y.; Soh, H. T., Probing the Limits of Aptamer Affinity with a Microfluidic SELEX Platform. *PLoS One* **2011,** *6* (11), 8.

180.   Li, Y. L.; Guo, L.; Zhang, F. C.; Zhang, Z. Y.; Tang, J. J.; Xie, J., High-sensitive determination of human alpha-thrombin by its 29-mer aptamer in affinity probe capillary electrophoresis. *Electrophoresis* **2008,** *29* (12), 2570-2577.

181.   Park, B. J.; Sa, Y. S.; Kim, Y. H.; Kim, Y., Spectroscopic and Electrochemical Detection of Thrombin/5 '-SH or 3 '-SH Aptamer Immobilized on (porous) Gold Substrates. *Bull. Korean Chem. Soc.* **2012,** *33* (1), 100-104.

182.   Mani, R. J.; Dye, R. G.; Snider, T. A.; Wang, S. P.; Clinkenbeard, K. D., Bi-cell surface plasmon resonance detection of aptamer mediated thrombin capture in serum. *Biosens. Bioelectron.* **2011,** *26* (12), 4832-4836.

183.   Yang, H.; Ji, J.; Liu, Y.; Kong, J. L.; Liu, B. H., An aptamer-based biosensor for sensitive thrombin detection. *Electrochem. Commun.* **2009,** *11* (1), 38-40.

184.   Ocana, C.; Pacios, M.; del Valle, M., A Reusable Impedimetric Aptasensor for Detection of Thrombin Employing a Graphite-Epoxy Composite Electrode. *Sensors* **2012,** *12* (3), 3037-3048.

185.   Hianik, T.; Ostatna, V.; Sonlajtnerova, M.; Grman, I., Influence of ionic strength, pH and aptamer configuration for binding affinity to thrombin. *Bioelectrochemistry* **2007,** *70* (1), 127-133.

186.   Centi, S.; Tombelli, S.; Minunni, M.; Mascini, M., Aptamer-based detection of plasma proteins by an electrochemical assay coupled to magnetic beads. *Anal. Chem.* **2007,** *79* (4), 1466-1473.

187.   Ostatna, V.; Vaisocherova, H.; Homola, J.; Hianik, T., Effect of the immobilisation of DNA aptamers on the detection of thrombin by means of surface plasmon resonance. *Anal. Bioanal. Chem.* **2008,** *391* (5), 1861-1869.

188.   Sun, D.; Sun, L.-P.; Guo, T.; Guan, B.-O., Label-Free Thrombin Detection Using a Tapered Fiber-Optic Interferometric Aptasensor. *Journal of Lightwave Technology* **2018,** *37* (11), 2756-2761.

189.   Gosai, A.; Yeah, B. S. H.; Nilsen-Hamilton, M.; Shrotriya, P., Label free thrombin detection in presence of high concentration of albumin using an aptamer-functionalized nanoporous membrane. *Biosensors and Bioelectronics* **2019,** *126*, 88-95.

190.   Jemal, A.; Murray, T.; Ward, E.; Samuels, A.; Tiwari, R. C.; Ghafoor, A.; Feuer, E. J.; Thun, M. J., Cancer statistics, 2005. *CA: a cancer journal for clinicians* **2005,** *55* (1), 10-30.

191.   Tahmasebi, F.; Noorbakhsh, A., Sensitive Electrochemical Prostate Specific Antigen Aptasensor: Effect of Carboxylic Acid Functionalized Carbon Nanotube and Glutaraldehyde Linker. *Electroanalysis* **2016,** *28* (5), 1134-1145.

192.   Jeong, S.; Han, S. R.; Lee, Y. J.; Lee, S. W., Selection of RNA aptamers specific to active prostate-specific antigen. *Biotechnol. Lett.* **2010,** *32* (3), 379-385.

193.   Savory, N.; Abe, K.; Sode, K.; Ikebukuro, K., Selection of DNA aptamer against prostate specific antigen using a genetic algorithm and application to sensing. *Biosens. Bioelectron.* **2010,** *26* (4), 1386-1391.

194.   Yang, Z. G.; Kasprzyk-Hordern, B.; Goggins, S.; Frost, C. G.; Estrela, P., A novel immobilization strategy for electrochemical detection of cancer biomarkers: DNA-directed immobilization of aptamer sensors for sensitive detection of prostate specific antigens. *Analyst* **2015,** *140* (8), 2628-2633.

195.   Souada, M.; Piro, B.; Reisberg, S.; Anquetin, G.; Noel, V.; Pham, M. C., Label-free electrochemical detection of prostate-specific antigen based on nucleic acid aptamer. *Biosens. Bioelectron.* **2015,** *68*, 49-54.

196.   Kong, R. M.; Ding, L.; Wang, Z. J.; You, J. M.; Qu, F. L., A novel aptamer-functionalized MoS2 nanosheet fluorescent biosensor for sensitive detection of prostate specific antigen. *Anal. Bioanal. Chem.* **2015,** *407* (2), 369-377.

197.   Hao, T. T.; Wu, X. L.; Xu, L. G.; Liu, L. Q.; Ma, W.; Kuang, H.; Xu, C. L., Ultrasensitive Detection of Prostate-Specific Antigen and Thrombin Based on Gold-Upconversion Nanoparticle Assembled Pyramids. *Small* **2017,** *13* (19), 6.

198.   Jang, H. S.; Park, K. N.; Kang, C. D.; Kim, J. P.; Sim, S. J.; Lee, K. S., Optical fiber SPR biosensor with sandwich assay for the detection of prostate specific antigen. *Optics Communications* **2009,** *282* (14), 2827-2830.

199.   Su, L.-C.; Chen, R.-C.; Li, Y.-C.; Chang, Y.-F.; Lee, Y.-J.; Lee, C.-C.; Chou, C., Detection of prostate-specific antigen with a paired surface plasma wave biosensor. *Anal. Chem.* **2010,** *82* (9), 3714-3718.

200.   Duan, F.; Zhang, S.; Yang, L.; Zhang, Z.; He, L.; Wang, M., Bifunctional aptasensor based on novel two-dimensional nanocomposite of MoS2 quantum dots and g-C3N4 nanosheets decorated with chitosan-stabilized Au nanoparticles for selectively detecting prostate specific antigen. *Anal. Chim. Acta* **2018,** *1036*, 121-132.

201.   Goddard, N. J.; Gupta, R., Speed and sensitivity–Integration of electrokinetic preconcentration with a leaky waveguide biosensor. *Sensors and Actuators B: Chemical* **2019,** *301*, 127063.

202.   Gupta, R.; Goddard, N., A novel optical biosensor with internal referencing. *Freiburg, Germany* **2013**.

203.   Alamrani, N. A.; Greenway, G. M.; Pamme, N.; Goddard, N. J.; Gupta, R., A feasibility study of a leaky waveguide aptasensor for thrombin. *Analyst* **2019,** *144* (20), 6048-6054.